NASA TECHNICAL MEMORANDUM

NASA TM X-72819

NASA TM X-72819

THIRD WORKING MEETING ON

GALLIUM ARSENIDE SOLAR CELLS

NASA - LANGLEY RESEARCH CENTER

September 25-26, 1975

Compiled by Gilbert H. Walker

This informal documentation medium is used to provide accelerated or special release of technical information to selected users. The contents may not meet NASA formal editing and publication standards, may be revised, or may be incorporated in another publication.

NATIONAL AERONAUTICS AND SPACE ADMINISTRATION

LANGLEY RESEARCH CENTER, HAMPTON, VIRGINIA 23665

1. Report No. TMX-72819	2. Government Accession No.	3. Recipient's Catalog No.

4. Title and Subtitle
Third Working Meeting on Gallium Arsenide Solar Cells

5. Report Date
March 1976

6. Performing Organization Code

7. Author(s)
Compiled by Gilbert H. Walker

8. Performing Organization Report No.

10. Work Unit No.

9. Performing Organization Name and Address
NASA Langley Research Center
Hampton, VA 23665

11. Contract or Grant No.

13. Type of Report and Period Covered
Technical Memorandum

12. Sponsoring Agency Name and Address
National Aeronautics and Space Administration
Washington, DC 20546

14. Sponsoring Agency Code

15. Supplementary Notes
Papers presented at the Third Working Meeting on Gallium Arsenide Solar Cells at Langley Research Center, September 25-26, 1975.

16. Abstract

Research results are reported for GaAs Schottky barrier solar cells, GaAlAs/GaAs heteroface solar cells, and GaAlAs/GaAs graded band gap solar cells. Related materials studies are presented. A systems study for GaAs and Si solar concentrator systems is presented.

17. Key Words (Suggested by Author(s))
Solar Cells
Gallium Arsenide
Schottky Barriers
Energy Conversion

18. Distribution Statement
Unclassified
Unlimited

19. Security Classif. (of this report)	20. Security Classif. (of this page)	21.
Unclassified	Unclassified	

For sale by the National Technical Information Service, Springfield, Virginia 22161

Foreward

Figures in this document were used as provided by the authors with no attempt to improve the quality.

Table of Contents

Introduction to the Third Working Meeting on

Gallium Arsenide Solar Cells

September 25-26, 1975

In the early to mid 1960's the U.S. Air Force contracted with RCA to develop gallium arsenide (GaAs) solar cells. The program terminated in 1965 with 7% efficient cells made by silicon-solar-cell-like technology. In 1969, the Electronic Materials Working Group of OART reviewed this area and recommended that NASA initiate a GaAs solar cell development program using the improved technologies developed specifically for GaAs. In the spring of 1971, Langley took over management of a grant from OART and began the first Langley program on GaAs solar cells.

This was the third GaAs Solar Cell Meeting. The first meeting, October 1972, resulted in a decision to reduce research on diffused cells and activate plans to make two-layer cells. The second meeting, February 1974, highlighted substantial efficiency gains for GaAs cells and demonstrated the need for improved GaAs material to achieve higher efficiency solar cells.

This third meeting emphasized (a) efficiency over 14%, (b) initial results on cells with the improved GaAs, and (c) new thrusts in the program. Dramatic new thrusts were a cell with a built-in field for high collection efficiency (not reported) and a systems study on GaAs cells with solar concentrators for terrestrial application.

Three other NASA solar cell programs were presented: (1) Dr. James Hutchby of Langley discussed his graded bandgap GaAlAs cell; (2) Dr. Richard Stirn, JPL, presented his recent advances with Schottky barrier GaAs cells; and (3) Dr. Mike Godlewski from Lewis Research Center presented a brief overview of his center's silicon solar cell research. This document contains the summaries of the papers presented.

CURRENT STATUS OF SILICON SOLAR CELL TECHNOLOGY

Henry W. Brandhorst, Jr.

NASA-Lewis Research Center

Cleveland, Ohio

E-8534

ABSTRACT

In quest of higher efficiency, major progress has occurred in solar cell technology during the last five years. In this period cell efficiency has climbed about 50 percent. Technical approaches leading to increased output include back surface fields (n^+-p-p^+ structures), shallow junctions, improved antireflection coatings, surface texturizing, and fine grid patterns on the cell surface. The status of current solar cell technology and its incorporation into cell production is discussed.

Research and development leading to improved performance and reduced cost are also described.

INTRODUCTION

During the last five years, the efficiency of silicon solar cells has increased dramatically. In 1970, the average outer space efficiency of silicon solar cells was 10.5%. In 1975, laboratory cells have reached efficiencies above 15% and production cells are in the 13% range. Most of the increased output has resulted from increased short-circuit current, with only minor increases in voltage being reported. It is appropriate to review the past accomplishments so that the future potential of the cell and the pertinent research problems can be clearly defined.

STATE OF PRESENT TECHNOLOGY

Short-Circuit Current

Short-circuit current can be increased in two ways. First, the amount of light entering the cell can be increased by reducing the surface area covered by the grid pattern and by reducing the reflectivity of the surface.

Grid Pattern: In 1970, the standard grid pattern on a 2x2 cm cell covered about 10% of the cell surface. By use of improved metal masks or photoresist technology, average coverage is now in the 5-7% range.

Antireflection Coatings: The conventional antireflection coating in 1970 was a quarter wavelength coating of SiO. However, when the cells were covered with adhesive and a coverslip, a loss in current of about 3% was obtained. Reoptimization of the antireflection coating to account for the cover glass required coatings with a higher refractive index such as TiO_x, Ta_2O_5 and Nb_2O_5. As shown in Table I, the use of these coatings led to an increase in current of about 5% on covering and an advantage over a glassed SiO cell of about 7%.

Texturizing: The most important advance in increasing the amount of light entering the cell came through surface texturizing. The use of the basis chemical etches such as KOH, NaOH or hydrazine in 100 silicon surfaces results in surfaces covered with a myriad of pyramids as shown in figure 1. This surface yields two benefits. One benefit arises from multiple reflections experienced by the incoming beam as shown in figure 2. This reduces bare surface reflectivity from 33% to about 11%. Addition of a Ta_2O_5 antireflection coating and a cover glass leads to a reflectivity of only 3% compared to about 10% average reflectivity for a smooth cell coated with SiO.

The second benefit arises because light is refracted as it enters the silicon and travels obliquely through the cell. Collection efficiency increases because light is absorbed closer to the junction. Also more infrared light is absorbed because the path length is greater than the silicon thickness and because the light is totally internally reflected from the smooth back surface. These factors also increase cell current.

Shallow Junctions: To reduce the effects of poor collection efficiency in the diffused region (due to anomalous phosphorus diffusion profiles and low lifetimes), shallow junctions have been used. Sheet resistances in the 150 to 500 Ω/□ range resulting from phosphorus diffusion in the 800° C temperature range yield junction depths on the order of 0.1 μm. These have led to substantial increases in the blue region of the cell spectral response.

Increased Minority Carrier Lifetime: The minority carrier lifetime measured in n$^+$-p solar cells ranges from 6 to 10 microseconds. Studies have shown that the front and back surface recombination velocities and the wafer thickness significantly influence the measured lifetime. For example, a

300 μm thick cell has an 8 μsec lifetime while a 100 μm thick n^+-p cell has a lifetime of only about 1 μsec. Use of a back surface p^+ field (n^+-p-p^+ structure) yields an essentially zero surface recombination velocity plane. Accordingly, the lifetime increases to about 30 μsec in 300 μm thick devices. This increase in lifetime yields an increase in short-circuit current of only a few percent but leads to a more important effect on cell open-circuit voltage.

Open-Circuit Voltage: Efforts to increase the voltage have explored several areas. The inclusion of a back surface field in 10 Ω-cm cells produced an increase of about 50 mV in open-circuit voltage. However, almost no effect was observed for 1 Ω-cm material. It is believed now that the increased voltage results from the presence of the near zero surface recombination velocity p^+-p low-high junction coupled with the increased lifetime noted above.

Device Performance and Production Status

Increased device performance results from inclusion of the above technologies into the cell. However, transition from the laboratory to cost effective production is difficult and represents a significant barrier to rapid introduction of new, marketable solar cell devices. Table II summarizes the technologies used and the production status of current improved efficiency cells. Table III compares the performance of the 1970 cell with selected new technology cells, all with cover glasses. The 13% efficient Helios cell is in high volume production at Spectrolab. The violet cell nearing production by OCLI, was not included in Table III since it has the same features of the Helios cell but with a slightly higher voltage which leads to a 13.5% efficiency. The highest performance, 15.3%, is achieved by the CNR cell. This cell remains in laboratory production at the COMSAT laboratory.

From Table III it is clear that most of the improved output comes from increased short-circuit current. The increased voltage comes from use of the p^+ back surface field and lower resistivity material. Improved fill factor is the result of both improved grid geometry and junction processing procedures. A comparison of the spectral response of a CNR cell and a 1970 cell is shown in figure 3. The CNR cell has a quantum yield (electrons collected per incident photon) above 90% over most of the response region. Thus it appears that little further improvement in short-circuit current can be anticipated in the future.

FUTURE RESEARCH AND TECHNOLOGY TRENDS

Although developments to date have been significant and exciting, additional research and development opportunities exist. Efficiency increases can be expected and cost reductions by orders of magnitude can be predicted. Basic research and high technology will both play a significant role.

Open-Circuit Voltage

The last substantial barrier to achieving the maximum practical efficiency of about 19% is the open-circuit voltage. Although simple diode theory predicts an increasing voltage with decreasing resistivity, contrary results are obtained experimentally as shown in figure 4. The highest voltage reported for 0.1 Ω-cm material is 0.61 V instead of the 0.7 V calculated. Also the base region minority carrier lifetimes in the 0.1 and 0.01 Ω-cm cells are sufficiently great so as to yield much larger open-circuit voltages. Thus it appears that a low emitter efficiency of the diffused region is the cause of poor voltages. Several effects may act to reduce the voltage. These include band gap narrowing, increased interband transition rates and defect clustering. These mechanisms also influence bipolar transistor current gain and frequency response and hence are an area that should receive great attention. The kinship between solar cells and transistors is rather close at this time.

Technological approaches aimed at increasing cell voltage have examined alternate dopants, ion implantation and epitaxial structures. Of these, epitaxy seems to offer the most advantage at this time. By use of heavily doped substrates, and doping gradients within both the base and the emitter region, open-circuit voltages above 630 mV have been achieved. While this gain is modest, it may be the harbinger of things to come.

Short-Circuit Current

The one remaining research area related to current is determination and reduction of cell surface recombination velocity. Preliminary measurements of the surface recombination velocity on diffused solar cell surfaces yield values between 5 and 10×10^3 cm/sec, which is much lower than had previously been estimated. However, reduction to a value below 10^3 cm/sec is required before full short-circuit current can be achieved.

Wrapping the front contact around to the back of the cell eases interconnection of cells and may increase cell current and power by reducing front surface blockage. Simply wrapping the diffused junction around the cell edge has resulted in unacceptable leakage currents. Development of wrap-around contacts for high efficiency cells warrants further study.

Low Cost Technology

The final barrier to widespread use of solar cells is cost. The ERDA National Photovoltaic Program is clearly focussed on this target. Both automated, high rate cell production and new technologies will be required to meet stringent cost requirements. Table IV summarizes some of the low cost, non-vacuum technologies that are currently being investigated for automated production. Cell costs have been reduced from $80/watt for space cells to under $10/watt for present terrestrial cells. The use of large circular wafers up to 10 cm

diameter have aided this reduction. Automation is expected to reduce cell costs to $2/watt in the next few years. Additional major technological advances to reduce the cost of polycrystalline silicon and development of low cost single crystal silicon ribbon growth or wafer preparation together with further gains through automation are expected to yield 10-50¢/watt arrays by 1985.

SUMMARY

The progress made in improvement of the silicon solar cell has yielded a 50% increase in cell efficiency in the last five years. Current laboratory cells have reached an efficiency above 15% and continuing efforts are aiming at the 19% practical limit. The future holds research and development opportunities aimed at increased cell performance and ultra low cost production methods.

TABLE II-1 EFFECT OF COVER GLASSING ON SHORT-CIRCUIT CURRENT OF SOLAR CELLS

	SHORT-CIRCUIT CURRENT	
	SiO	Ta_2O_5
COATED CELL ONLY	142 mA	140 mA
COATED CELL WITH COVER GLASS AND ADHESIVE	138 mA	147 mA

TABLE II-2 SUMMARY OF PRESENT HIGH EFFICIENCY SOLAR CELLS

DESCRIPTION	STATUS
HELIOS CELL	
20 Ω-CM P^+ BACK SHALLOW JUNCTION THIN GRID FINGERS Ta_2O_5 AR COATING	IN PRODUCTION BY SPECTROLAB
VIOLET CELL	
2 Ω-CM P^+ BACK VERY SHALLOW JUNCTION FINE GRID FINGERS Ta_2O_5 AR COATING	NEARING PRODUCTION BY OCLI
COMSAT NON-REFLECTIVE CELL	
ETCHED, LOW REFLECTION SURFACE OTHERWISE LIKE VIOLET CELL	LABORATORY, NOT OPTIMIZED COMSAT CORP.

TABLE II-3 - PERFORMANCE COMPARISON OF SILICON SOLAR CELLS

	1970 PRODUCTION CELL	HELIOS CELL	CNR CELL
SHORT CIRCUIT CURRENT, I_{sc}	138 mA	157 mA	181 mA
OPEN-CIRCUIT VOLTAGE, V_{oc}	545 mV	585 mV	595 mV
MAXIMUM POWER, P_{max}	55 mW	70 mW	83 mW
FILL FACTOR*, FF	73%	76%	77%
EFFICIENCY (AMO), η	10.2%	13%	15.3%

$$*FF = \frac{P_{max}}{V_{oc} I_{sc}} \times 100$$

TABLE II-4 - NEAR TERM SOLAR CELL COST REDUCTION APPROACHES

IMPROVE MATERIALS UTILIZATION

- USE LARGER DIAMETER SINGLE CRYSTAL INGOTS
- REDUCE SAWING LOSSES
  - USE ROUND CELLS
  - REDUCE KERF LOSS

AUTOMATE CELL MANUFACTURING PROCESSES

- ELIMINATE VACUUM PROCESSES
  - USE SCREEN PRINTING FOR CONTACTS
  - USE "SPIN ON" TECHNIQUES FOR ANTIREFLECTION COATINGS
- ELIMINATE GASEOUS DOPANT SOURCES
  - USE "SPIN ON" TECHNIQUES
  - USE ION IMPLANTATION

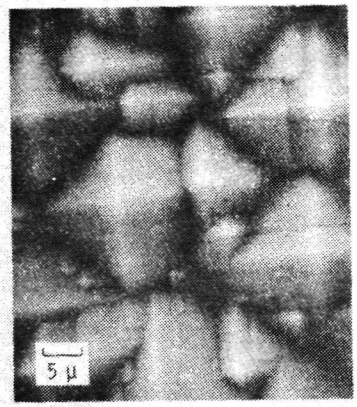

PERPENDICULAR TO SAMPLE

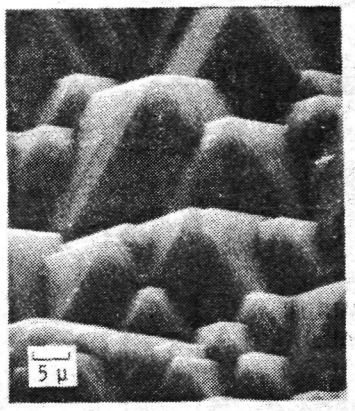

45° OBLIQUE VIEW

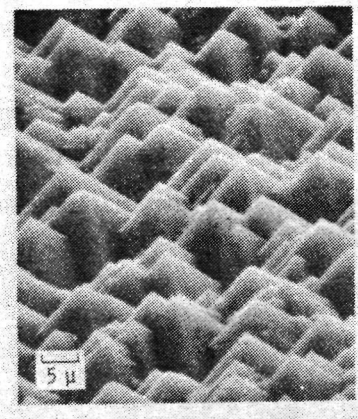

45° OBLIQUE VIEW ROTATED 70°

CS-73708

Figure II-1. - Views of texturized surface.

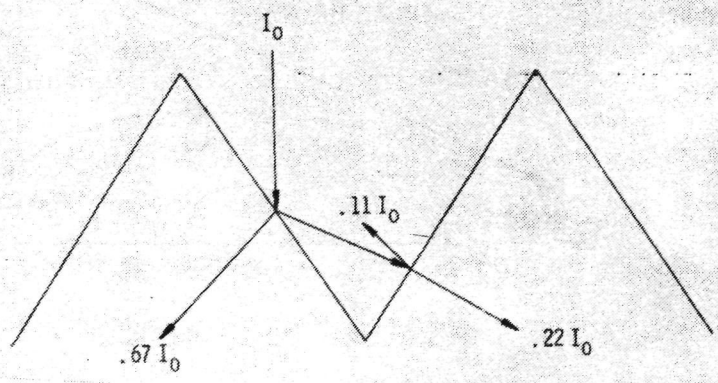

Figure II-2. - Optical path diagram of tetrahedral texturized surface.

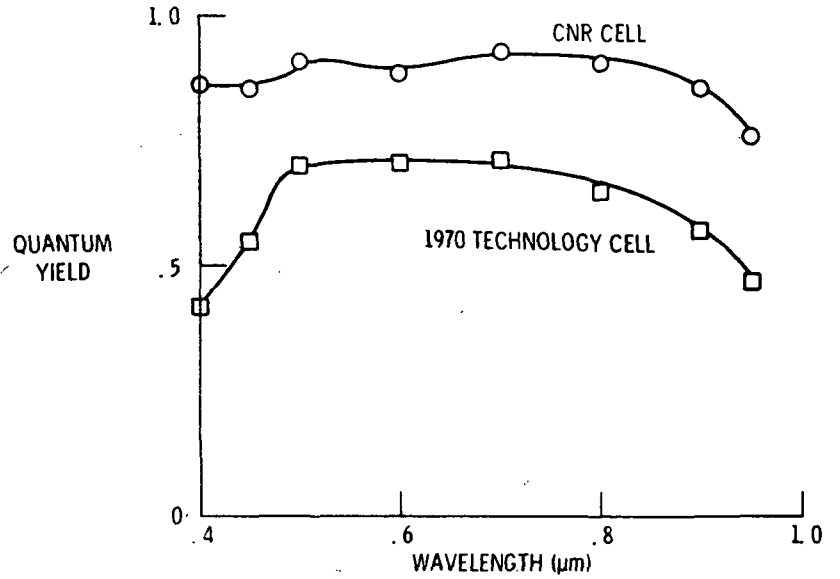

Figure II-3. - Quantum yield comparison of solar cells.

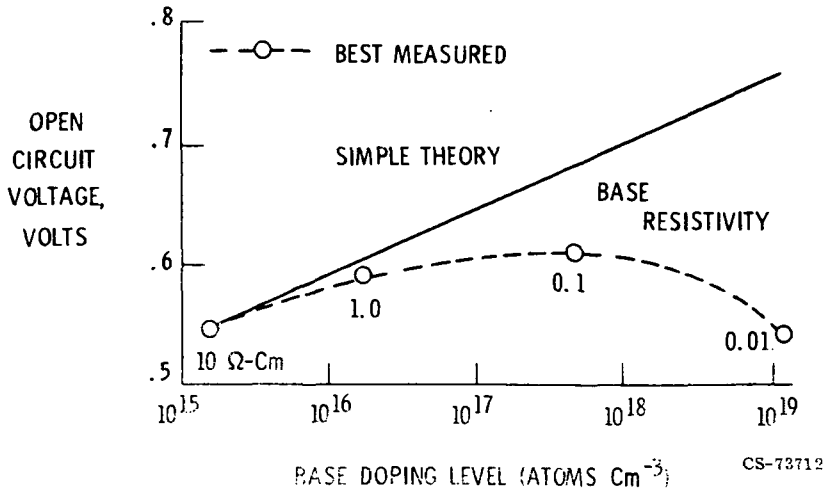

Figure II-4. - Dependence of solar cell open circuit voltage on doping level.

THE IBM PROGRAM ON GaAs SOLAR CELLS

H. J. Hovel, J. Woodall

The program at IBM consists basically of 4 parts:

1) materials studies,

2) optimization of the "basic structure" for operation at AMO,

3) the investigation of exploratory structure,

4) a study of temperature effects on GaAs cells (Figure 1).

The materials studies are centered around the growth of very thin, sub-micron GaAlAs layers of high Al content and methods of contacting the resulting solar cell structure (Figure 2) that result in low contact resistances. The advantages of thin GaAlAs layers can be seen in Figures 3 to 6, where theoretical calculations of the spectral response, photocurrent, and AMO efficiency are shown for the "basic structure" (p-p-n). Figure 3 shows the spectral response for various GaAlAs thicknesses (86% Al). The response to high energy photons is strongly enhanced for thicknesses below 1 μm. The experimental results shown in Figure 4 agree well with the computed ones. The computed short circuit currents at AMO are shown in Figure 5. The top line represents the photocurrent that would be obtained from highly perfect conditions: $S_{top} = 10^5$ cm/sec, $S_{interface} = 4 \times 10^3$ cm/sec, $\chi_j = 0.8\mu$, $L_{GaAlAs} = 0.81\mu$, $L_{pGaAs} = 4.5\mu$, $L_{nGaAs} = 3\mu$. The second line is for more "typical" device parameters: $S_{top} = 10^6$, $S_{int} = 10^4$, $\chi_j = 0.8\mu$, $L_{GaAlAs} = 0.27\mu$, $L_{pGaAs} = 1.8\mu$, $L_{nGaAs} = 1.96\mu$, where S denotes recombination velocity and L denotes diffusion length. The AMO efficiencies in the two cases are shown in Figure 6. Values of 15% should be obtainable for GaAlAs thicknesses above 2μ, and considerably better

efficiencies could be obtained with sub-micron thick layers. "Limit" efficiencies are several points higher. (It should be emphasized that these are idealized values; contact area masking would reduce these by around 0.95, and reflection by 0.97.)

A table of measured values for various devices is given as Figure 7. Open circuit voltages are generally in the 0.95-0.99 volt range at 20°C; lower values are obtained when "poor quality" substrates are used. Short circuit currents (corrected for contact area) are usually about 22-23 mA/cm^2, slightly lower than expected. Most of the devices have been 12% efficient or over (contact area corrected) with several units over 13%. The efficiencies are much less dependent on junction depth than originally expected, which is a confirmation that the interface recombination velocity in the devices is negligible and that the electron diffusion length in the pGaAs is well in excess of 4μ.

The small dependence of photocurrent and efficiency on junction depth led to research on the first of the two exploratory structures, Figure 8. It should be possible to overcome the common problem of poor quality substrates by fabricating deep junction devices where all of the relevant light is absorbed in the pGaAs and a poor lifetime in the base would not affect the photocurrent. This can only be successful if the diffusion length in the pGaAs considerably exceeds the junction depth. The wide pGaAs region can be produced by epitaxial growth, such as a Ge doped epitaxial layer, or by allowing the Zn to diffuse in farther than usual. The deep Zn diffusion method has proven successful by the additional step of "leaching" the device in the Ga melt so that fast-diffusing lifetime killers such as Cu can be removed from the sample into the Ga. Figure 9 shows calculated

spectral responses for a p-p-n cell with a hole diffusion length of 0.35μ and various electron diffusion lengths in the pGaAs. The measured response for the leached cell SCB62 is also shown, indicating a L_n of over 4μ even though the measured starting L_p was 0.35μ . This cell was over 14% AMO efficient (contact area corrected). Figure 10 shows the calculated efficiencies for deep junction cells and how they compare with the previous values. The slightly lower efficiencies are due to the higher expected dark currents in the poor substrate devices.

Figure 10 also shows the calculated efficiencies versus junction depth for the second type of exploratory structure depicted in Figure 8, a very shallow junction device. Figure 11 shows the spectral responses of such cells compared to various GaAlAs-GaAs structures. The GaAlAs devices are superior to the straight GaAs junction under almost any conditions at low and intermediate photon energies, while the GaAs junction has an advantage at high energies. The AMO efficiencies (Fig. 10) are several points lower. The only reason for pursuing this structure therefore is an economic one, and it has a low priority in IBM's program compared to the other structures.

The final phase of the program involves temperature studies on GaAlAs-GaAs p-p-n cells. Figure 12 shows how the absorption coefficient of GaAs varies with temperature. The shift to lower photon energies should considerably enhance the photocurrent. The effect of the absorption coefficient on the calculated spectral response is given in Figure 13a, and the additional effect of the expected diffusion length dependence on temperature is shown in Figure 13b. The GaAlAs structure is an excellent tool for studying diffusion length-temperature behavior because of the absence of surface

recombination complications. Figure 14 shows how the base diffusion length can be studied using a shallow junction device, where the response is derived entirely from the base. Figure 15 shows how the electron diffusion length in the pGaAs can be studied using a deep junction device where none of the response is derived from the base. The measured spectral responses of a deep junction device are shown in Figure 16, and the best fit calculated responses are given in Figure 17. A considerable improvement in diffusion length with increasing temperature is indicated, as suggested earlier by Vilms and Spicer (J. Appl. Phys. 36, 2815 (1965)). The measured diffusion lengths in several devices are given in Figure 18, along with the Vilms and Spicer data. The improvement with temperature should translate into higher photocurrents with increasing temperature.

The calculated photocurrent as a function of temperature for several conditions are shown in Figure 19. If the shift in absorption edge alone were acting, a concave-upward increase is predicted. If the diffusion length improvement alone were involved, a concave-downward, saturating result is predicted, as expected. When both variations are taken into account, a linear improvement with temperature is predicted. Linear changes of photocurrent with temperature are almost always observed experimentally, although the measured values are affected more strongly by temperature than predicted, partly due to excess infra-red radiation in the Xenon solar simulator but possibly due to other improvements in the collection efficiency presently unaccounted for.

Figure 20 shows the open circuit voltage, short circuit current, and the contact area corrected and uncorrected efficiencies of one device as a

function of temperature using a Xe light source. The efficiency varies slowly with temperature up to about 100°C and more rapidly thereafter. Corrected values (obtainable in practice after better contact grids are employed) of 9% at 250°C and 6% at 300°C are indicated. Devices with shallower junctions and made from "good" substrates have given similar values.

I B M GaAs SOLAR CELL PROGRAM

1. Basic Structure Optimization, AMO
2. Exploratory Structures
3. Temperature Effects
4. Materials Studies

III-1

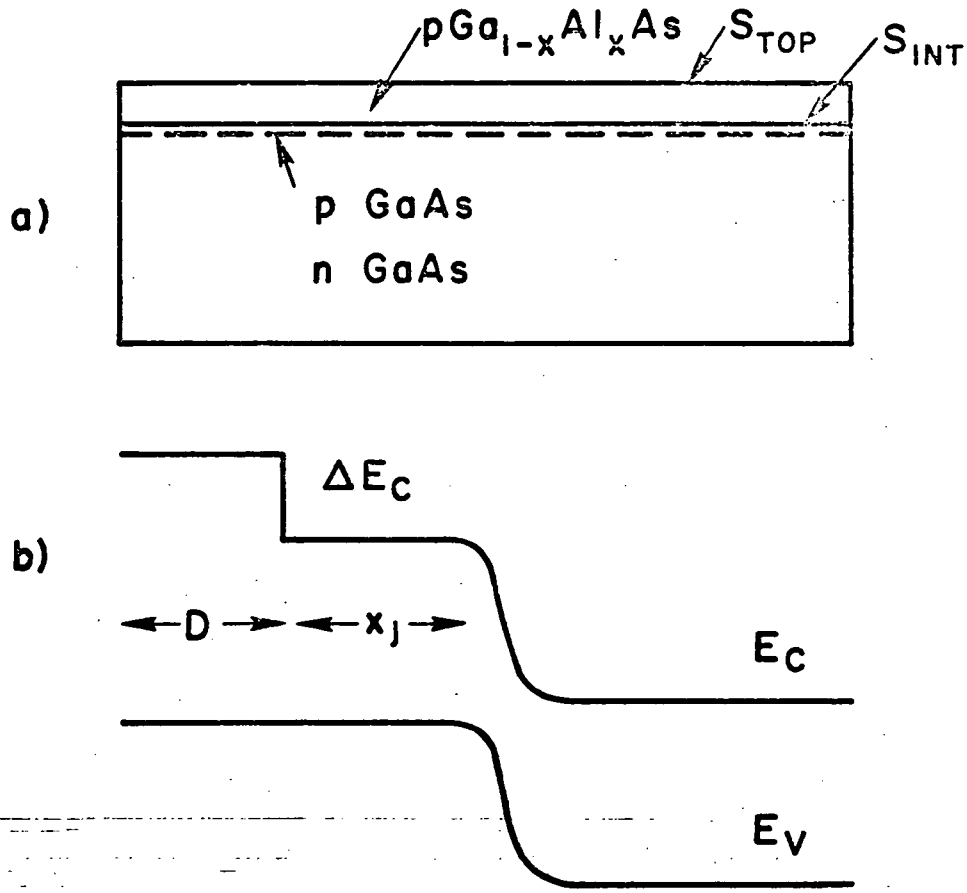

III-2

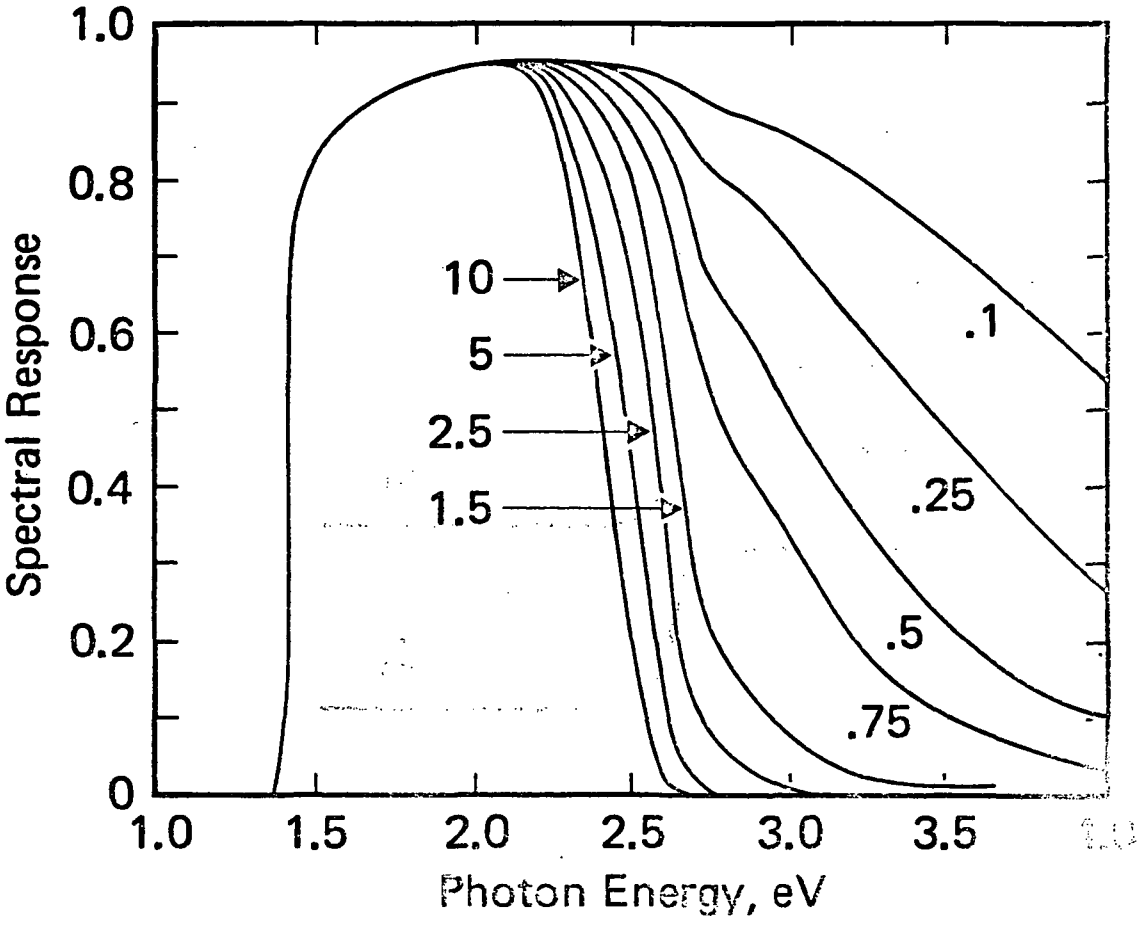

III-3 Spectral responses for decreasing GaAlAs thickness, parameters of Table 1.

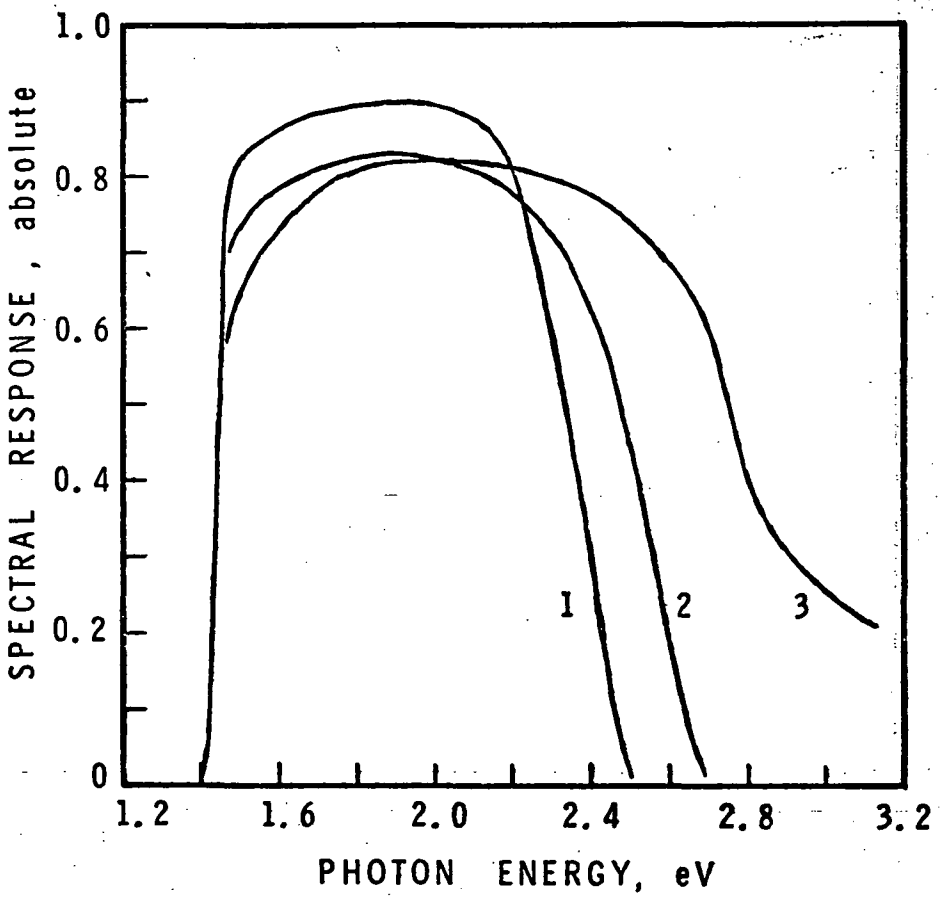

III-4 Measured spectral responses. 1: x_j=0.8u, D=5.5u ; 2: x_j=1.1u, D=1.8u ; 3: x_j=1.1u, D=0.6u.

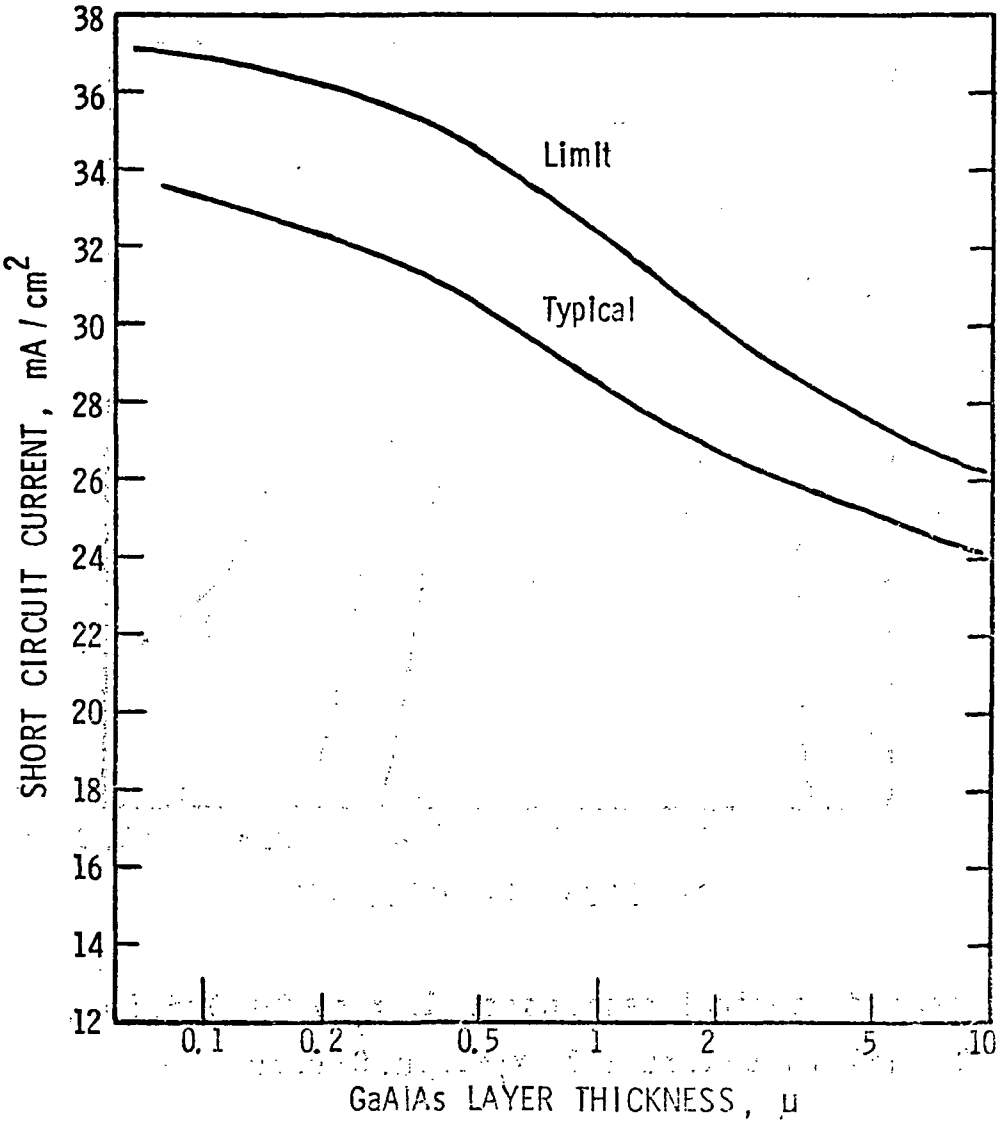

III-5 Short Circuit Currents of 2 Types of GaAs Solar Cells, AM0

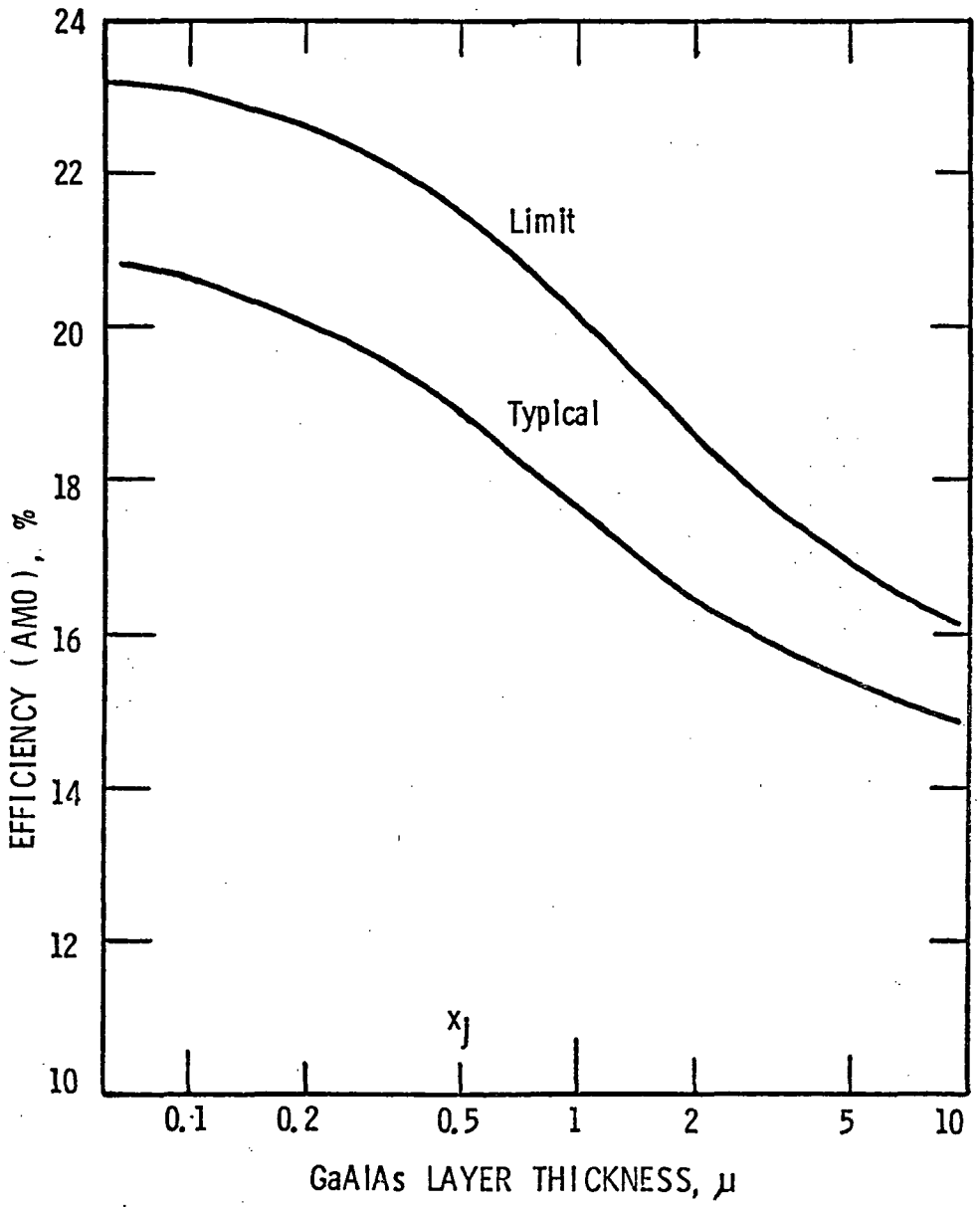

III-6 Efficiencies of 2 Types of GaAs Solar Cells, AM0

DEVICE	D	x_j	V_{oc}	FF	n	Subs.
288	14	0.8	.960	.812	11.9	good
287	5.5	0.8	.950	.779	12.2	good
449	5.5	0.8	.955	.800	11.8	poor
scb46	0.6	1.1	.953	.744	12.5	poor
scb15	1.8	1.1	.960	.788	11.9	poor
scb16	1.8	1.4	.958	.751	10.5	poor
452-3	2-4	1.8	.962	.752	12.6	poor
453-3	2-4	1.8	.955	.774	12.0	poor
454-3	2-4	1.8	.962	.772	13.4	poor
289	16	2.7	.970	.743	11.3	good
335-2	11	2.8	.946	.796	12.2	good
323	2-4	2.8	.956	.785	12.3	good
scb64	0.6	3.0	.909	.682	10.2	poor
scb62	0.6	3.0	.980	.802	14.5	poor, leach
298	11	3.5	.980	.807	12.1	good

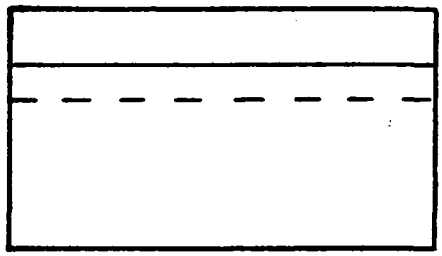

pGaAlAs
pGaAs
nGaAs

BASIC
STRUCTURE

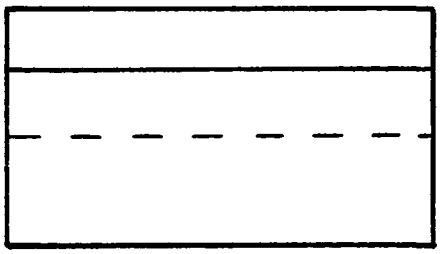

pGaAlAs
pGaAs
nGaAs

DEEP
JUNCTION

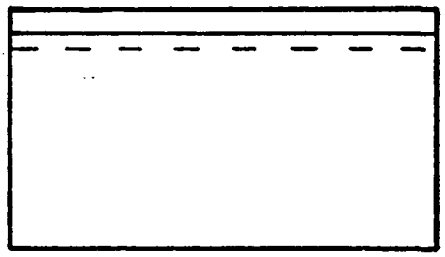

nIn_2O_3
n, p GaAs
p, n GaAs

SHALLOW
JUNCTION

III-8

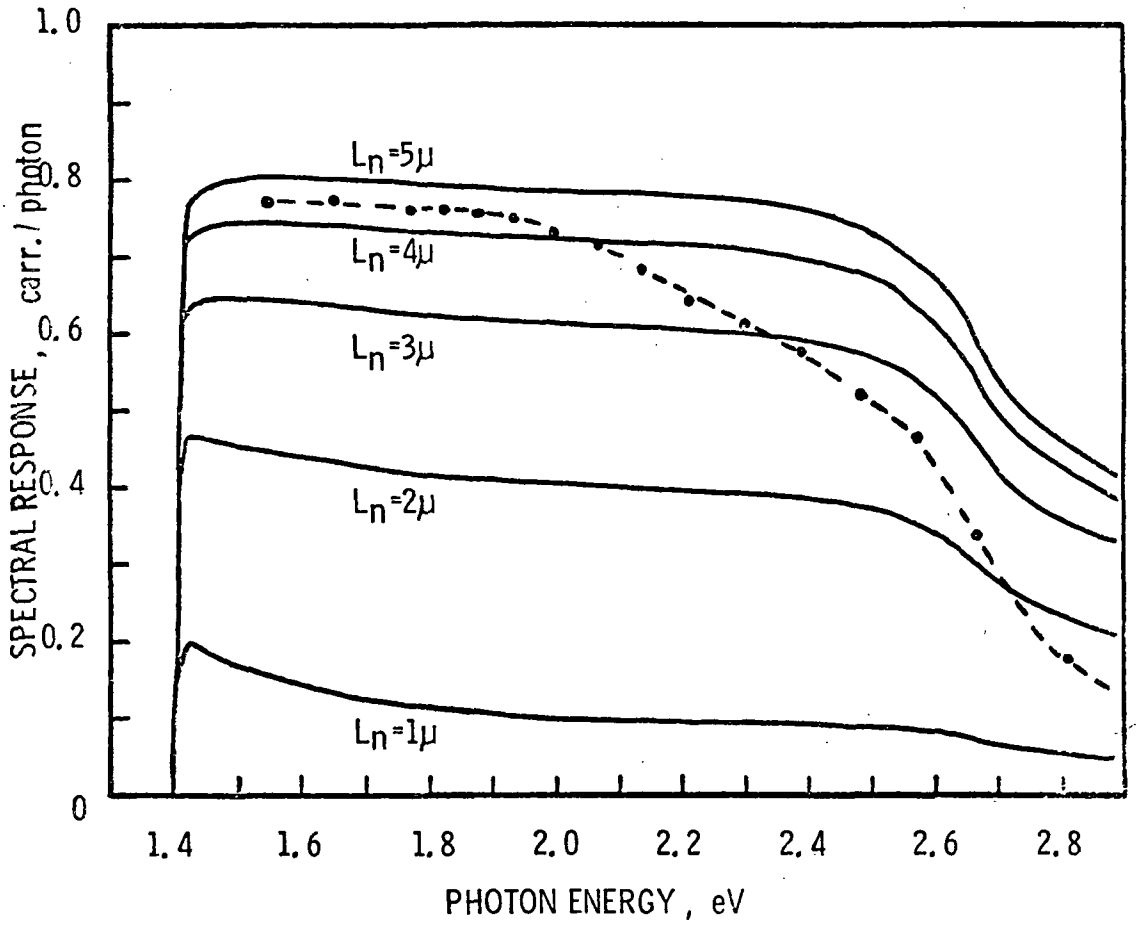

III-9 Spectral Responses For Poor Quality Substrates

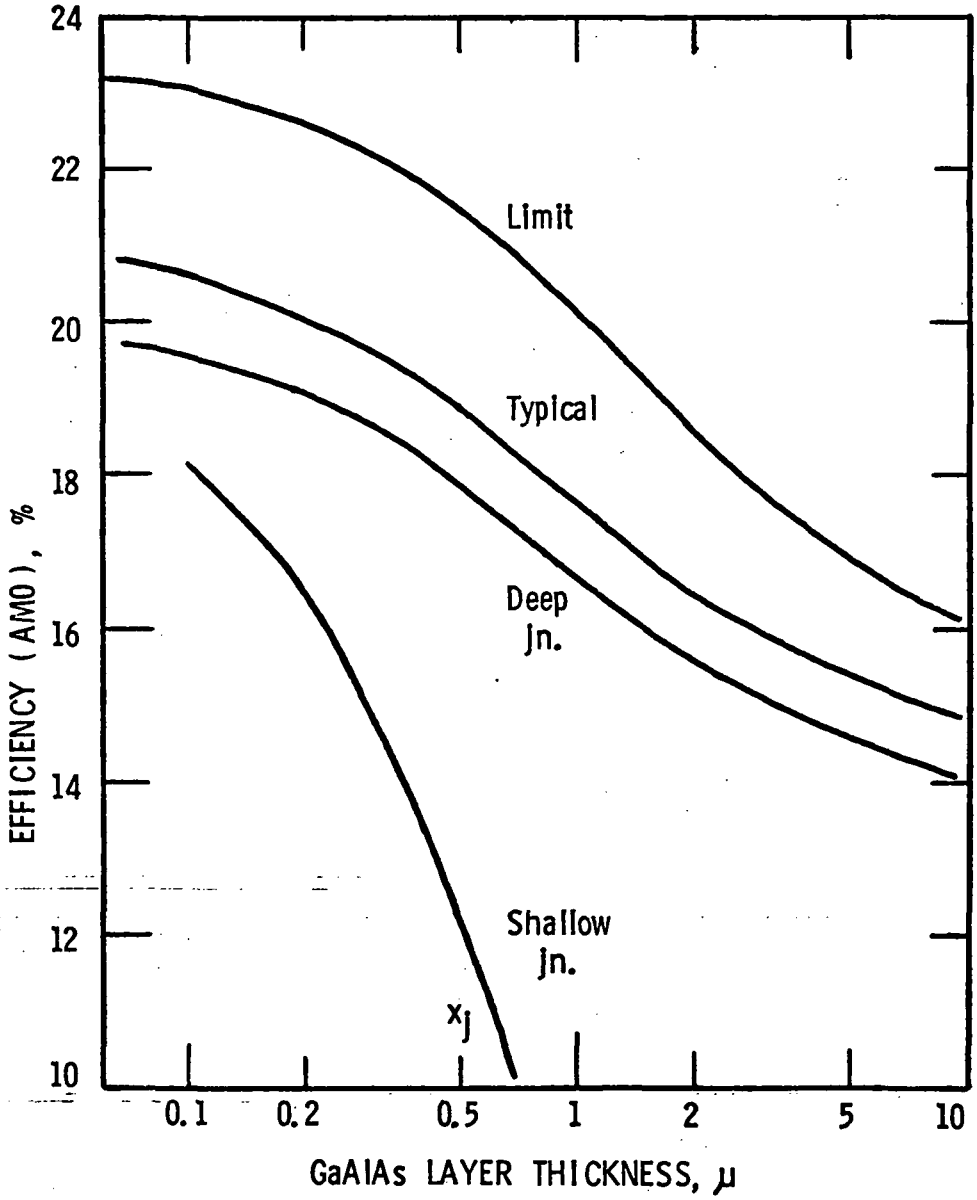

III-10 Efficiencies of 4 Types of GaAs Solar Cells, AMO

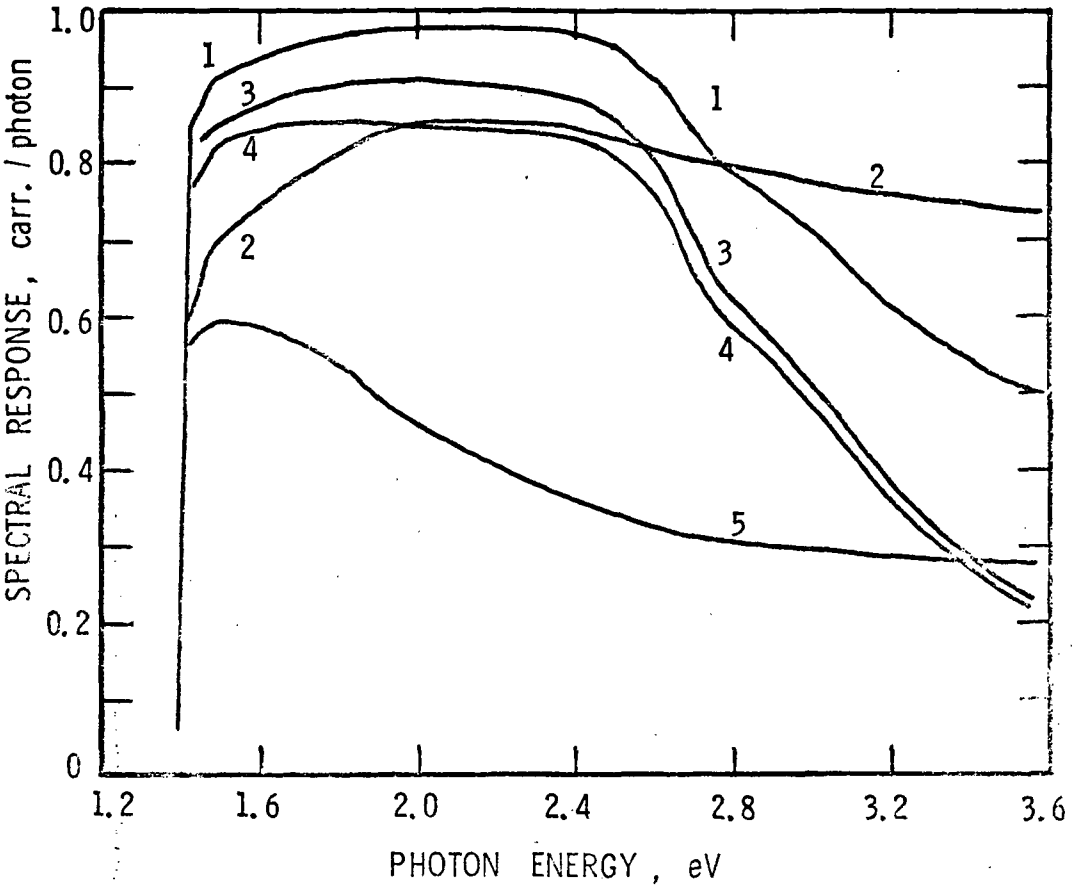

III-11 Spectral Responses of GaAs Solar Cells. 1: GaAlAs, Limit. 2: GaAs, $x_j = 0.15\mu$. 3: GaAlAs, Typical. 4: GaAlAs, Deep Junction. 5: GaAs, $x_j = 0.75\mu$.

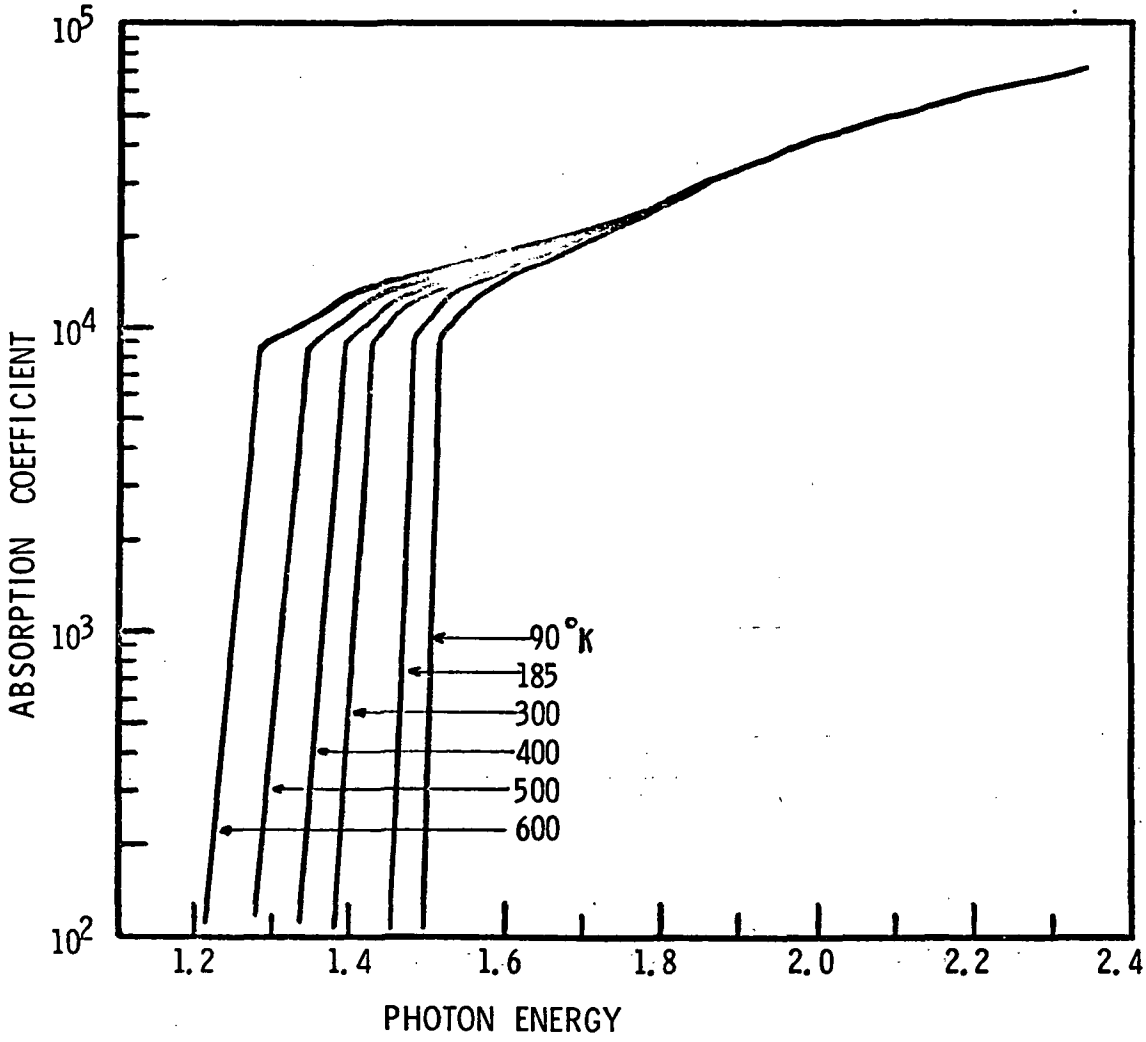

III-12 ABSORPTION COEFFICIENT OF GaAs versus TEMPERATURE

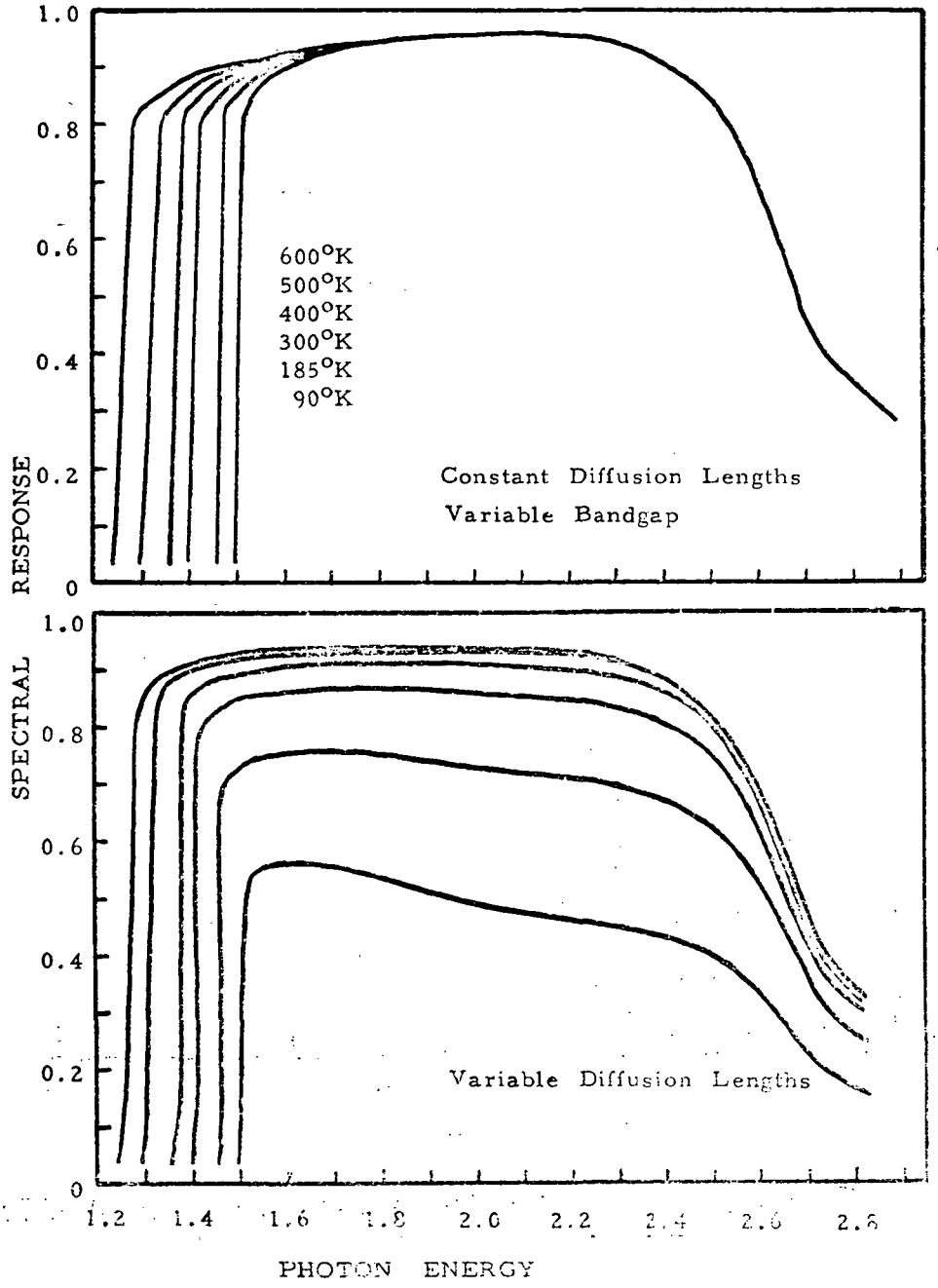

III-13 Calculated spectral responses for two conditions

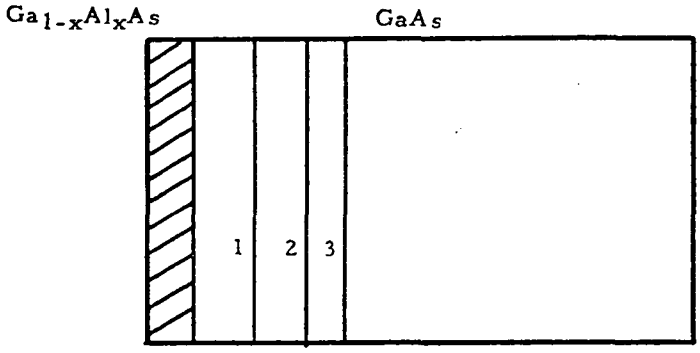

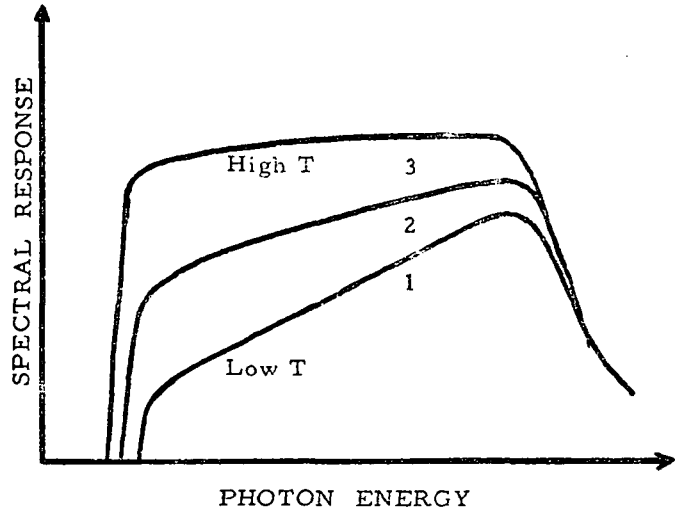

III-14 DEVICES WITH SHALLOW JUNCTIONS

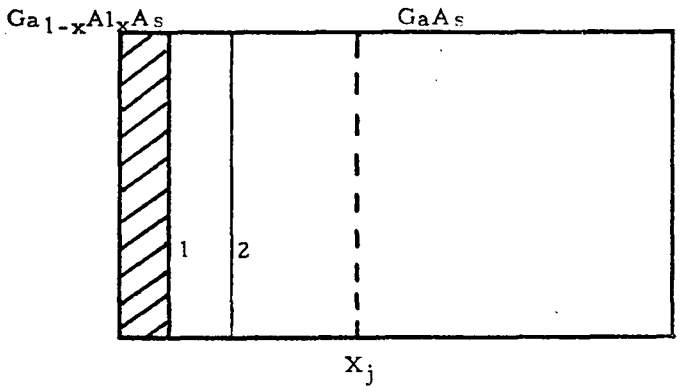

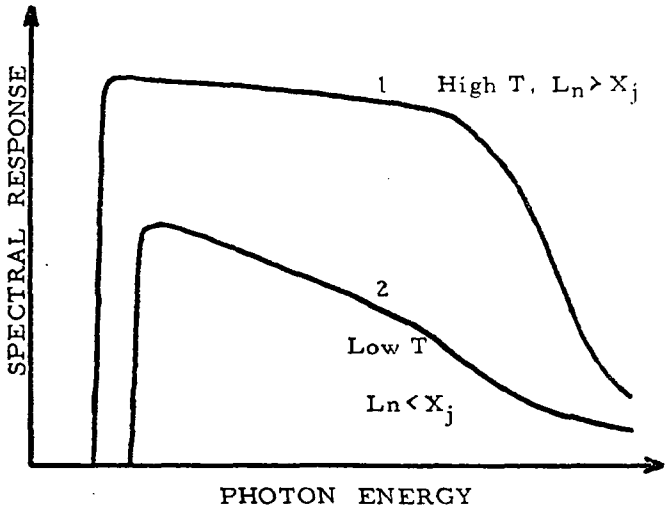

III-15 DEVICES WITH DEEP JUNCTIONS

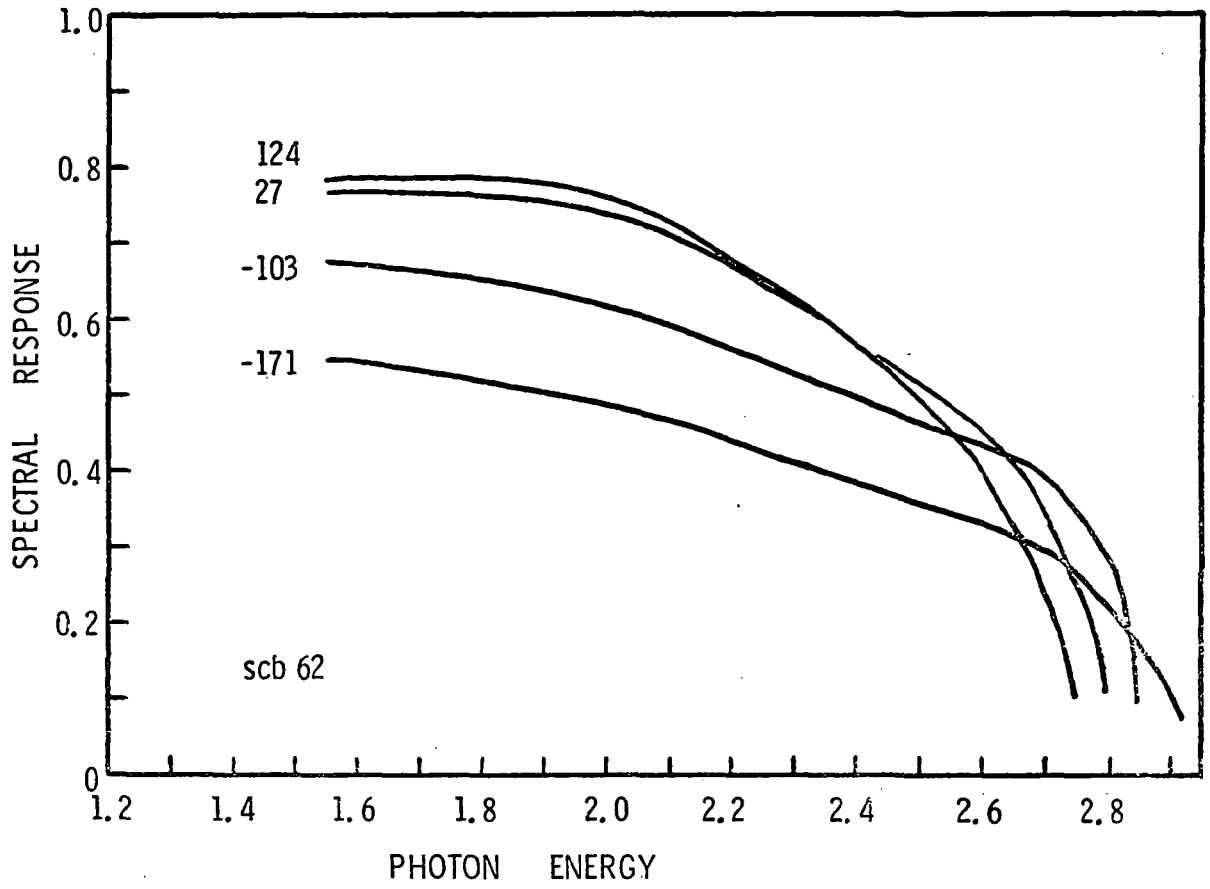

III-16 MEASURED RESPONSES OF A CELL WITH A 3μ JUNCTION

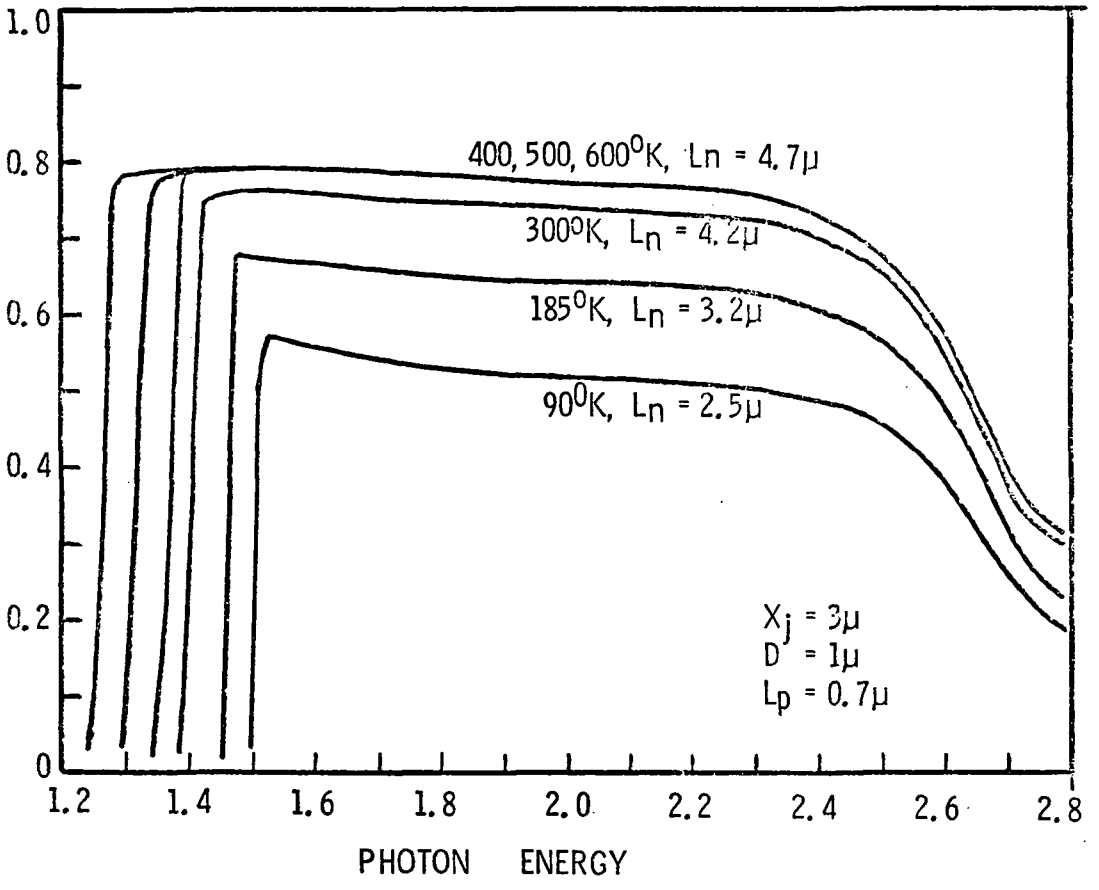

III-17 CALCULATED RESPONSES, DEEP JUNCTIONS

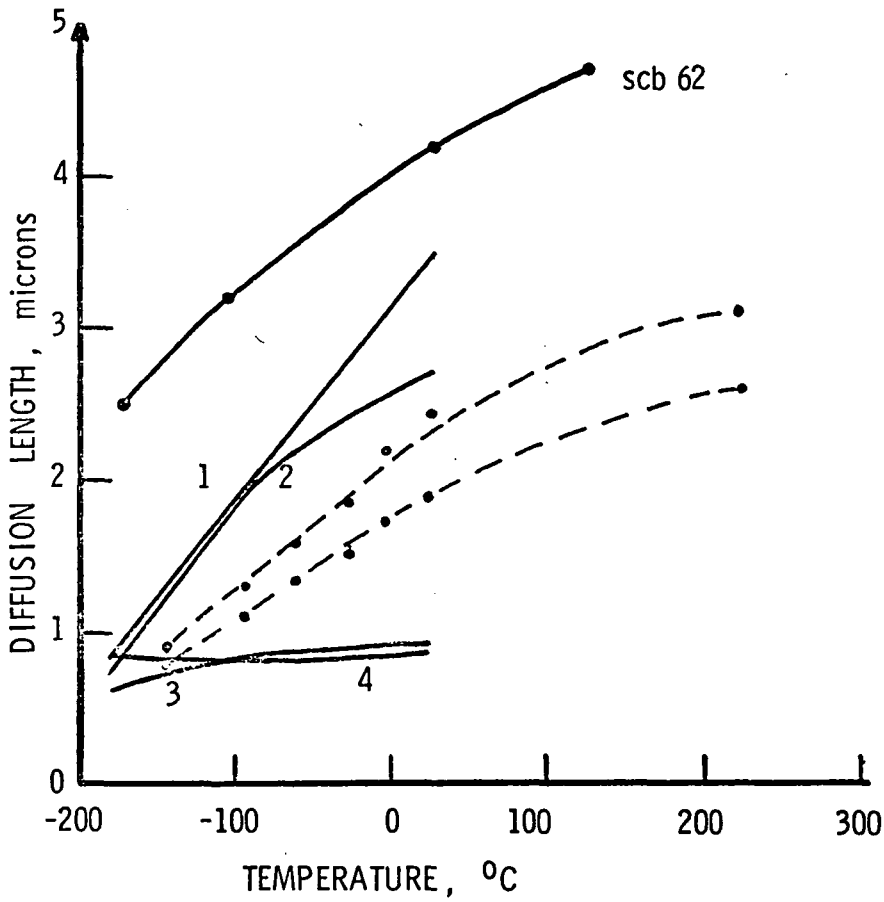

1. L_n. $N_a = 6 \times 10^{17}$
2. L_n. $N_a = 2 \times 10^{18}$ ref. 5
3. L_n. $N_a = 1 \times 10^{18}$

4. L_p. $N_d = 2 \times 10^{18}$ ref. 7

III-18 Diffusion length versus temperature.

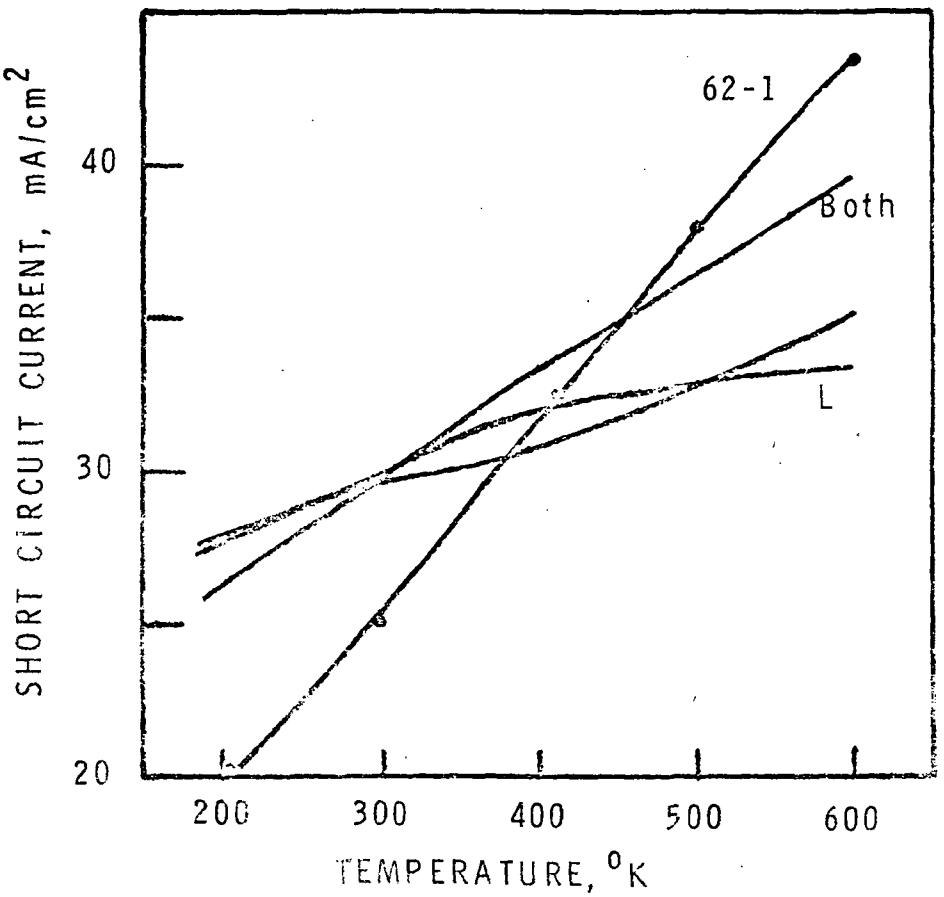

FII-19 Variation in J_{sc} at AM0 for: 1) variable, 2) L variable, 3) both variable. Exper. result also shown. GaAs parameters constant in all cases.

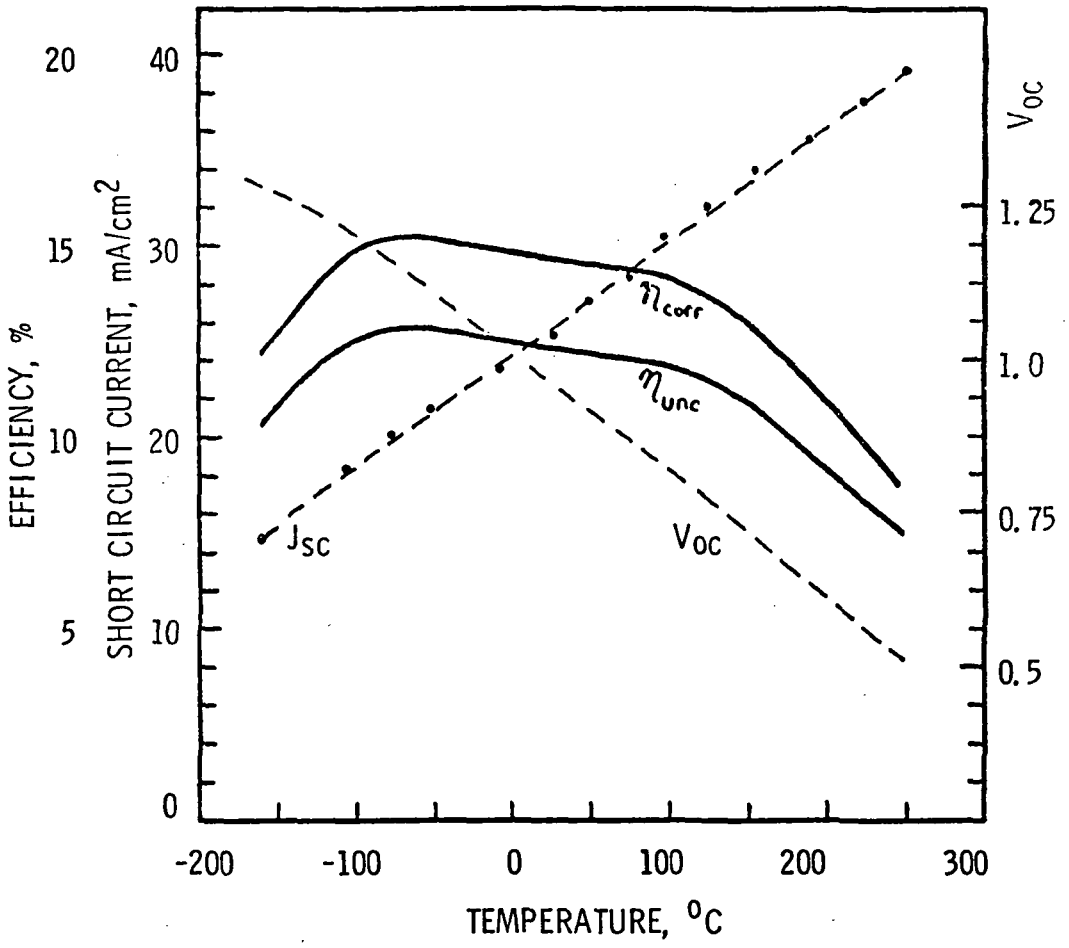

III-20 Open circuit voltage, short circuit current, and efficiency under Xenon light (135 mW/cm^2).

CARNEGIE-MELLON PROGRAM

ON

GaAlAs-GaAs SOLAR CELLS

D. L. Feucht and A. G. Milnes

The work at Carnegie-Mellon University has been concerned with investigation of large area (1x2 cm) aluminum gallium arsenide heteroface solar cells. Three aspects of the work are discussed in this summary. First the growth procedures and the problems in the resulting growths, second, lifetime measurements from various manufacturers and processes and third, nonuniformity in cell properties over the 1x2 cm areas.

Fig. 1 shows the general structure of the cell. Two different growth procedures have been used as outlined in Figs. 2 and 3. Growths using the 950°C growth procedure have not been sufficiently smooth possibly due to degradation of the substrate surface at the high temperatures prior to growth. Altering the growth procedure and using a lower growth temperature as shown in Fig. 3 has resulted in much smoother looking growths over the whole surface. Studies of the diffusion of zinc into the GaAs to form the p-n junction indicate that the zinc diffuses primarily during the heatup time of the boat prior to when the substrate is covered by the melt. The results of several runs are shown in Fig. 4. Run 88A indicates much of the zinc diffusion occurs prior to the growth. The zinc diffusion depth can be controlled by the amount of zinc added to the melt and the time and temperatures prior to growth.

An important parameter for good solar cell performance is the diffusion length of holes in the n type material as it greatly affects the current collection efficiency. We have continued to investigate Lp as a function of N_D, the growth processes and the supplier. The physical structure and the scanning electron microscope technique used are shown in Figs. 5 and 6. The typical

ln i response of the Schottky barrier versus distance is plotted in Fig. 7 and 8 for short and long diffusion length material. The turn over of the response for the short diffusion length material of Fig. 7 is due to the finite size of the injected beam while the upward curvature near the barrier for the long diffusion length material is due to recombination at the surface and a geometric effect. To understand the effects of surface recombination in this geometry we have calculated the current collected by the barrier using the model depicted in Fig. 9. The results as shown in Figs. 10 and 11 demonstrate that the curvature depends both upon the diffusion length and the surface recombination velocity. It is clear that for long diffusion length material the apparent diffusion length measured by this technique is a strong function of the recombination velocity of the surface on which the electron beam impinges. In Fig. 12 the diffusion length is shown as a function of electron concentration for a variety of samples. In the doping range of 5×10^{15} to $10^{17} cm^{-3}$ only vapor phase or liquidphase material have values greater than 2 or 3 microns, which, based on previous calculations, appears as the minimum value for good solar cell performance.

The 1 x 2cm heteroface cells we have fabricated have exhibited relatively low open circuit voltages 0.7 to 0.8 volts and low current collection efficiencies. To determine whether this was characteristic of the solar cell or whether this was the result of bad areas on the cell we have investigated the uniformity of the cell by two methods. One of the methods employs a flying spot scanner, developed at the National Bureau of Standards and the second involves defining mesas on the cell and measuring the characteristics of small regions. The flying spot scanner depicted in Fig. 13 provides two types of output signals. One is the output from a photodetector which measures the reflected light from the sample and the other is the actual photovoltage developed by the cell. These can be used individually or mixed to modulate both the intensity and deflection in the y direction. Figs. 14-17 show the surface fea-

tures and corresponding photoresponse over several regions of two cells. While much of the areas give good response there are regions where the response is very low.

In the second method we have taken large area cells which showed poor response and defined smaller areas and mesas to investigate the uniformity of the cell characteristics. Fig. 18 outlines the steps for determining the mesa solar cell performance. The performance of larger area regions measured under the NASA Lewis AMO simulator and mesas from the same 1 x 2cm cells are given in Fig. 19. The results indicate there are regions of quite high efficiency but also others of lower efficiency which must drag down the overall performance of the larger area cells.

Areas of our planned work on $Al_xGa_{1-x}As$-GaAs solar cells are outlined in Fig. 20.

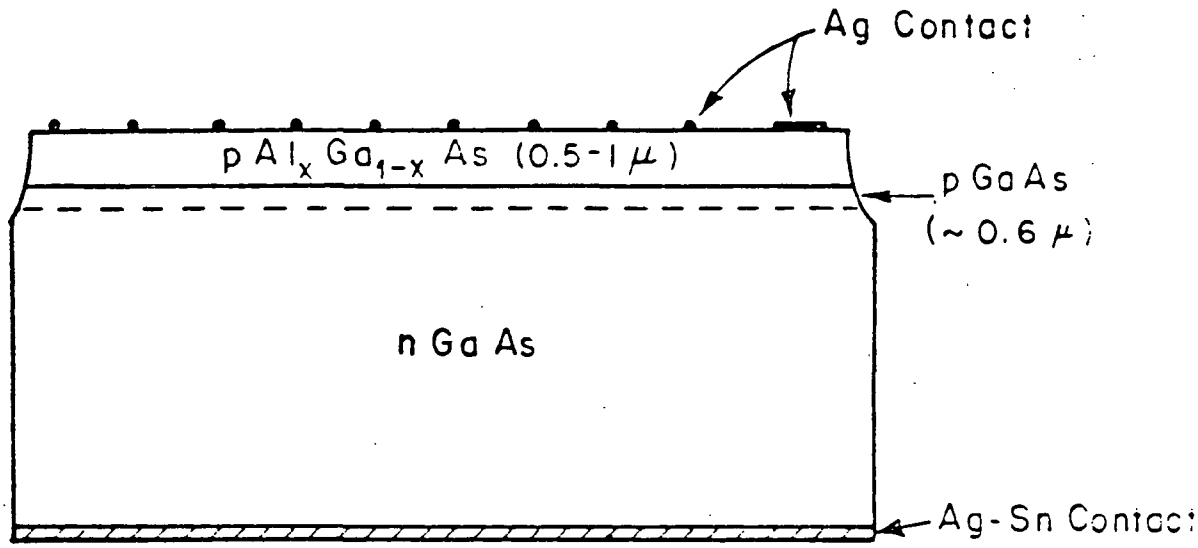

Al$_x$ Ga$_{1-x}$ As - Ga As Solar Cell Cross Section.

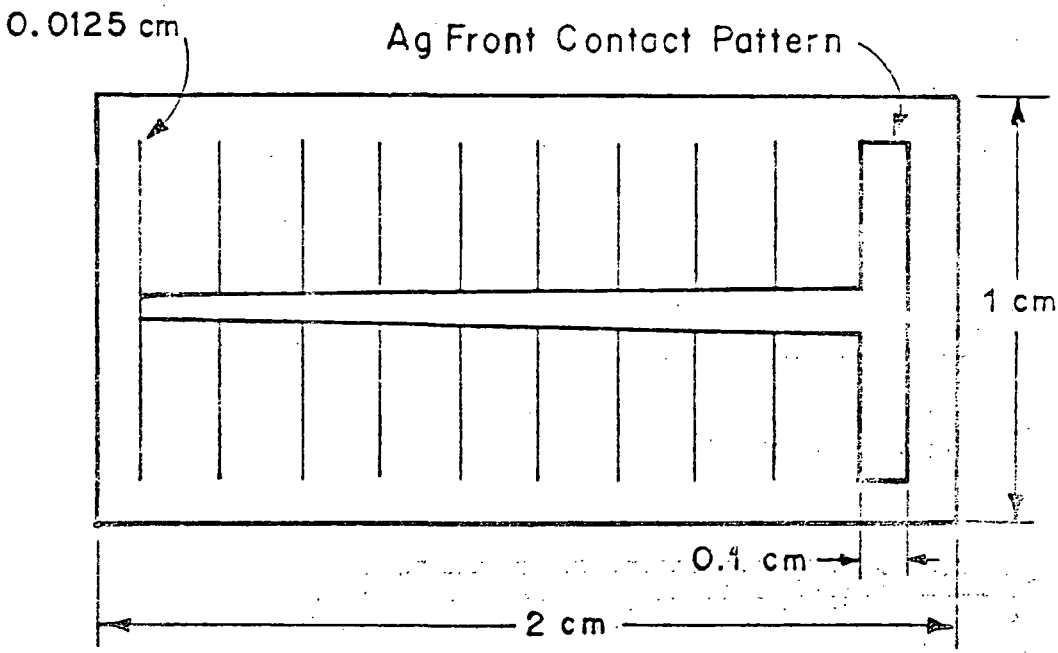

Top of Cell With Contact Pattern.

IV-1

Top View

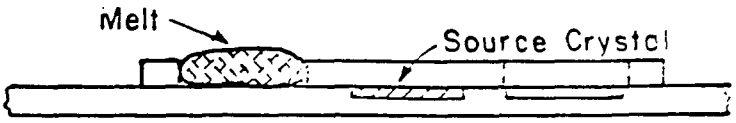

(1) Load source crystal, source pieces and gallium; bake at 1000°C overnight.

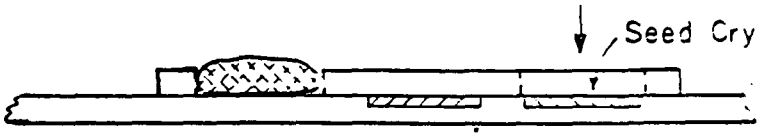

(2) Load seed, Zn & Al through right hand opening.

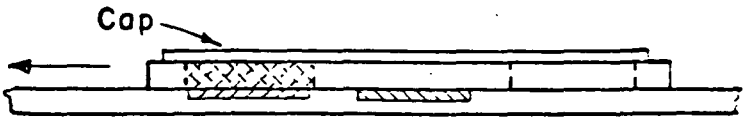

(3) Heat to 950°C and allow to come to equilibrium with seed crystal covered by carbon.

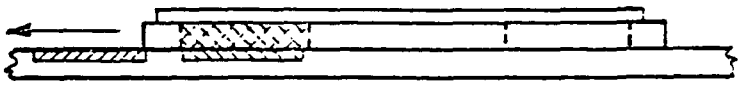

(4) Grow with seed beneath melt at a cooling rate of 0.5°C/minute.

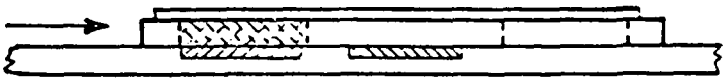

(5) Terminote growth by moving slider in reverse direction.

IV-2 Schematic diagram of current growth procedures, with prebake of melt, using special boat top with larger right hand opening.

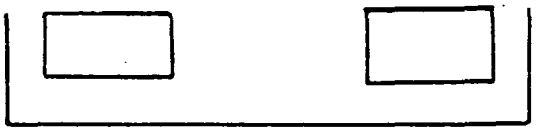

Top View

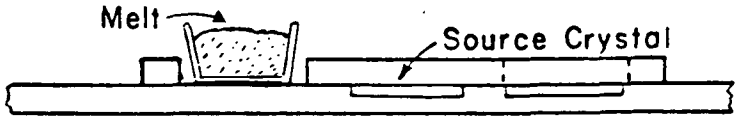

(1) Load Ga in crucible and bake with boat at 1000°C.

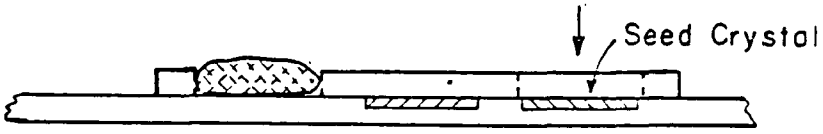

(2) Load Ga, Zn, Al; Load seed through right hand opening.

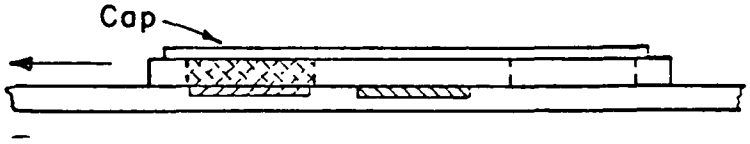

(3) Heat to 850°C for 15min; cool to 800°C at 10°C/min with seed covered by carbon.

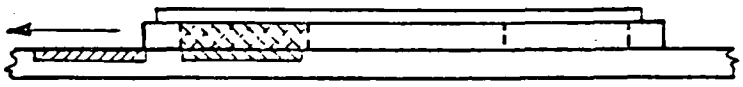

(4) Move slider at 800°C so seed is below melt and cool at 10°C /min to 797°C.

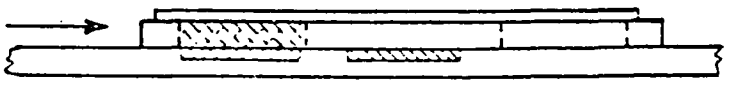

IV-3

JUNCTION DEPTH STUDIES

Run	Substrate Doping (cm^{-3})	Temperature Cycle	wt. Zn(gm)	wt. Ga(gm)	d_j(cm)
88A	2.5×10^{16}	850°C-15 min (no growth)	.022	4.0	0.83
161	8×10^{16}	851°C for 17 min growth 850-845°C @ 2°C/min	.0275	5.0	1.0
162	5.7×10^{17}	870°C for 15 min cool to 820°C @ 10°C/min growth to 815°C	.0147	5.0	0.80
154	7×10^{17}	900°C for 60 min growth 900-895°C @ .50°C/min	.0110	5.0	0.70
156	7×10^{17}	900°C for 60 min growth 900-895°C @ .50°C/min	.0065	5.0	0.56
157	3.5×10^{16}	900°C for 60 min growth 900-895°C @ .50°C/min	.0052	5.0	0.67

TL-4

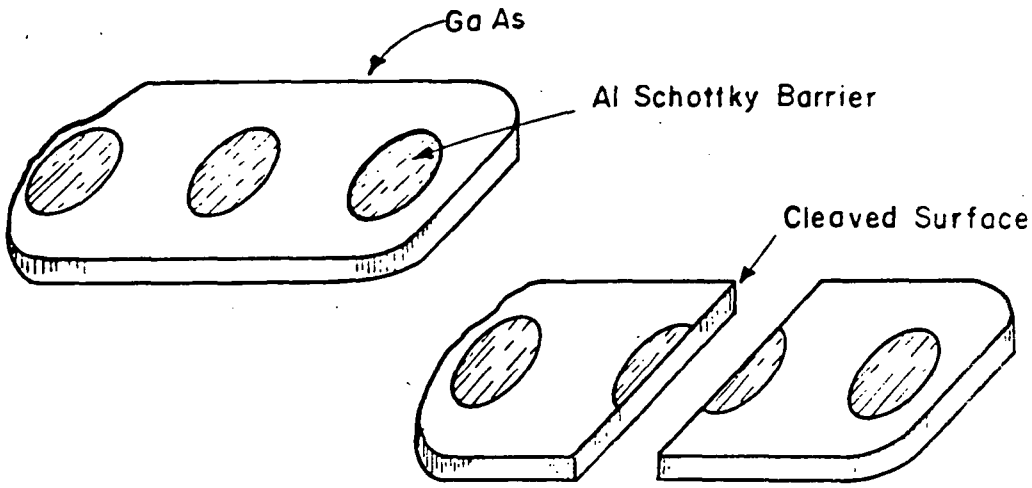

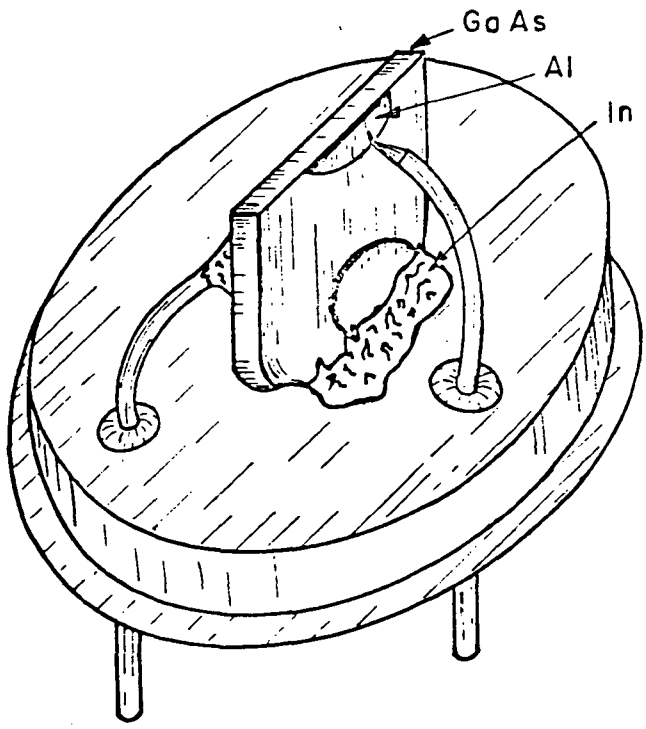

IV-5

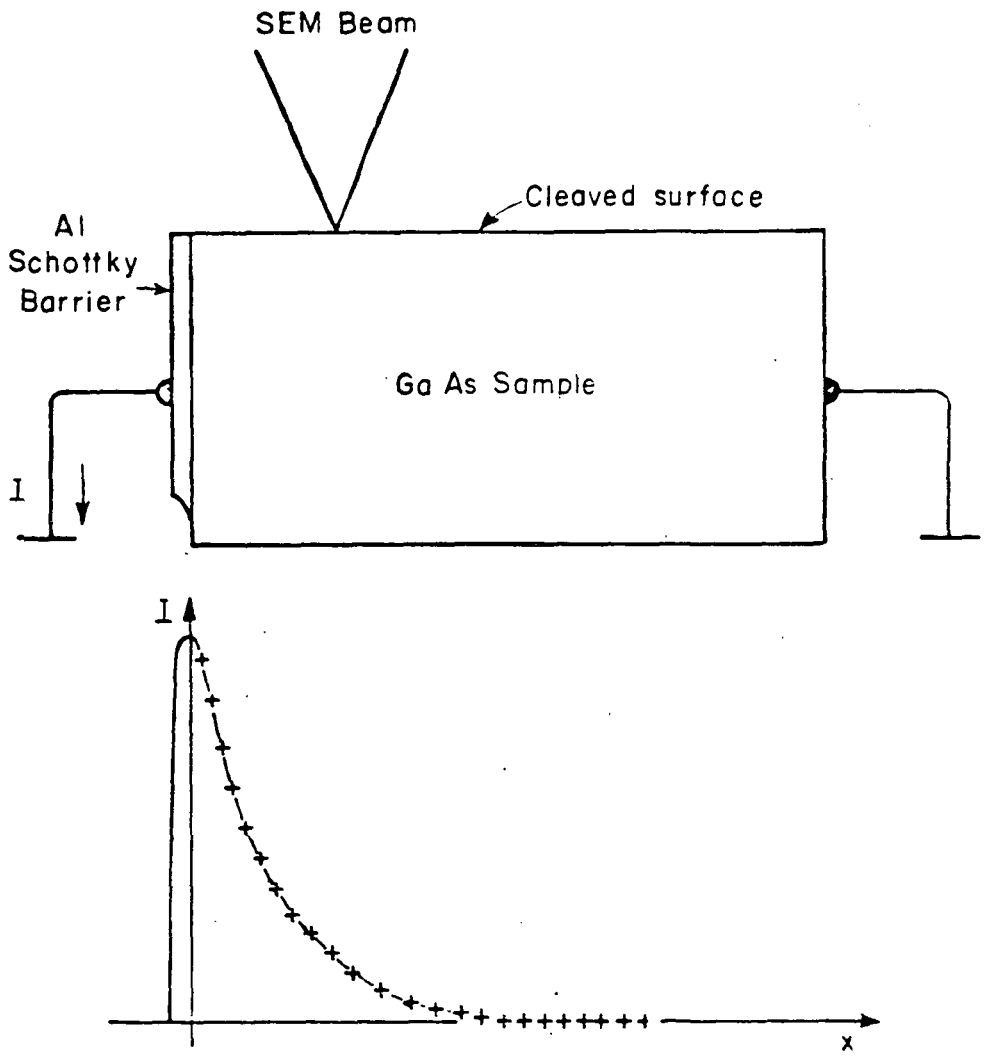
SEM Beam
Cleaved surface
Al
Schottky
Barrier
Ga As Sample
I
I
x

IV-6

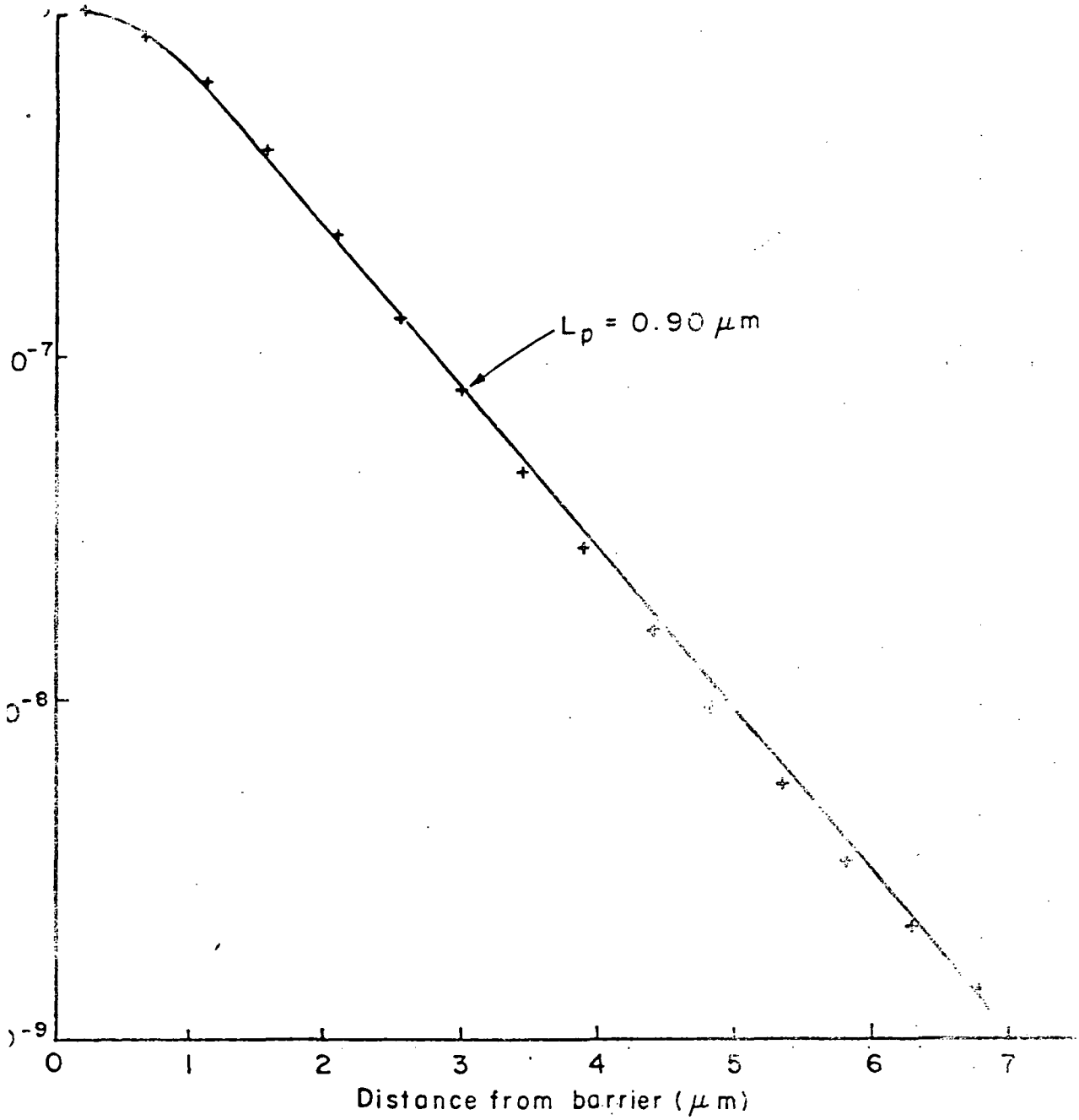

IV-7

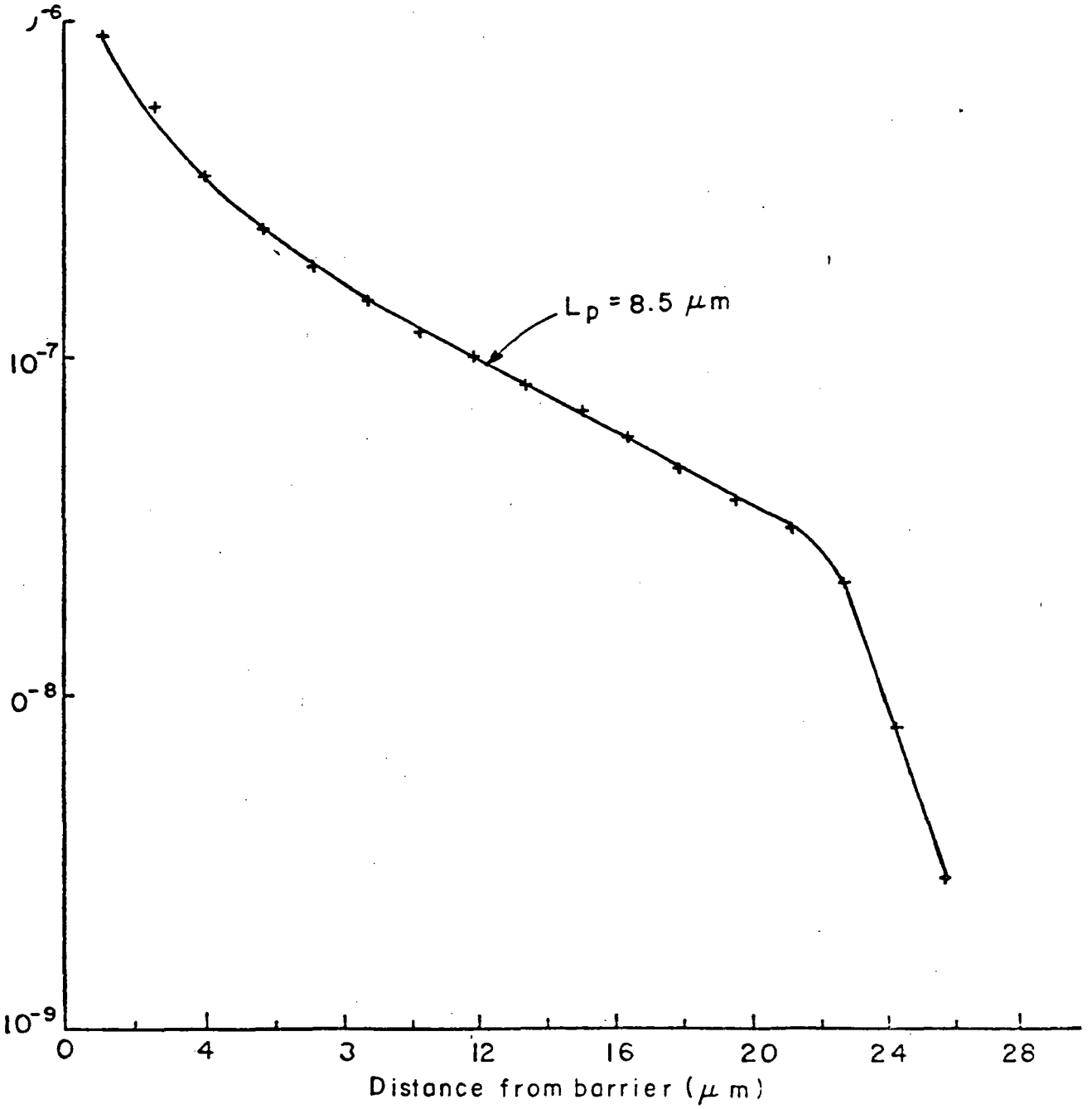
10^{-6}
10^{-7}
10^{-8}
10^{-9}
$L_p = 8.5\ \mu m$
0
4
3
12
16
20
24
28
Distance from barrier (μ m)

IV-8

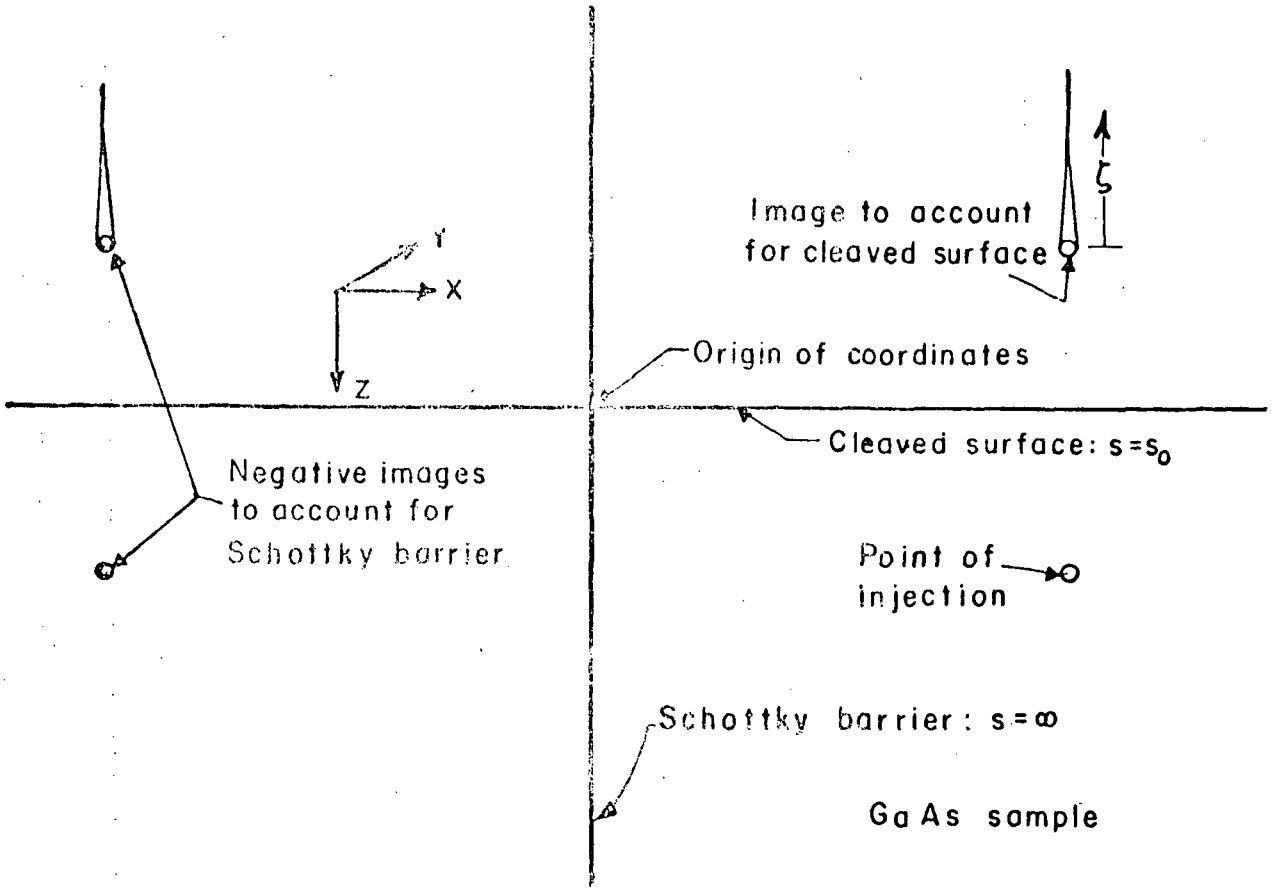
Y
X
Z
Image to account
for cleaved surface
ζ
Origin of coordinates
Cleaved surface: s=s0
Negative images
to account for
Schottky barrier
Point of
injection
Schottky barrier : s=∞
Ga As sample

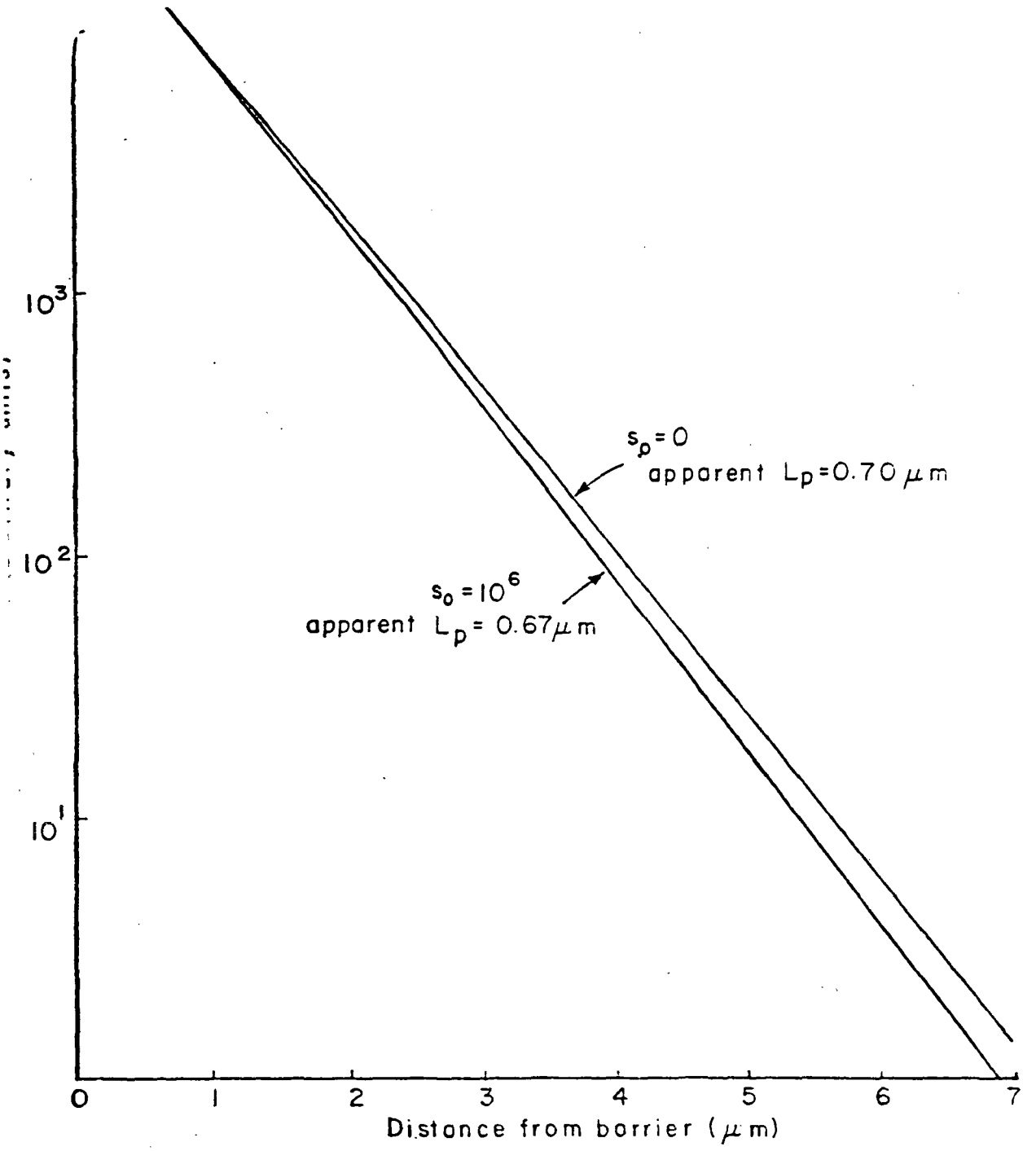
10^3
10^2
10^1
$s_p = 0$
apparent $L_p = 0.70\,\mu m$
$s_0 = 10^6$
apparent $L_p = 0.67\,\mu m$
0
1
2
3
4
5
6
7
Distance from borrier (μm)

IV-10

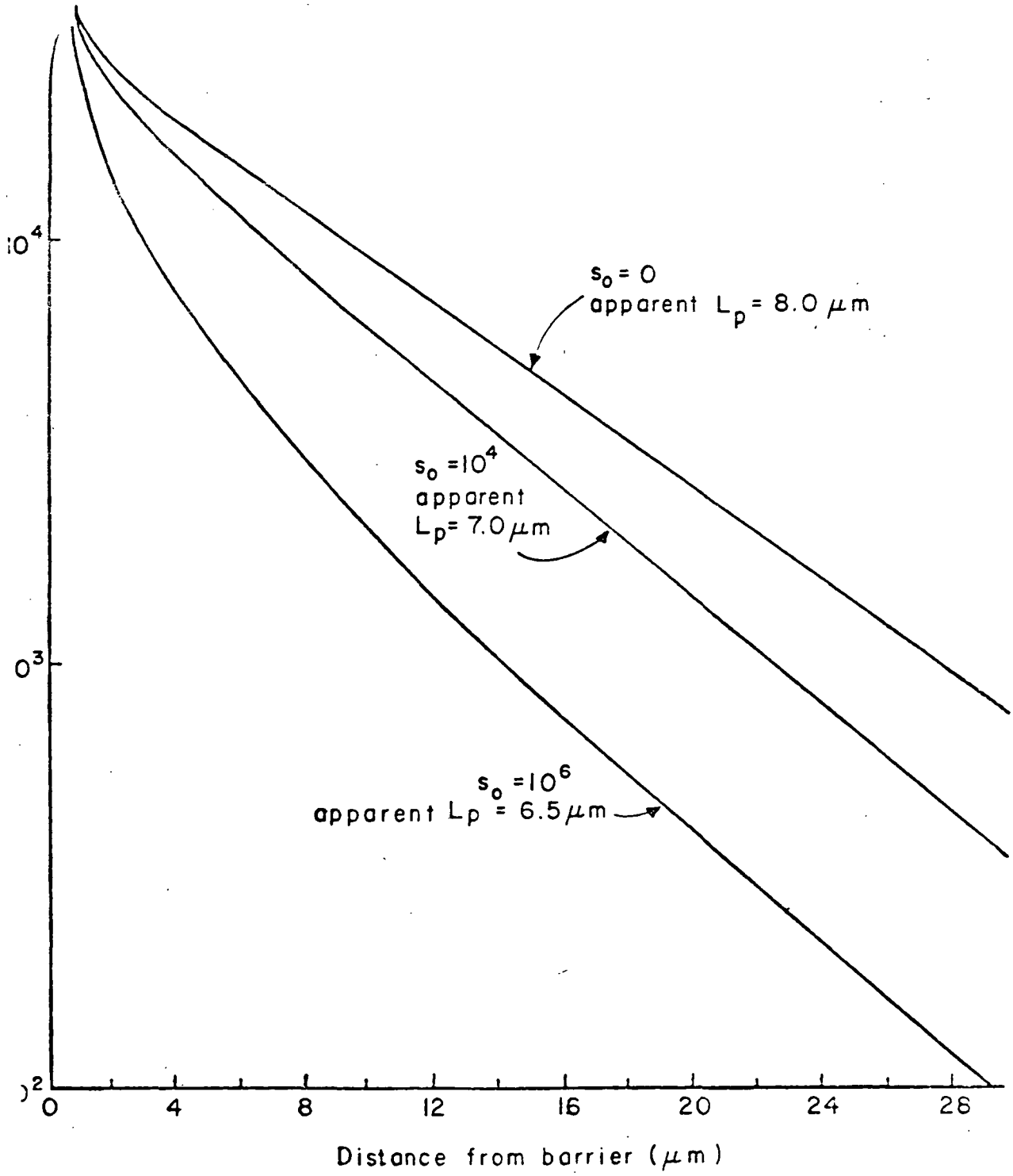
10^4
10^3
10^2
$s_o = 0$
apparent $L_p = 8.0\ \mu m$
$s_o = 10^4$
apparent
$L_p = 7.0\ \mu m$
$s_o = 10^6$
apparent $L_p = 6.5\ \mu m$
0
4
8
12
16
20
24
28
Distance from barrier (μm)

IV-11

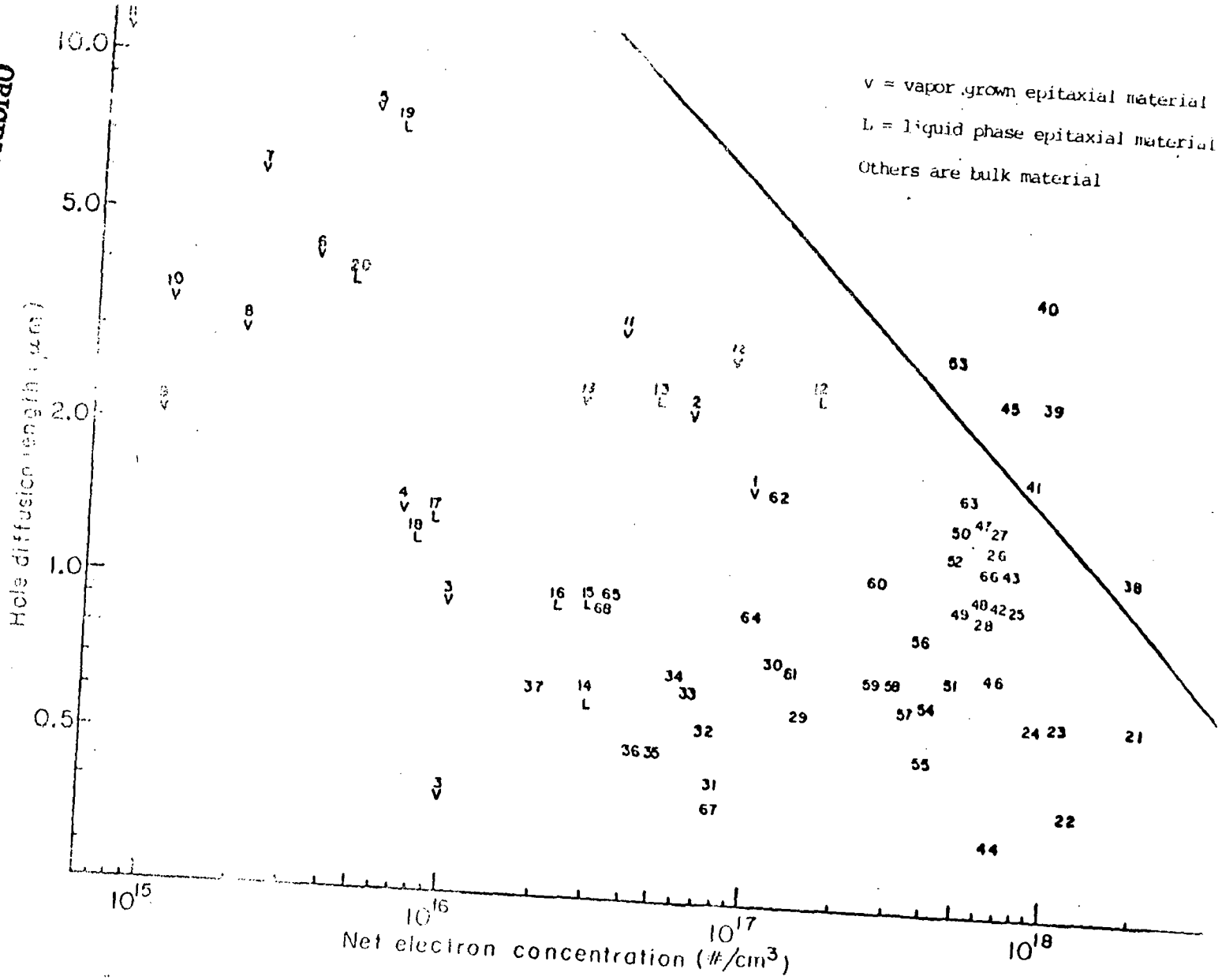

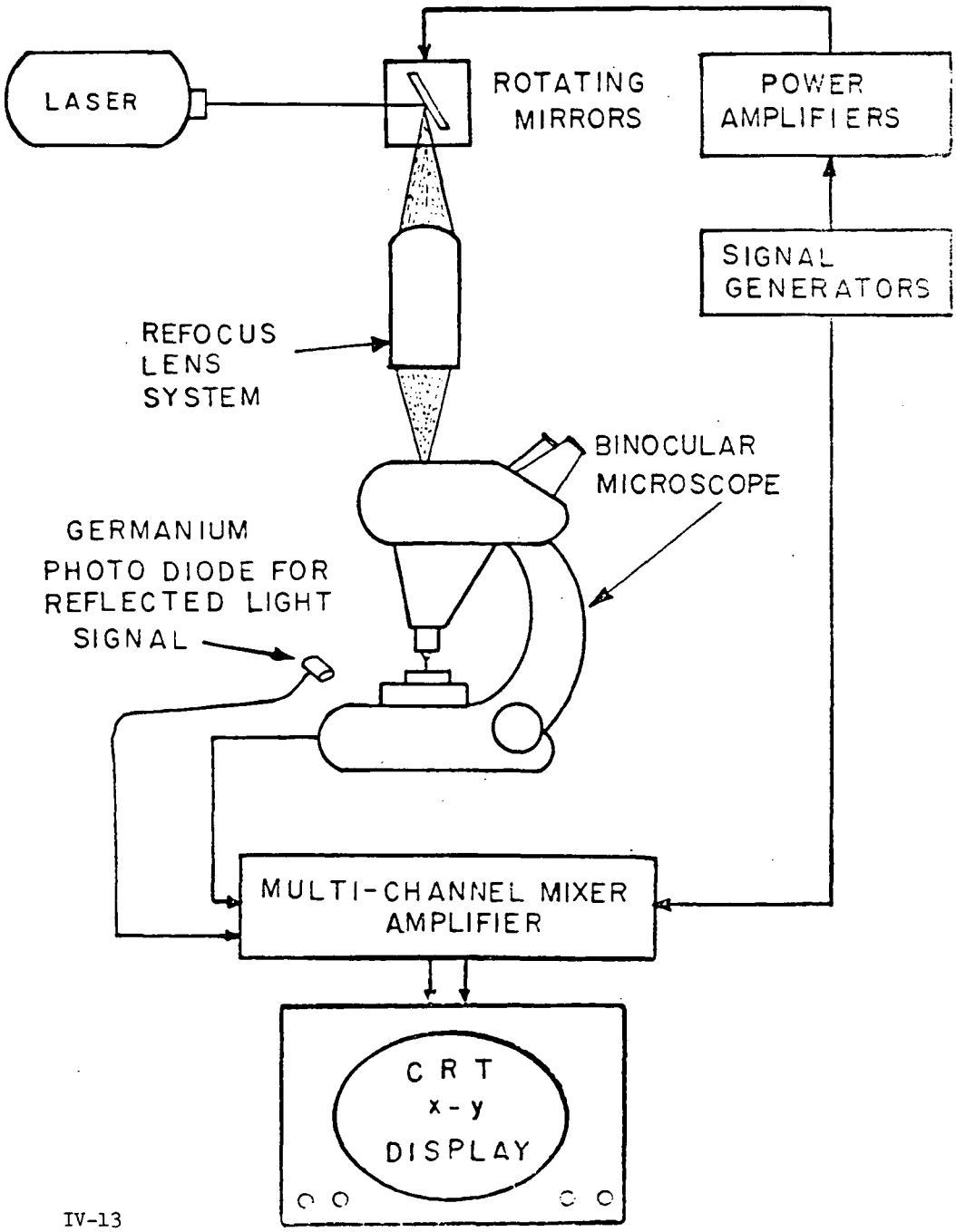
LASER
ROTATING MIRRORS
POWER AMPLIFIERS
SIGNAL GENERATORS
REFOCUS LENS SYSTEM
BINOCULAR MICROSCOPE
GERMANIUM PHOTO DIODE FOR REFLECTED LIGHT SIGNAL
MULTI-CHANNEL MIXER AMPLIFIER
C R T x - y DISPLAY

IV-13

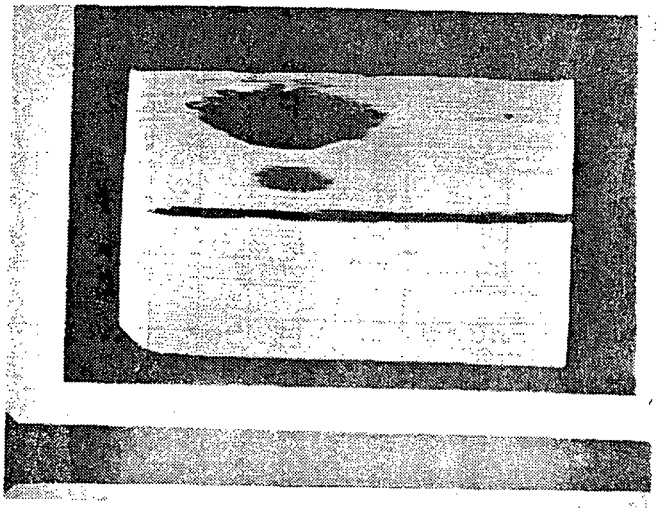

a

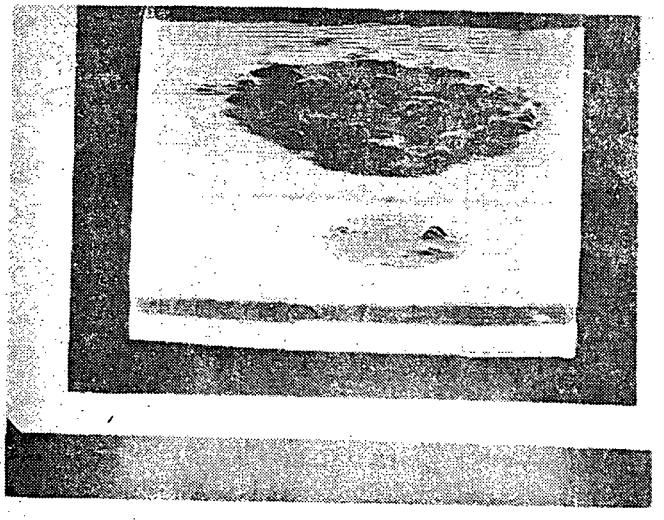

b

IV-14 Poor response area near contact finger (Pg 16).

a. y deflection and intensity modulated by photoresponse.

b. Increased magnification; y deflection [illegible] light and intensity by photoresponse.

a

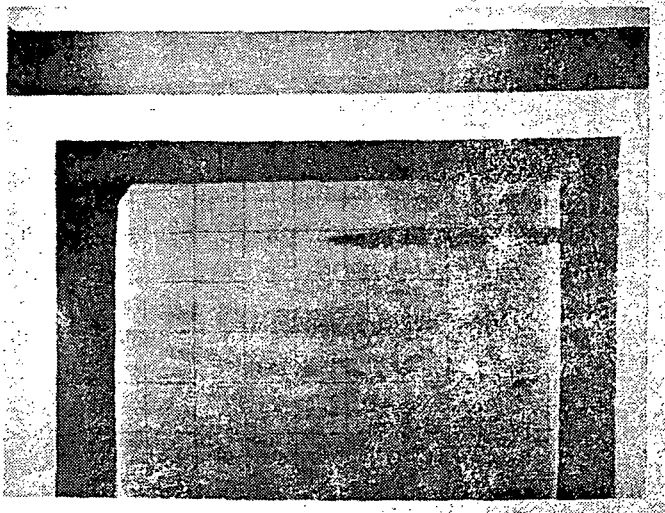

b

IV-15 Surface blemish near contact bar (Run 162)

Run 162 a. Intensity modulated by reflected light.

b. Intensity modulated by photoresponse.

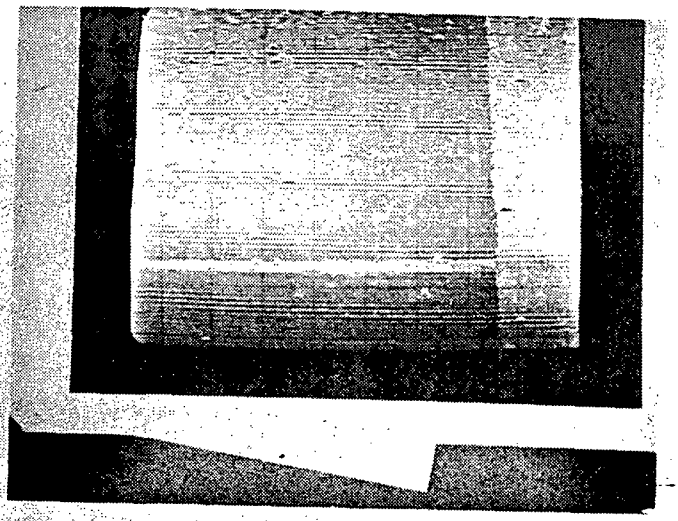

a

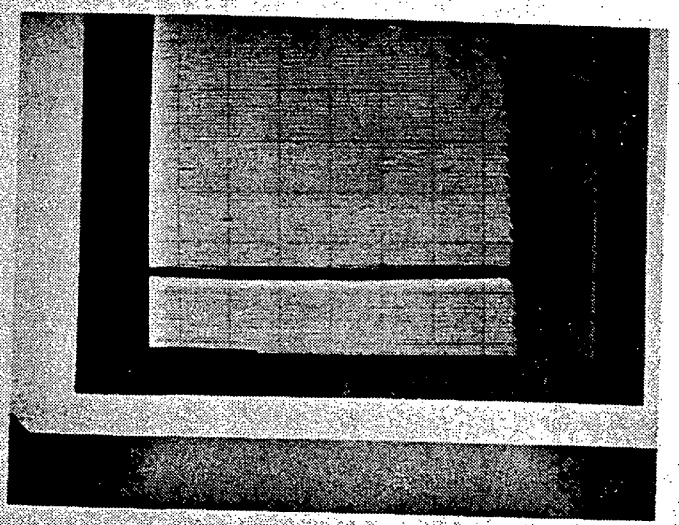

b

IV-16 Uniform response area near contact finger (Run 162).

a. y deflection and intensity modulated by reflected light.

b. y deflection and intensity modulated by photoresponse.

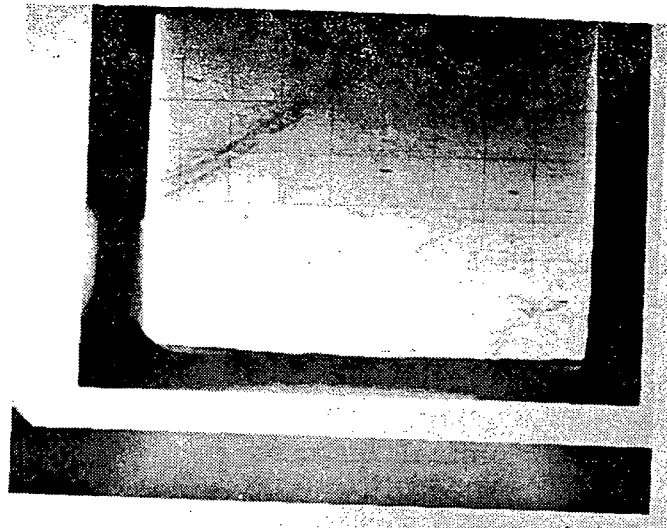

a

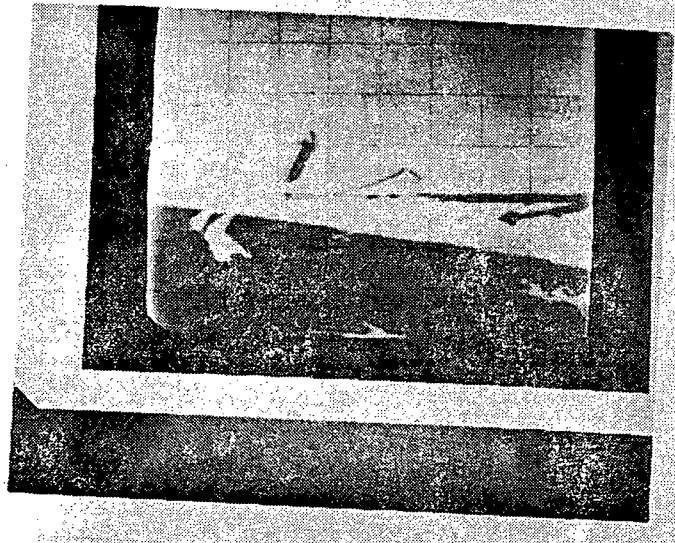

b

IV-17 Cell area near contact bar (Run 165).

a. y deflection and intensity modulated by reflected light.

b. Intensity modulated by photoresponse.

STEPS FOR DETERMINING MESA SOLAR CELL PERFORMANCE

1. Etch Mesa Diodes; $A=0.01cm^2$

2. Measurements

   2.1 Spectral Response

   2.2 Dark V-I

   2.3 N_D of Substrate by C-V

   2.4 Active and Total Area of Mesa

3. Calculate I_{sc} (AMO) from 2.1

4. Find V_{oc}, V_{mp} and J_{mp} from 3 and 2.2

5. Calculate η, f.f.

IV-18

HETEROFACE SOLAR CELL PERFORMANCE

CMU Cell #	area (cm^{-2})	Voc (V)	Jsc (ma cm^{-2})	ff	η (AMO)%*
151	.386	.91	18.23	.76	9.3
151.3	.020	.98	23.02	.82	13.6
151.2	.013	.97	23.02	.82	13.5
158	.817	.87	21.67	.63	8.7
158.3	.028	.94	25.93	.80	14.2
158.2	.034	.93	25.93	.74	13.2
160	.130	.93	25.88	.51	9.1
160.21	.018	.97	31.50	.83	18.7
160.105	.0053	.66	31.50	.71	10.7
164	.508	.81	21.0	.74	9.2
164.2	.0015	.85	24.78	.81	12.6
164.1	.0028	.80	24.78	.77	11.2
165	.238	.82	19.7	.67	8.2
165.6	.0054	.86	25.47	.81	12.9
165.2	.0026	.443	25.47	.70	5.8
166	.668	.88	21.0	.69	9.3
166.1	.0089	.94	20.83	.80	11.4
166.4	.0133	.80	20.83	.77	9.5

Cell numbers without decimals are large samples characterized under simulated AMO (NASA Lewis) illumination.

Cell numbers with decimals are mesa samples with characteristics computed from the spectral response (NASA Lewis) of the large samples and the current voltage measurements made on the mesa diodes.

*This value is adjusted down by 12% for contact area loss and then up by 16% for antireflection coating gain from original bare cell measurements. The 16% correction corresponds to a refractive index of 2.9 for 0.8 mole fraction of AlAs.

FUTURE WORK ON $Al_xGa_{1-x}As$-GaAs SOLAR CELLS

1. Further Investigation of Non-uniformity of Cell Response.
   a) Flying Spot Scanner
   b) Mesaing into Small Cells

2. Improving LPE Growths to get Large Area Cells

3. Effect of Substrate Doping and Properties on Cell Performance

4. Double Epitaxial Layer Heteroface Cells

Characterization of GaAlAs-GaAs Solar Cells

by

Gilbert H. Walker
NASA - Langley Research Center

Summary

Two parameters which limit the efficiency of GaAs solar cells are surface recombination velocity and minority carrier diffusion length. The research described in this paper is directed toward solving these problems.

The efficiency of GaAs solar cells has been increased by epitaxially growing a thin window of GaAlAs on the surface of the GaAs solar cell. The critical parameter here becomes the recombination velocity at the GaAs-GaAlAs interface. The spectral response of GaAlAs-GaAs solar cells was measured using a xenon light source and a monochromator. From these data the recombination velocity at the GaAlAs/GaAs interface was calculated to be approximately 10^5 cm/sec. A study was also conducted to determine the effect of the GaAlAs layer thickness on the spectral response of the solar cells. It was found that the normalized spectral response at 2.4 eV of the cells increased from 0.2 to 0.8 as the GaAlAs layer thickness was decreased from 2.0 μm to 1.0 μm

Another parameter which reduces the efficiency of GaAs solar cells is the low hole diffusion length in the base n-type GaAs. Surveys of commercially available n-GaAs, which is doped in the range of 1 to

5×10^{17} carriers/cm^3, have shown that the hole diffusion length is typically less than 1 μm. A hole diffusion length greater than 3 μm is required for the most efficient GaAs solar cell. One method for increasing the hole diffusion length is to decrease the carrier concentration in the base material. In order to investigate this method of increasing the solar cell efficiency, GaAlAs/GaAs solar cells were fabricated with three different base carrier concentrations. It was found that for base dopings of 1×10^{18}, 6×10^{16}, and 3×10^{16} there was no correlation in either open circuit voltage or efficiency; however, the short circuit current density increased from 17.24 ma/cm^2 for carrier concentration of 1×10^{18} carriers/cm^3 to 22.35 ma/cm^2 for a carrier concentration 3×10^{16} carriers/cm^3. The fill factor decreased from 0.67 to 0.46.

INTERFACE RECOMBINATION VELOCITY CALCULATION

$$J_{PH}(\lambda) = \left[J_{JUNCTION}(\lambda) + J_{BASE}(\lambda) + J_{DEPLETION\ REGION}(\lambda)\right]\left[1 - R(\lambda)\right]$$

$$J_{JUNCTION}(\lambda) = f(S_G)$$

MATERIAL PARAMETERS USED IN CALCULATIONS

$d_j = 0.8\ \mu m$

$L_a = 0.27\ \mu m$

$S_a = 10^6\ CM\ SEC^{-1}$

$T_a = 10^{-9}\ SEC$

$L_n = 2.0\ \mu m$

$T_n = 10^{-8}\ SEC$

$L_p = 1.0\ \mu m$

RESULTS

INTERFACE RECOMBINATION VELOCITY $\approx 10^5\ CM\ SEC^{-1}$

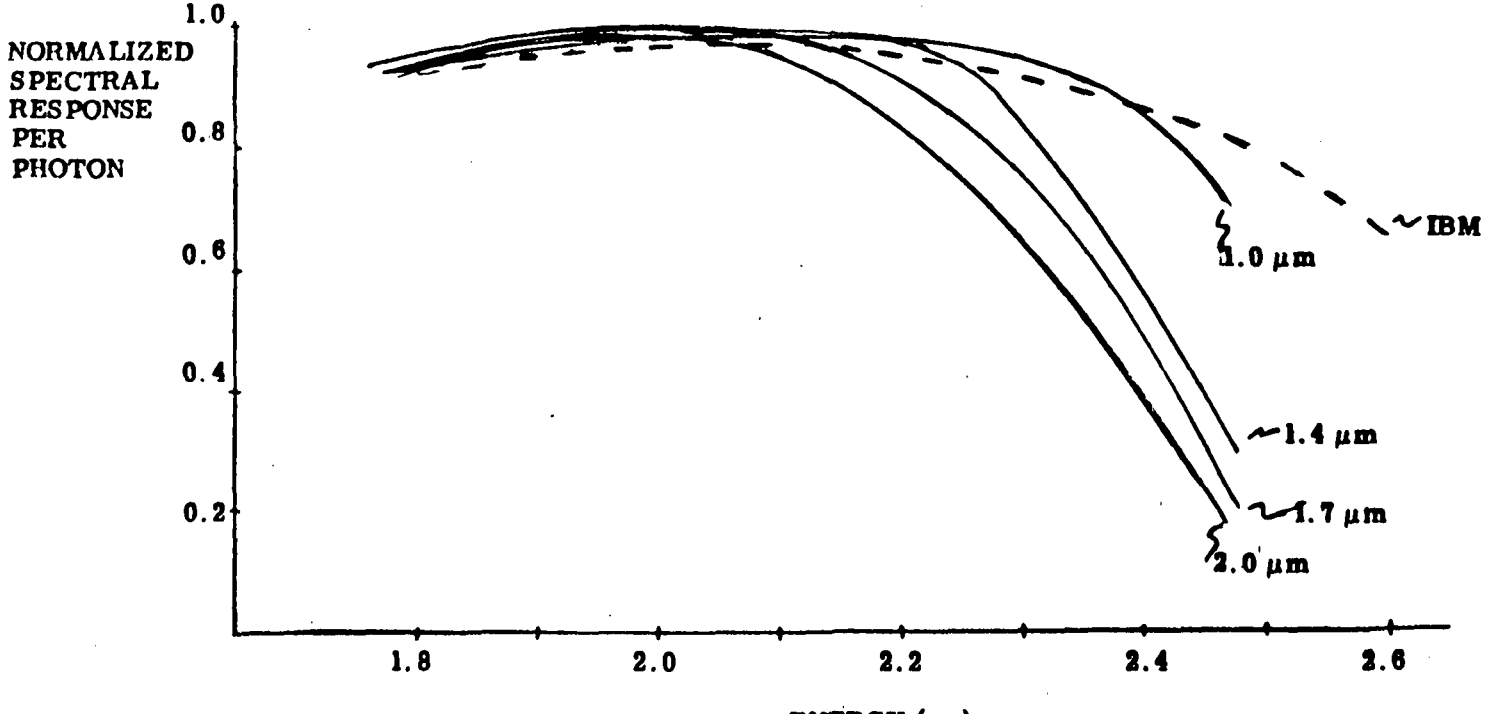

SPECTRAL RESPONSE OF GaAlAs GaAs SOLAR CELLS WITH VARYING GaAlAs THICKNESS

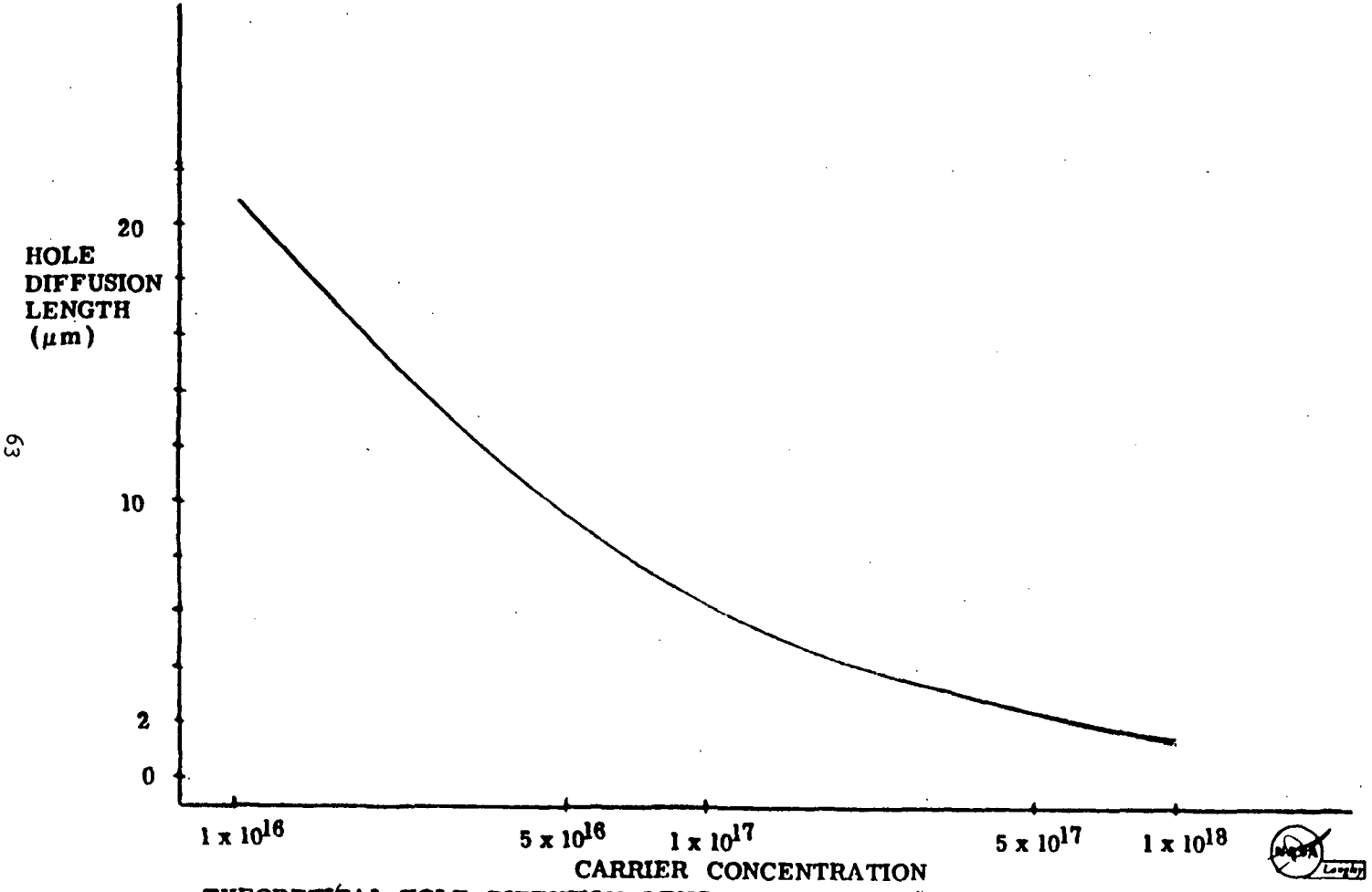

THEORETICAL HOLE DIFFUSION LENGTH MAXIMUM (RYAN EBERHARDT, 1972)

$Ga_{1-x}Al_xAs$ HETEROFACE SOLAR CELL

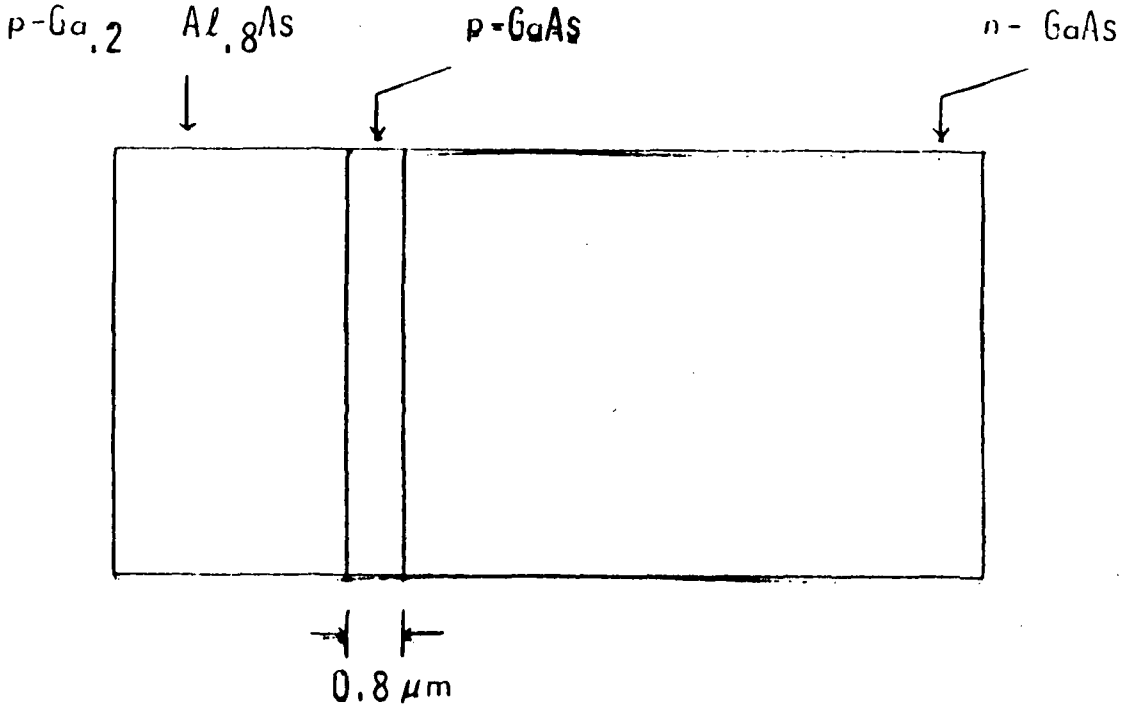

EFFECT OF SURFACE RECOMBINATION VELOCITY ON GaAs SOLAR CELL EFFICIENCY FOR A 0.25 MICRON p-n JUNCTION DEPTH

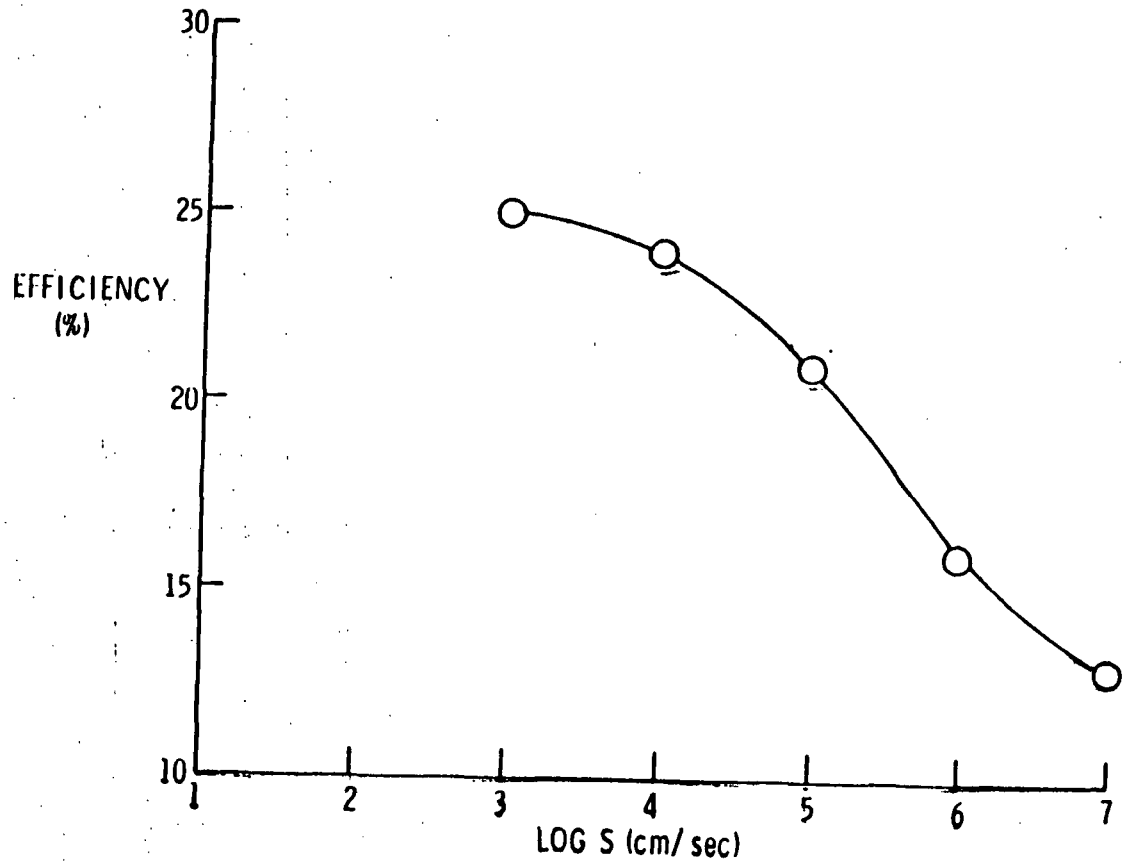

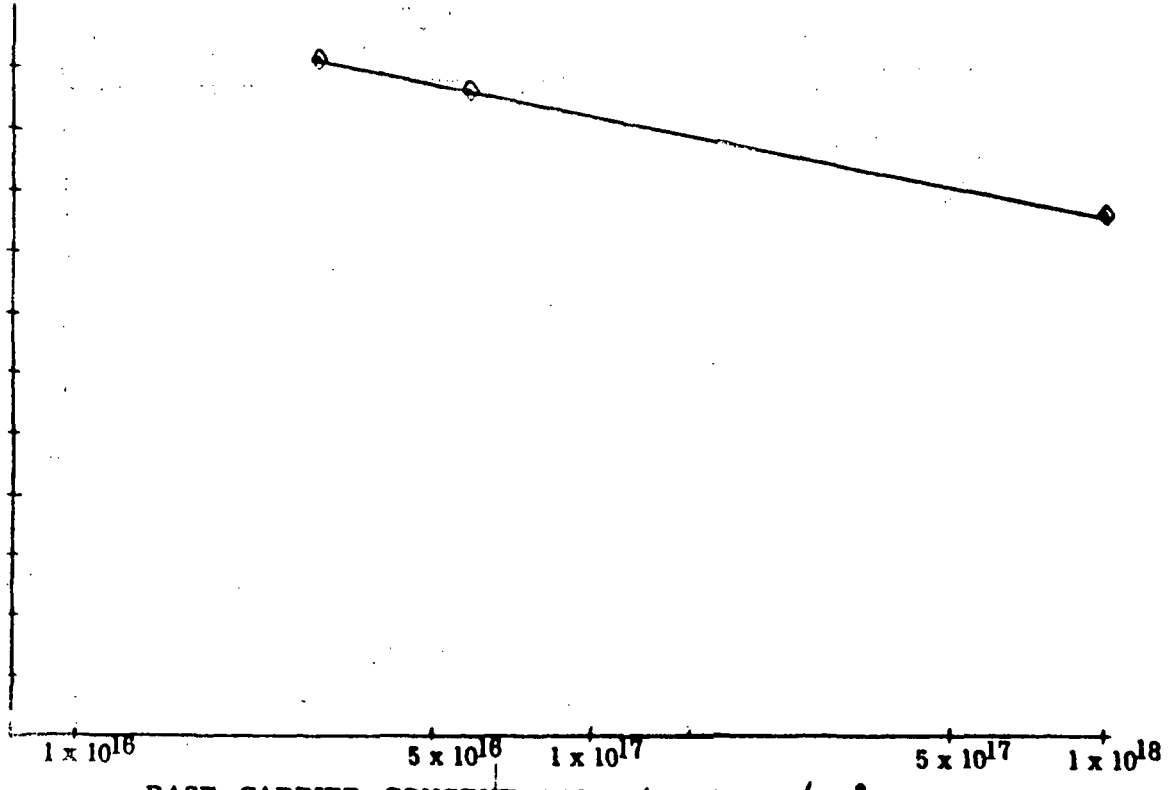

VARIATION OF SHORT CIRCUIT CURRENT DENSITY WITH BASE CARRIER CONCENTRATION

GaAlAs GaAs SOLAR CELL CHARACTERISTICS UNDER AMO ILLUMINATION

BASE CARRIER CONCENTRATION	OPEN CIRCUIT VOLTAGE	SHORT CIRCUIT CURRENT DENSITY	FILL FACTOR	EFFICIENCY
3×10^{16}	.88 v	22.35 ma/cm^2	.46	6.52 %
6×10^{16}	.825 v	21.45 ma/cm^2	.60	6.75 %
1×10^{18}	.865 v	17.24 ma/cm^2	.67	7.23 %

Third Working Meeting on GaAs Solar Cells
Sept 25-26, 1975

GaAs Surface Barrier Solar Cells

Richard J Stirn- JPL

ABSTRACT

The conversion efficiency of metal-semiconductor GaAs solar cells has been markedly improved by the addition of a heat treatment step before the metal deposition. Output voltages at open circuit are now about 0.70 volts as compared to 0.45 volts without the effect. Conversion efficiencies are about 12% AMO and 15% AMI. However, most of the time, but not always, deposition of the grid by vacuum evaporation lowers the open-circuit voltage by about 0.1 volts. The reason for this behavior and means to avoid it are still being investigated.

The uniqueness of the AMOS solar cell is shown by the fact that an open-circuit voltage greater than the built-in potential (0.75 volts in our samples with doping of 2×10^5 cm $^{-3}$) can be obtained when illuminating the cell with high intensity light. The obvious implication is that this may occur even at normal sunlight intensities. Indeed, one recent cell (ungridded) has shown a voltage of 0.75 volts.

A model that allows for such voltage outputs has been developed by Prop. S. Fonash of Pennsylvania State University - field shaping by localized states. We have demonstrated that other possible causes such as majority carrier transport control by thin oxide tunneling and barrier height modification by fixed charge do not play a significant role in the GaAs AMOS cell. A simplified step function model for localized state density distribution (assumed acceptor-like) has been shown to describe the experimental dark forward current-voltage characteristics.

An experimental program to investigate the chemical nature of the oxide-semiconductor interface using ESCA (Electron Spectroscopy by Chemical Analysis) has begun. These investigations are to determine the exact elemental form, which, when bonded with either the Ga or As atoms or their oxidized compounds, give the desired interfacial states distribution and density for optimum open-circuit voltage and fill factor.

Experiments on the 60A° - thick gold-GaAs system with an ellipsometer having a variable compensator have determined the effective complex index of refraction. Good agreement between the predicted and measured reflectance at all wavelengths of interest show the accuracy of the measured index of refraction. Calculations show that the ideal index of refraction for an antireflection (AR) coating matched to air is 2.35, and 3.0 when matched to a cover glass adhesive with index of 1.4. Unfortunately we have been able to obtain an index of only about 2.0 for unannealed Ta_2O_5. Other materials including Nb_2O_5 will be investigated and reflectance minima at about 0.55μ used in order to further improve the output current in general and the blue response specifically.

Double layer metal-semiconductor solar cells fabricated at JPL using crystals grown at Stanford University by LPE have shown that the expected higher open-circuit voltages are obtained (≈0.8 volts with no AMOS processing), but that the collection efficiency of carriers generated in the GaAs layer is much too small. The AlGaAs, with about 40% Al, is about 1 micron thick. If layers can be grown with thicknesses between 0.2 to 0.5μ with light doping, much better collection should result because of the presence of the built-in electric field at the interface.

Preliminary experiments with 1Mev electrons on "baseline" Au-GaAs cells have shown markedly superior radiation resistance as compared to silicon solar cells. However, irradiations have not been made on voltage-enhanced AMOS cells to date because of funding limitations.

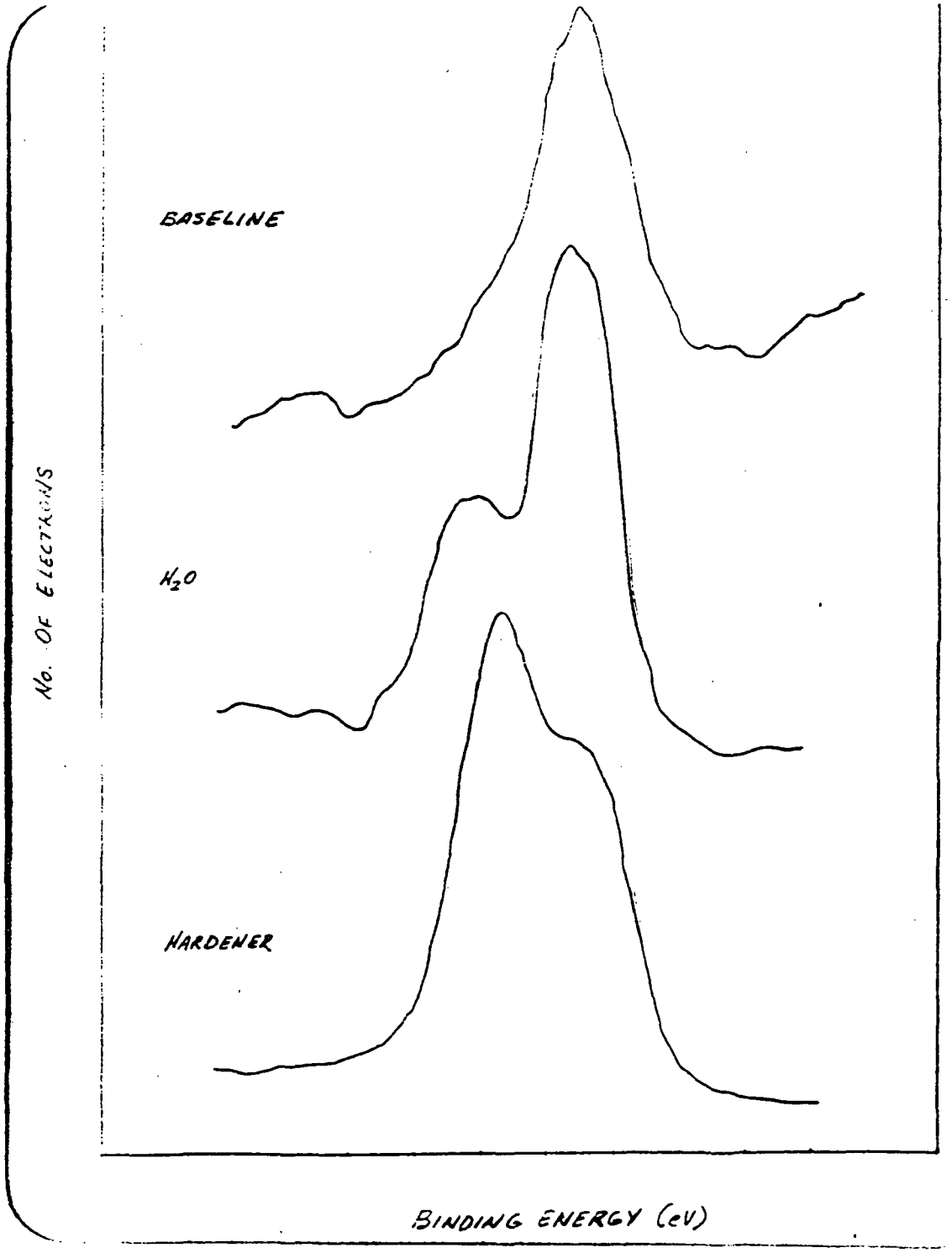
BASELINE
H_2O
HARDENER
No. OF ELECTRONS
BINDING ENERGY (eV)

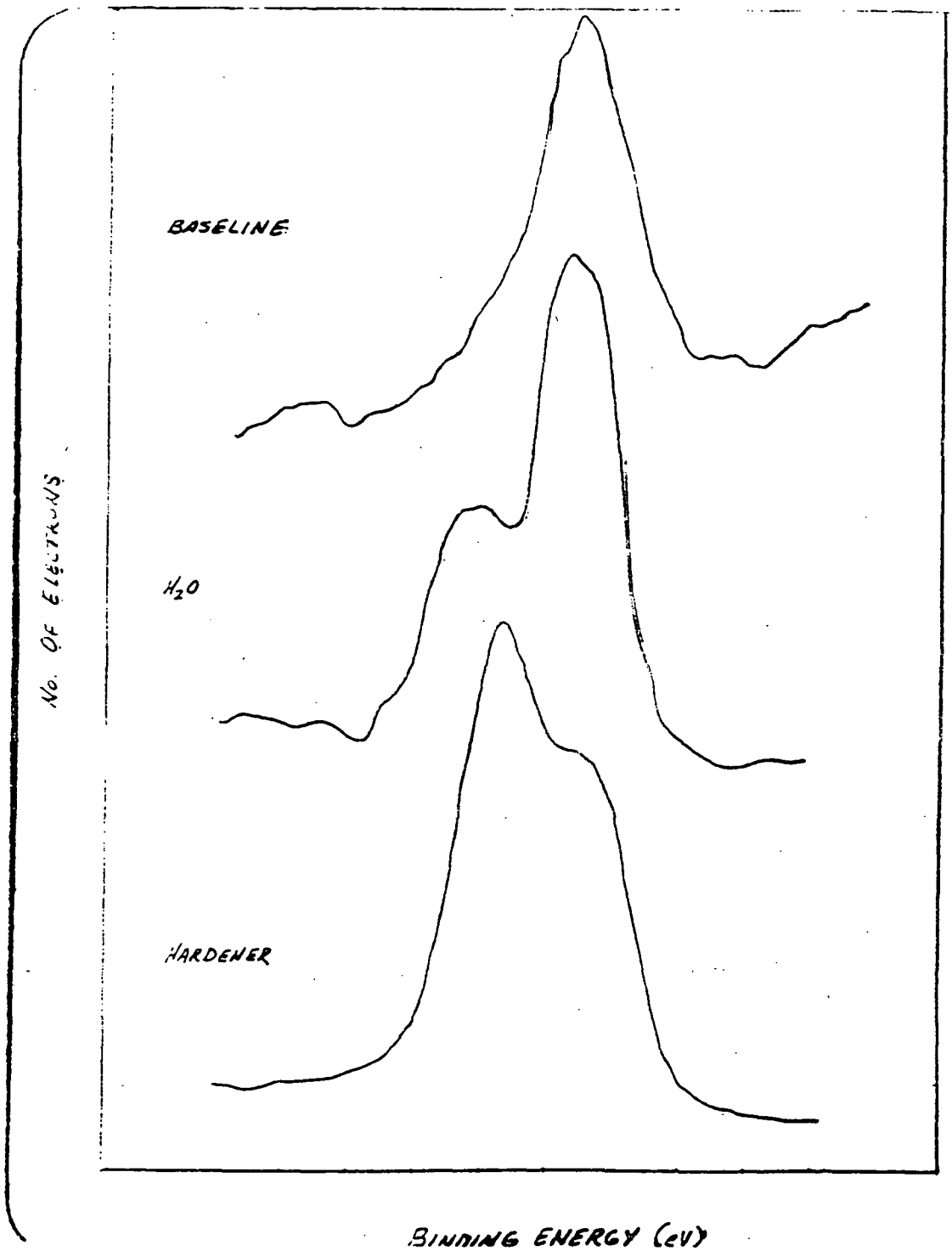

VI-2

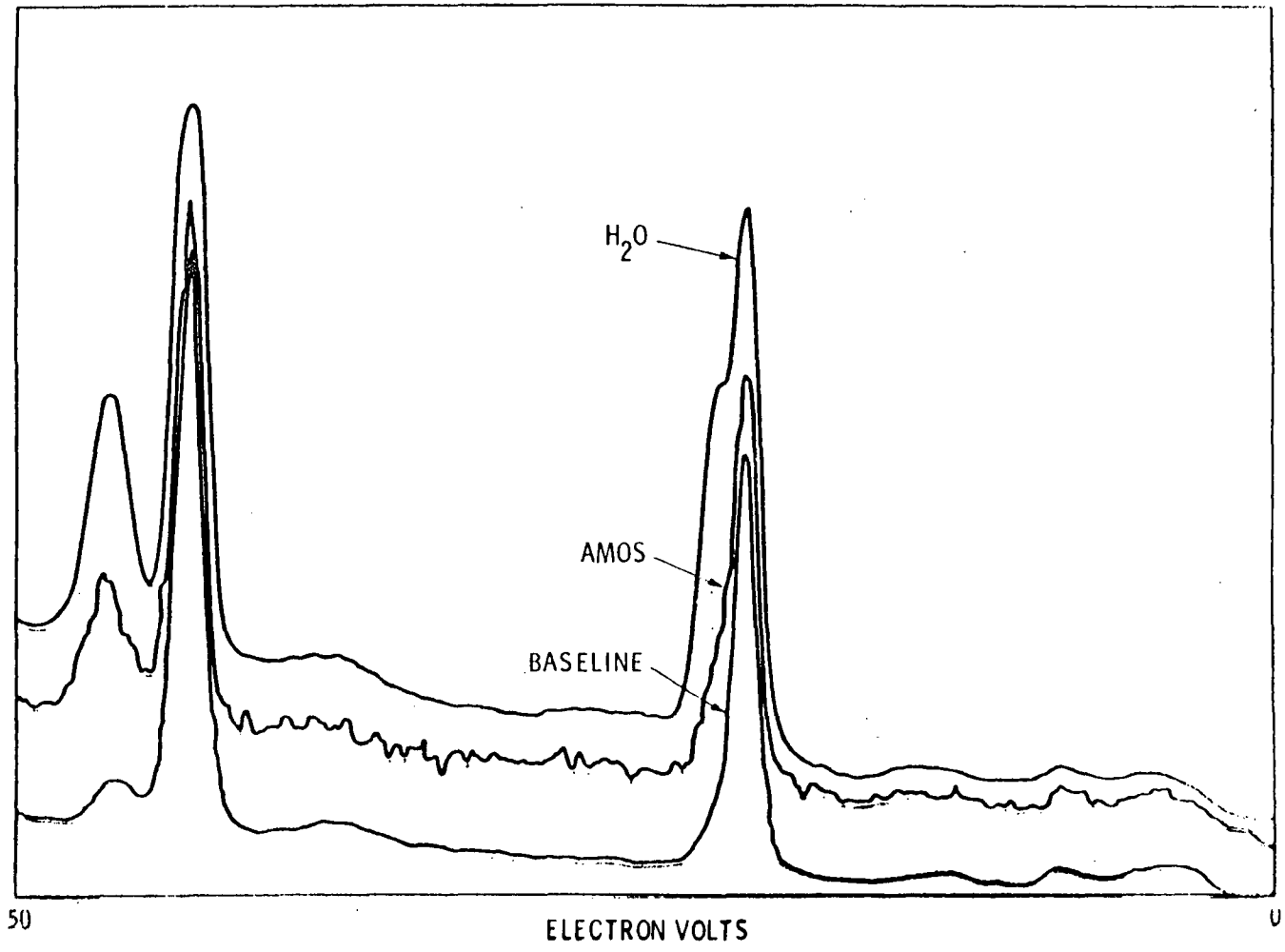
H_2O
AMOS
BASELINE
50
ELECTRON VOLTS
0

AMOS SOLAR CELL

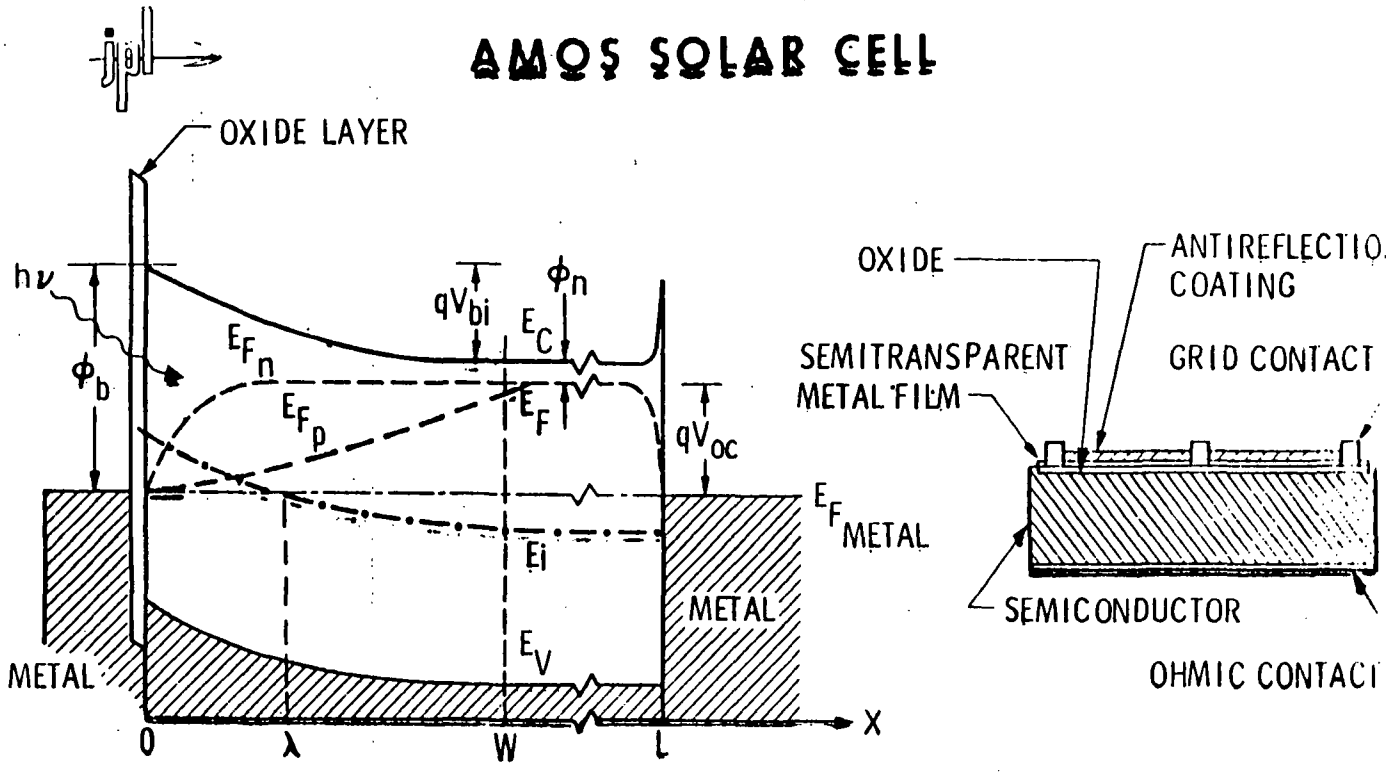

LOCALIZED STATE DENSITY MODEL FOR AMOS

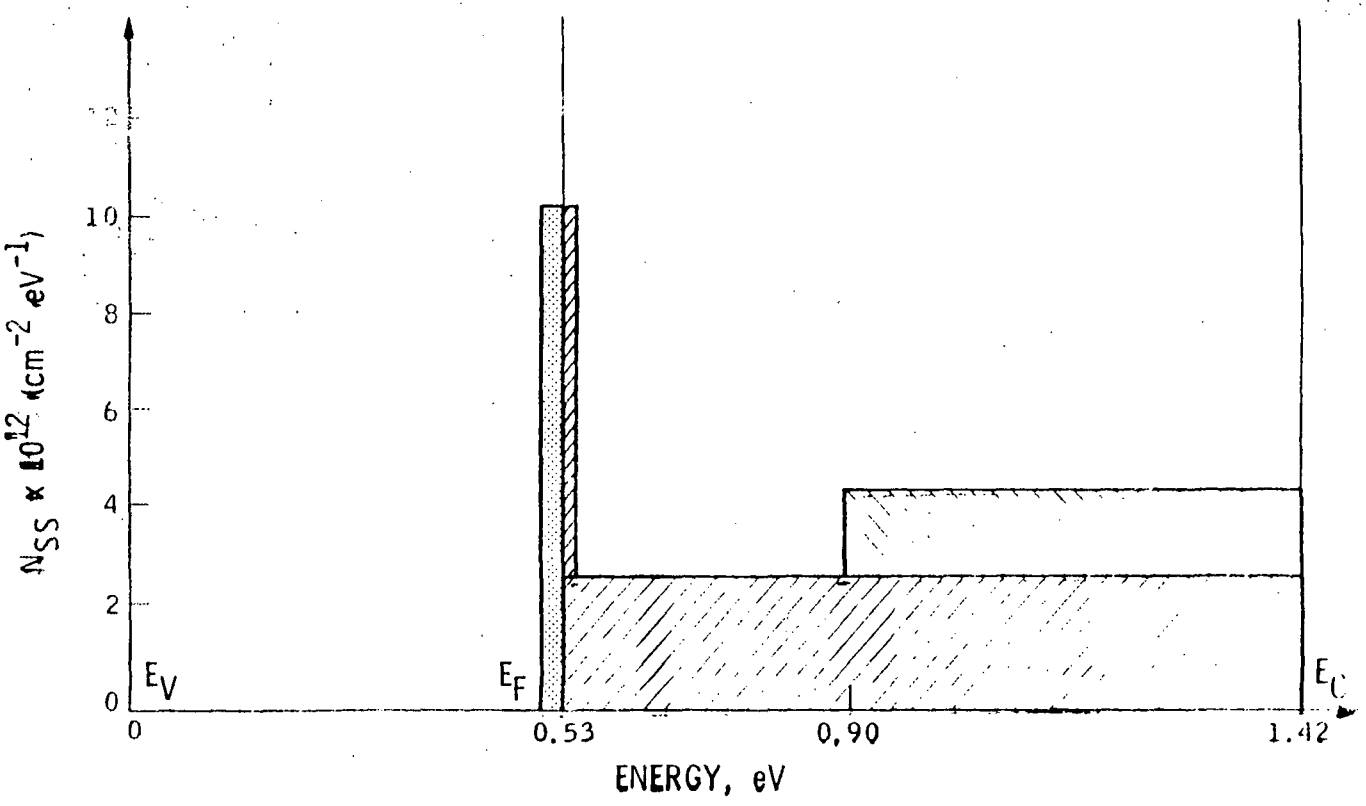

EXPERIMENTAL DARK FORWARD I-V CURVES

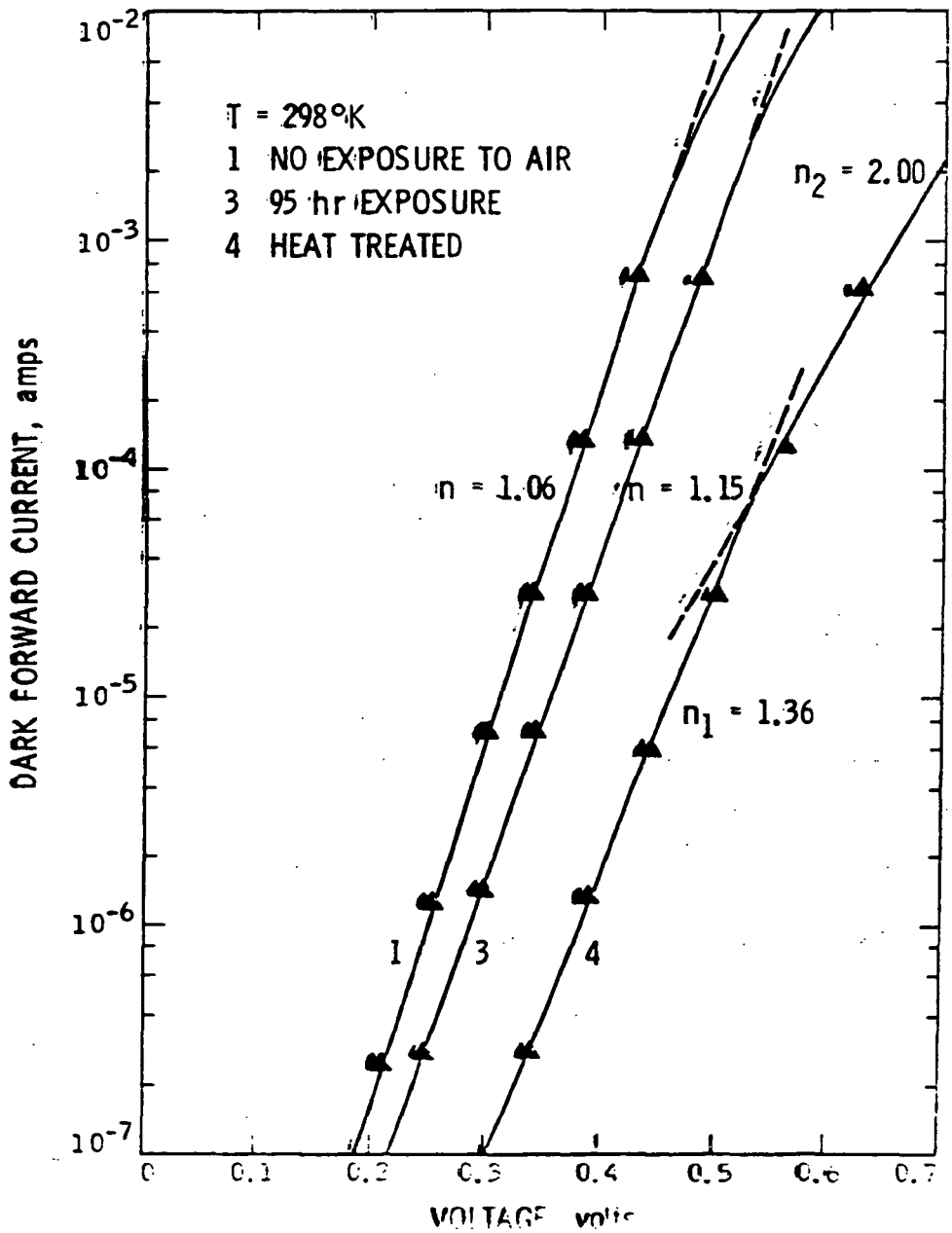

FIELD SHAPING BY LOCALIZED STATES

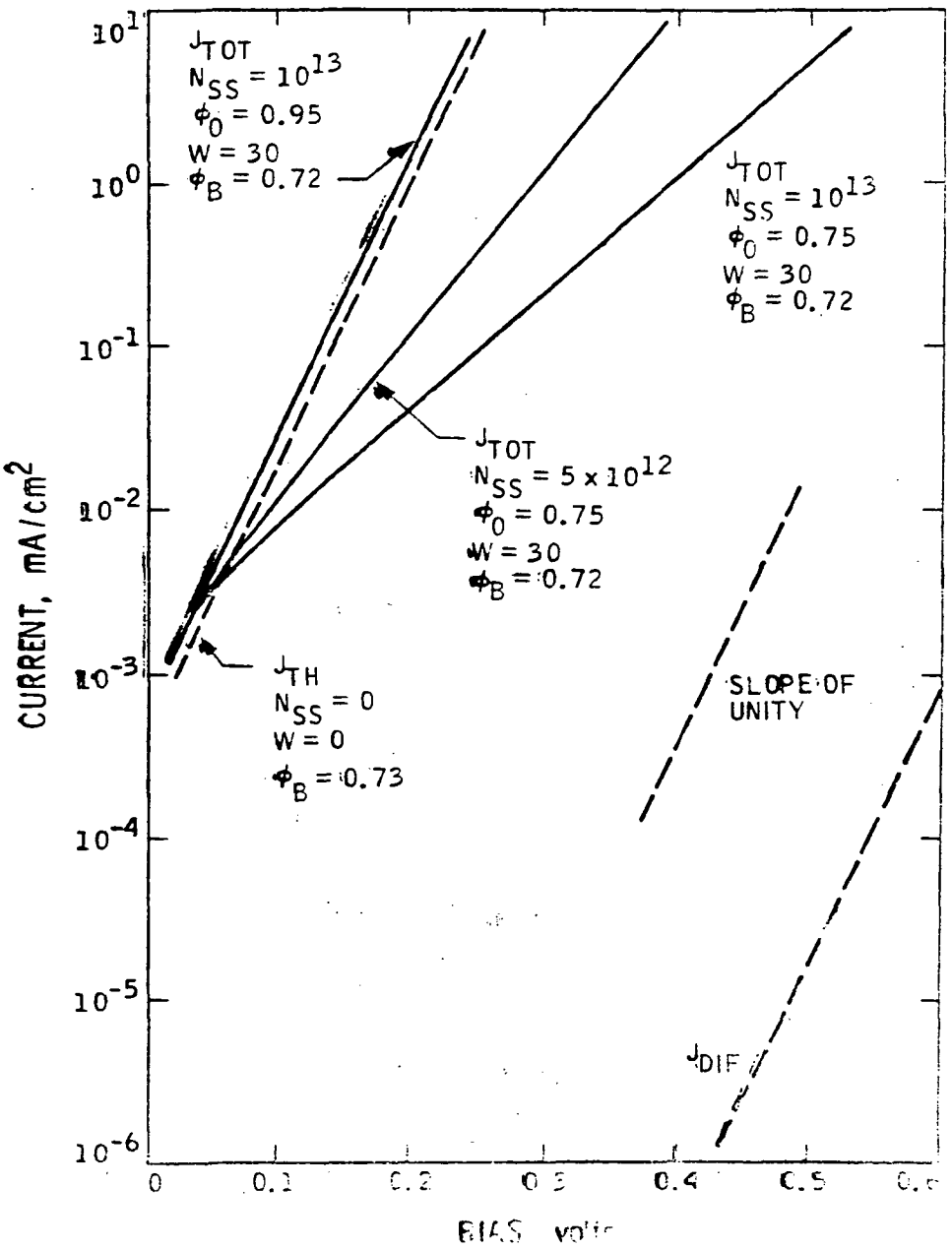

EFFECT OF FIXED CHARGE ON BARRIER HEIGHT

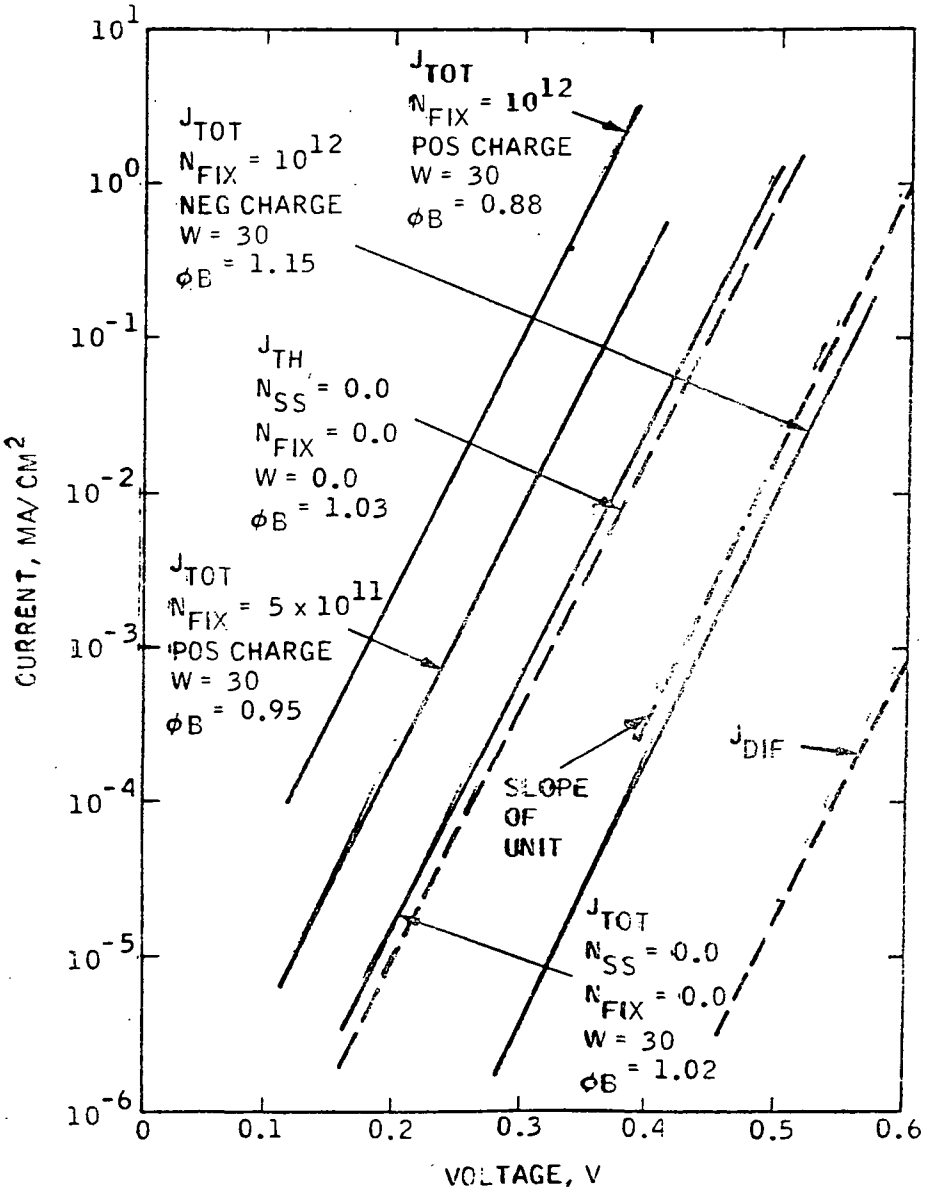

TRANSPORT CONTROL BY TUNNELING

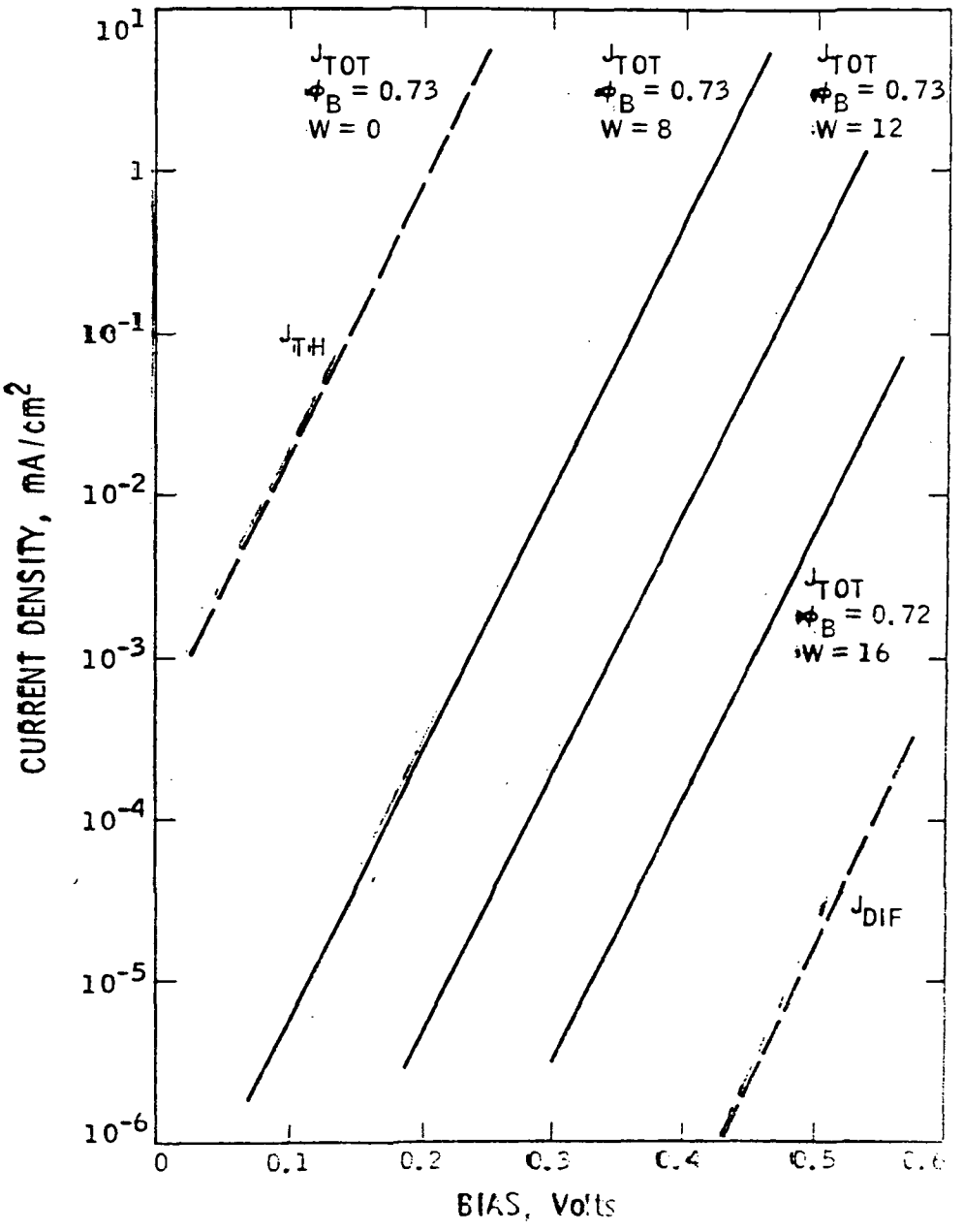

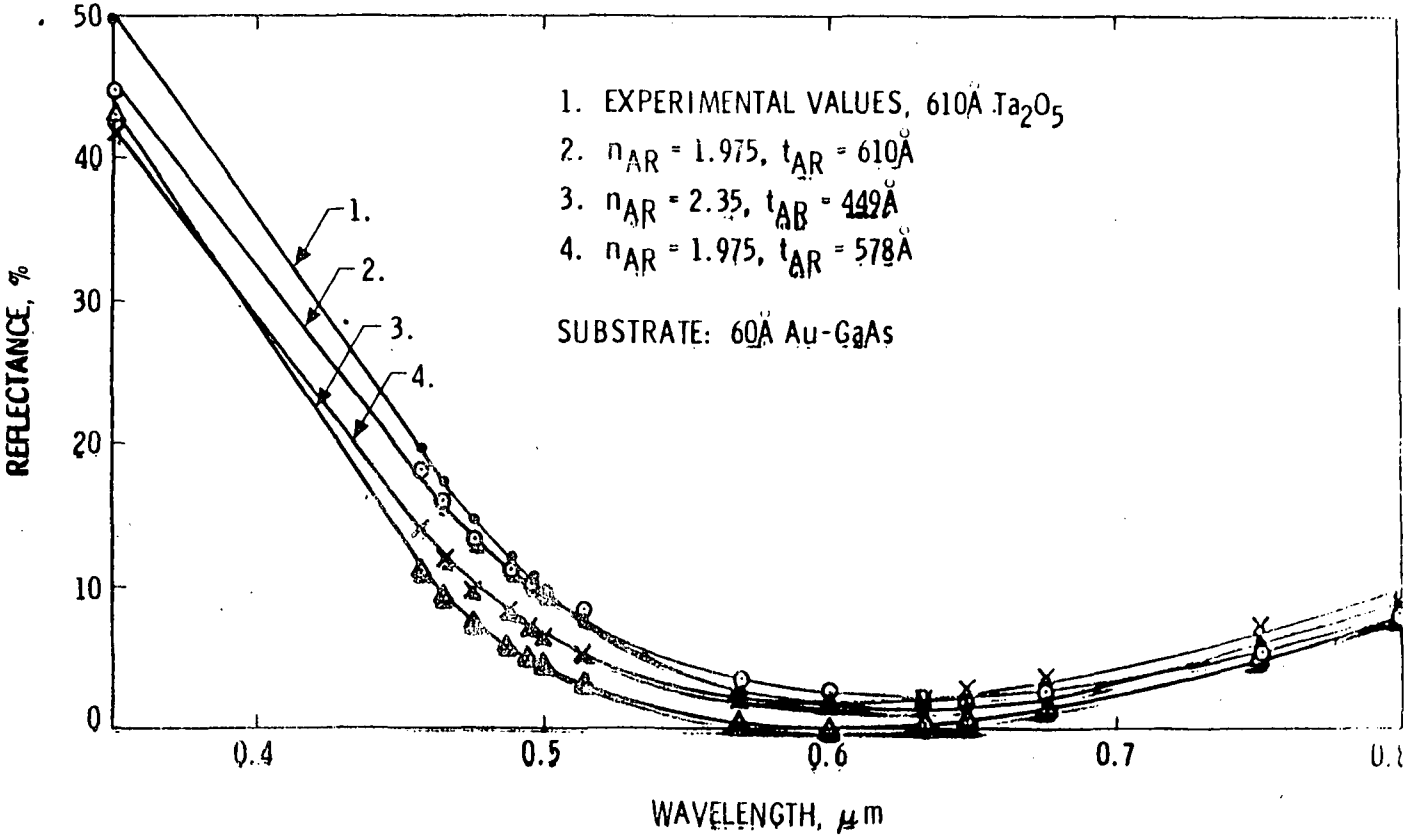
1. EXPERIMENTAL VALUES, 610Å Ta_2O_5
2. n_{AR} = 1.975, t_{AR} = 610Å
3. n_{AR} = 2.35, t_{AR} = 449Å
4. n_{AR} = 1.975, t_{AR} = 578Å
SUBSTRATE: 60Å Au-GaAs
REFLECTANCE, %
WAVELENGTH, μm
50
40
30
20
10
0
0.4
0.5
0.6
0.7

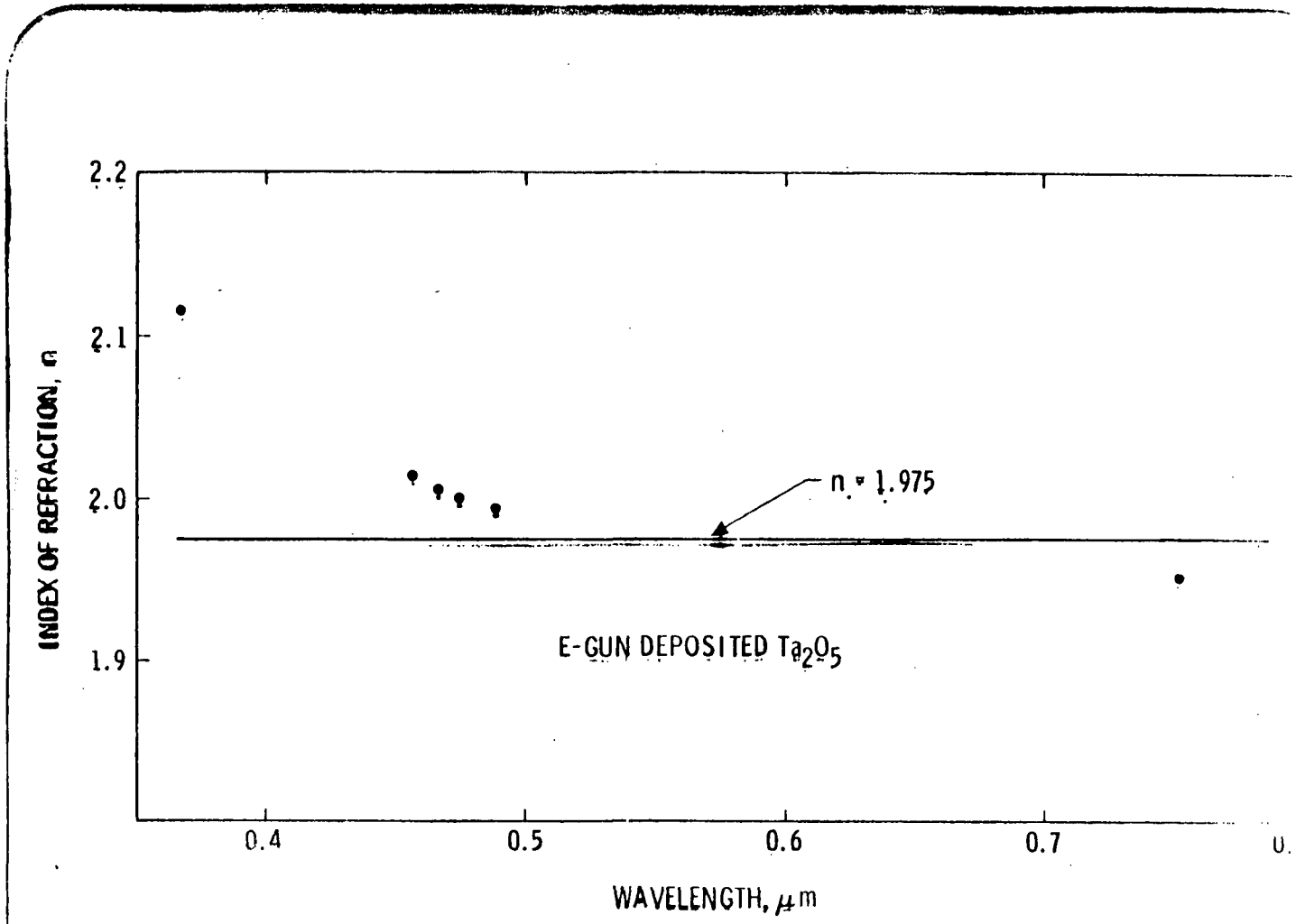
2.2
2.1
2.0
1.9
INDEX OF REFRACTION, n
n = 1.975
E-GUN DEPOSITED Ta_2O_5
0.4
0.5
0.6
0.7
WAVELENGTH, μm

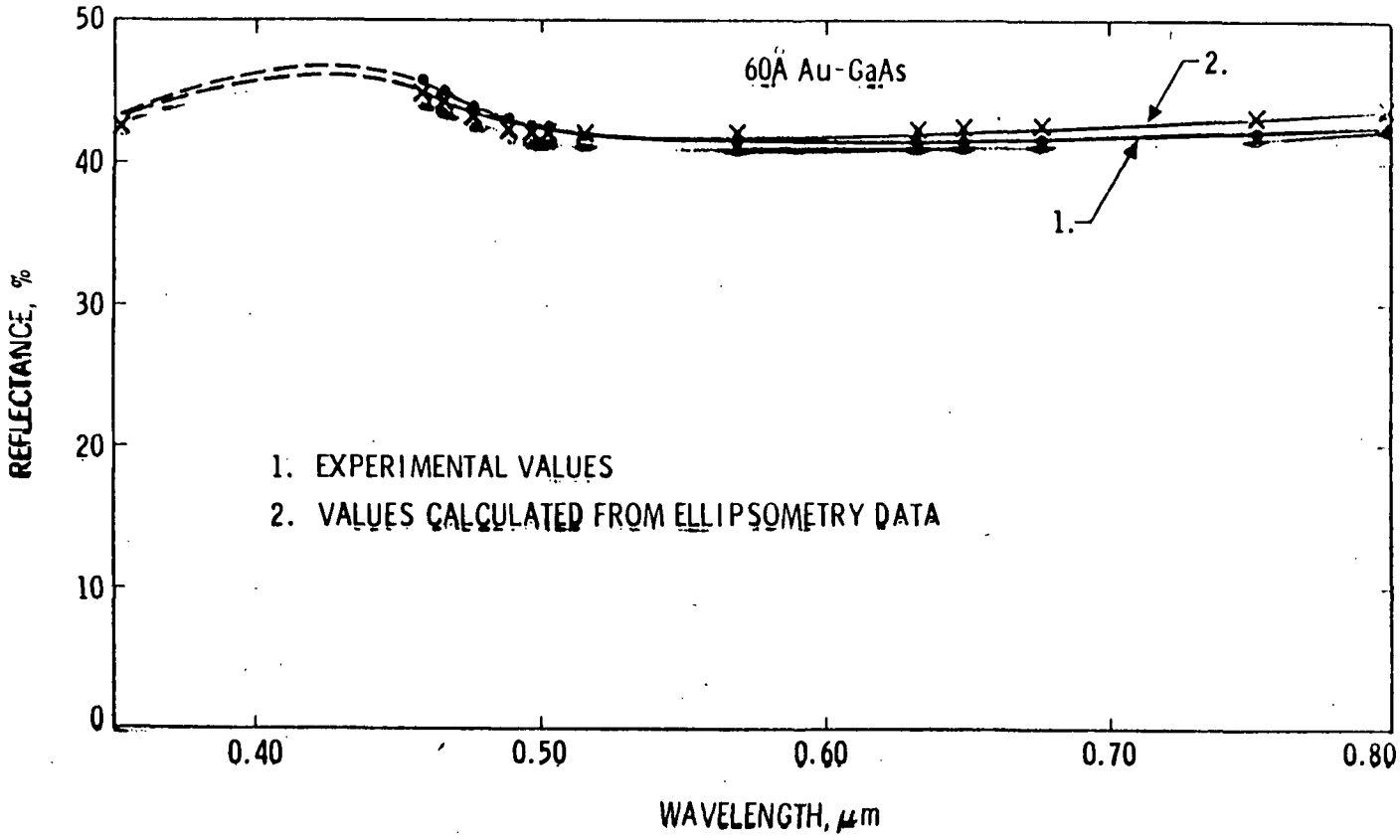
60Å Au-GaAs
2.
1.
1. EXPERIMENTAL VALUES
2. VALUES CALCULATED FROM ELLIPSOMETRY DATA
REFLECTANCE, %
50
40
30
20
10
0
0.40
0.50
0.60
0.70
0.80
WAVELENGTH, μm

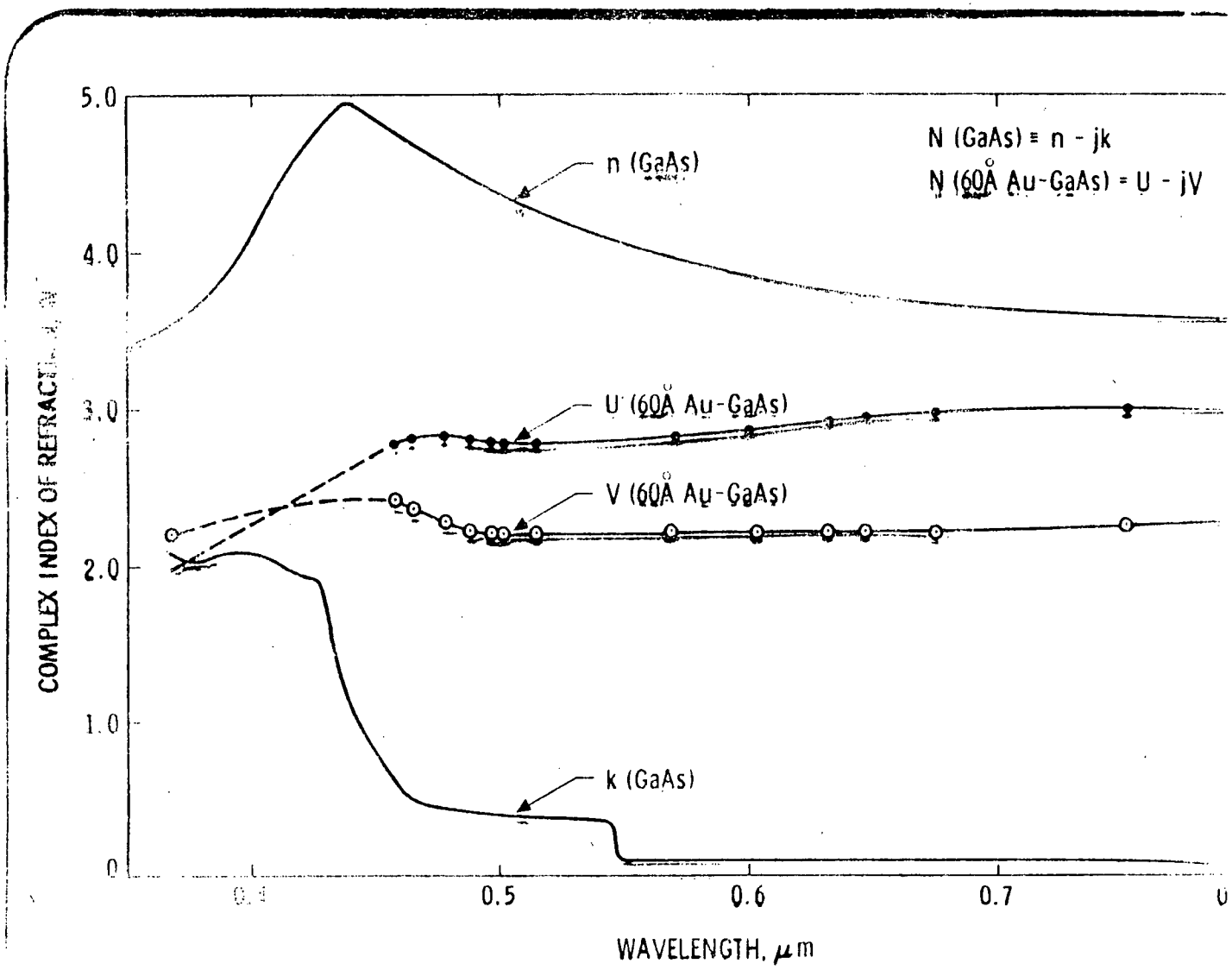

OPEN CIRCUIT VOLTAGE OF AMOS CELL AT VERY HIGH LIGHT INTENSITY

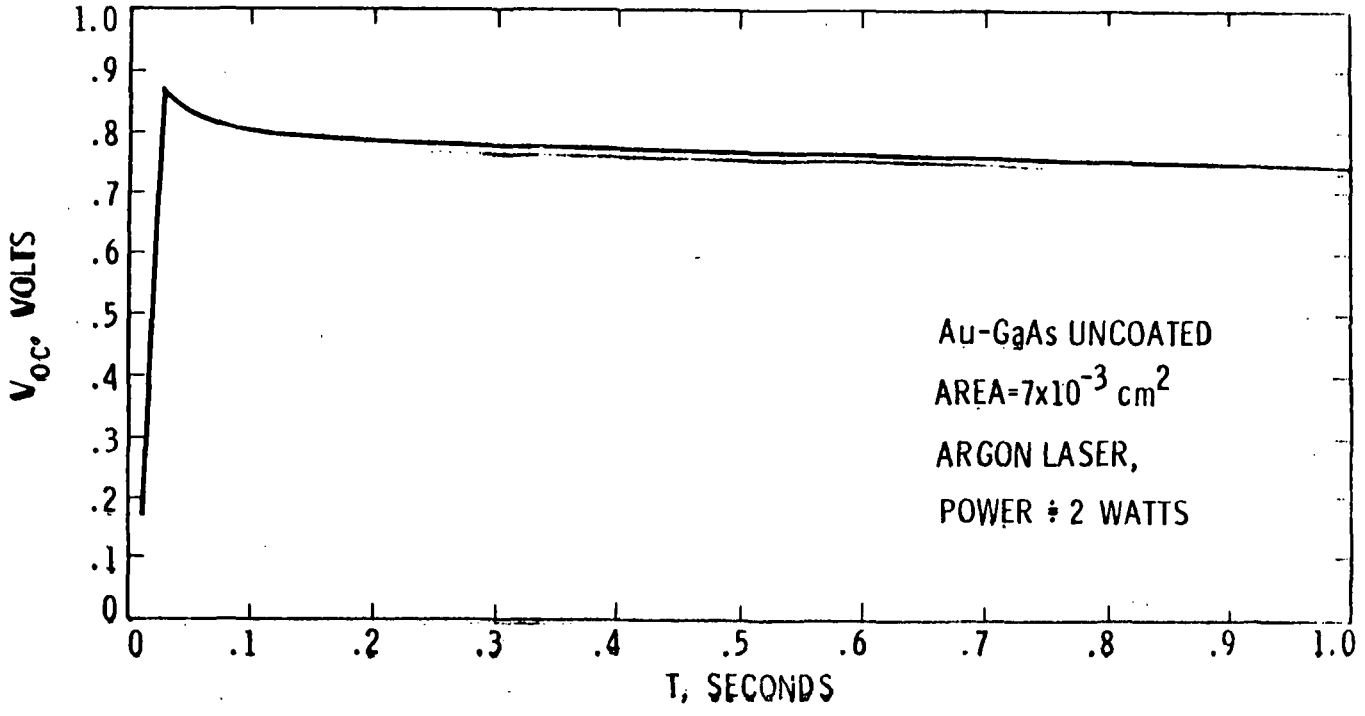

LIGHT I-V CURVE FOR AMOS CELL

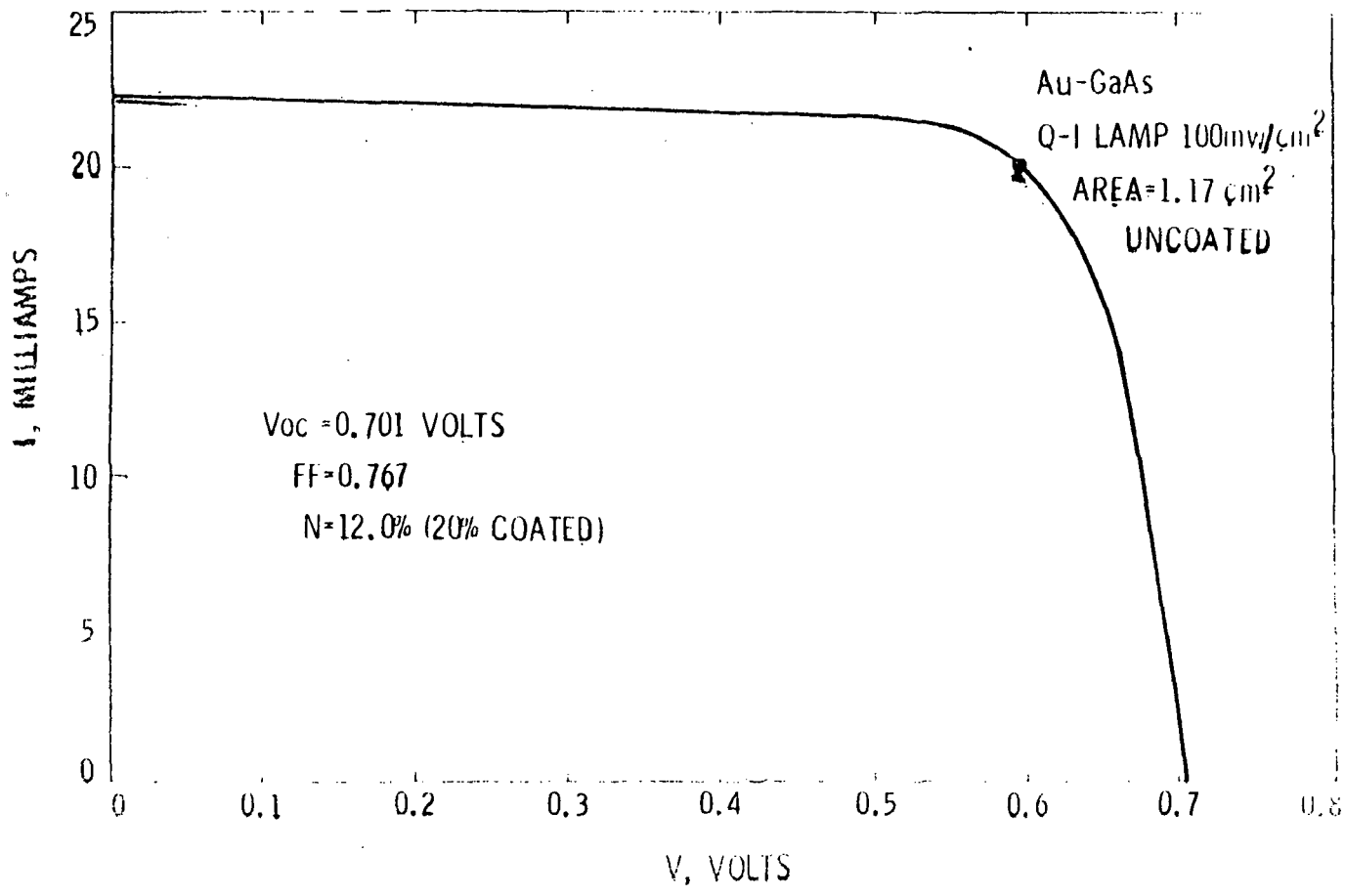

LIGHT I-V CHARACTERISTICS

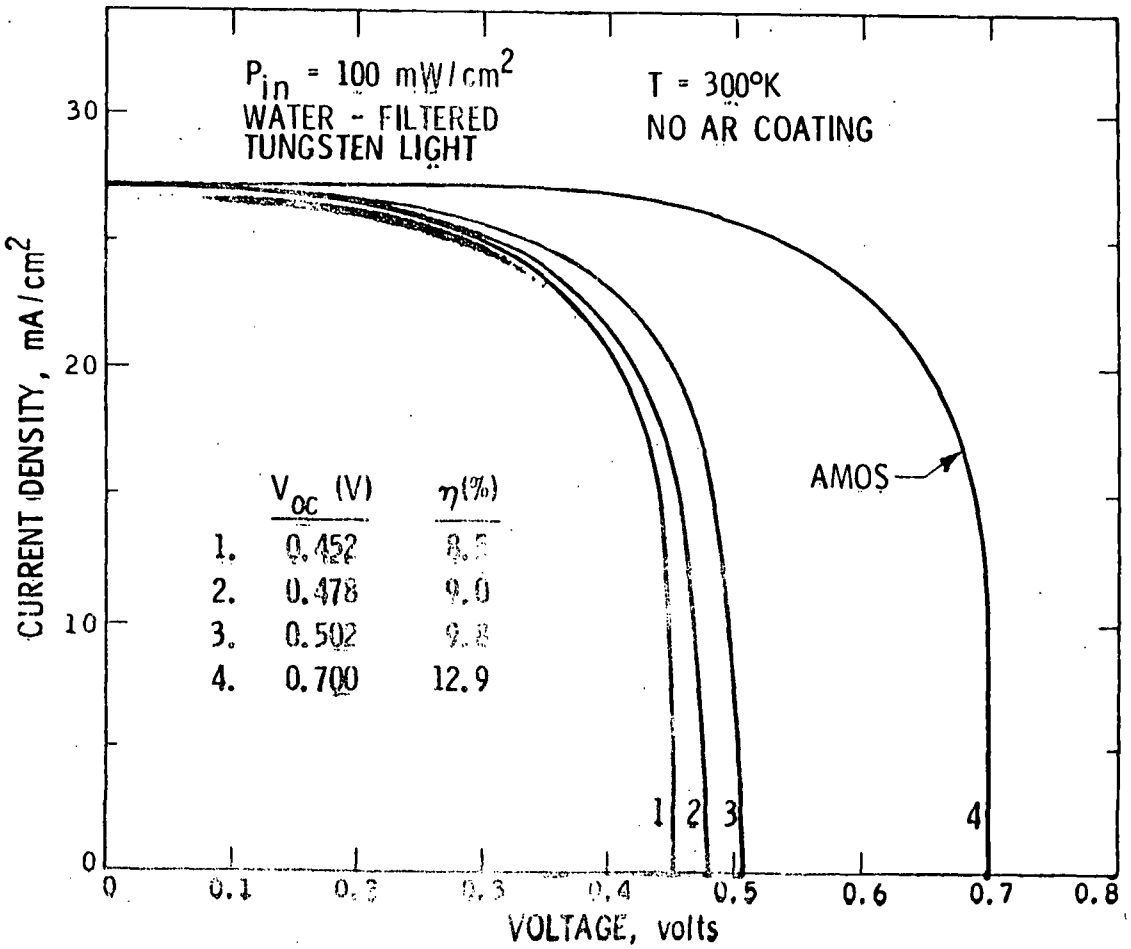

ABSOLUTE SPECTRAL RESPONSE

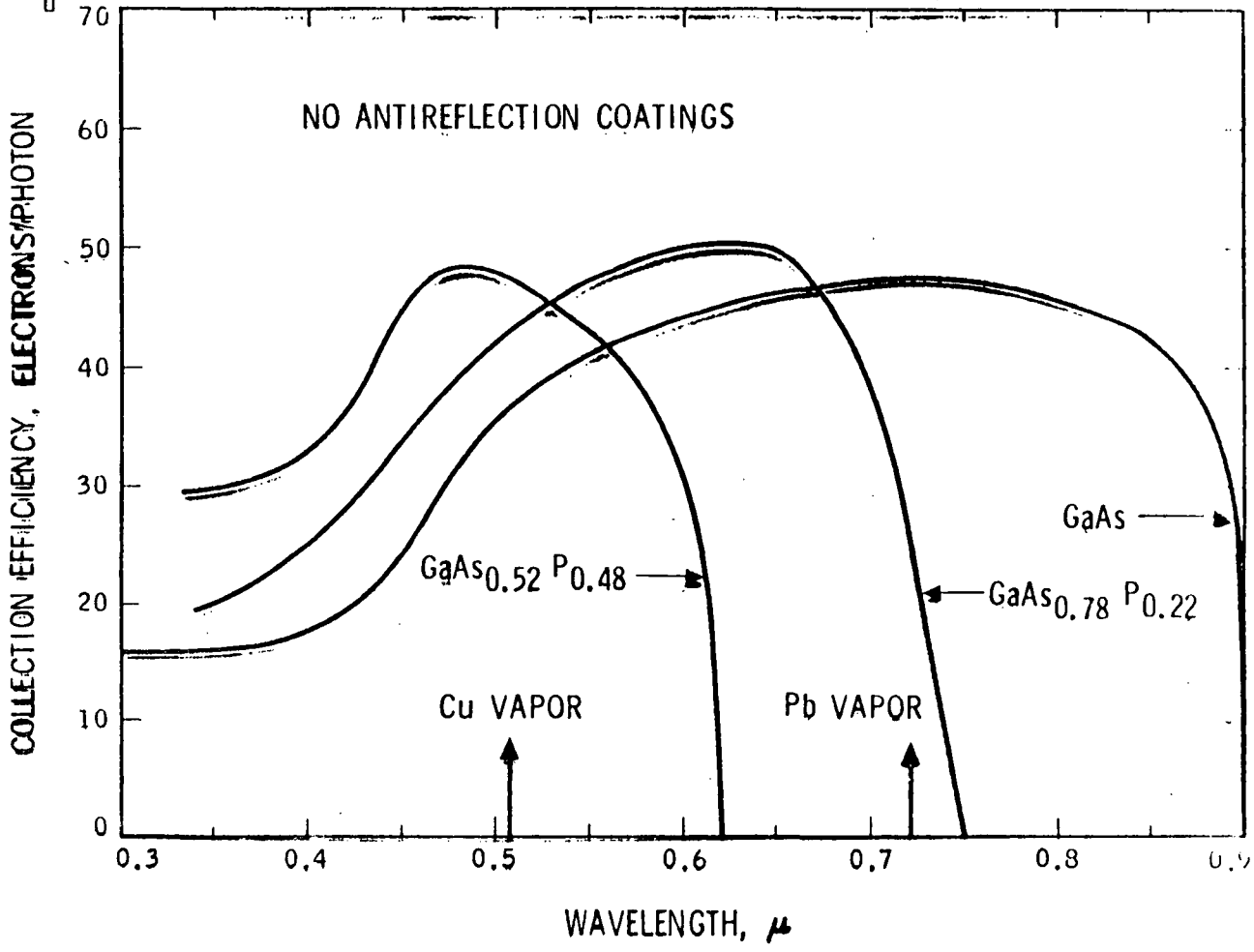

SCHOTTKY BARRIER GaAs SOLAR CELLS (AMOS)

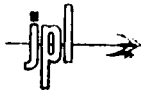

Richard J. Stirn

JET PROPULSION LABORATORY
CALIFORNIA INSTITUTE OF TECHNOLOGY

THIRD WORKING MEETING ON GaAs SOLAR CELLS
SEPTEMBER 24-25, 1975

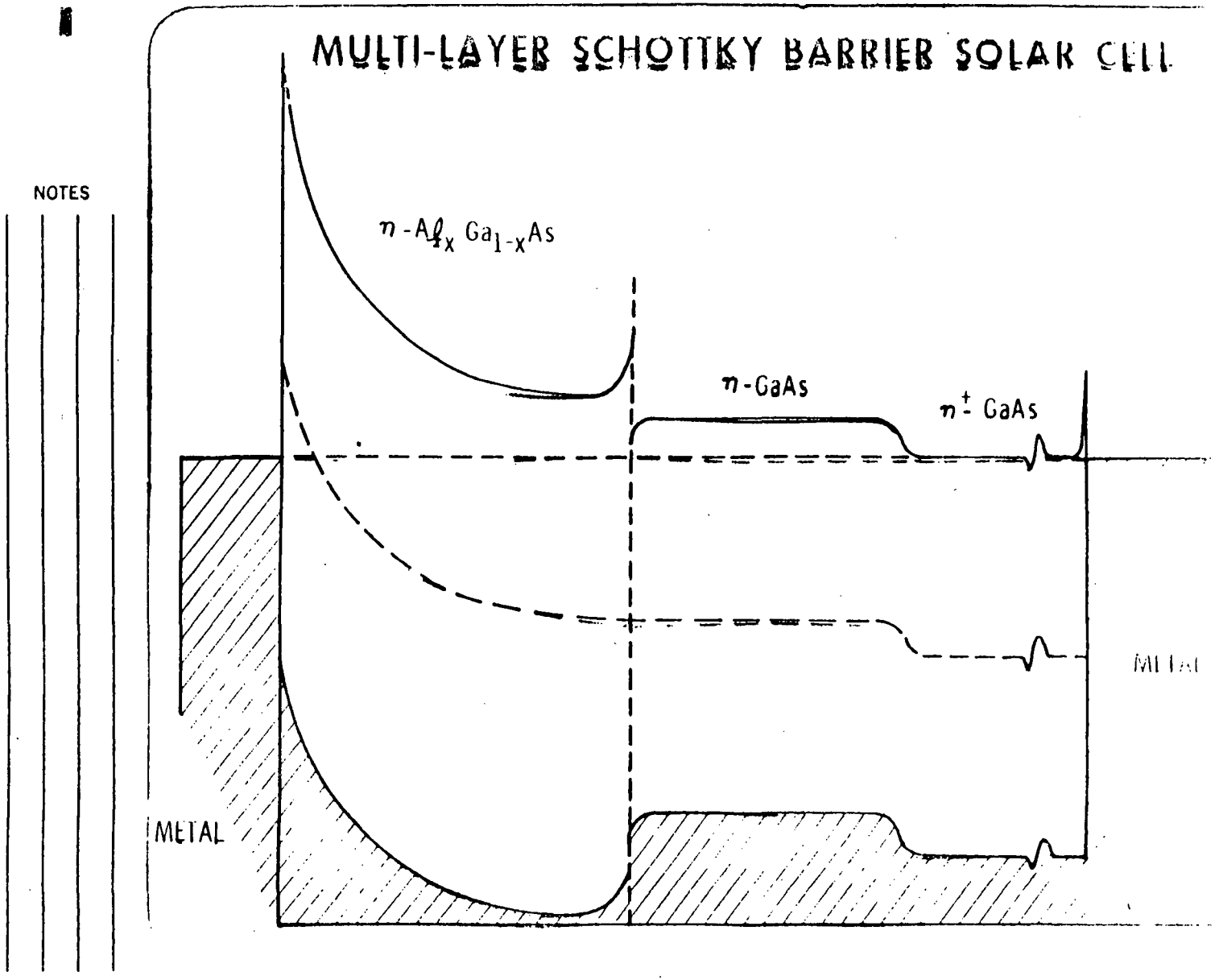
MULTI-LAYER SCHOTTKY BARRIER SOLAR CELL
NOTES
n -Al$_x$ Ga$_{1-x}$As
n-GaAs
n$^+$ GaAs
METAL
METAL

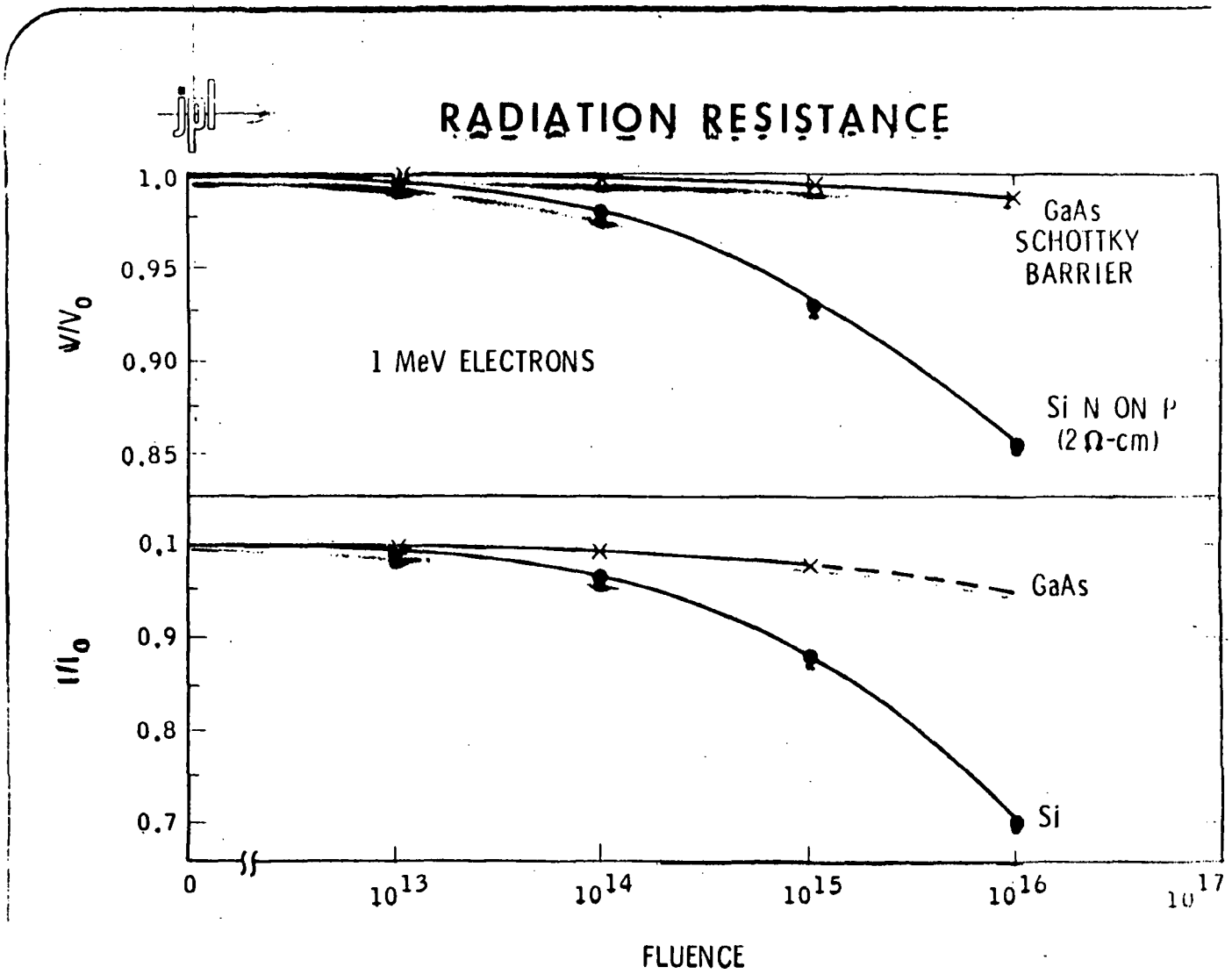
RADIATION RESISTANCE
1.0
0.95
0.90
0.85
V/V0
1 MeV ELECTRONS
GaAs
SCHOTTKY
BARRIER
Si N ON P
(2 Ω-cm)
0.1
0.9
0.8
0.7
I/I0
GaAs
Si
0
10^13
10^14
10^15
10^16
10^17
FLUENCE

GALLIUM ARSENIDE GRATING SOLAR CELLS: STATUS REPORT

SEPTEMBER, 1975 NASA GRANT NGR-40-002-093
BROWN UNIVERSITY
PROVIDENCE, RI

Report Presented by E. E. Crisman

Abstract

A grating pattern of zinc stripes, alloyed into the surface of a single crystal, GaAs, n-type wafer, has been used to produce a p/n junction for photovoltaic conversion. A PV cell has also been constructed with a very shallow junction between the zinc fingers. This second device is produced by taking advantage of the high ratio between diffusion coefficients of zinc for a phosphor silica glass/GaAs interface and GaAs bulk. Problems of uniform zinc deposition are discussed and initial results are presented.

- - - - -

Previously [1], we have reported silicon photovoltaic devices made by alloying fine stripes of aluminum (a p-type dopant) into the surface of n-type, 1 to 10Ω-cm silicon wafers. Devices made by this procedure have, to date, exhibited 8% efficiencies with short circuit currents equal to or greater than commercial cells and with extended response into the high energy photon regime. The object was to produce a device with characteristics superior to present day commerical solar cells by a simplified process which would avoid many of the steps involved in "standard" solar cell fabrication.

A similar effort has been undertaken to construct such "grating" type cells on GaAs wafers.* Zinc was used as the p-type dopant, since a relatively low (412°C) eutectic exists for the zinc-gallium arsenide system. (This temperature

*The work reported here constitutes essentially the M.S. thesis material of L. J. Walker currently with the Southern Company of Atlanta, Georgia.

is also compatible with the heat treatment temperature required to bond ohmic indium contacts to the opposite face of the base wafer.)

Figure 1 is a schematic representation of a grating cell. The base wafer contacts were made by electroplating In onto that surface following the method described by Fainer et al. [2]. In our case, we used a 0.1 molar $In(SO_4)_3$ solution and a current of 300 mA/cm^2. In properly fabricated grating cells, the line width should be as narrow as possible and the spacing between grating lines should be less than twice the minority carrier diffusion length in the base wafer. In the best n-GaAs described in the literature, the hole diffusion length is about 5μ; this means that the line spacing should be about 10μ. We did not use n-GaAs of this quality since our main purpose in this preliminary work was to develop techniques for making such cells from n-GaAs. For this same reason, we used a much coarser grid pattern than that which would be optimum. Scaling the grid dimensions down to say 1μ stripes, 10μ apart would not be difficult.

The first problem to be surmounted is the deposit of a fine-grain layer of Zn on GaAs: the grain size must be small compared to finger width. We found that this goal could not be accomplished by simple evaporation of Zn directly onto the GaAs. Figure 2 shows the best film obtained by direct evaporation of Zn; a 2 micron wide strip is shown on the figure for reference. The GaAs substrate was at or slightly above room temperature. Evaporation was performed at 5×10^{-2} torr pressure. Visual appearance of the film was a mat gray, and the zinc conglomerates were of the order of 8 microns in length. Using a method suggested by Holland [3] attempts were made to induce larger nucleation densities by evaporating a thin layer of tin before the zinc. Figure 3 shows the result of this approach with about 6Å of Sn evaporated @ 5×10^{-5} torr on a substrate at 25°C. Grains of about 1μ were produced in this fashion. Further reductions in zinc grain

sizes were induced by heating the substrate before the zinc evaporation. Figures 4 and 5 show the results for substrate temperatures of 56°C and 70°C respectively. The grain sizes for these two temperatures were 0.4 micron and 0.1 micron. We found that the nucleating layer of tin led to reduced grain size in Zn layers between 2 and 30 microns thick and that grain size decreased as the substrate temperature increased from room temperature to 100°C. For our cells we selected a Zn thickness of about 0.4μ. As the first step in cell fabrication, an Sn-Zn layer was evaporated on n-type GaAs (Te doped to 1.4×10^{17} /cc) whose diffusion length, as reported by the supplier, was 0.75 microns. After evaporation the cell was coated with GAF PR-102 photoresist and exposed through a mask with 35μ lines spaced 50μ apart. After developing, Transene Brand Aluminum Etch was used to remove the zinc. The remaining photoresist was stripped and the cell heated to 500°C with quick cooling to room temperatures @~100°/min. The surface of the cell after heat treatment was examined using a 7.5 Kev energy scanning electron microprobe beam. By operating the cell in the electron-voltaic mode and connecting the cell output to the z(intensity)-axis of the display scope, the picture shown in figure 6 was generated. Here, the bright vertical lines are regions having a photovoltaic sensitivity; these stripes occur at the Zn/GaAs interfaces. The completely dark areas are the uncoated regions between fingers, and the dark areas with occasional light spots are the zinc figures. The light spots are places where the zinc film was thin enough to allow 7.5 KeV electron penetration into the junction below the zinc. Such a sensitivity vs. position picture is to be expected since the diffusion length was < 1μ for the base material and the stripe spacings were about 50 microns. By adding the device output to the vertical deflection plates of the display scope, pictures such as those of figures 7 and 8 can be generated. In the first of these the microprobe beam is allowed to travel only once across the

sample at a given position. The sensitive regions at the edges of the fingers are now quite evident as spike-like projection; there is also some response indicated in regions where the beam penetrates the finger region. The regions between the fingers show no response. In figure 8 another method of display is shown in which the microprobe beam is swept across the sample in the y- as well as the x-direction to give a 3-dimensional map of response versus position. The surface of the sample was subjected to electron microprobe examination to determine whether there was any zinc in the region between the fingers; the conclusion was that Zn was confined to the Zn-stripes only. Since this sample was constructed primarily to define the processing steps further measurements were not made on it. No significant photovoltaic response was expected because of the large proportion of dead area. To date we have managed to define with our photoresist technique 1.5μ line patterns spaced 3.5μ apart, and this layout will be used on subsequent devices when material with longer diffusion lengths are received.

A variation on the finger pattern approach, also being pursued by us, is based on the work of Baliga and Ghandi [4] who have measured diffusion of certain metals along the interface between phosphor-silica glass and GaAs. They have measured ratios for interface/bulk diffusion rates of up to 20/1 for zinc and 500/1 for tin by controlling the phosphor content in the glass layer (and hence the interface stresses resulting when the sample is cooled after glass formation). We hope that extremely thin (< 500Å) junctions can be formed in the inter-finger region by this method thereby relaxing the requirement that the spacing be maintained at about 1 to 2 diffusion lengths. At the same time the sheet resistance will be kept low because of relative large number of fingers present. For our work we have used the thermal decomposition of ethyltriethoxysilane, $(C_2H_5)Si(OC_2H_5)_3$, with trimethyl phosphate, $(CH_3O)_3PO$, on 2 x 10^{17} /cc, Te doped, 0.008Ω-cm gallium arsenide with a

2.7μ diffusion length and a <100> ±2° orientation. A layer between 2500Å and 3000Å of the glass was grown at 700°C in an argon transporting atmosphere. Using the 35/50 micron mask as above, windows were opened in the glass layer and diffusion was carried out in a sealed silica ampoule loaded with 1 gm of arsenic and 5 gms of zinc and evacuated before sealing to 1×10^{-5} torr. Diffusion occurred for 10 min. at 800°C. The electron microprobe map of the zinc distribution over the surface shown in figure 9 indicates that zinc is present in the region between the mask openings. When this same region is examined via the electron-voltaic (intensity enhanced) mode in figure 11, it is evident that there is some response from most of the region between the diffusion fingers. (Large "dead" spots which have no counterpart in the optical, secondary electron (figure 10) or zinc K-α maps are also evident.) A number of deflection enhanced electron-voltaic scans were produced at varying voltages of the microprobe beam energy. These are shown in figures 12 through 16 for 30.1 KeV (∿3.0μ penetration), 27.3 Kev (∿2.5μ), 24.4 Kev (∿2.0μ), 17.3 Kev (∿1.0μ), and 12.2 Kev (∿0.5μ). From these we conclude that the junction depth between the fingers was 2-3 microns rather than the planned 1000Å. This is also supported by the rather low response to 140 mw/cm^2 illumination shown in the i-V plot for this device (figure 17).

These preliminary results indicate that it is possible to produce a photovoltaic device on GaAs by alloying a grating of well separated Zn stripes and by the laterial Zn diffusion technique. Since the cells produced to date are far from optimum design, no estimate of ultimate efficiency can be made at this time. However, by analogy with grating cells produced on silicon, it is reasonable to expect short circuit currents comparable to or greater than those of cells produced by standard diffusion methods. If the open circuit voltage of the alloyed Zn junction is comparable to that of diffused Zn junctions, the efficiency of cells produced by this low temperature, simple method should be comparable to that of standard Zn diffused cells.

1. "Summary of Theoretical and Experimental Investigations of Silicon Grating Type Photovoltaic Cells," NASA Grant NRG-40-002-093/2, Brown University, 1975.

2. Fainer, M. Sh., Obukhovskii, Ya. A., Sysolv, L. A., and Gaisinskii, V. B., Soviety Physics--Semiconductors, 3, 11, pp. 1465-66, 1970.

3. Holland, L., Vacuum Deposition of Thin Films, Chapman & Hall, London, 1958.

4. Baliga, B. J., and Ghandi, S. K., IEEE Trans. on Electronic Devices, ED-21, 7, pp. 410-415, 1974.

DIS

C.2

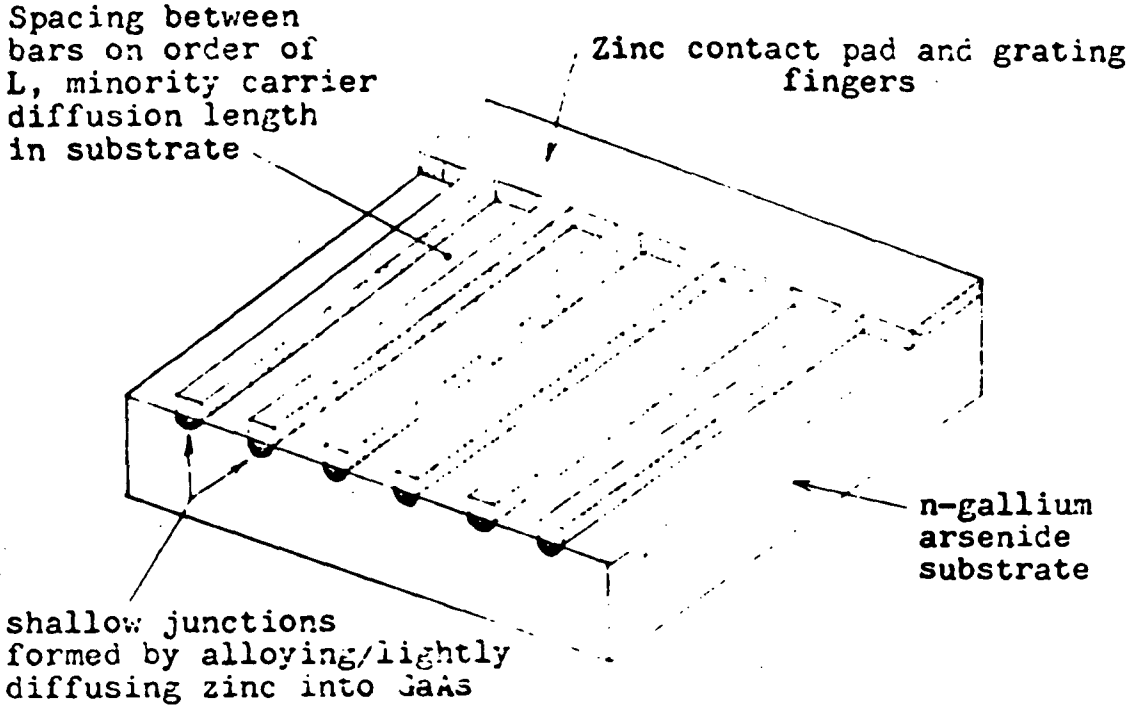

VII-1 THE GRATING STRUCTURED CELL

Fig. VII-2 Zinc film on gallium arsenide with no nucleating layer. Secondary electron SEM at 5000X, substrate temperature 24-25°C. Width of deposited zinc conductive bar superimposed.

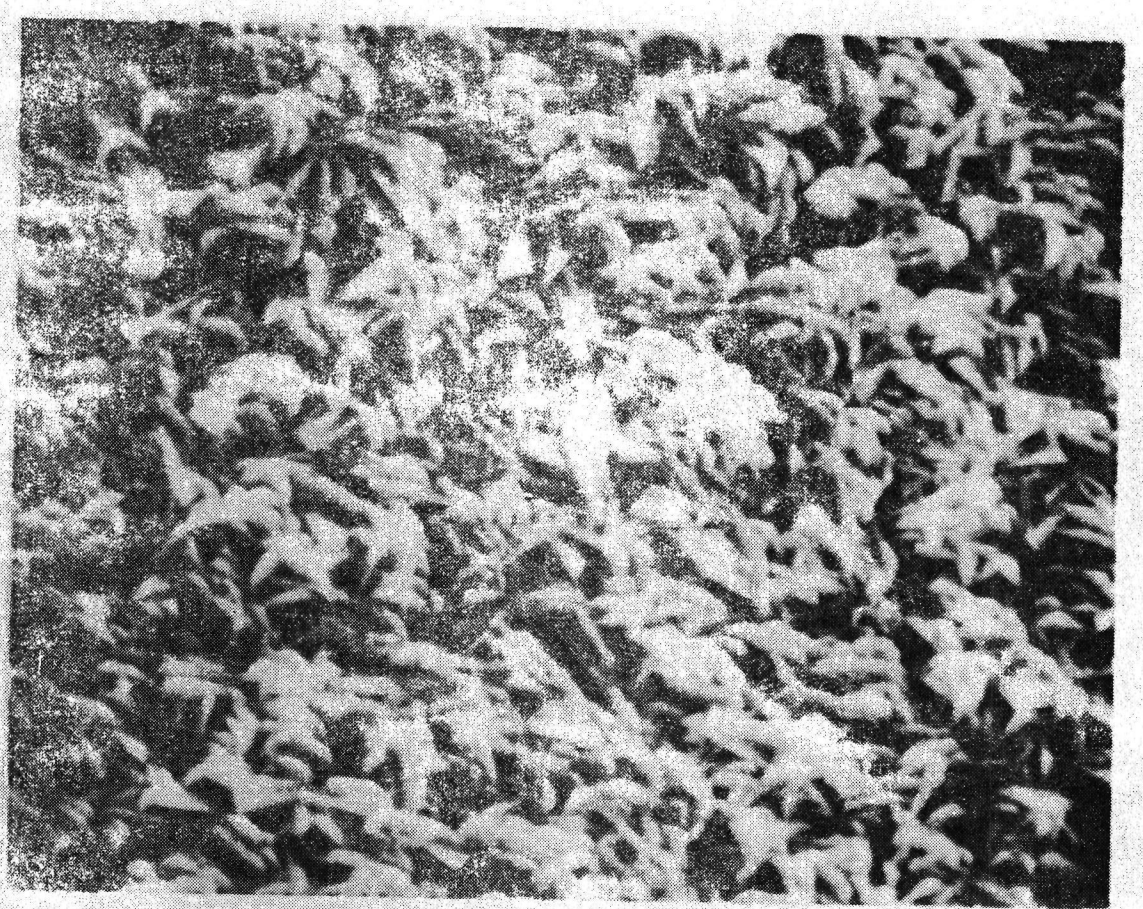

Fig. 11a-Zinc on GaAs with approximately 6 angstroms of nucleating tin. Secondary electron SEM at 5000X, substrate temperature 24-25°C.

Fig. VII-4 Zinc on GaAs with approximately 2 angstroms of nucleating tin, seconds elevation and at 5000X [illegible] during evaporation.

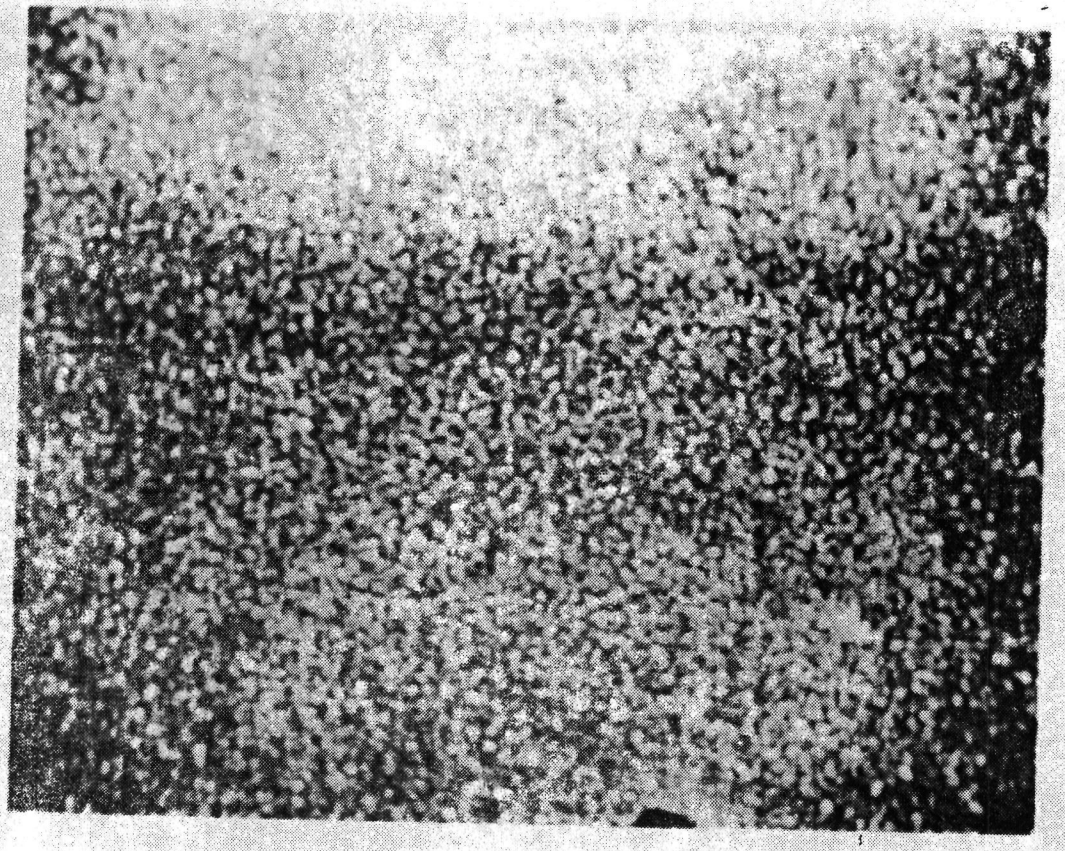

Fig. VII-5 Zinc on GaAs with approximately 8 angstroms nucleating tin. Secondary electron SEM at 5000 X, substrate temperature 70°C during evaporation. SEM taken near edge of sample. One of the smoothest zinc films obtained. Visual appearance totally specular.

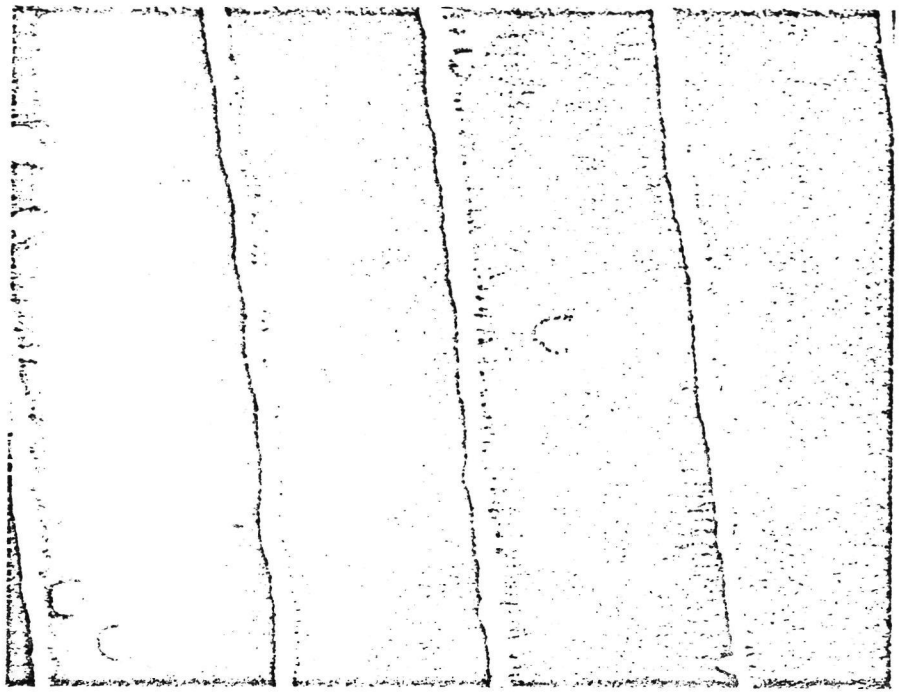

Intensity enhanced electron-voltaic response. Brighter bands represent regions of peak cell short circuit current as produced by a 7.5 Kev electron beam sweeping across cell (spot size approx. 5000 Å). Occasional bright spots due to beam penetration of zinc contact fingers. Magnification 500X.

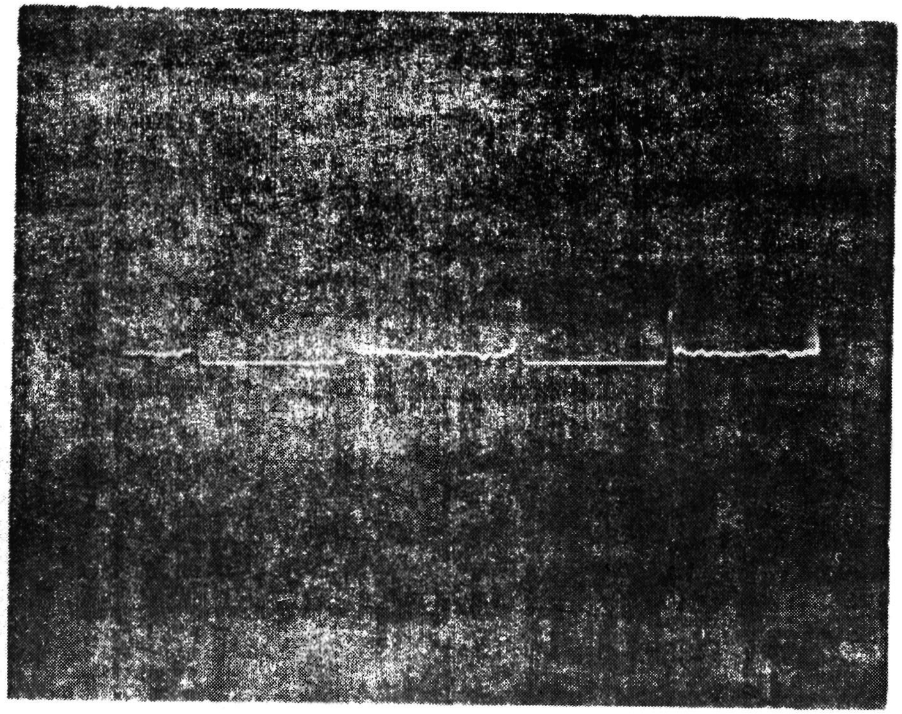

Fig. VII-7 Deflection-modulated electron-voltaic response of cell. Magnification 500X. Cross-sectional view of short circuit current (vertical deflection) as cell responds to single sweep of a 7.[illegible] [illegible] spot size approximately [illegible]. [illegible] deflection introduces a current [illegible] as measured by [illegible]ley [illegible] [illegible] 610 CR, slightly modulated [illegible] between [illegible] due to response from [illegible]. Width of bars ~ 10 microns, of spa[illegible] [illegible] response) ~ [illegible] microns.

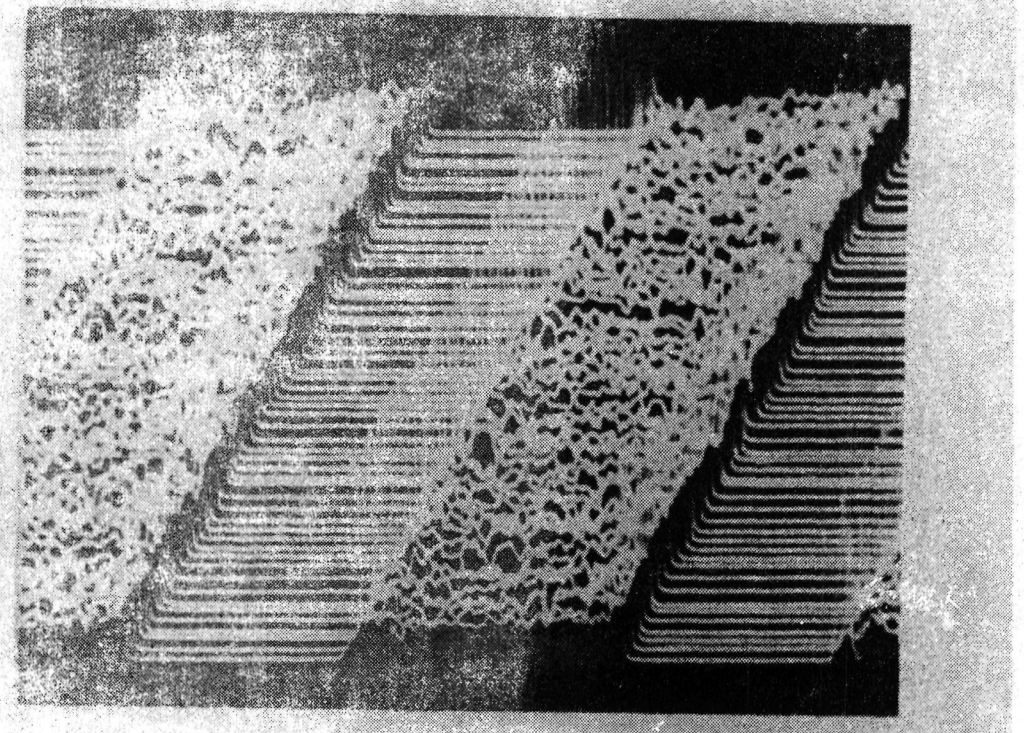

Fig. [illegible] Three-dimensional deflection-modulated electron-voltaic response of cell. Magnification 500X. View of short circuit current (vertical deflection) as cell responds to raster sweep of 7.5 Kev electron beam. Spot size approximately 5000 angstroms. Peak deflection 0.44 Amp as measured on Kiethley [illegible] electrometer. Slightly modulated areas between peaks due to response from beneath [illegible] bars. Width of bars - 50 microns, [illegible] spaced (smooth areas) - 35 microns.

Figure VII-2 GaAs, JM4-G1-19-n-a, map of Zn-K radiation, 30kV, I_{abs} = 0.2μamp, b.d. = 0.3 microns, magnification 500x, notice [illegible] at the arrows and [illegible] to arrows in figure 15. (SEM 29)

Figure 01-IIA GaAs, JM4-01-19-n-a, [illegible]
Image: 30kV, b.c.c. = 0.2 amp, o.d. = [illegible]
Magnification 500x, (SEM 28).

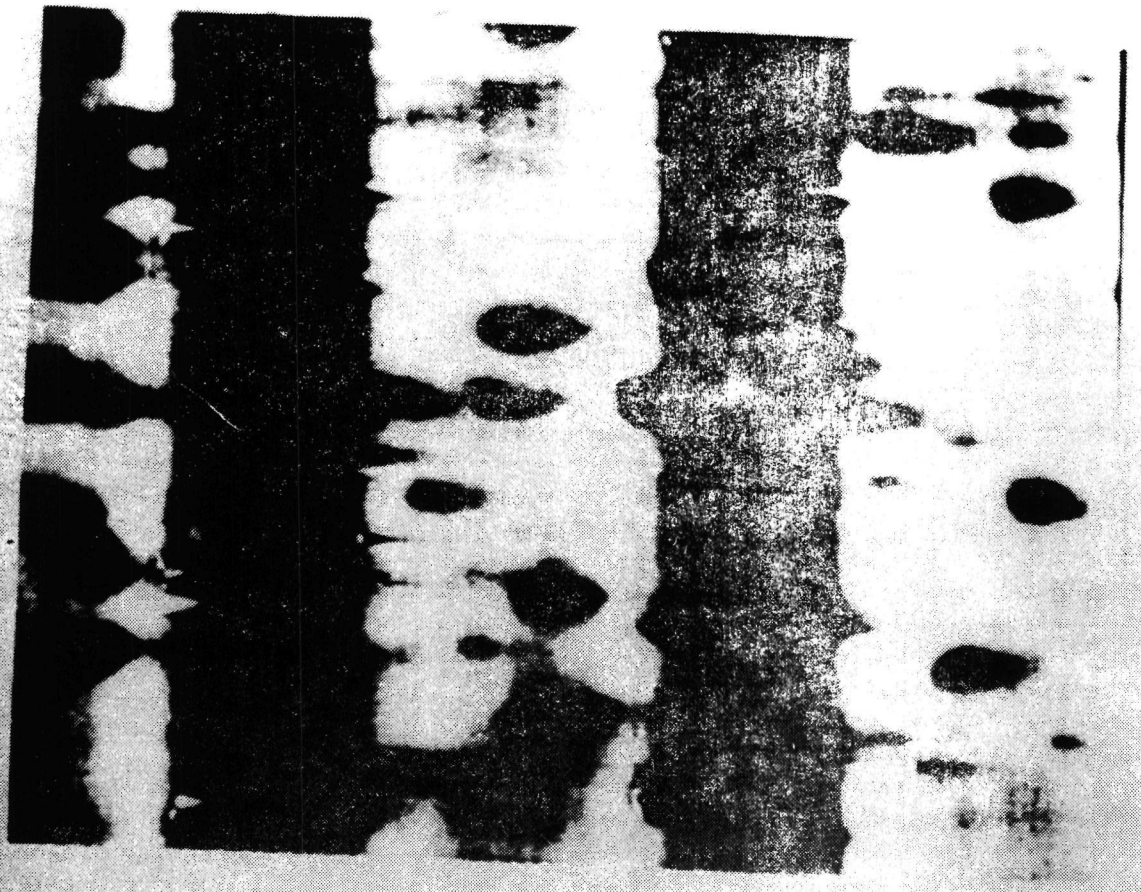

Figure VII-11 GaAs, JW4-G1-19-n-a, EBIC, 30kV, b.c.=0.2 amp, b.d.= 0.3 microns, Magnification 500x. (SEM 26)

VII-12

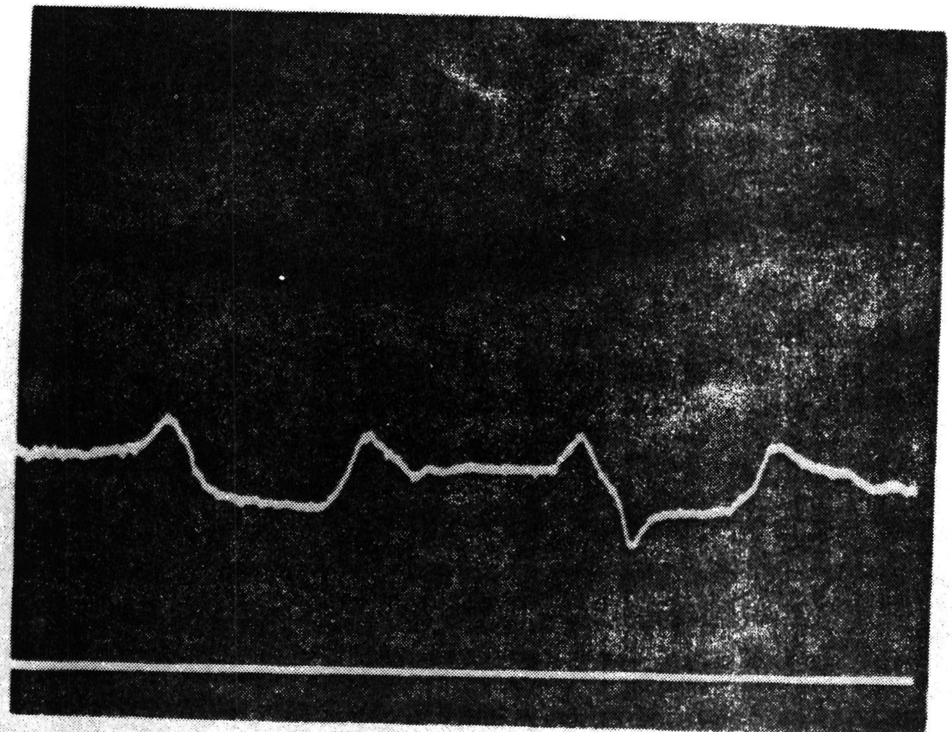

Figure VII-13 InAs, J-Gi-10-a, [illegible] profile with reference line 0 [illegible], 27 [illegible], [illegible] = 0.[illegible]μ[illegible], [illegible]d.= 0.3 microns, magnification [illegible]x. (SEM 34) [illegible]aximum (just off finger)= .[illegible]μ[illegible], minimum (on zinc finger)= .04μamp, [illegible] fingers= .05μamp.

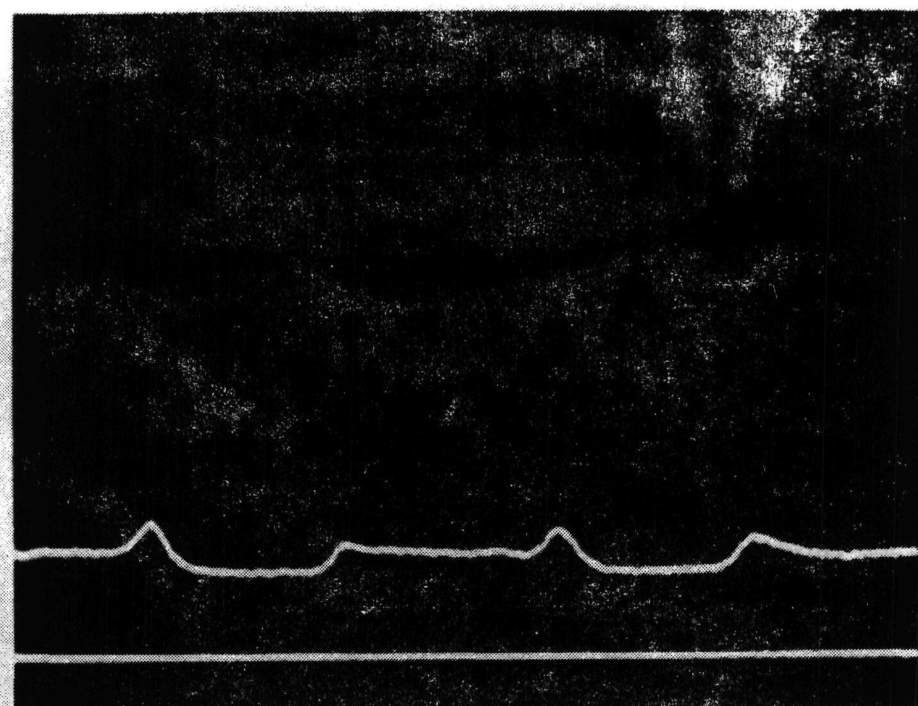

Figure VII-14 GaAs, JW[illegible] EBIC profile with reference line 0 amp, [illegible]kV, [illegible] = 0.[illegible] μamp, [illegible] = 0.5 microns, magnification [illegible]0x. ([illegible] 31) Maximum (just off finger) = .[illegible] μamp, minimum (on finger) = .[illegible] μamp, between fingers = .[illegible]5 μamp.

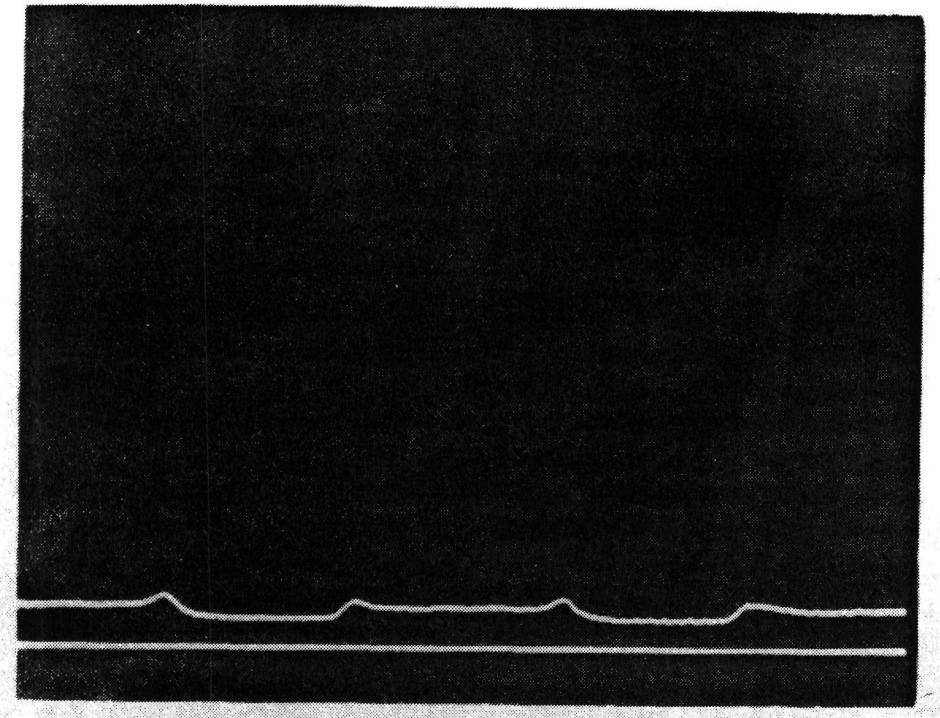

Figure VII-15 GaAs, JW4-D1-19-n-a, EBIC profile with reference line 0 amp, 17.3kV, p.c.= 0.8μamp, p.i.= .5 amp, ramification 500x. (SEM 32) Maximum (just off finger)= .0135μamp, minimum (on finger)= .007μamp, between finger= .01μamp.

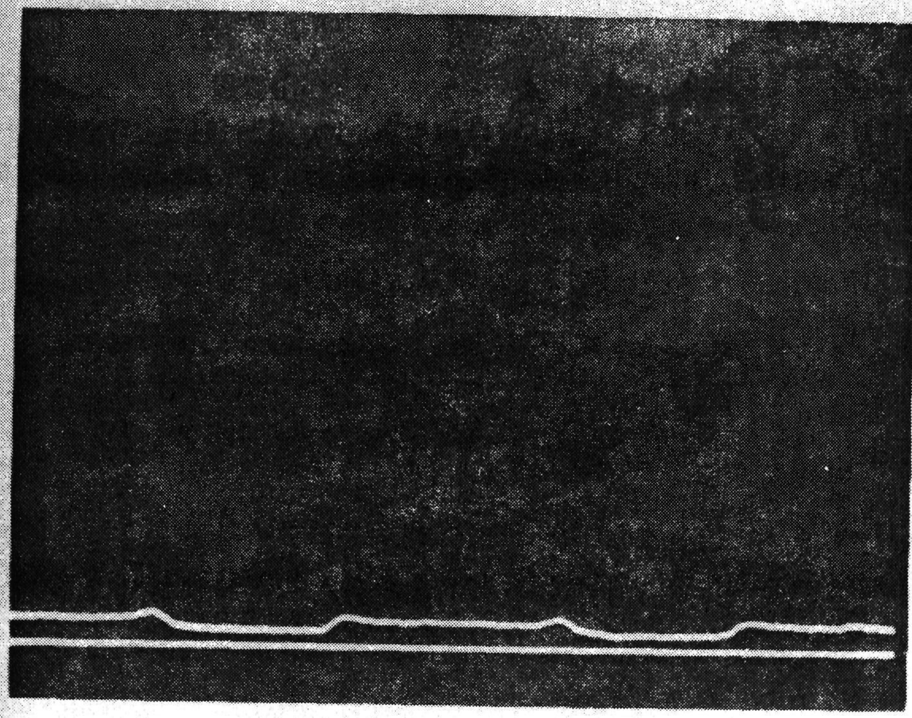

Figure VII-16 GaAs, JW4-G1-19-n-a, EBIC profile with reference line 0 amp, 12.2kV, b.c.= 0.4μamp, b.d.= 0.5 microns, magnification 50X. [illegible] 3) Maximum (just off finger)= .0085μamp, minimum (on finger)= .004μamp, between fingers = .0[illegible]μamp.

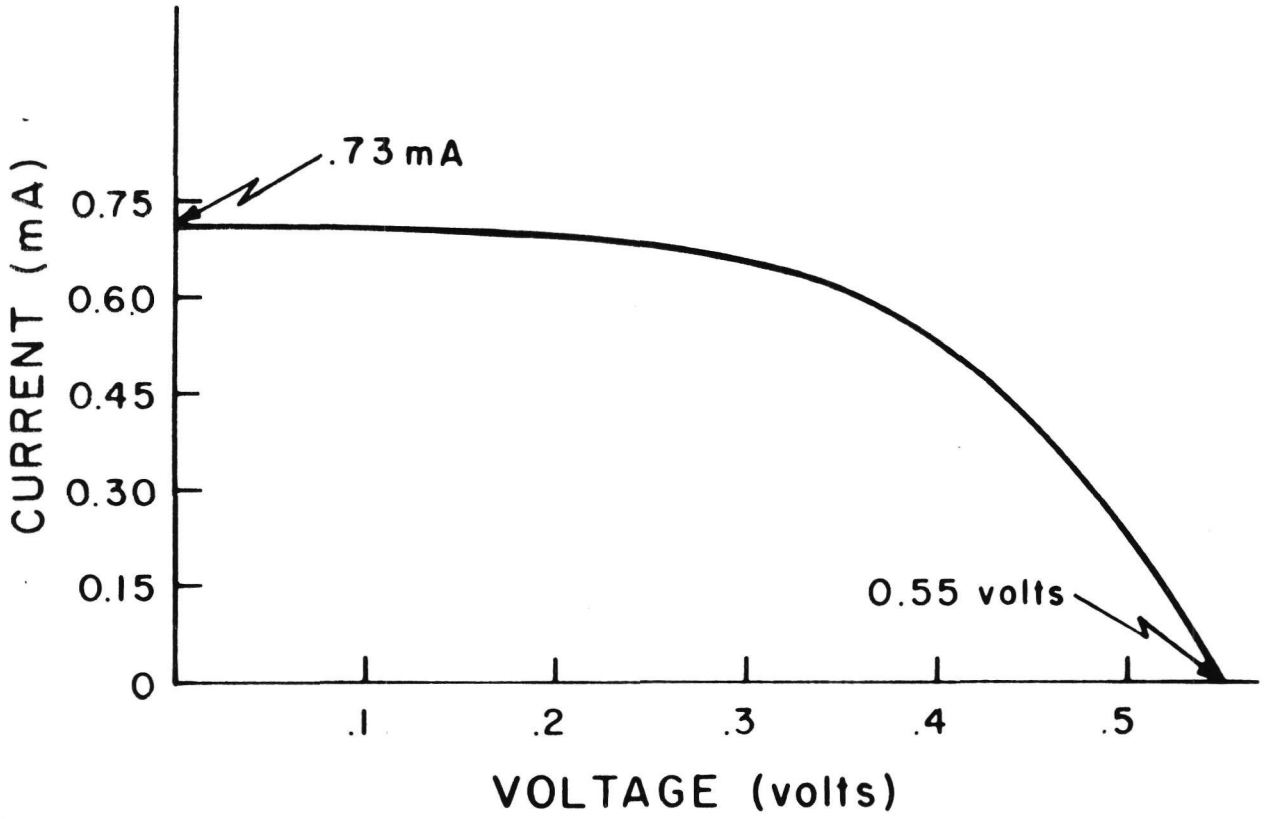

VII-17 Ga As SAMPLE # JW4 GI-19-n ILLUMINATED I-V CHARACTERISTIC @ AMO WITH SILICON CELL UNP-1 AS REFERENCE.

THEORETICAL AND EXPERIMENTAL EVALUATION OF A HIGH EFFICIENCY GRADED BAND-GAP N/P $Al_xGa_{1-x}As$-GaAs SOLAR CELL

J. A. Hutchby
NASA Langley Research Center
Hampton, Virginia 23665

and

R. Sahai and J. S. Harris
Science Center, Rockwell International
Thousand Oaks, California 91360

ABSTRACT

Theoretical and experimental analyses show that the higher energy spectral response of an n/p $Al_xGa_{1-x}As$-GaAs graded band-gap solar cell is substantially greater than that of a similar n/p $Al_xGa_{1-x}As$-GaAs heteroface cell, particularly for wavelengths below 0.5 μm. The theoretical analysis includes all practical energy loss mechanisms such as photon reflection; surface, bulk, and junction recombination currents; and series resistance. It predicts air mass zero (AMO) efficiencies of 16.7% for standard transport parameters and a surface recombination velocity (S) of 1×10^6 cm/sec and 17.7% for $S = 1 \times 10^5$ cm/sec.

Small, preliminary n/p graded band-gap structures have been fabricated using a new LPE, melt mixing growth technique to obtain the graded composition $Al_xGa_{1-x}As$ layer approximately 0.5 μm thick. Comparison of the measured spectral responses of the graded band-gap cell with similar n/p heteroface structures ($x = 0.85$) demonstrates substantial improvement provided by the graded cell for wavelengths between 0.60 μm and 0.35 μm. Preliminary electrical measurements performed in a calibrated AMO solar simulator on structures with a Si_3N_4 anti-reflection film indicate maximum power conversion efficiency of 13.6% (for zero contact area). This efficiency corresponds to measured short-circuit current density, J_{SC}, of 27.7 ma/cm^2, open-circuit voltage, V_{OC}, of 0.88 volts, and fill factor, FF, of 0.76. Individual values of J_{SC}, V_{OC}, and FF as high as 28.2 ma/cm^2, 0.95 volts, and 0.78 have been measured, each for a separate cell.

INTRODUCTION

It is well known, from the standpoint of optical band-gap energy, that GaAs is a near optimum material for solar cell fabrication, and is predicted to have a maximum theoretical air mass zero (AMO) power conversion efficiency of 24% compared to 20% for Si (1). However, in early work with GaAs p-on-n diffused cells, maximum AMO efficiencies of only 9.3% were achieved (2). A major difficulty in obtaining higher efficiencies is the significant current loss through surface recombination of photogenerated minority carriers, which are created near the surface (within approximately 1 μm) due to the direct nature of optical absorption in GaAs. The highest experimental AMO efficiencies of 11.7%-14.7% (corrected for zero contact area) were reported by Hovel and Woodall (3, 4) for the $Al_xGa_{1-x}As$-GaAs heteroface cell. In their device the surface $Al_xGa_{1-x}As$ layer is typically greater than one diffusion length thick (0.6-2 μm) and the p-n junction is located in the GaAs substrate approximately 1 μm - 3 μm below the metallurgical junction. Thus, the main function of the surface layer is to reduce the surface recombination velocity (S) of the GaAs surface and to reduce the series resistance of the cell; i.e., photons absorbed in the $Al_xGa_{1-x}As$ layer do not contribute significantly to the short-circuit current. Most recently, James (5) claims 19% AMO efficiency for his thin-window heteroface cell, based on an indirect analytical/experimental measurement.

Another method proposed to reduce surface recombination loss is that of a built-in electric field in the surface layer to accelerate photogenerated excess minority carriers toward the p-n junction and reduce the time required for their collection (6-12). Such a field can be accomplished by varying either the doping concentration or the energy band-gap in the surface layer.

Use of a band-gap gradient in the surface region of an n/p cell to generate the built-in field is illustrated in Figure 1. The field is proportional to the valance band gradient. A preliminary analysis of a near optimum n/p graded band-gap $Al_xGa_{1-x}As$-GaAs cell including all significant energy loss mechanisms shows that AMO efficiencies greater than 17% can be expected (10).

The purpose of this paper is to present theoretical and experimental evidence suggesting improved blue-uv response expected for the graded band-gap cell compared to the heteroface cell, and to report the first experimental efficiencies obtained for the graded composition cell.

THEORETICAL ANALYSIS AND EXPERIMENTAL TECHNIQUES

The analysis is performed using the standard continuity and current density expressions for the bulk material assuming $S = 1 \times 10^5 - 1 \times 10^6$ cm/sec

at y = 0 and S → ∞ at y = 125 μm. The injected excess carrier concentrations at the p-n junction are assumed to be given by the standard Boltzmann boundary condition. In the graded $Al_xGa_{1-x}As$ layer the hole transport parameters are assumed to be constant, but the position dependence of the absorption coefficienct requires a numerical solution. An analytical solution is used for the GaAs region. The hole diffusion length (l_{po}) in the $Al_xGa_{1-x}As$ layer and the electron diffusion length (l_{no}) in the GaAs substrate are assumed to have empirical dependences on impurity concentration. A near optimum cell with surface donor and base acceptor concentrations of $N_D = 4 \times 10^{17}$ cm^{-3} and $N_A = 2 \times 10^{17}$ cm^{-3} and graded composition layer thickness (equal to junction depth) of 1 μm is assumed. Furthermore, junction recombination current density, series resistance of the cell, and surface reflection losses (assuming an optimized SiO anti-reflection coating) are considered. The analysis is performed for AMO insolation of 139.0 mw/cm^2.

Growth of the n-type, Te doped ($1\text{-}2 \times 10^{18}$ cm^{-3}) graded composition layer is accomplished by transient diffusion of Al through a Ga melt to the growth interface during a continuous growth of $Al_xGa_{1-x}As$. The Al concentration at the growth interface increases with time due to a continuous increase of Al concentration in the melt during the growth cycle, and is typically x = 0.85 when the cycle is terminated. The substrate is p-type Ge doped ($2\text{-}3 \times 10^{17}$ cm^{-3}), epitaxially grown (4 μm - 6 μm thick) GaAs. Many of the initial growths resulted in a uniform composition layer 0.8 μm thick at the surface which was chemically etched to expose the 0.4 μm - 0.6 μm graded composition region. Devices are fabricated from 0.075 inch cleaved squares using ohmic contacts provided by Au/Ge (12% Ge) on the n-side and Ag/Mn (5% Mn) on the p-side. The final process is deposition of a near optimum Si_3N_4 anti-reflection coating. Absolute spectral response measurements were obtained using a Cary-14 spectrophotometer in conjunction with a calibrated Si photodetector and a He-Ne laser used to obtain an absolute response at 0.6328 μm. Power conversion efficiency measurements were obtained using an AMO solar simulator calibrated using a ballon flown Si cell.

RESULTS AND DISCUSSION

The most dramatic effect the presence of a graded composition layer has on the theoretical performance of a GaAs solar cell is a substantial increase in power conversion efficiency with increasing aluminum gradient. Figure 2 shows the theoretical dependence of efficiency (including a large 12.8% contact area) upon the surface mole fraction of Al, X_{ALO}, for two values of S and for both assumed and degraded values for ℓ_{po}. In each case, X_{ALO} has a profound effect upon efficiency up to the direct-indirect transition, above which a decrease in surface field causes a slight drop in efficiency. Although the presence of an electric field decreases the sensitivity of efficiency to S and ℓ_{po}, these parameters (particularly the latter) are still important to achieving high efficiencies. As can be seen, an optimized cell having $\ell_{no} = 7.6$ μm, $\ell_{po} = 2.1$ μm, and $S = 1 \times 10^5$ cm/sec is predicted to have an efficiency of 17.7% AMO. The same call with $S = 1 \times 10^6$ cm/sec has a predicted efficiency of 16.6% AMO.

Figures 3 and 4 show the total theoretical spectral response and the contributions from the surface $Al_xGa_{1-x}As$ region and the base GaAs region for $X_{ALO} = 0$ and $X_{ALO} = 0.30$, respectively. A plot of the theoretical reflection coefficient, R, for an optimum SiO anti-reflection coating is also provided. The graded Al concentration increases current collected from both the surface and base regions of the cell. The additional current collected from the surface region is due to increased collection efficiency, whereas the additional contribution from the base region is mainly due to an increased concentration of higher energy photons absorbed in this region near the junction. The reduced response at high energies ($\lambda < 0.5$ μm) is due to both increased photon absorption closer to a lossy surface and to reflection. Comparison of the theoretical spectral response given in Figure 4 for the n/p graded band-gap cell with the theoretical spectral response for a somewhat similar p/n heteroface cell given by Hovel and Woodall (13) and shown in Figure 4 indicates a similar response for low energy photons ($\lambda > 0.59$ μm) but a substantially increased response for the graded band-gap cell at higher energies. This increased blue response is the primary advantage gained by the graded band-gap cell.

Several experimental graded band-gap cells recently fabricated have reasonably good efficiences and demonstrate improved response to the blue-uv solar spectrum. The best cell examined has an efficiency of 13.6% AMO (corrected for zero contact area), corresponding to a short circuit current density $J_{SC} = 27.7$ ma/cm^2, open circuit voltage $V_{OC} = 0.88$ volts, and fill factor FF = 0.76 based on a solar constant of 135.3 mw/cm^2. Most of the cells tested had corrected efficiency values between 12.0% and 13.5%. Individual values of J_{SC}, V_{OC}, and FF as high as 28.2 ma/cm^2, 0.95 volts, and 0.78 were each measured for different cell structures; i.e., no single cell concurrently has these high values for J_{SC}, V_{OC}, and FF. The spectral responses of a graded band-gap cell ($X_{ALO} = 0.35$) and a nearly identical n/p $Al_{.85}Ga_{.15}As$-GaAs heteroface cell compared in Figure 5 demonstrate the improved blue-uv response expected for the graded composition cell. Both cells have an $Al_xGa_{1-x}As$ layer thickness of approximately 0.5 μm.

In conclusion, both theoretical and experimental results indicate that the graded band-gap $Al_xGa_{1-x}As$-GaAs solar cell has an improved response to blue-uv photons compared to the heteroface cell. Further improvement of the low open circuit voltage and fill factor should provided AMO efficiencies of 15%. However, further refinements of the growth and characterization of the graded composition $Al_xGa_{1-x}As$ layer are required to obtain efficiencies in excess of 16% AMO.

REFERENCES

(1) J. J. Loferski, J. Appl. Phys. 27, 777 (1956). The AMO condition is identical to the condition of m = 0 and w = 0 given in this reference.

(2) S. C. Tsaur, A. G. Milnes, R. Sahai, and D. L. Feucht, in Proceedings of the Fourth International Symposium on GaAs and Related Compounds, Conference Series No. 17 (The Institute of Physics, London, England, 1973), p. 156.

(3) H. J. Hovel and J. M. Woodall, J. Electrochem. Soc. 120, 1246 (1973).

(4) H. J. Hovel and J. M. Woodall, in Conference Record of the Eleventh IEEE Photovoltaic Specialists Conference - 1975 (IEEE, New York, 1975), p. 433.

(5) L. W. James, 1975 IEDM, December 1-3, 1975, Washington, DC.

(6) M. Wolf, Proc. IRE 48, 1246 (1960).

(7) M. Wolf, Proc. IEEE 51, 674 (1963).

(8) B. Ellis and T. S. Moss, Solid-State Electron. 13, 1 (1970).

(9) Y. Marfaing, in Proceedings of the International Colloquium on Solar Cells (Gordon and Breach, New York, 1970), p. 67.

(10) J. A. Hutchby, Appl. Phys. Letters 26, 457 (1975).

(11) J. A. Hutchby, in Conference Record of the Eleventh IEEE Photovoltaic Specialists Conference - 1975 (IEEE, New York, 1975), p. 414.

(12) M. Konagai and K. Takahashi, J. Appl. Phys. 46, 3547 (1975).

(13) H. J. Hovel and J. M. Woodall, in Conference Record of the Tenth IEEE Photovoltaic Specialists Conference - 1974 (IEEE, New York, 1973), p. 25.

FIGURE CAPTION

Figure 1. Energy band diagram for $Al_xGa_{1-x}As$-GaAs graded band-gap solar cell.

Figure 2. Dependence of power conversion efficiency on X_{ALO}. O:S = 1 x 10^5 cm/sec, ℓ_{po} = 2.1 μm; ◻:S = 1 x 10^6 cm/sec, ℓ_{po} = 2.1 μm; ◇:S = 1 x 10^5 cm/sec, ℓ_{po} = 0.52 μm; △:S = 1 x 10^6 cm/sec, ℓ_{po} = 0.52 μm.

Figure 3. Calculated spectral response data for n/p cell with X_{ALO} = 0 (GaAs cell), ◇: total spectral response; O - spectral response of surface n-type layer; ◻: spectral response of p-type base region; △: reflection coefficient.

Figure 4. Calculated spectral response data for n/p cell with X_{ALO} = 0.30 (graded band-gap cell). ◇: total spectral response; O - spectral response of graded band-gap surface layer; ◻: spectral response of GaAs base region; △: reflection coefficient; ◆: total theoretical spectral response of p/n heteroface $Al_xGa_{1-x}As$-GaAs cell for a $Al_xGa_{1-x}As$ thickness of 0.5 μm and a total junction depth of 1.0 μm. (Ref. 13)

Figure 5. Experimental spectral response data for n/p graded band-gap cell (X_{ALO} = 0.35), ◆, and for n/p $Al_{.85}Ga_{.15}As$-GaAs heteroface cell, ■, compared with calculated spectral response for a similar graded band-gap (X_{ALO} = 0.35) cell, ◇. The $Al_xGa_{1-x}As$ layer thickness for each case is 0.5 μm.

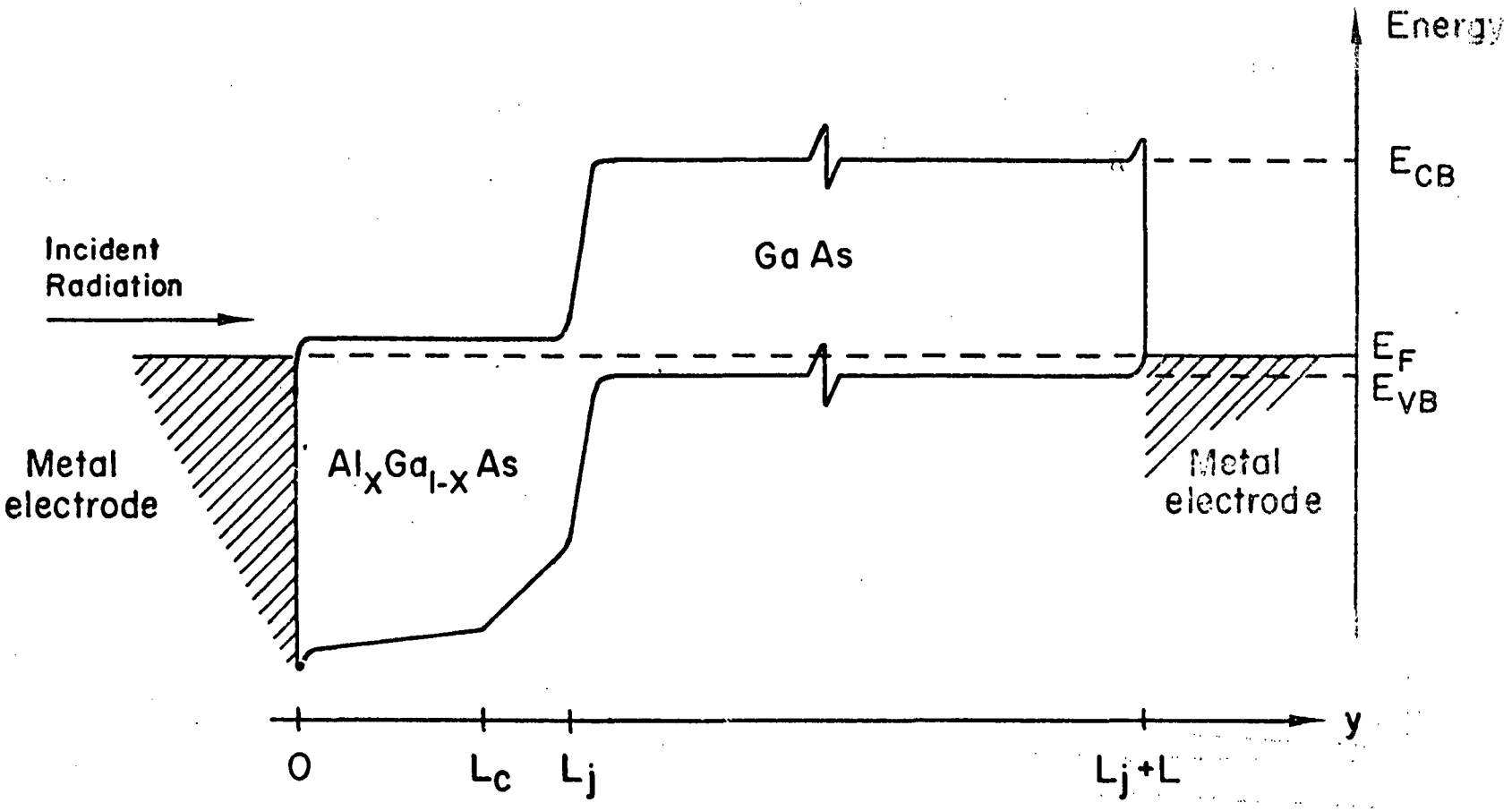
Energy
E_{CB}
Incident
Radiation
Ga As
E_F
E_{VB}
Metal
electrode
$Al_xGa_{1-x}As$
Metal
electrode
y
0
L_c
L_j
L_j+L

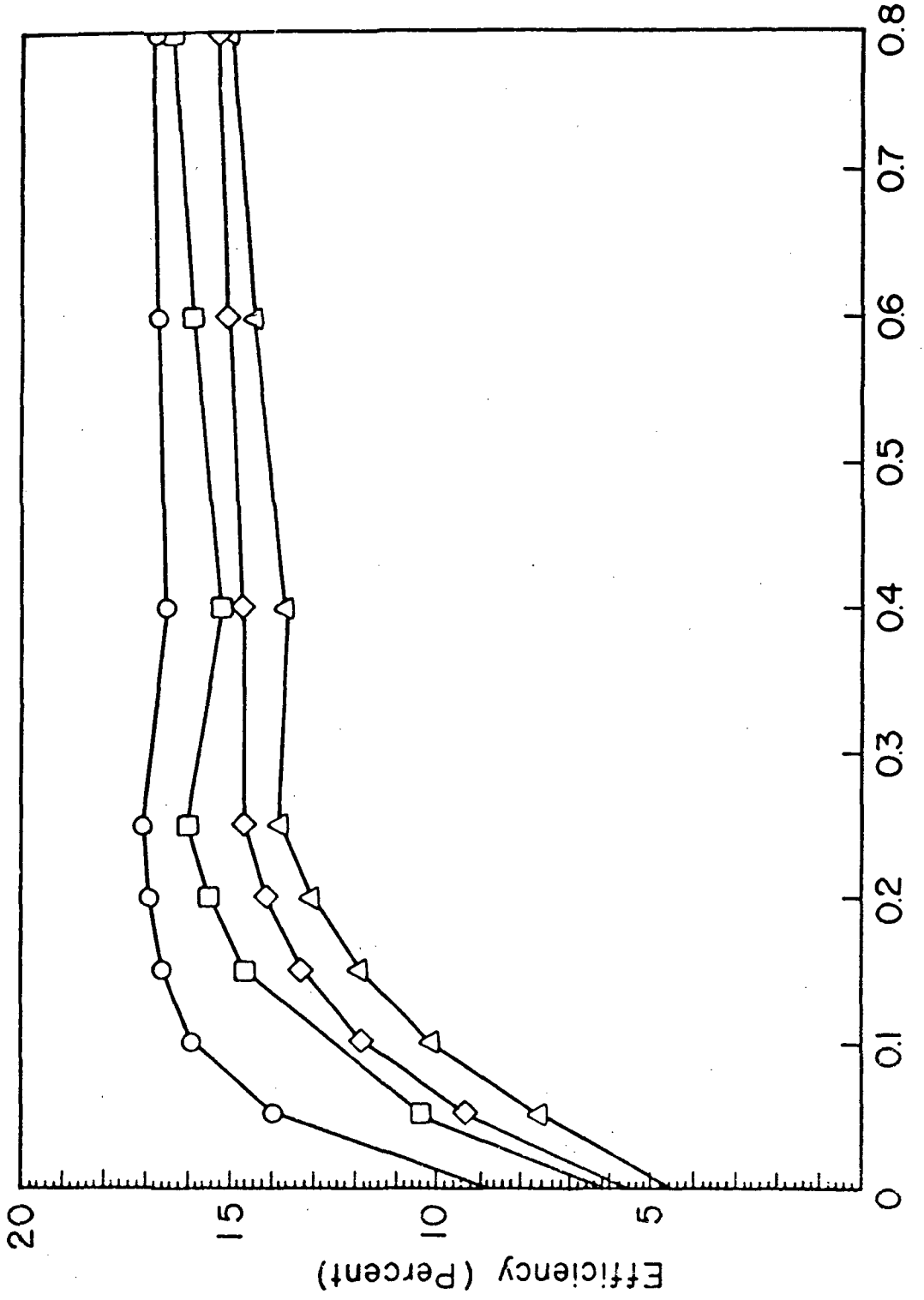

VIII-2

SPECTRAL RESPONSE

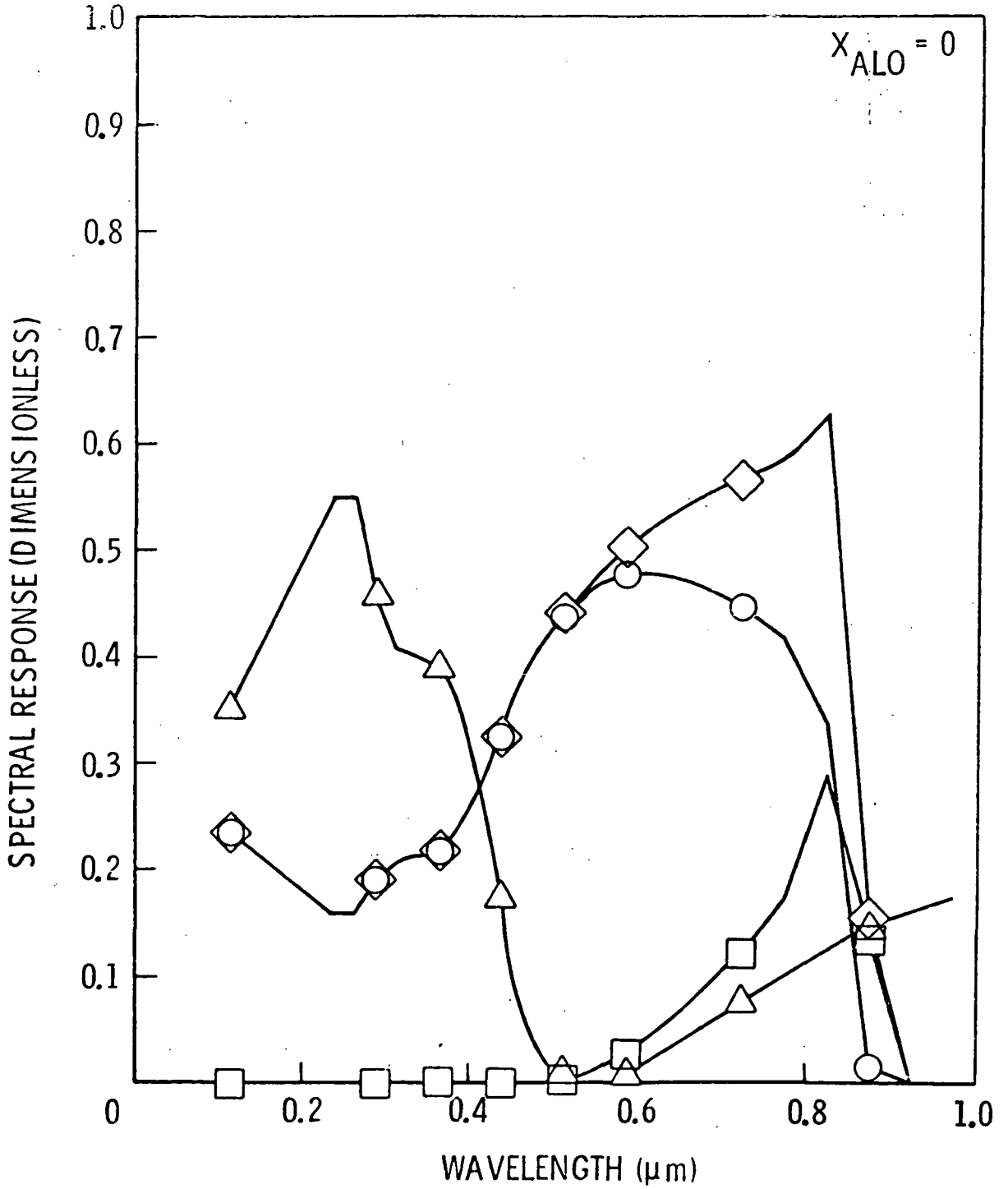

VIII-3

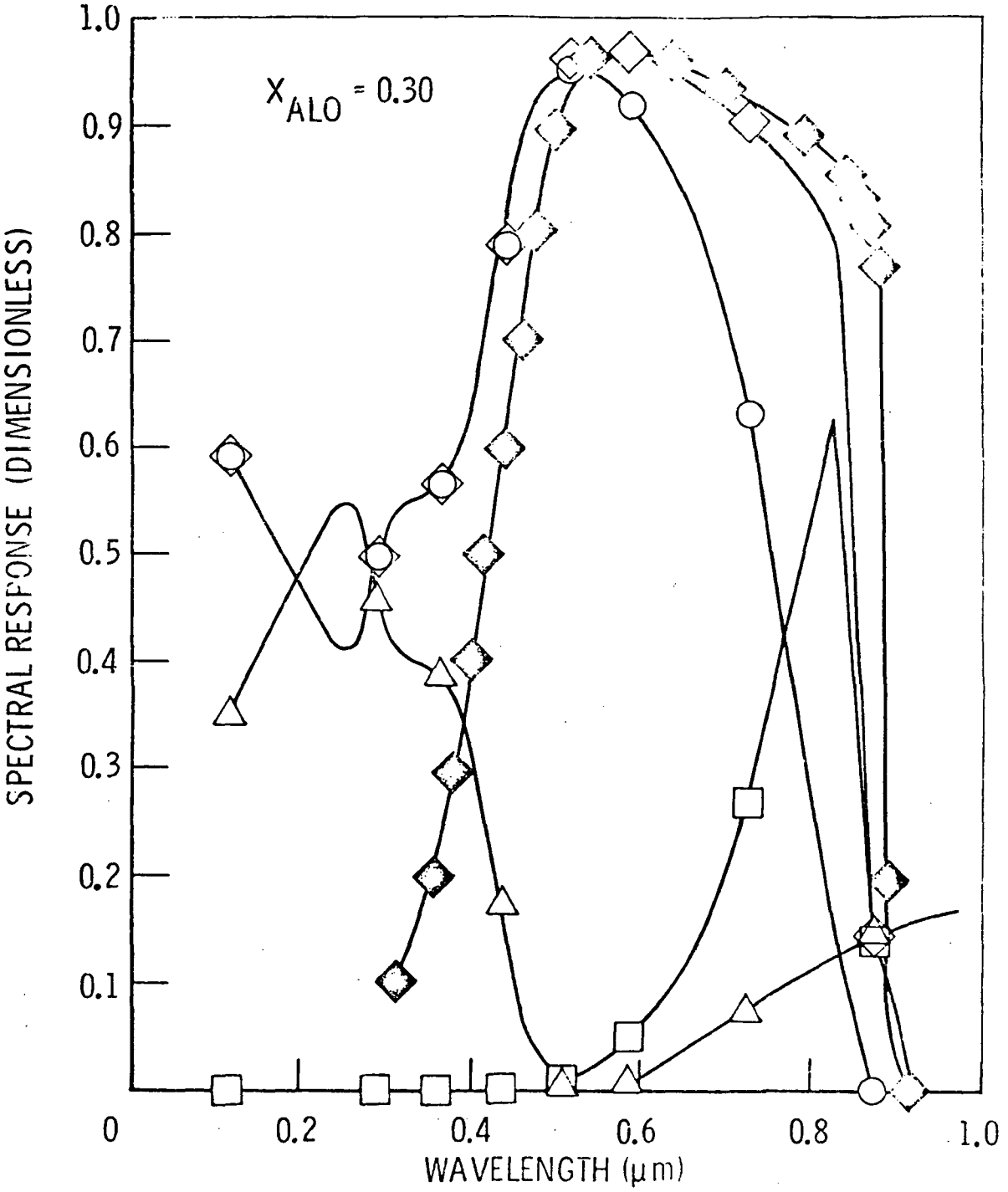
X_{ALO} = 0.30
SPECTRAL RESPONSE (DIMENSIONLESS)
WAVELENGTH (μm)
1.0
0.9
0.8
0.7
0.6
0.5
0.4
0.3
0.2
0.1
0
0.2
0.4
0.6
0.8
1.0

VIII-4

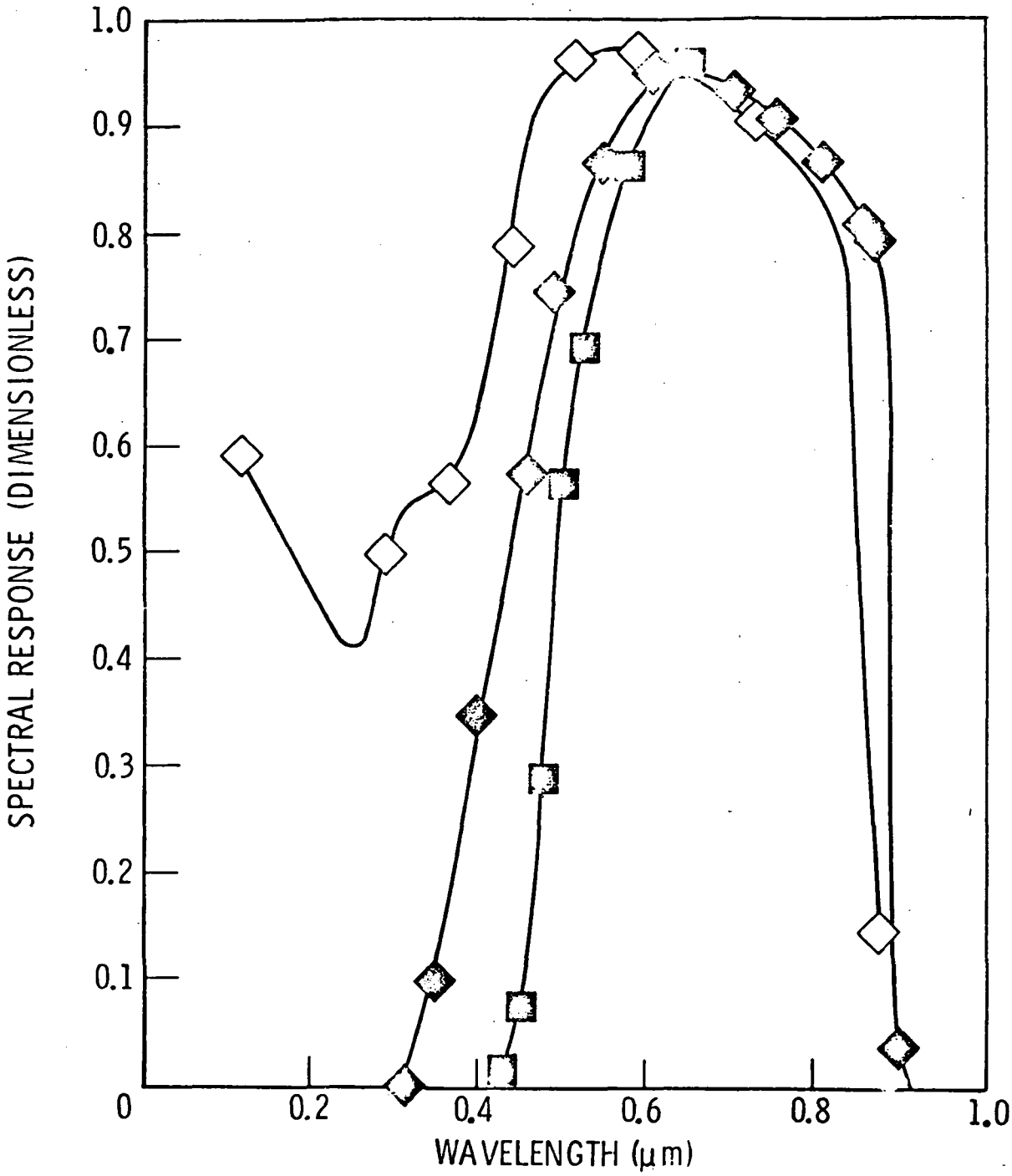
SPECTRAL RESPONSE (DIMENSIONLESS)
1.0
0.9
0.8
0.7
0.6
0.5
0.4
0.3
0.2
0.1
0
0.2
0.4
0.6
0.8
1.0
WAVELENGTH (μm)

VIII-5

SURFACE PHOTOVOLTAGE SPECTROSCOPY

Summary

Surface photovoltage spectroscopy is uniquely suited for the study of the energy position and dynamic parameters of high energy gap semiconductor surfaces. In the case of GaAs surfaces the study of their electronic characteristics is significantly aided by the surface piezoelectric effect which is essentially analogous to the classical field effect; it permits the direct determination of the capture cross section of the surface states for electrons. Due to finite communication of the GaAs surface states with the bulk, surface photovoltage spectroscopy is much more effective at low temperatures; it was recently found, for example, that partially filled surface states are present even below the Fermi level. Photo-piezoelectric effects have permitted the determination of the surface stress (surface energy) of GaAs and its changes in various ambient atmospheres. A new technique was developed for determining the surface recombination velocity in GaAs employing scanning electron microscopy. This new technique will now permit relating the surface state configuration with surface recombination velocities. This is an essential step in pursuing the study of surface recombination processes relevant to the conversion efficiency of GaAs photovoltaic cells.

Harry C. Gatos

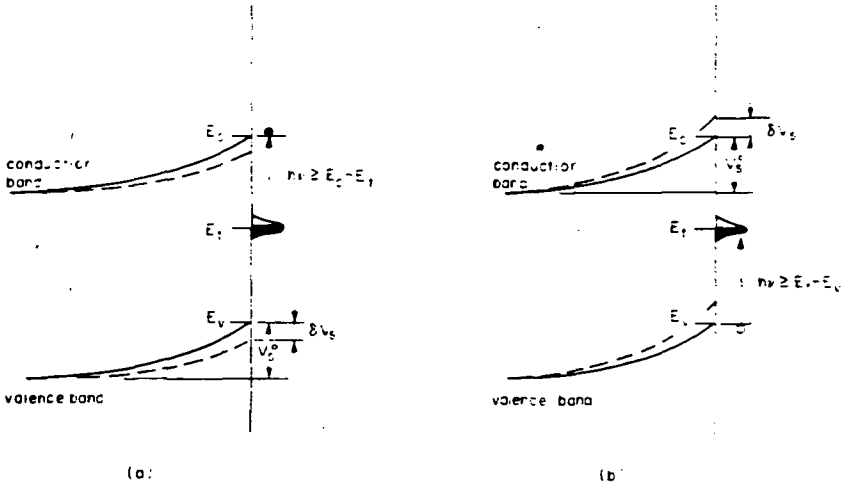

Fig. 1. Schematic representation of origin of photovoltage (a) surface state depopulation (decrease in surface barrier) and (b) surface state population (increase in surface barrier, i.e., photovoltage inversion or photovoltage quenching effect).

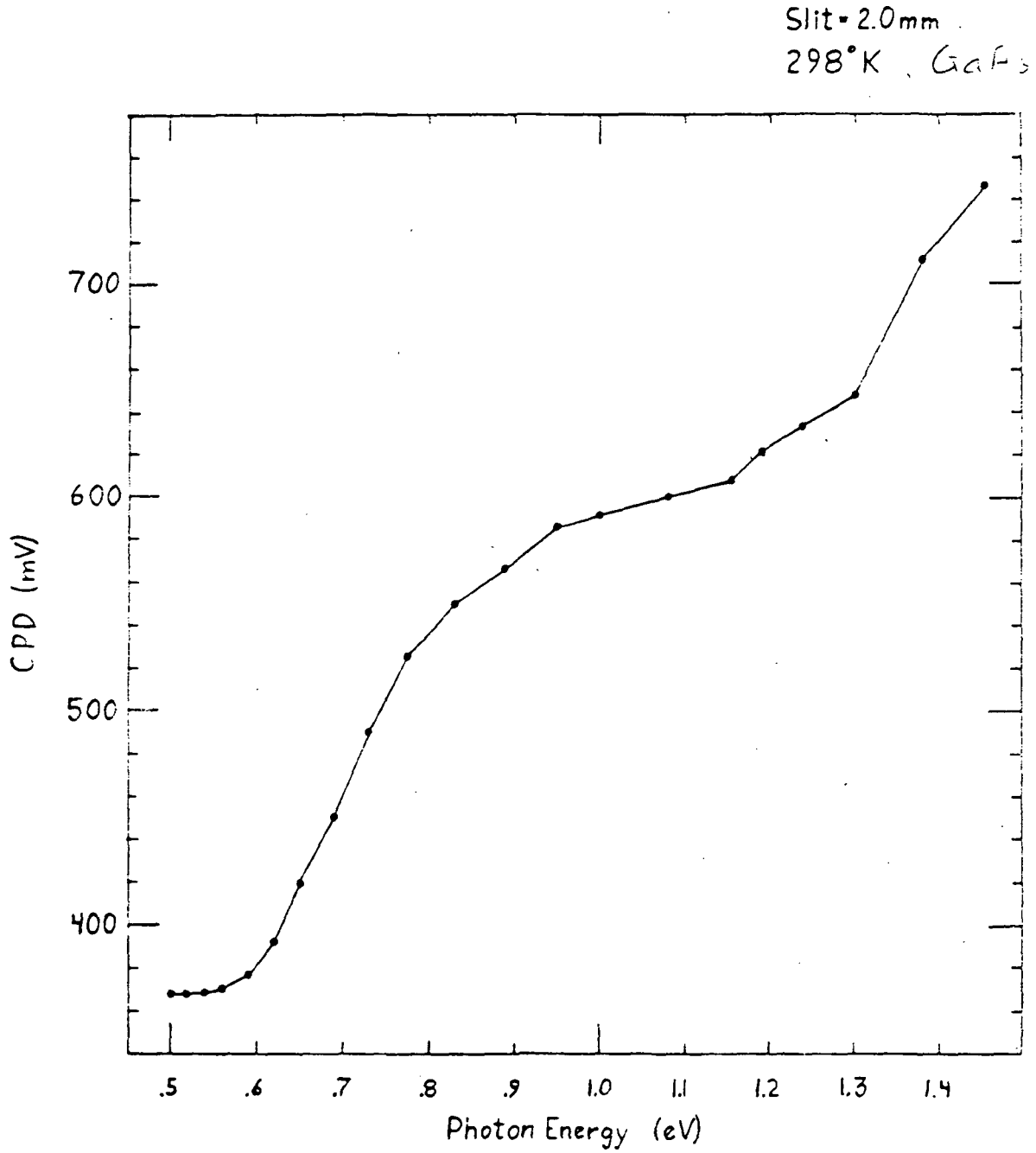
Slit = 2.0mm
298°K . GaP
700
600
500
400
CPD (mV)
.5
.6
.7
.8
.9
1.0
1.1
1.2
1.3
1.4
Photon Energy (eV)

IX-2

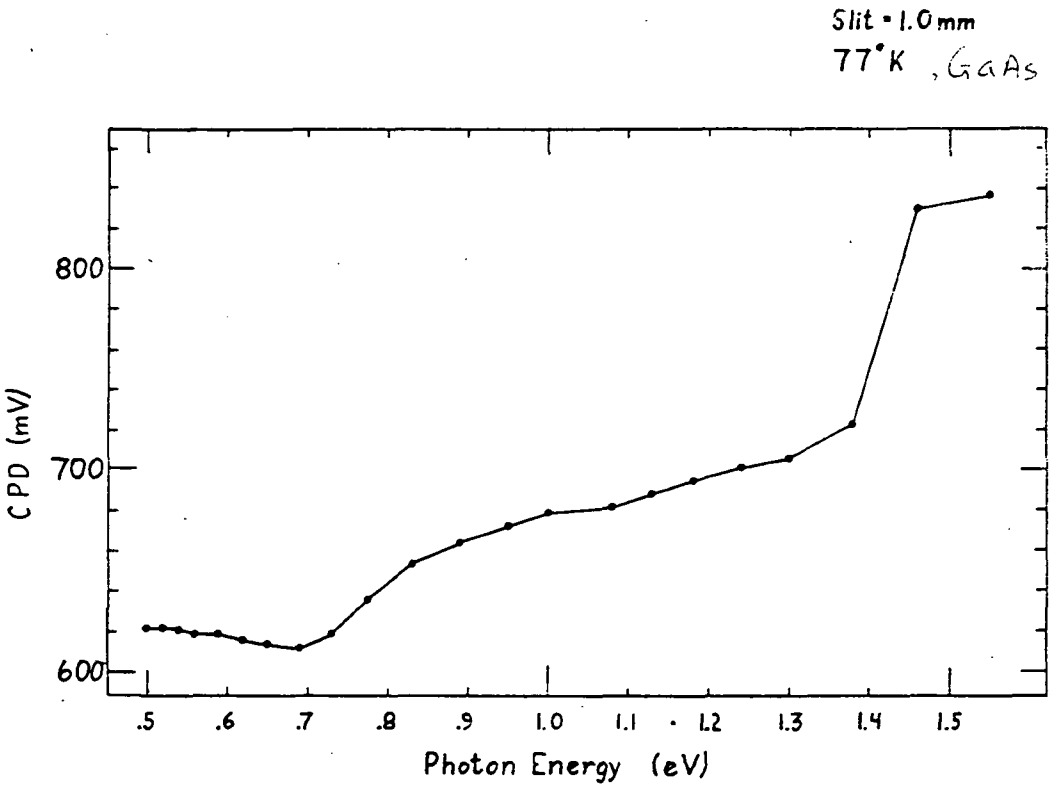
Slit • 1.0 mm
77°K , GaAs
800
700
600
CPD (mV)
.5
.6
.7
.8
.9
1.0
1.1
1.2
1.3
1.4
1.5
Photon Energy (eV)

IX-3

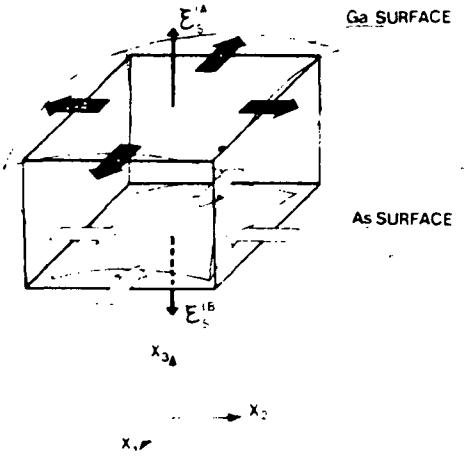

Fig. 7. Schematic representation of mechanical bending of a GaAs wafer due to the converse piezoelectric effect at the surface. Arrows represent the surface stresses, σ_{x_2}, due to the electric field on the opposite surfaces of the wafer; [in CdS the surface stresses are opposite to those in GaAs since GaAs and CdS crystals exhibit opposite polarities[21]].

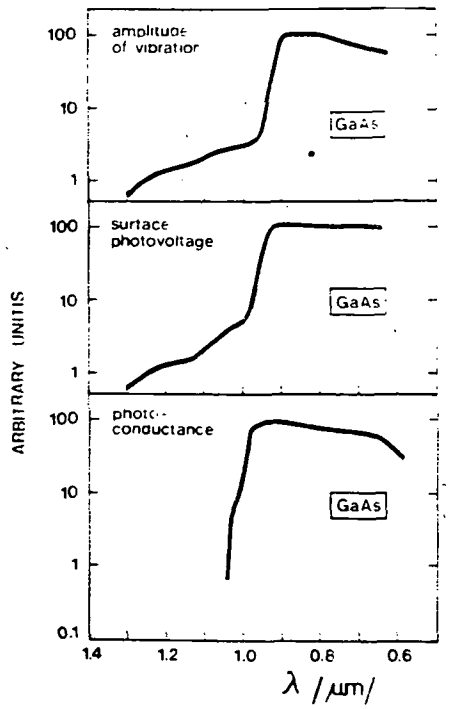

Fig. 4. Typical spectra of the amplitude of the photomechanical vibration, surface photovoltage and photoconductance of an (111) GaAs wafer. Measurements were carried out at room temperature and at an ambient pressure of 10^{-5} torr. frequency of light-chopping ≃ 98 Hz

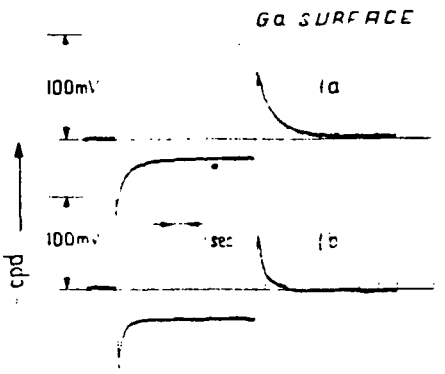

Fig. 3. Typical cpd transient resulting from bending and subsequent unbending of the wafer. Measurements carried out on a Ga surface. Curves a and b correspond to wet air and ozone, respectively. Upon bending the Ga surface was under tension. The radius of bending, R, was approximately 10 cm. A decrease in cpd corresponds to an increase in surface barrier.

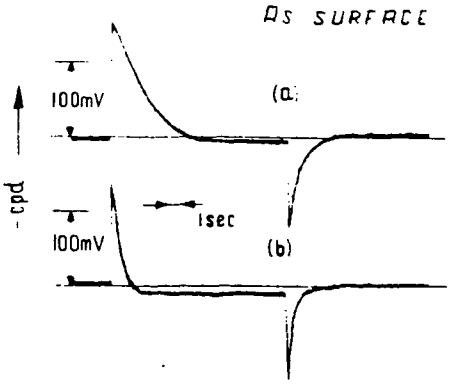

Fig. 4. Typical cpd transients resulting from bending and subsequent unbending of the wafer. Measurements carried out on As surfaces. Curves a and b correspond to wet air and ozone, respectively. Upon bending the As surface was under tension. The radius of bending, R, was approximately 10 cm. An increase in cpd corresponds to a decrease in surface barrier.

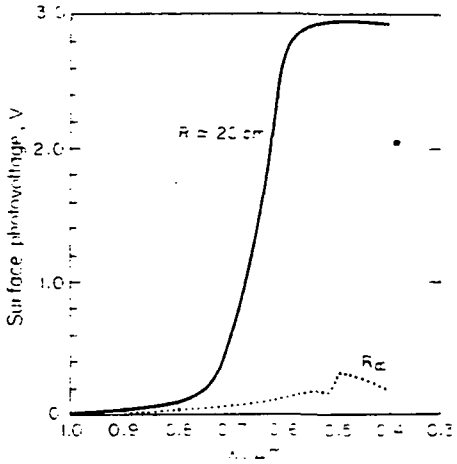

Fig. 1. The effect of mechanical bending on photovoltage of (00.1) surfaces of n-type CdS at room ambient.

325

IX-8 Typical oxygen-induced changes in CPD and resistivity in the presance of a depletion layer at the surface under an oxygen pressure of 40 Torr. The sample was bent at a radius of curvature R = -30 cm at the time indicated by arrows.

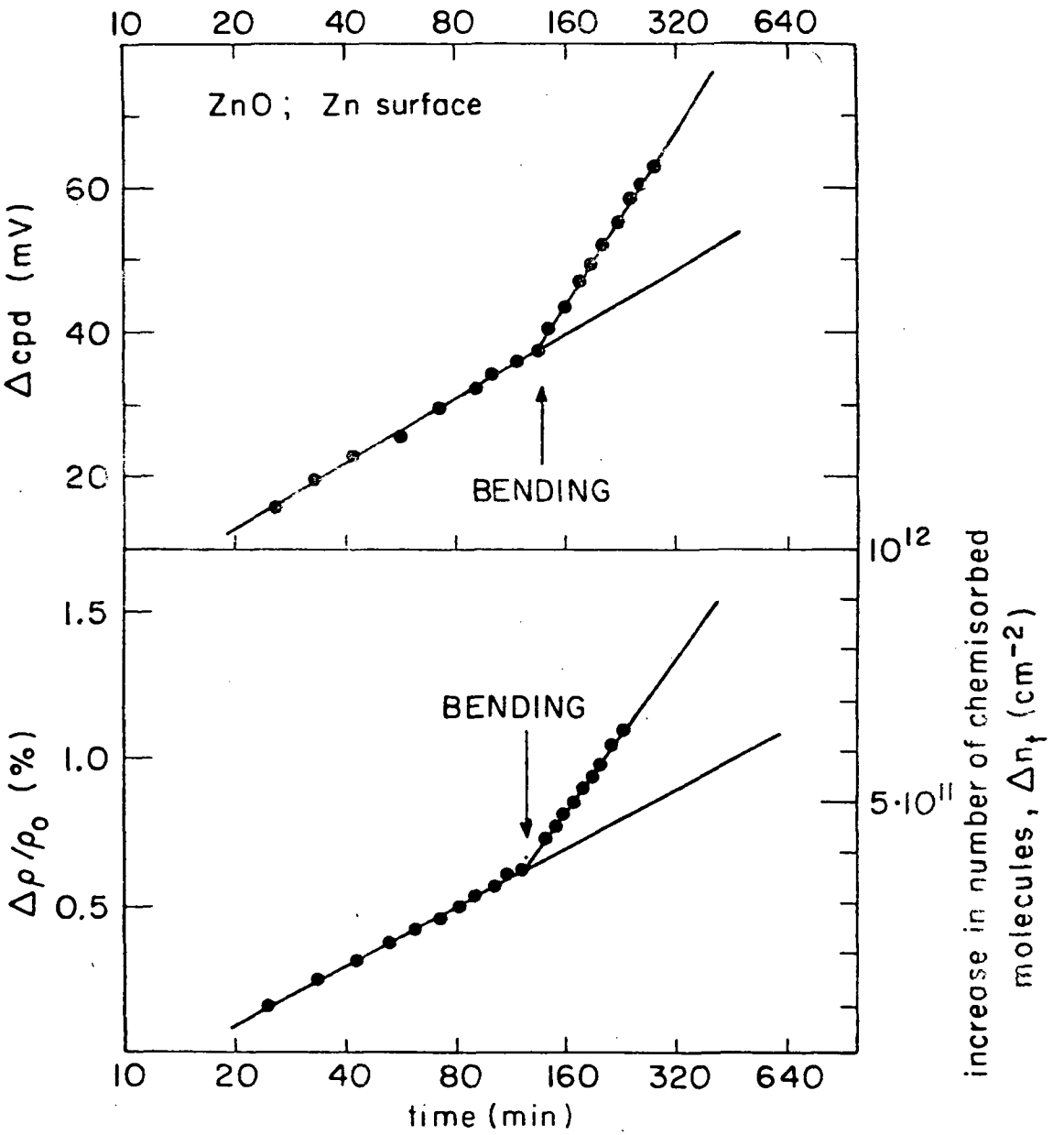

IX-9

Bending-induced changes in the rate of oxygen adsorption on the surface of ZnO, in terms of the quantity d(ΔCPD)/dlnt under a pressure of 100 Torr. At t_1, t_2, t_3 and t_4 the sample was bent to a radius of curvature, $R_1 \simeq 30$ cm, $R_2 \simeq -30$ cm, $R_3 \simeq 45$ cm, and $R_4 \simeq 15$ cm, respectively.

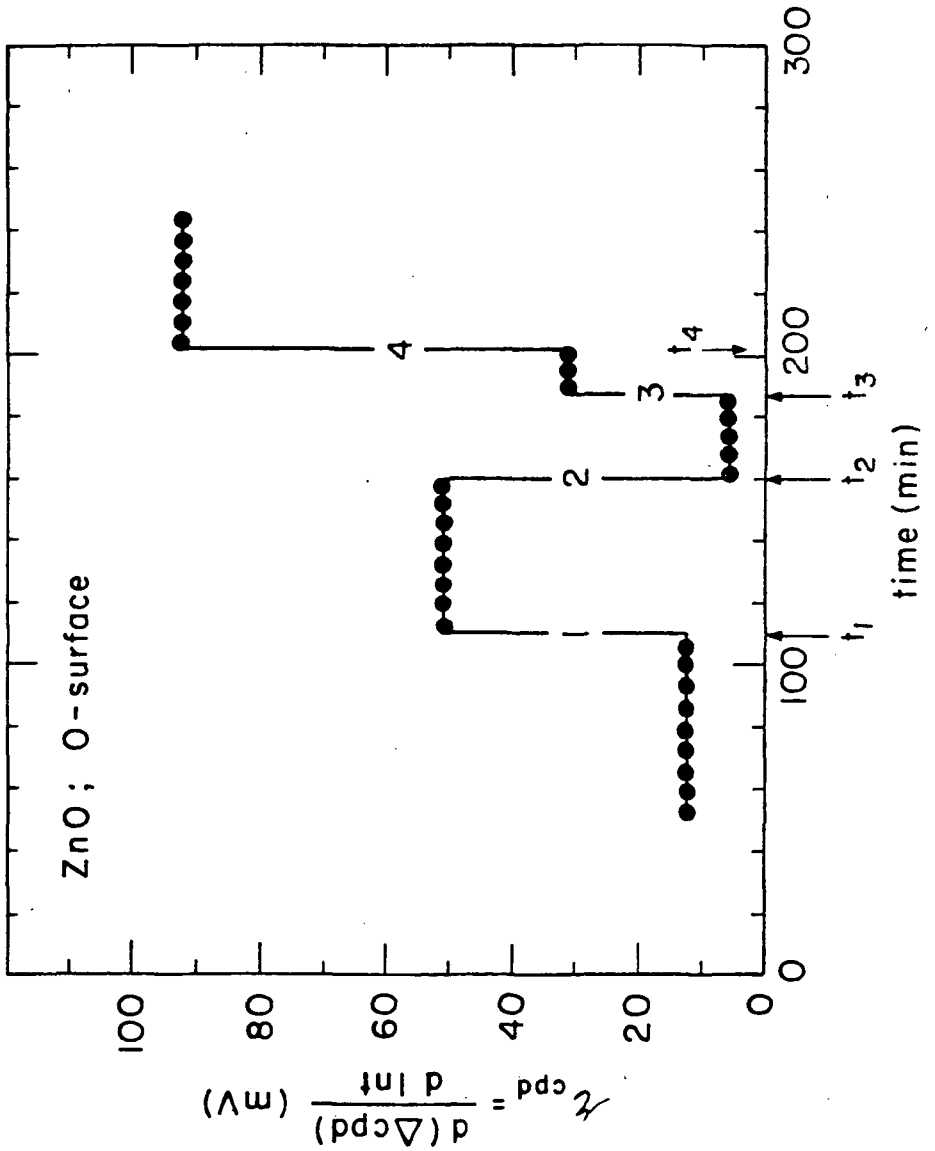

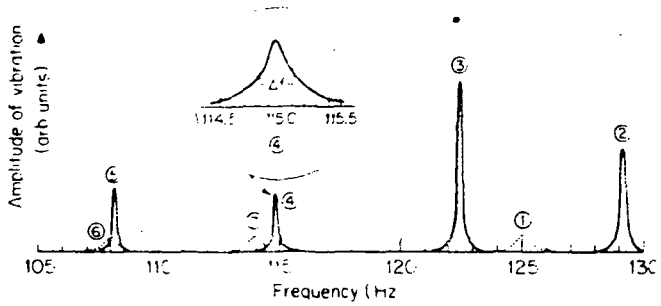

FIG. 2. Normal mode of vibration of a 12-μm-thick (111) GaAs wafer for different ambient conditions: (1) room atmosphere just after etching; (2) 30 min in 10^{-4} Torr; (3) 48 h in 10^{-5} Torr; (4) 10^{-6} Torr after corona discharge; (5) 10^{-6} Torr; outgassing at ≃ 200°C for 3 h; (6) immediately after exposure to room atmosphere; (7) 2 h after exposure to room atmosphere.

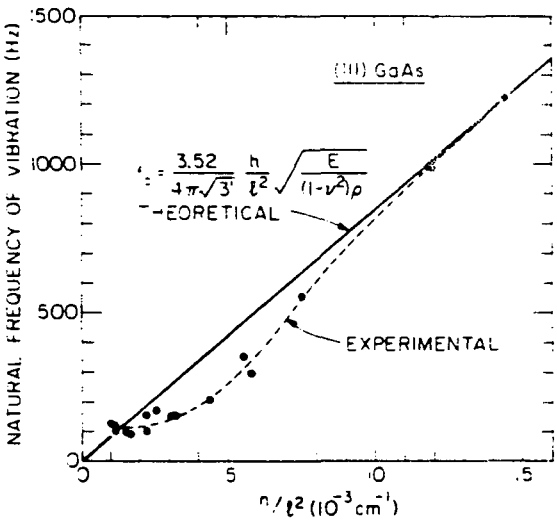

FIG. 1. Natural frequency of vibration of thin (111) GaAs crystals (in a cantilever configuration) as a function of crystal dimensions (h/ℓ^2). Measurements were carried out on freshly etched samples.

IX-11

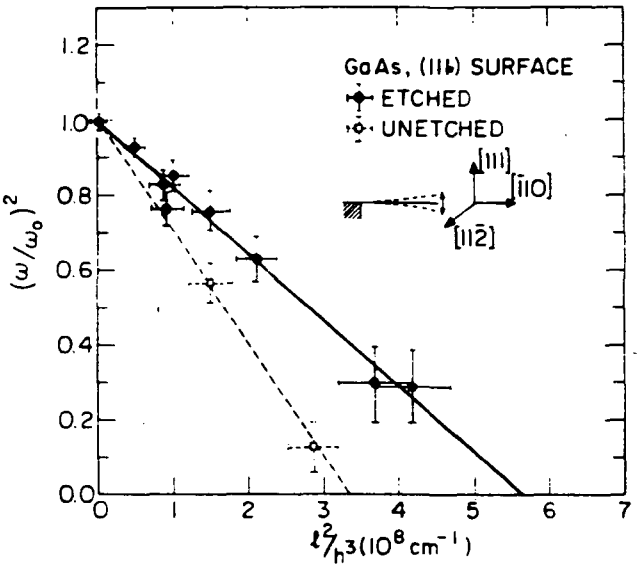

FIG. 4. Dependence of $(\omega/\omega_0)^2$ on l^2/h^3 for a freshly etched and an unetched (111) GaAs wafer. Measurements were carried out at room atmosphere. The indicated precision limits of the experimental data are associated primarily with uncertainties in thickness measurements.

IX-12

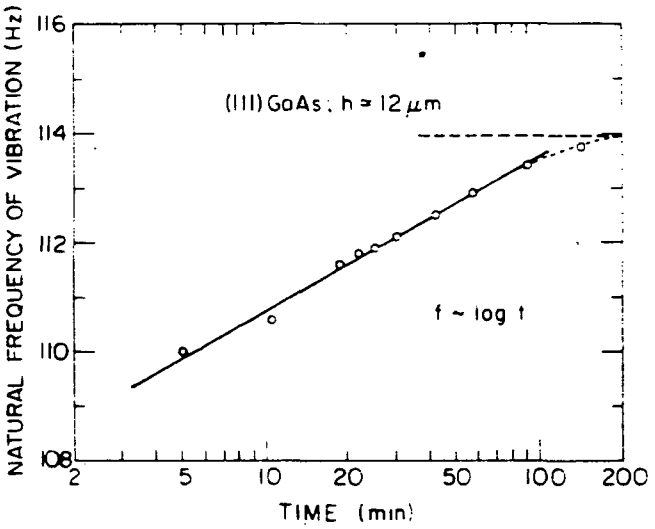

FIG. 3. Transient of the natural frequency of a 12-μm-thick (111) GaAs wafer upon exposure to room atmosphere (sequence 6→7 in Fig. 2).

IX-13

TABLE I

Surface-piezoelectric and photo-piezoelectric effects associated with surface depletion layers in polar semiconductors

Phenomenon	Conditions	Measured quantity	Resulting information	Observed in	References
Surface piezoelectric effect	$S \neq 0$, $I = 0$	cpd versus mechanical strain	Surface barrier height, identification of A and B surfaces	CdS	2 6 4
Piezoelectric modulation of surface charges	$S \neq 0$, $I = 0$	cpd transients	Dynamic parameters of surface states	CdS GaAs ZnO	3 4 6
Stress-induced amplification of photovoltage	$S \neq 0$, $I \neq 0$	Photovoltage versus mechanical strain	Processes associated with photovoltage identification of light-induced electronic transitions	CdS	5 3
Illumination-induced bending	$S = 0$, $I \neq 0$	Light-induced changes in radius of curvature	Piezoelectric contribution to surface stress	CdS GaAs	1 and present paper
Photomechanical vibration	$S = 0$, $I \neq 0$, chopped illumination	Amplitude of vibrations versus $h\nu$ and illumination intensity	Electrical and mechanical properties of surfaces	CdS GaAs	1 and present paper

S external stress applied to the crystal; I = incident illumination.

IX-15

Experimental configuration used in the effective diffusion length measurements.

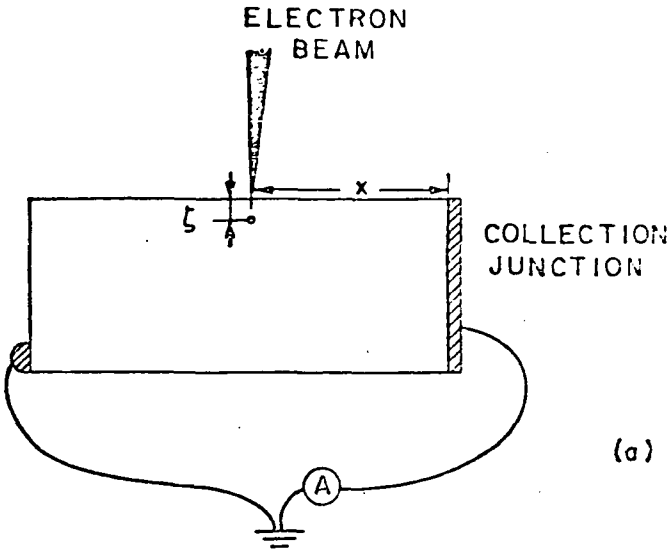

(a)

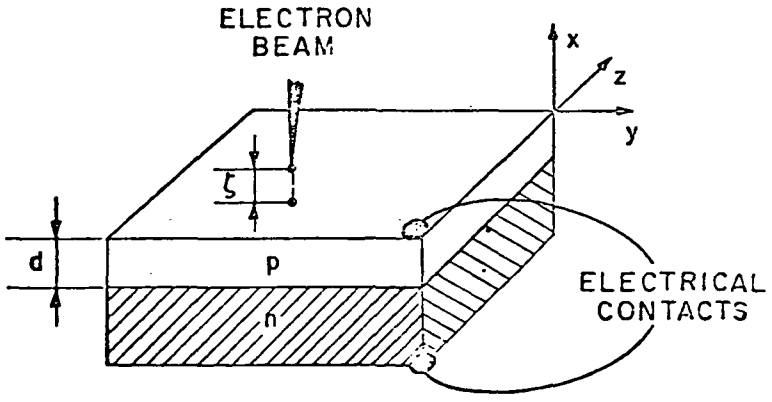

(b)

IX-16 (a) The ~~electric~~ current generated by electron beam vs. a distance between generation point and the collecting junction. (b) The effective diffusion length vs. accelerating voltage and the penetration depth of electron beam.

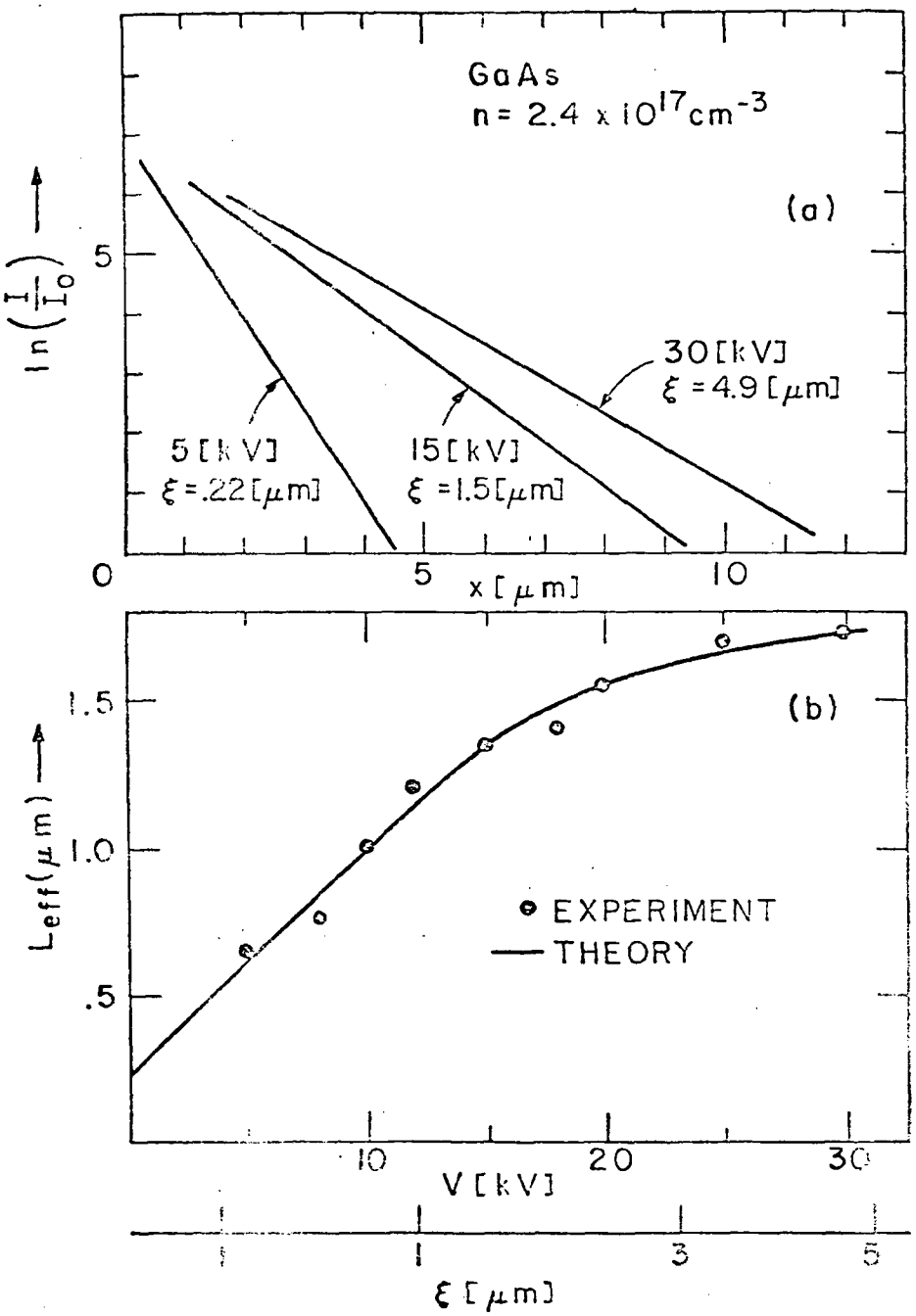

IX-17 Surface recombination velocity in GaAs vs. the majority carrier concentration; o - present results, ref. 9 - ●, ref. 10 - ▲.

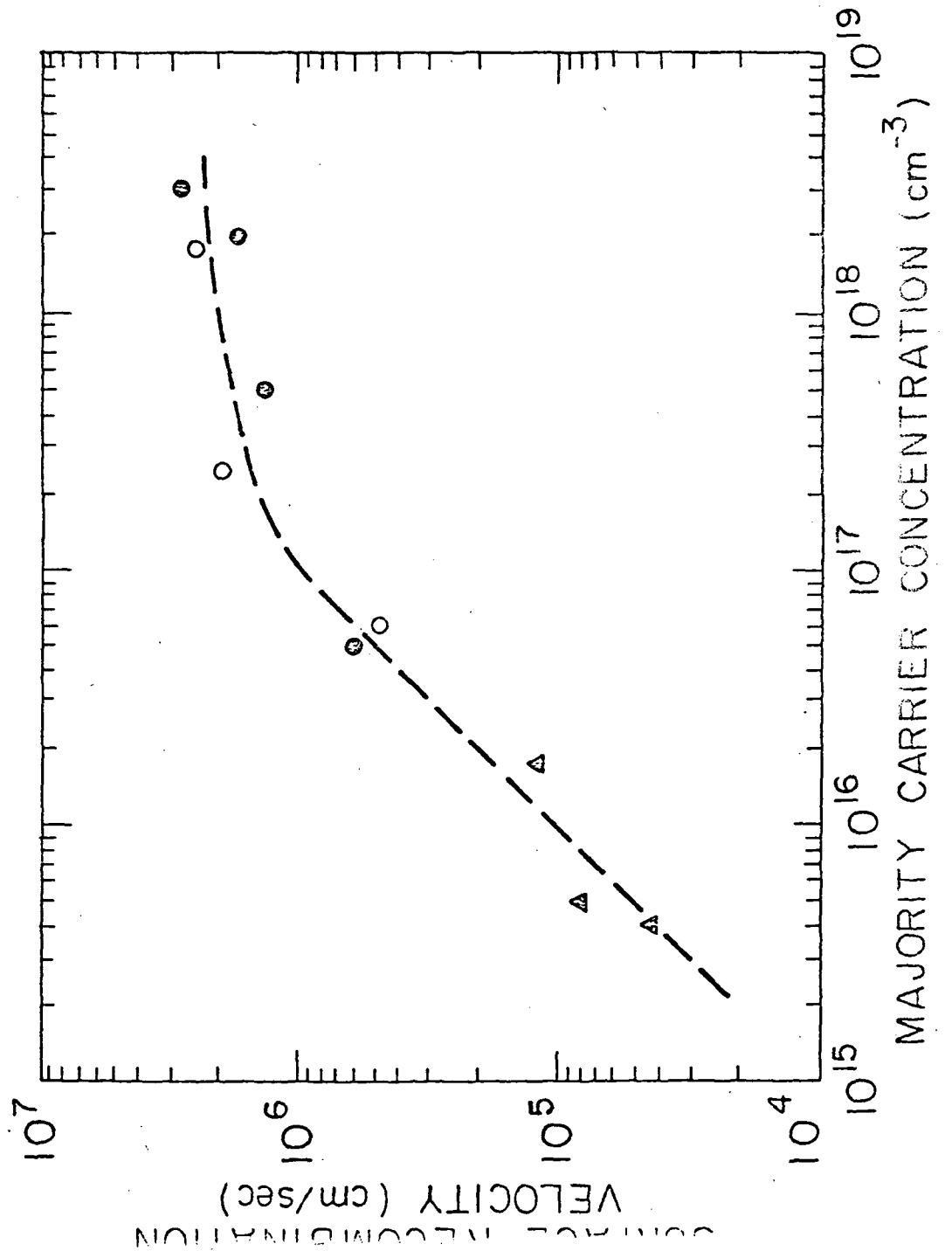

IX-18

Fig. 3 $\ln[1 - (\frac{L_{eff}}{L_b})^2]$ as a function of the penetration depth of the electron beam, in L_b arbitrary units. Curve I corresponds to the expanded scale (I), curves II correspond to the scale (II).

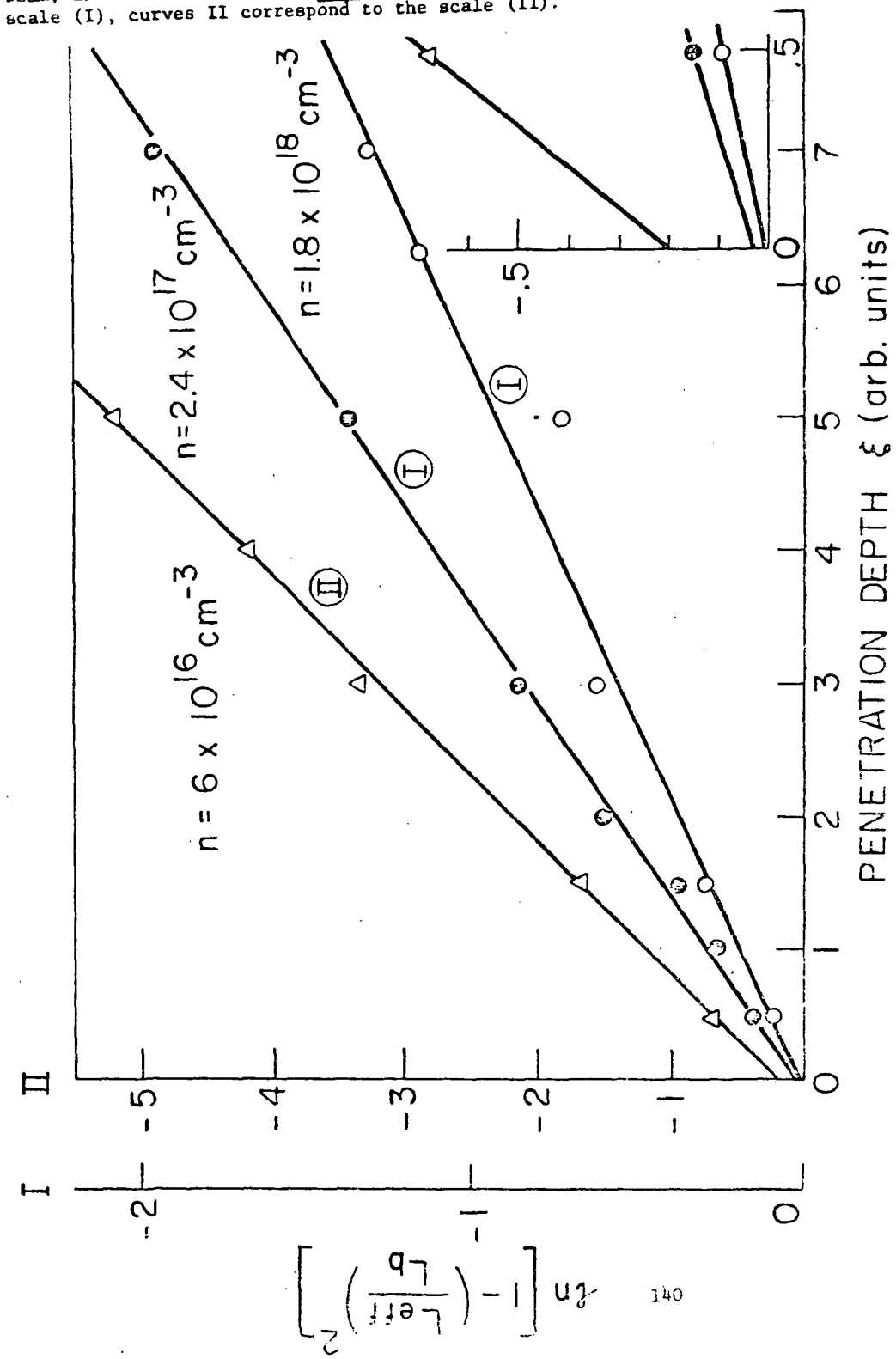

SURFACE STATES AND SURFACE RECOMBINATION ON WIDE BAND-GAP SEMICONDUCTORS

C. E. BYVIK

SURFACE STATES AND SURFACE RECOMBINATION OF WIDE BAND-GAP SEMICONDUCTORS

C. E. Byvik NASA Langley Research Center

Analyses of the material properties of semiconductors for use as solar cells have indicated that wide band-gap semiconductors are theoretically the most efficient materials for energy conservation in space and terrestrial applications. A wide band-gap material that is readily available and has near optimum properties for use as a solar cell is gallium arsenide. However, the GaAs solar cells fabricated to date have exhibited efficiencies short of that theoretically attainable. This reduced efficiency has been attributed to the physical properties of surface states that lead to a high surface recombination velocity. In order to achieve the goal of efficient solar cells, an objective of this program is to characterize the properties of the surface of GaAs that lead to the decreased efficiency observed for this material.

The research to date has led to the following results: (1) the energy position of the observed surface states coincide closely to energy positions observed for bulk impurities; (2) these energy states, their position and their capture cross-sections, appear to be independent of surface treatment and crystal orientations; (3) the calculated surface recombination velocity using the measured quantities for the density of states, and capture cross sections as well as the surface voltage agrees with the measured surface recombination velocity to within an order of magnitude; (4) the surface voltage varied from sample to sample but was relatively insensitive to changes in ambient gases such as water vapor and oxygen; and (5) only depletion layers have been observed both in this laboratory and as reported by others for GaAs. These results indicate that deep bulk impurities pinned by the Fermi level at the surface may be responsible for the observed surface voltage and properties.

The present work consists of (1) an experimental effort to determine the effect of known deep bulk impurities in the interpretation of surface photovoltage spectroscopy, and (2) an analytical effort to include deep impurity states near the surface and determine their effect on surface voltage, surface photovoltage, and surface recombination.

To determine the impurities present in material used in this research, samples of tellurium doped GaAs from three manufacturers were analyzed for impurity content by ion probe mass spectrometry. The results of this analysis are shown in Table 1. Also indicated in the table are the types of impurity state in GaAs where known (i.e., donor or acceptor states) and the measured position of these states. It should be noted that the concentrations of the iron and copper impurities are of the same order as the carrier concentration and that they are acceptor states in GaAs. This result supports the proposed model since bulk acceptor states present in concentrations of the order of 10^{17} to $10^{18}/cm^3$ will be present at the surface with surface densities of the order of 10^{11} to $10^{12}/cm^2$ which coincides with measured surface state densities.

Results of an initial analytical effort to determine the effect of bulk impurity states present at the surface on the surface voltage indicate that the surface voltage is dependent on the position of the impurity level with respect to the Fermi level and pinned at the Fermi level. A next step is to determine the effect of a number of deep impurity levels on the surface voltage and the extent of the depletion layer. The consequence of the validity of this model is that by identifying and eliminating the impurities which result in surface states the efficiency of solar cells will be increased.

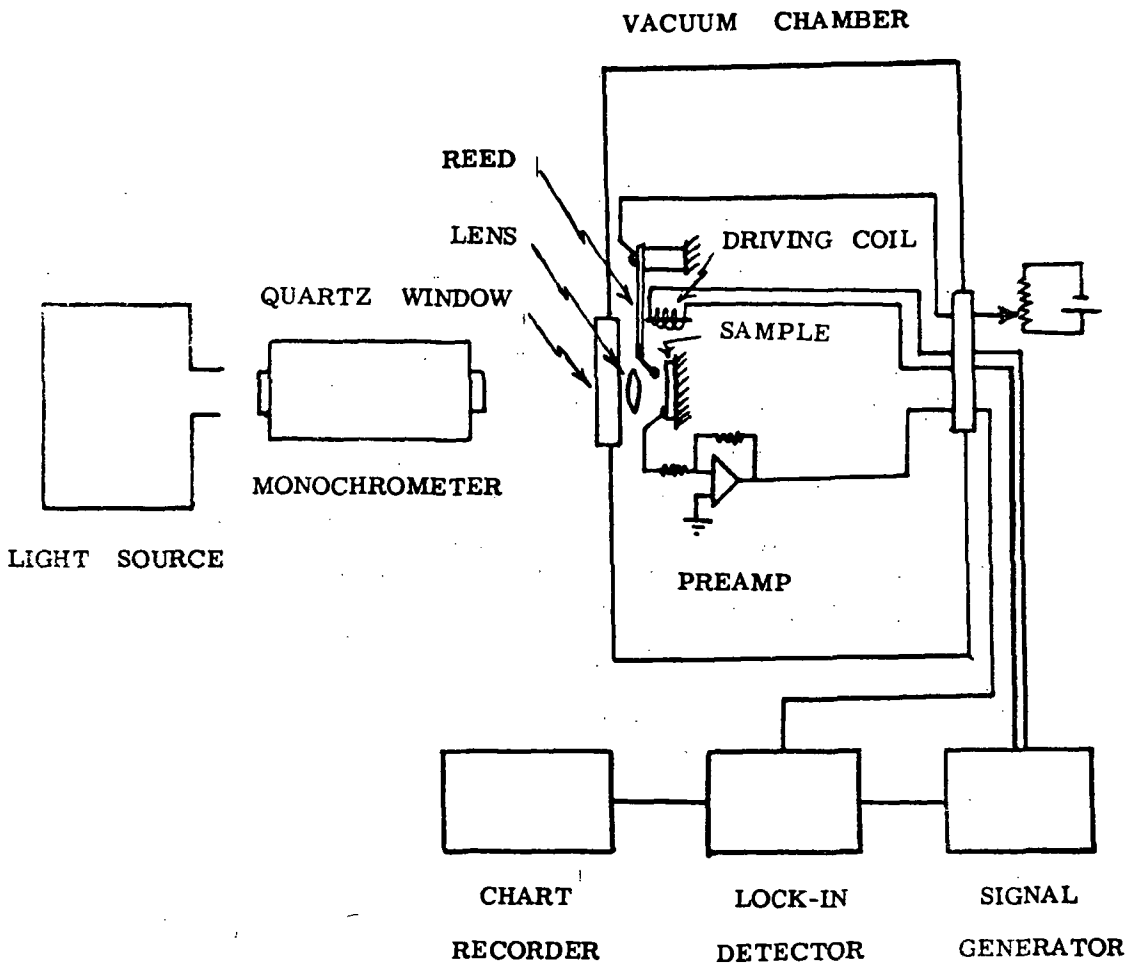

SCHEMATIC DIAGRAM OF THE EXPERIMENTAL SET-UP

X-1

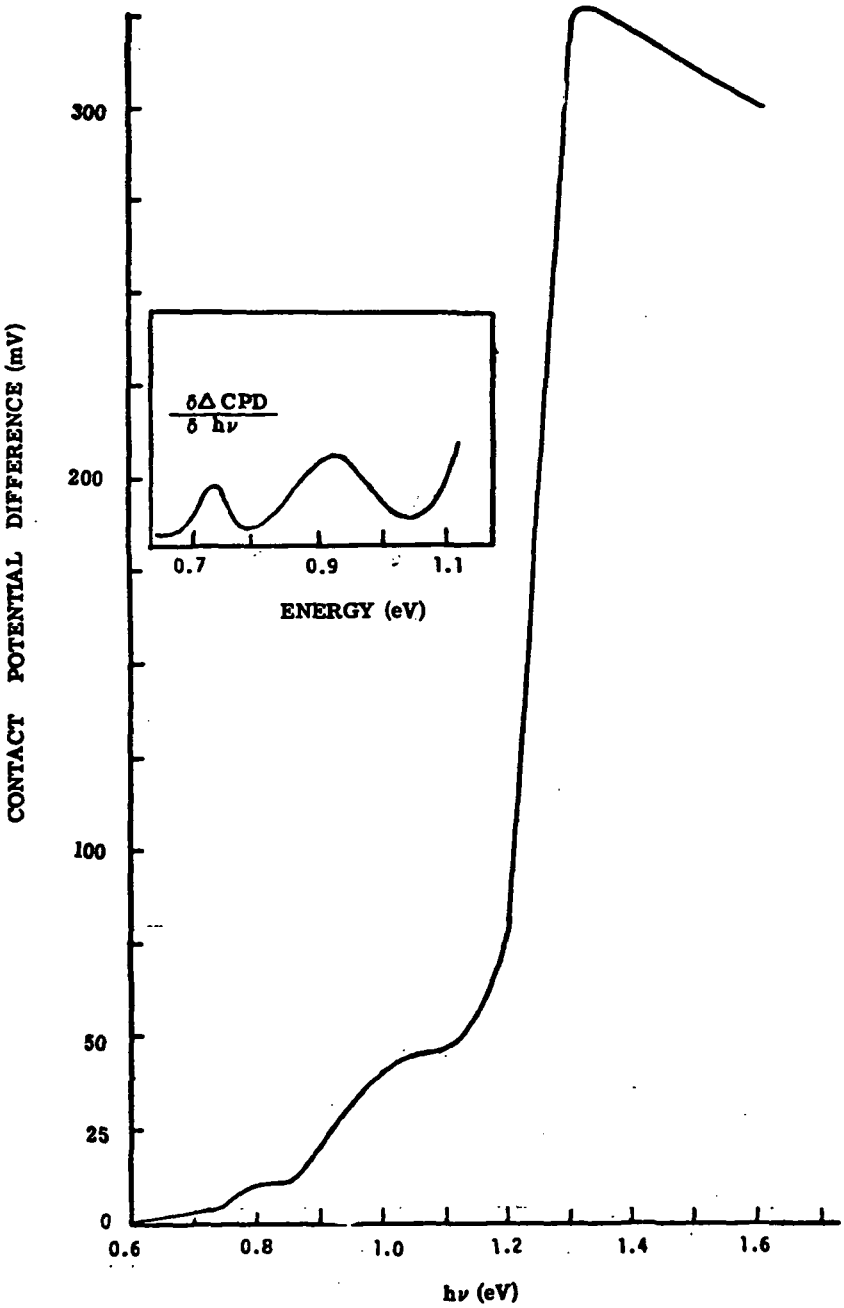

PHOTOVOLTAGE SPECTRUM OF THE (111) SURFACE OF GaAs (from GATOS)

X-2

SURFACE STATES REPORTED ON GALLIUM ARSENIDE

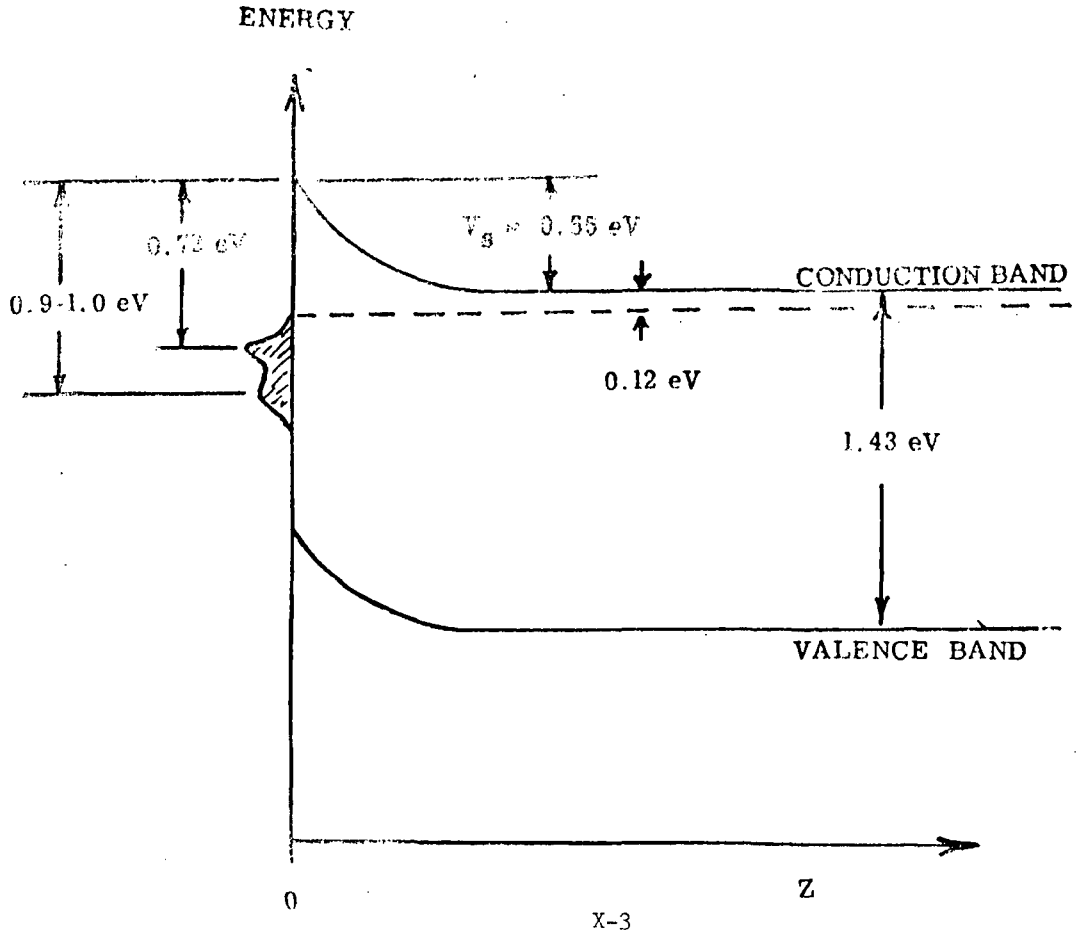

X-3

PHOTOVOLTAGE SPECTRUM OF (100) SURFACE OF n-TYPE GaAs IN VACUUM

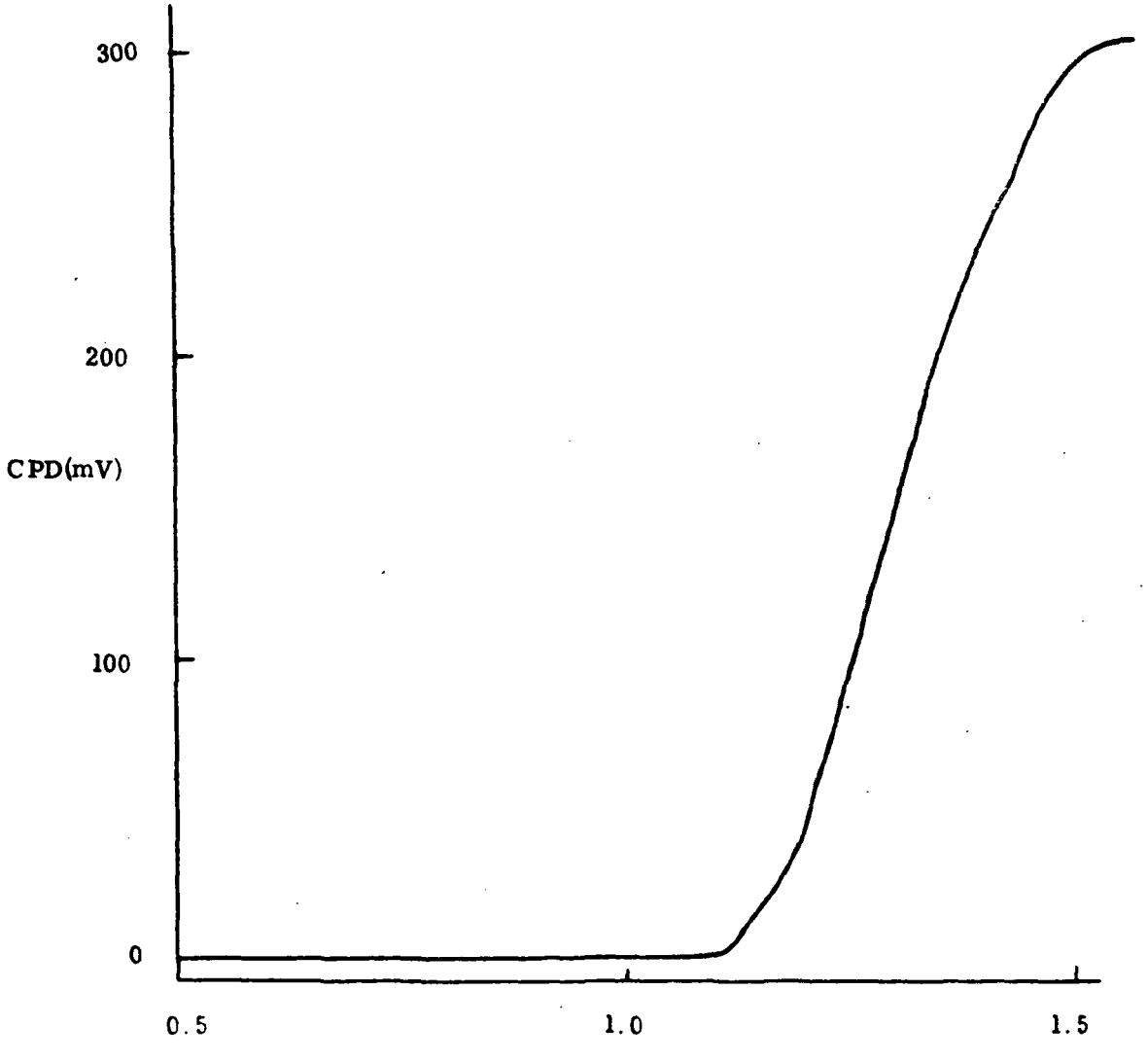

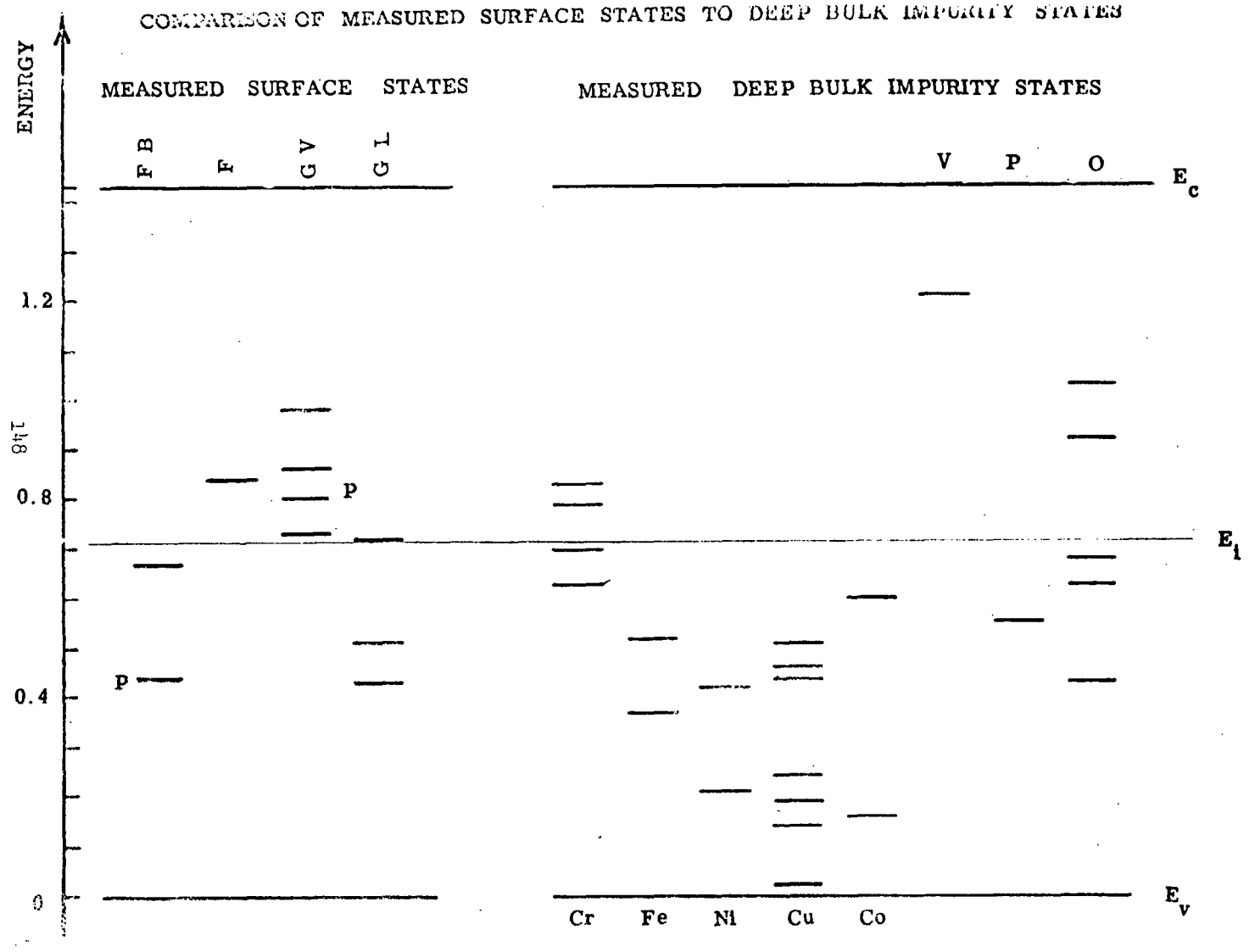

ION PROBE MASS SPECTROSCOPIC ANALYSIS OF THREE GALLIUM ARSENIDE SAMPLES

IMPURITY	Acceptor (A)	(E_c-E_t) (eV)	Sample	Boat Grown 1	Boat Grown 2	EPI Grown 3
			Carrier Concentration	3.8×10^{17}/cc	3.0×10^{17}/cc	1×10^{17}/cc
Cr	A	0.80, 0.73		0.088 x 10^{17}/cc	0.088 x 10^{17}/cc	0.044 x 10^{17}/cc
		0.40, 0.64				
Fe	A	1.06, 0.91		8.4	0.92	0.57
Cu	A	1.20, 1.28		2.0	0.26	0.44
		1.25, 1.19				
		0.99, 0.97				
		0.92				
P	D	0.88		6.6	2.6	6.6
Na				22	22	0.88
K				12	2.2	0.44
Ca				13	0.44	0.44
C	A	1.41		88	88	88
Al				0.88	1.3	1.3
Si	A, D	1.40, 1.33		120	16	2.5
		1.21, 0.006				

X-7 BULK IMPURITY MODEL RESULTING IN SURFACE STATES ON GALLIUM ARSENIDE

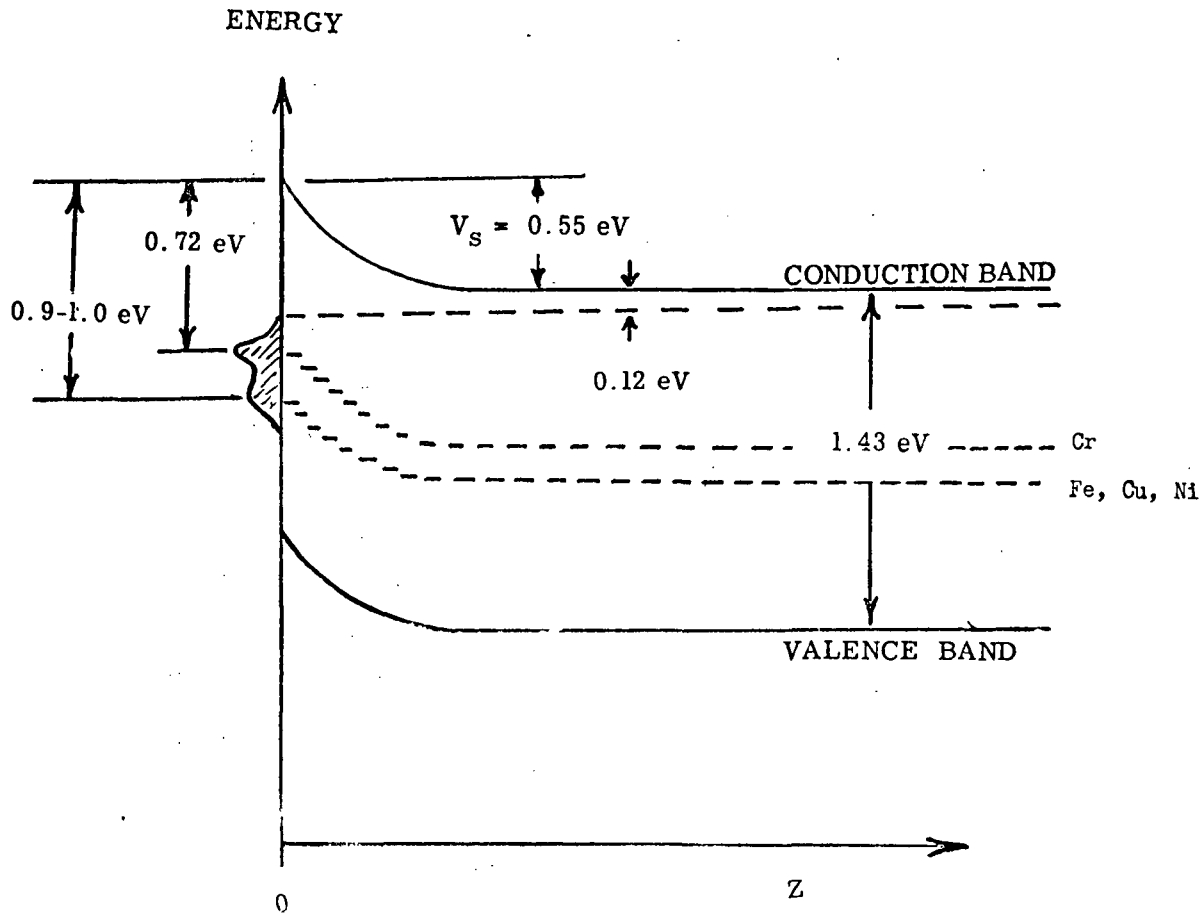

BULK IMPURITY MODEL OF SURFACE STATES AND SURFACE VOLTAGE

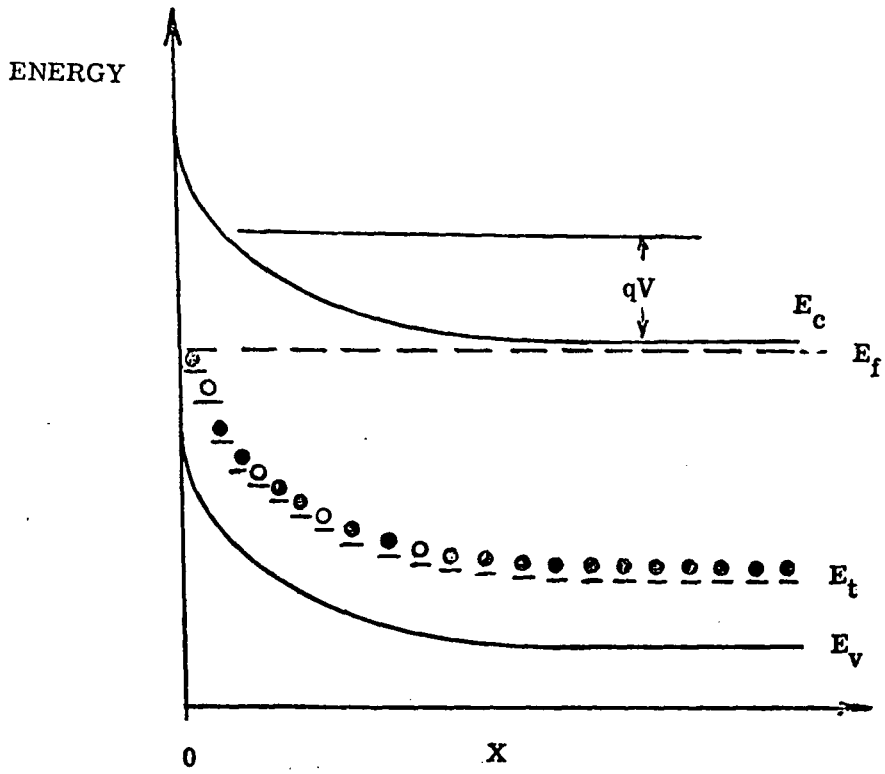

POISSON EQUATION

$$\frac{d^2V}{dx^2} = n - p - N_D + N_A f(E_t - E_f)$$

RATIO OF THE CENTERS OF CHARGE

$$\frac{L_c}{L_B} = (1 + 6 \times 10^{-18} N_A)^{1/2}$$

INVESTIGATION OF LIQUID EPITAXIAL GaAs:Si LAYERS

K. L. Ashley Southern Methodist University

Abstract

GaAs layers were obtained with liquid epitaxial crystal growth with Si as dopant where the temperature growth range was maintained at a sufficiently high level to obtain n-type material. Growth temperature range was 925 to 900° C. The doping level was in the 10^{16} cm^{-3} range. The object was to obtain n-type material with long electron hole diffusion length. p-n junctions were formed on some of the n layers obtained by growing an additional layer which was doped with Ge. These were used for obtaining reverse bias C-V data and optical microprobe information. The C-V data exhibited an internal shunt capacitance of unknown origin. Therefore, it was necessary to determine the magnitude of this capacitance before doping density information could be extracted from the C-V data. This was done by assuming that the total measured diode capacitance contained the depletion region capacitance in parallel with the unknown shunt capacitance, i.e.

$$C \text{ (total measured)} = K(V_a + V_b)^{-1/2} + C \text{ (shunt)}$$

where V_a and V_b are the applied and built in voltages.
A plot of C (total measured) versus $(V_a + V_b)^{-1/2}$ then yields C (shunt) as the intercept of the C (total measured) axis obtained by an extrapolation of the plotted data. This form of assumed capacitance proved to represent the behavior very well and permitted the use of the C-V data for obtaining doping density magnitudes which agreed with Hall effect results. Optical microprobe plots were also obtained with the p-n junction devices which indicated that the hole diffusion lengths were approximately 10 microns long.

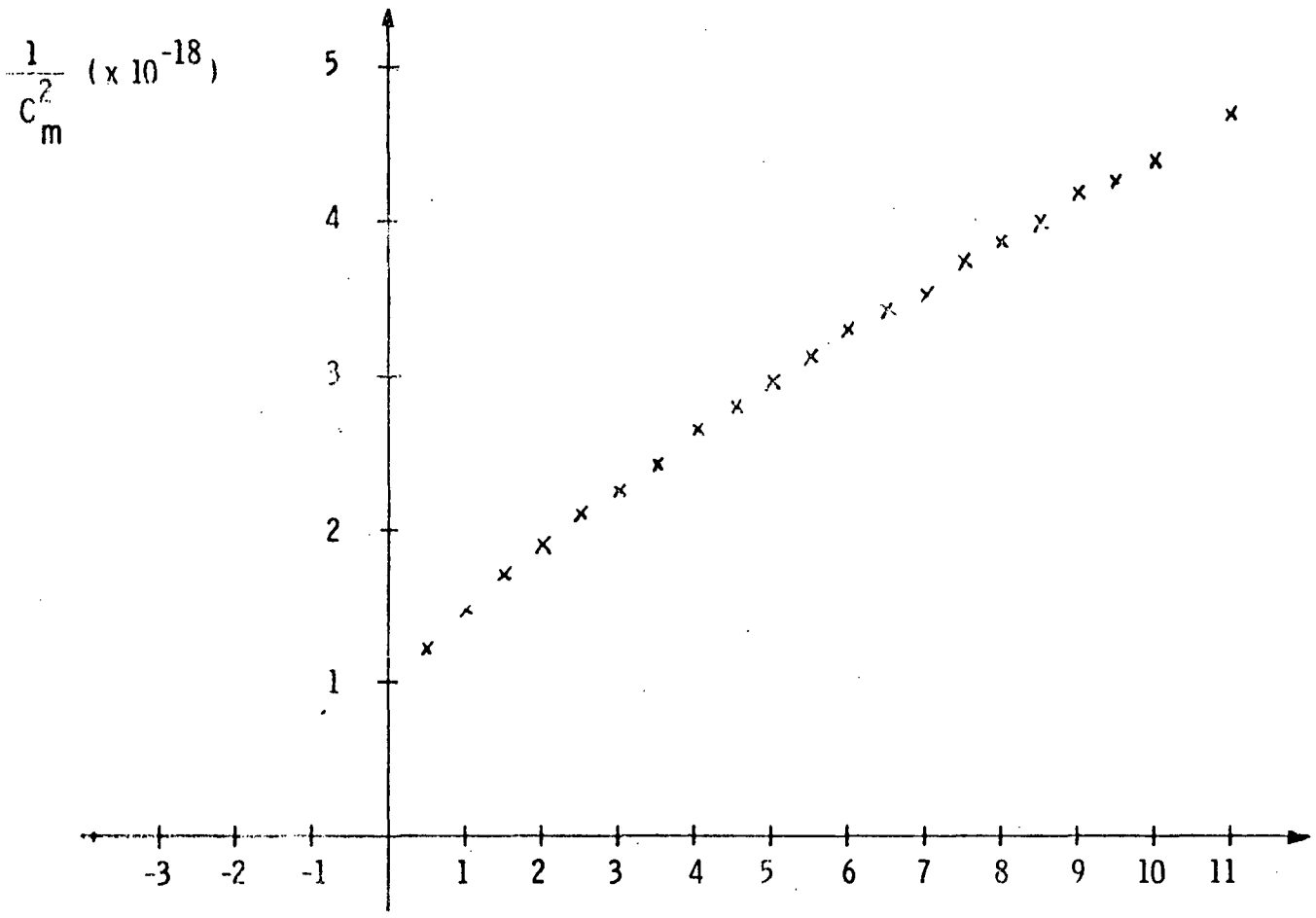
$\frac{1}{C_m^2}$ ($\times 10^{-18}$)
5
4
3
2
1
-3
-2
-1
1
2
3
4
5
6
7
8
9
10
11
REVERSE-BIAS VOLTS

Capacitance of abrupt, p + n junction with internal parallel capacitance

$$C_m = \frac{K}{(V_B + V_A)^{1/2}} + C_S$$

$$K = \left\{ \frac{q\epsilon N_D}{2} \right\}^{1/2}$$

$$\frac{1}{(C_m - C_S)^2} = \left\{ \frac{2}{q\epsilon N_D} \right\} (V_B + V_A)$$

$$\log(C_m - C_S) = -\frac{1}{2} \log(V_B + V_A) + \text{const.}$$

XI.2

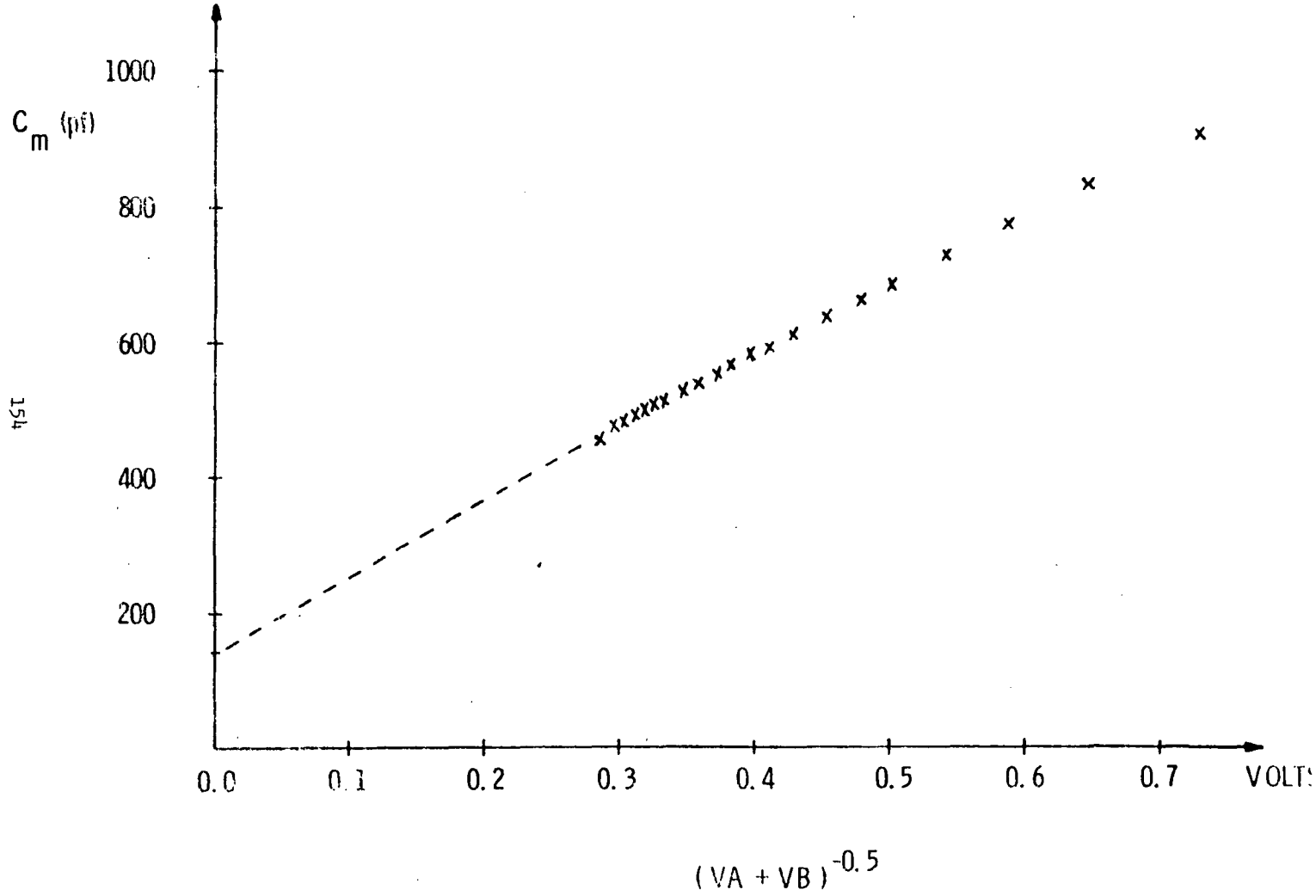
1000
800
600
400
200
C_m (pf)
0.0
0.1
0.2
0.3
0.4
0.5
0.6
0.7
VOLTS
$(VA + VB)^{-0.5}$

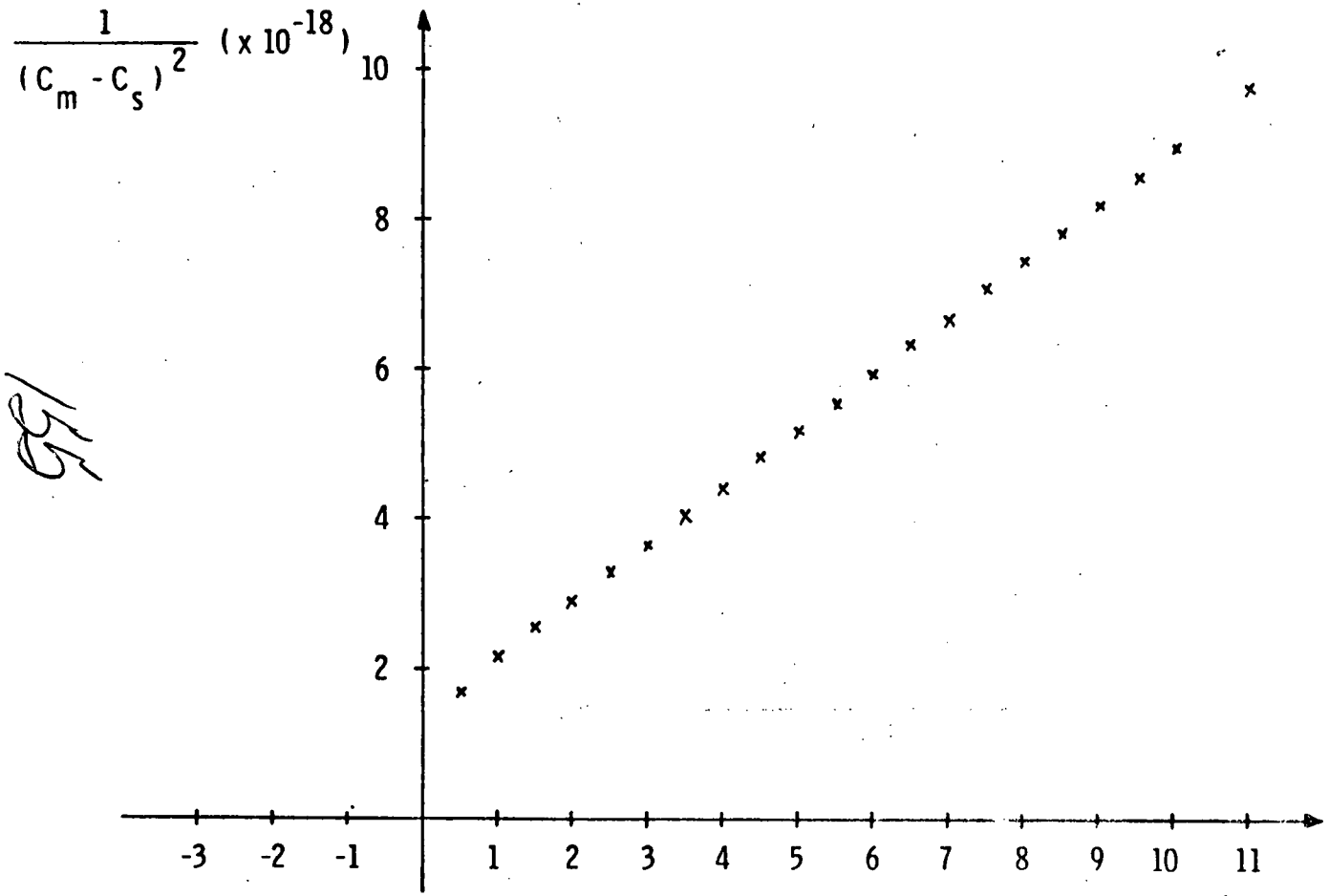
$\frac{1}{(C_m - C_s)^2}$ ($\times 10^{-18}$)
10
8
6
4
2
-3
-2
-1
1
2
3
4
5
6
7
8
9
10
11
REVERSE-BIAS VOLTS

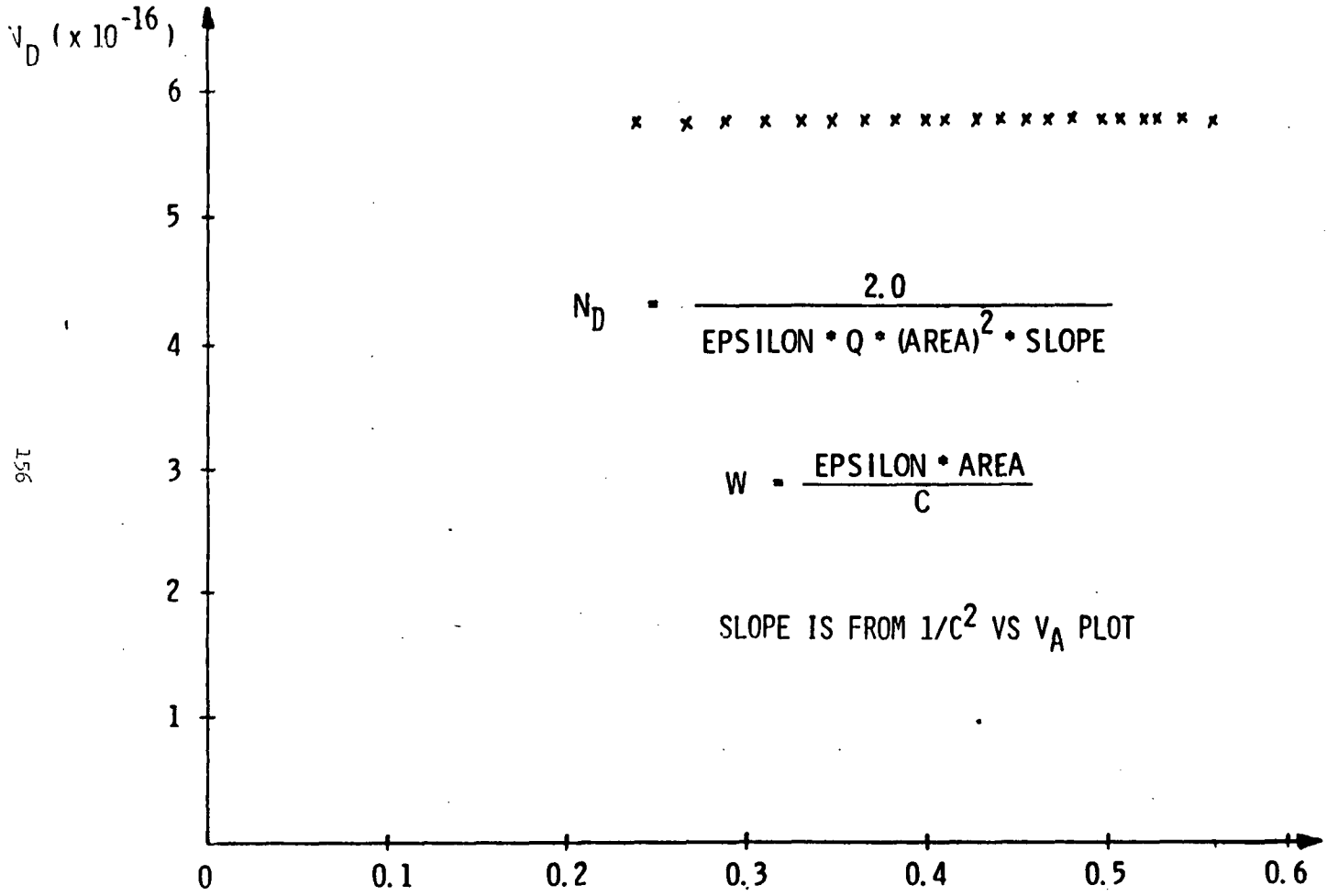
N_D (x 10^{-16})
6
5
4
3
2
1
0
0.1
0.2
0.3
0.4
0.5
0.6
$N_D = \frac{2.0}{EPSILON * Q * (AREA)^2 * SLOPE}$
$W = \frac{EPSILON * AREA}{C}$
SLOPE IS FROM $1/C^2$ VS V_A PLOT
DEPLETION REGION DISTANCE INTO THE N-SIDE (MICRONS)

Hg ARC EXCITATION SOURCE, λ = 5461 A

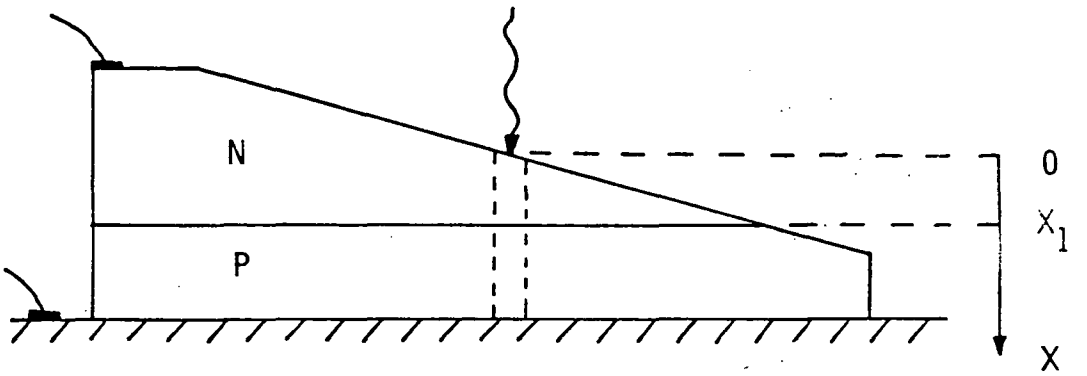

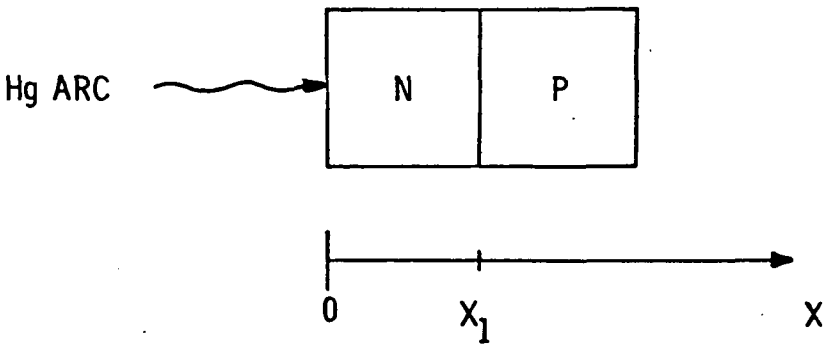

RELATIVE RESPONSE, R

$$R = \frac{v_d}{v_d + s} \times t$$

s = surface recombination velocity

v_d = diffusion velocity ($x = 0$)

$= D/L = L/\tau$

t = transport factor

$= 1/\cosh(x_1/L)$

$$R = \frac{1}{(s/v_d)\sinh(x_1/L) + \cosh(x_1/L)}$$

TWO EXTREME RESPONSE MODES

	Condition	$v_d(x = 0)$	Response
1	$x_1 \ll L_p$	D_p/x_1	1
2	$x_1 \gg L_p$	D_p/L_p	$\frac{2}{1 + s/v_d} e^{-x_1/L_p}$

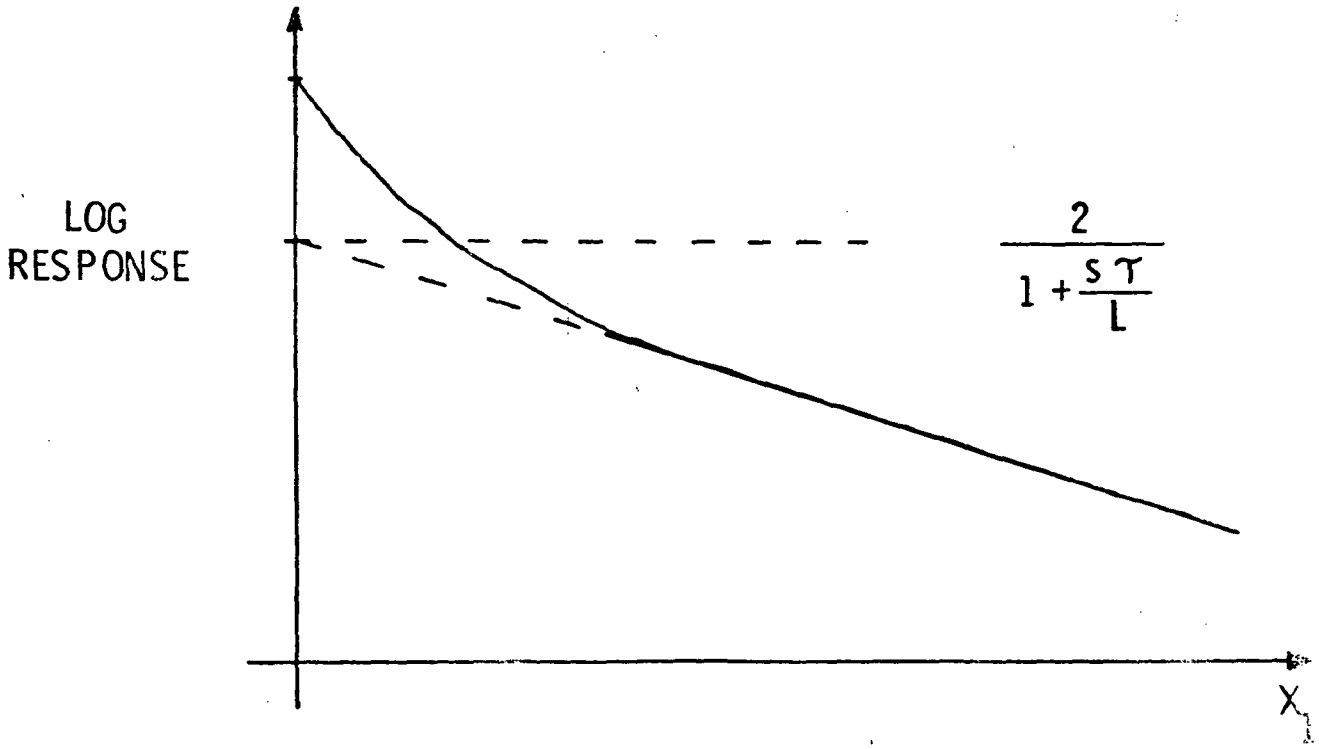
LOG
RESPONSE
$\frac{2}{1+\frac{s\tau}{L}}$
X

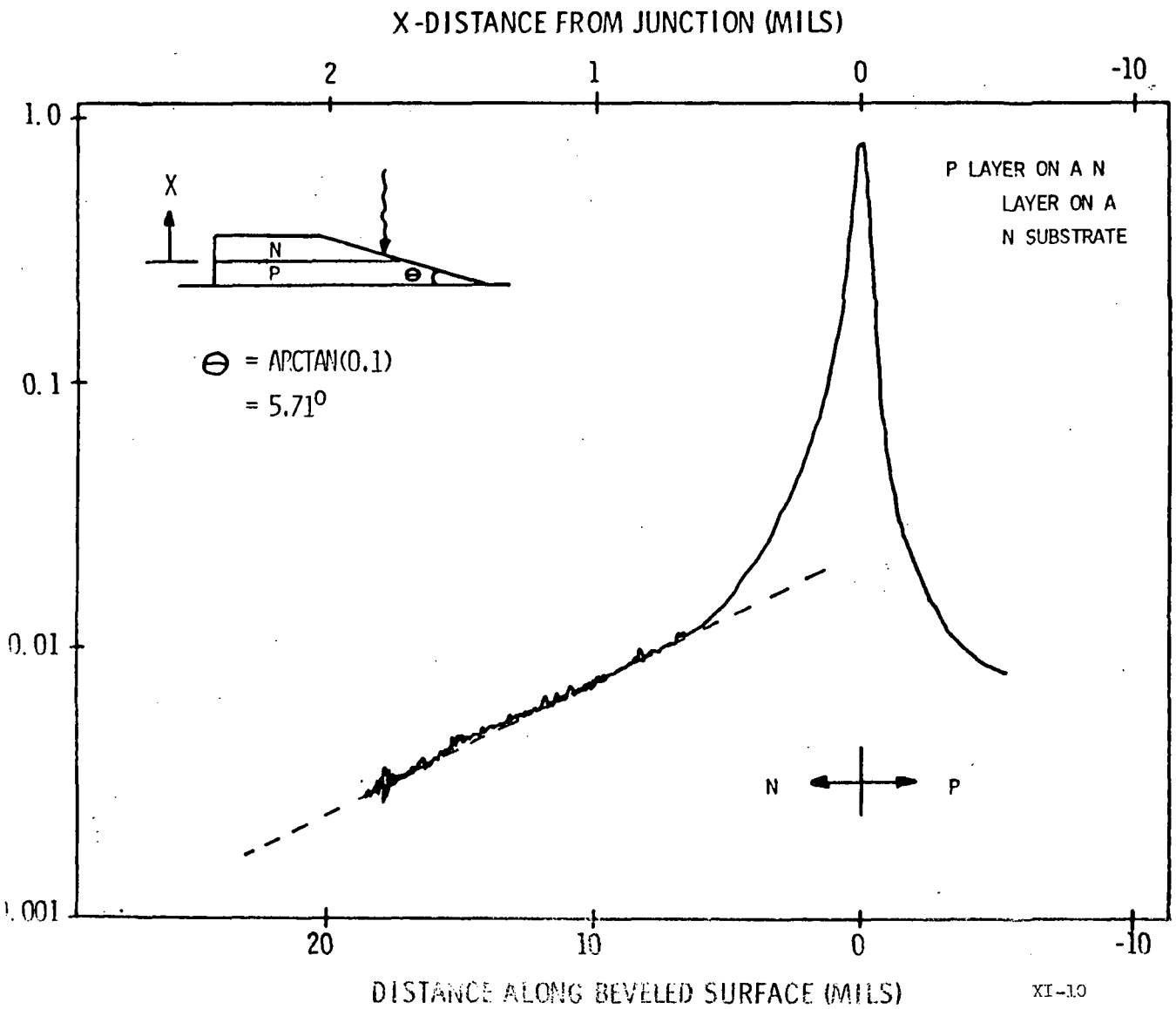
X-DISTANCE FROM JUNCTION (MILS)
2
1
0
-10
1.0
0.1
0.01
.001
X
N
P
Θ
Θ = ARCTAN(0.1)
= 5.71°
P LAYER ON A N
LAYER ON A
N SUBSTRATE
N
P
20
10
0
-10
DISTANCE ALONG BEVELED SURFACE (MILS)

XI-10

CALCULATION OF s

$x_1 = 0$ Intersection of large x_1 asymptote

$$= \frac{s/v_d + 1}{2} \simeq 50$$

$$s \simeq 100 v_d$$

With D = 5 ($\mu_p = 200$), $L_p = 10^{-3}$ cm^{-3}, ($v_d = 5 \times 10^3$)

$$s \simeq 5 \times 10^5 \text{ cm/sec}$$

XI-11

Math Modeling of GaAs and Si Terrestrial Solar Hybrid Systems

John Heinbockel and Sidney Roberts
Old Dominion University

Summary

Various silicon hybrid systems are modeled and compared with a GaAs hybrid system. The hybrid systems modeled produce electric power and also thermal power which can be used for heating or air conditioning. Various performance indices are defined and are used to compare system performance. The performance indices are: capital cost per electric energy out; capital cost for total energy out; capital cost per electric energy plus mechanical work; annual cost per annual electric power; and annual cost per electric power plus annual mechanical work. These performance indices indicate that concentrator hybrid systems can be cost effective when compared to present day energy costs.

Realistic costs and efficiencies of GaAs and Si are, respectively, $\$35000/m^2$ for 15 percent efficient solar cells and $\$1000/m^2$ for 10 percent efficient solar cells. The performance indices show that limiting values for annual costs are 10.3¢/KWH and 6.8¢/KWH for Si and GaAs, respectively. Results demonstrate that for a given flow rate there is an optimal operation condition for maximum photovoltaic output for concentrator systems. Also, high concentration hybrid systems produce a distinct cost advantage over flat plate hybrid systems.

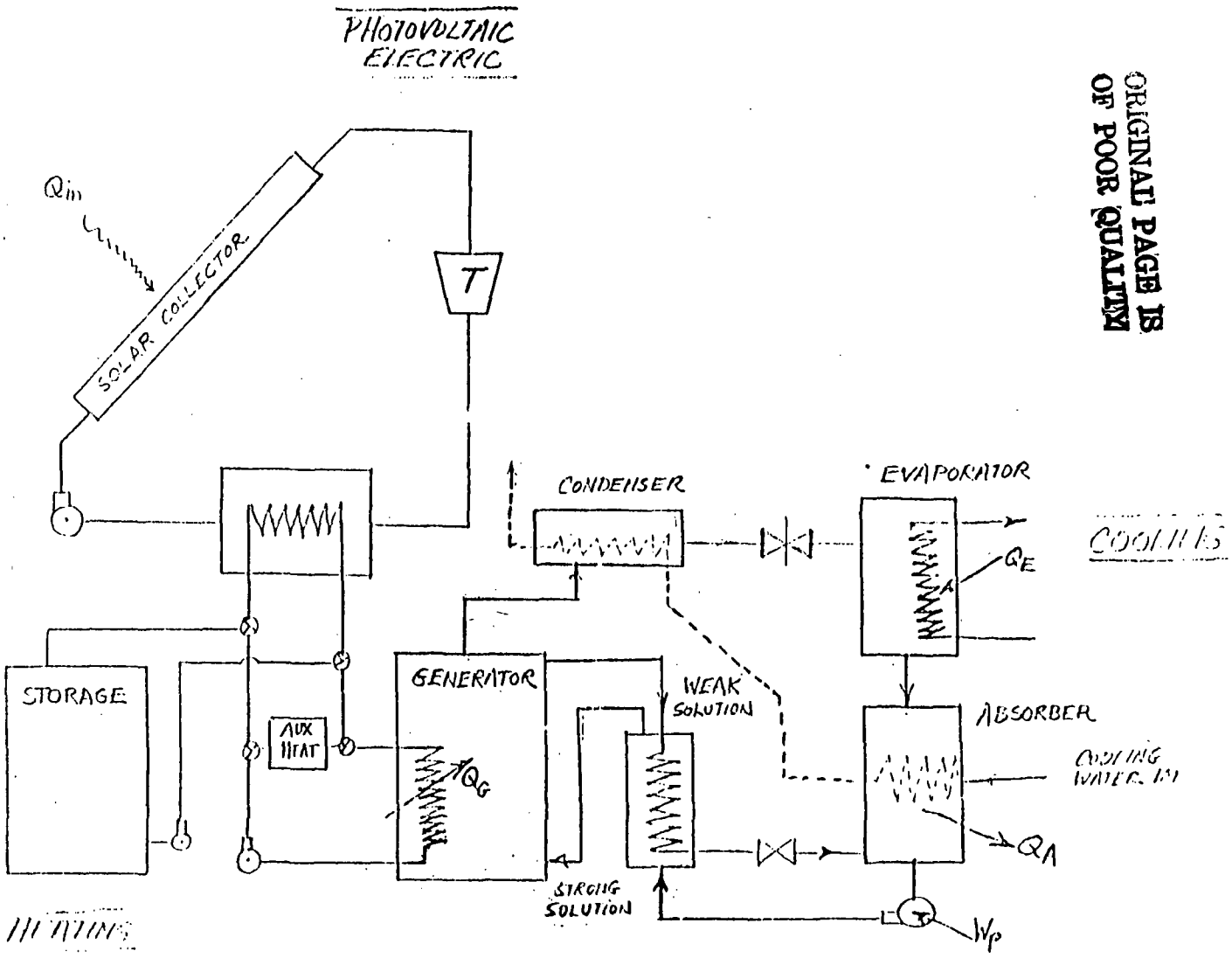

SYSTEM I

FLAT PLATE COLLECTOR FOR THERMAL ENERGY
FLAT PLATE COLLECTOR (SILICON SOLAR CELLS) FOR ELECTRICAL ENERGY

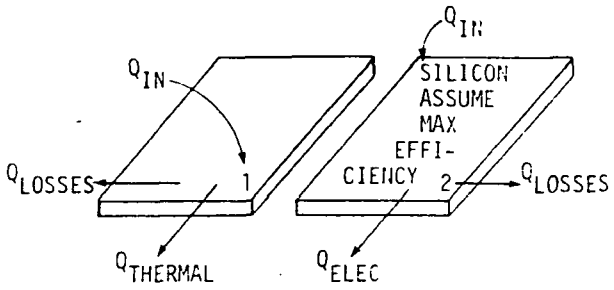

$$Q_{IN} = .84I_N \quad W/m^2$$

$$Q_{LOSS} = h_1(T_{CK} - T_{airK}) + \varepsilon\sigma(T_{CK}^4 - T_{airK}^4) \quad W/m^2$$

$$Q_{ELEC} = \eta_3 Q_{IN}$$

$$Q_{THERMAL} = \frac{\dot{m}C_o}{Aabs}\ T_C - T_F)$$

ENERGY BALANCE (SILICON PLATE)

$$Q_{IN} - Q_{ELEC} - Q_{LOSSES} = 0$$

$$(1 - \eta_3)(.84)I_N - h_1(T_{CK} - T_{airK}) - \varepsilon\sigma(T_{CK}^4 - T_{airK}^4) = 0$$

ENERGY BALANCE FOR THERMAL ENERGY

$$Q_{IN} - Q_{LOSSES} - Q_{THERMAL} = 0$$

$$Q_{THERMAL} = .84I_N - h_1(T_{CK} - T_{airK}) - \varepsilon\sigma(T_{CK} - T_{airK}) = \frac{\dot{m}C_p}{Aabs}\ (T_{CK} - T_{FK})$$

COST CON = $400\eta_2 + 10$ \$/m^2 η_2 = EFFICIENCY OF COLLECTOR = $\frac{Q_{THERMAL}}{Q_{IN}}$

COST FLAT PLATE PLUS SILICON - 1000. + 56.

SYSTEM II

FLAT PLATE COLLECTOR FOR THERMAL ENERGY HAVING SILICON
WITH EFFICIENCY OF SILICON AS FCN OF TEMPERATURE

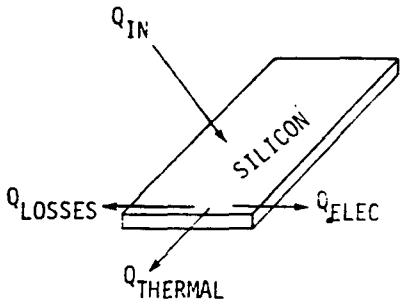

ENERGY BALANCE

$$Q_{IN} - Q_{ELEC} - Q_{LOSSES} - Q_{THERMAL} = 0$$

$$(1 - \eta_3)(.84)I_N - h_1(T_{CK} - T_{airK}) - \varepsilon\sigma(T_{CK}^4 - T_{airK}^4) = \frac{\dot{m}C_p}{Aabs}(T_{CK} - T_{FK})$$

PERFORMANCE INDEX P

$$P_1 = \frac{\text{CAPITAL COST}}{\text{PEAK(ELEC + MECH)POWER}} = \frac{(\text{COST FP}_1)Aabs + (\text{COST FP}_2 + \text{COST CELL})Aabs}{Q_{ELEC}\,Aabs + .5\left(1 - \frac{T_{FK}}{T_{CK}}\right)Q_{THERMAL}}$$

$$P_2 = \frac{\text{CAPITAL COST}}{\text{TOTAL POWER OUT}} = \frac{(\text{COST FP}_1)Aabs + (\text{COST FP} + \text{COST CELL})Aabs}{(Q_{ELEC} + Q_{THERMAL})Aabs}$$

$$P_3 = \frac{\text{CAPITAL COST}}{\text{ELEC POWER}} = \frac{(\text{COST FP}_1)Aabs + (\text{COST FP} + \text{COST CELL})Aabs}{Q_{ELEC}\,Aabs}$$

SYSTEMS III AND IV

III - GaAs SOLAR CELLS

IV - SILICON SOLAR CELLS

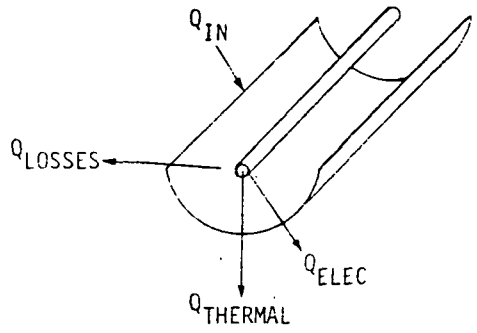

Aap = APERTURE AREA

Aabs ABSORBER AREA OF RECEIVER

As = SURFACE AREA OF RECEIVER

$C_{TH} = \frac{Aap}{Aabs}$ = THEORETICAL CONCENTRATION RATIO

$\frac{As}{Aabs} = 2$

COST CON = 100 + $\eta_1$80. $/m²

[INCLUDES TRACKING STRUCTURAL (WIND) SUPPORTS]

$Q_{IN} = \eta_1 I_N C_{TH}$ $\quad Q_{ELEC} = \eta_3 Q_{IN}$

$Q_{LOSSES} = 2h_1(T_{CK} - T_{airK}) + 2\varepsilon\sigma(T_{CK}^4 - T_{airK}^4)$

ENERGY BALANCE

$$Q_{IN} - Q_{ELEC} - Q_{LOSSES} = Q_{THERMAL}$$

$Q_{THERMAL} = \frac{\dot{m}C_p}{Aabs}(T_{CK} - T_{FK})$

PERFORMANCE INDEX P

$$P_1 = \frac{\text{CAPITAL COST}}{\text{PEAK(ELEC + MECH)POWER}} = \frac{(\text{COST CON})Aap + (\text{COST CELL})(Aabs)}{Q_{ELEC} \cdot Aabs + .5\left(1 - \frac{T_{FK}}{T_{CK}}\right) Q_{THERMAL} \cdot Aabs}$$

$$= \frac{\text{COST CON} + \frac{\text{COST CELL}}{C_{TH}}}{\frac{Q_{ELEC} + .5\left(1 - \frac{T_{FK}}{T_{CK}}\right) Q_{THERMAL}}{C_{TH}}}$$

$$P_2 = \frac{\text{CAPITAL COST}}{\text{TOTAL POWER}} = \frac{\text{COST CON} + \frac{\text{COST CELL}}{C_{TH}}}{\frac{Q_{ELEC} + Q_{THERMAL}}{C_{TH}}}$$

$$P_3 = \frac{\text{CAPITAL COST}}{\text{ELEC POWER}} = \frac{\text{COST CON} + \frac{\text{COST CELL}}{C_{TH}}}{\frac{Q_{ELEC}}{C_{TH}}}$$

SYSTEM V

CONCENTRATOR FOR THERMAL ENERGY AND SEPARATE FLAT PLATE COLLECTOR FOR ELECTRIC ENERGY WITH SILICON SOLAR CELLS

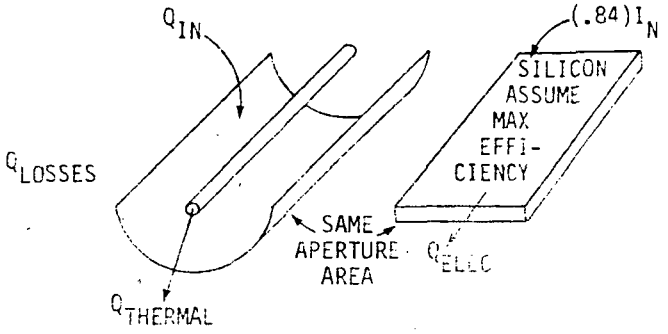

$$Q_{IN} = \eta_1 I_N C_{TH}$$

$$Q_{ELEC} = \eta_2 (.84) I_N$$

$$Q_{LOSSES} = 2h_1(T_{CK} - T_{airK}) + 2\varepsilon\sigma(T_{CK}^4 - T_{airK}^4)$$

$$Q_{THERMAL} = \frac{\dot{m}C_p}{Aabs}(T_{CK} - T_{FK})$$

ENERGY BALANCE

$$Q_{THERMAL} = Q_{IN} - Q_{LOSSES}$$

$$\text{COST CON} = \$100 + \eta_1 80.$$

PERFORMANCE INDEX P

$$P_1 = \frac{\text{CAPITAL COST}}{\text{PEAK(ELEC + MECH)POWER}} = \frac{(\text{COST CON})Aap + (\text{COST CELL} + \text{COST FP})Aap}{Q_{ELEC} \cdot Aap + .5\left(1 - \frac{T_{FK}}{T_{CK}}\right)Q_{THERMAL} \cdot Aabs}$$

$$= \frac{\text{COST CON} + \text{COST CELL} + \text{COST FP}}{Q_{ELEC} + .5\left(1 - \frac{T_{FK}}{T_{CK}}\right)\frac{Q_{THERMAL}}{C_{TH}}}$$

$$P_2 = \frac{\text{CAPITAL COST}}{\text{TOTAL POWER}} = \frac{\text{COST CON} + \text{COST CELL} + \text{COST FP}}{Q_{ELEC} + \frac{Q_{THERMAL}}{C_{TH}}}$$

$$P_3 = \frac{\text{CAPITAL COST}}{\text{ELEC POWER}} = \frac{\text{COST CON} + \text{COST CELL} + \text{COST FP}}{Q_{ELEC}} = \text{CONSTANT}$$

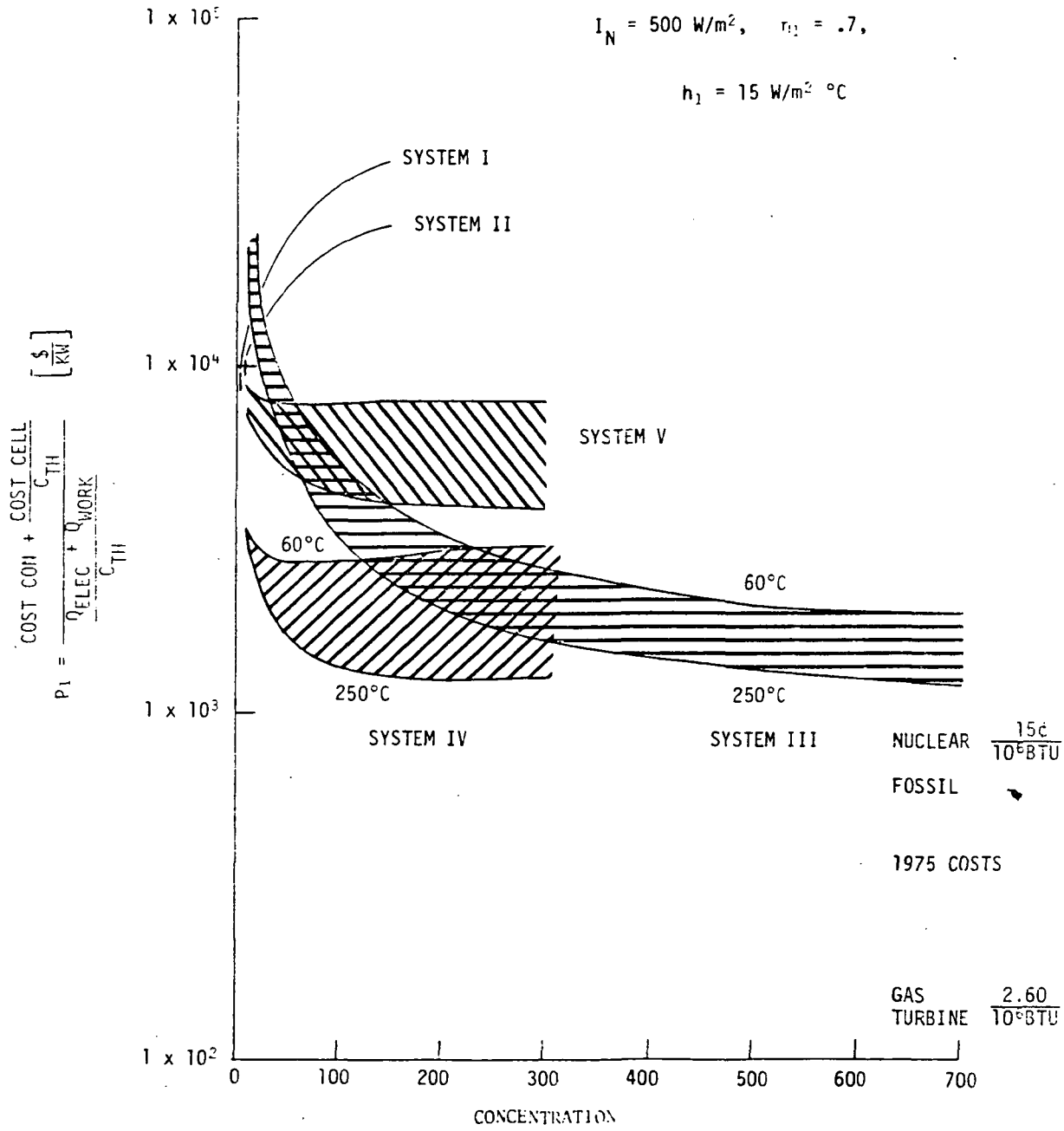
I_N = 500 W/m², η_1 = .7,
h_1 = 15 W/m² °C
SYSTEM I
SYSTEM II
SYSTEM V
60°C
60°C
250°C
250°C
SYSTEM IV
SYSTEM III
NUCLEAR 15¢/10⁶BTU
FOSSIL
1975 COSTS
GAS TURBINE 2.60/10⁶BTU
1 x 10⁵
1 x 10⁴
1 x 10³
1 x 10²
0
100
200
300
400
500
600
700
CONCENTRATION
$P_1 = \frac{\text{COST CON} + \frac{\text{COST CELL}}{C_{TH}}}{\frac{Q_{ELEC} + Q_{WORK}}{C_{TH}}}$ $\left[\frac{\$}{KW}\right]$

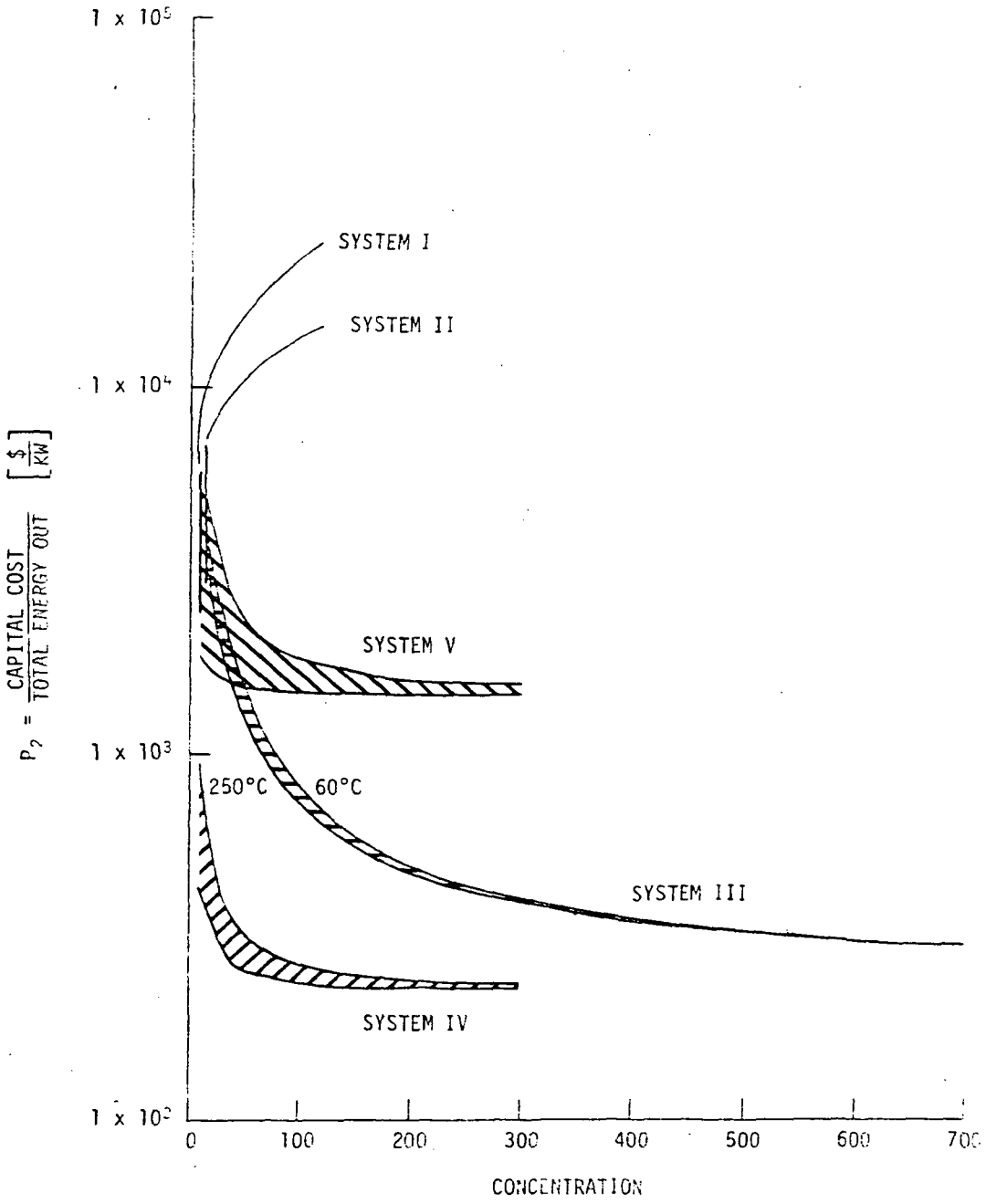
1 x 10⁵
1 x 10⁴
1 x 10³
1 x 10²
SYSTEM I
SYSTEM II
SYSTEM V
250°C
60°C
SYSTEM III
SYSTEM IV
0
100
200
300
400
500
600
700
CONCENTRATION
P2 = CAPITAL COST / TOTAL ENERGY OUT [$/KW]

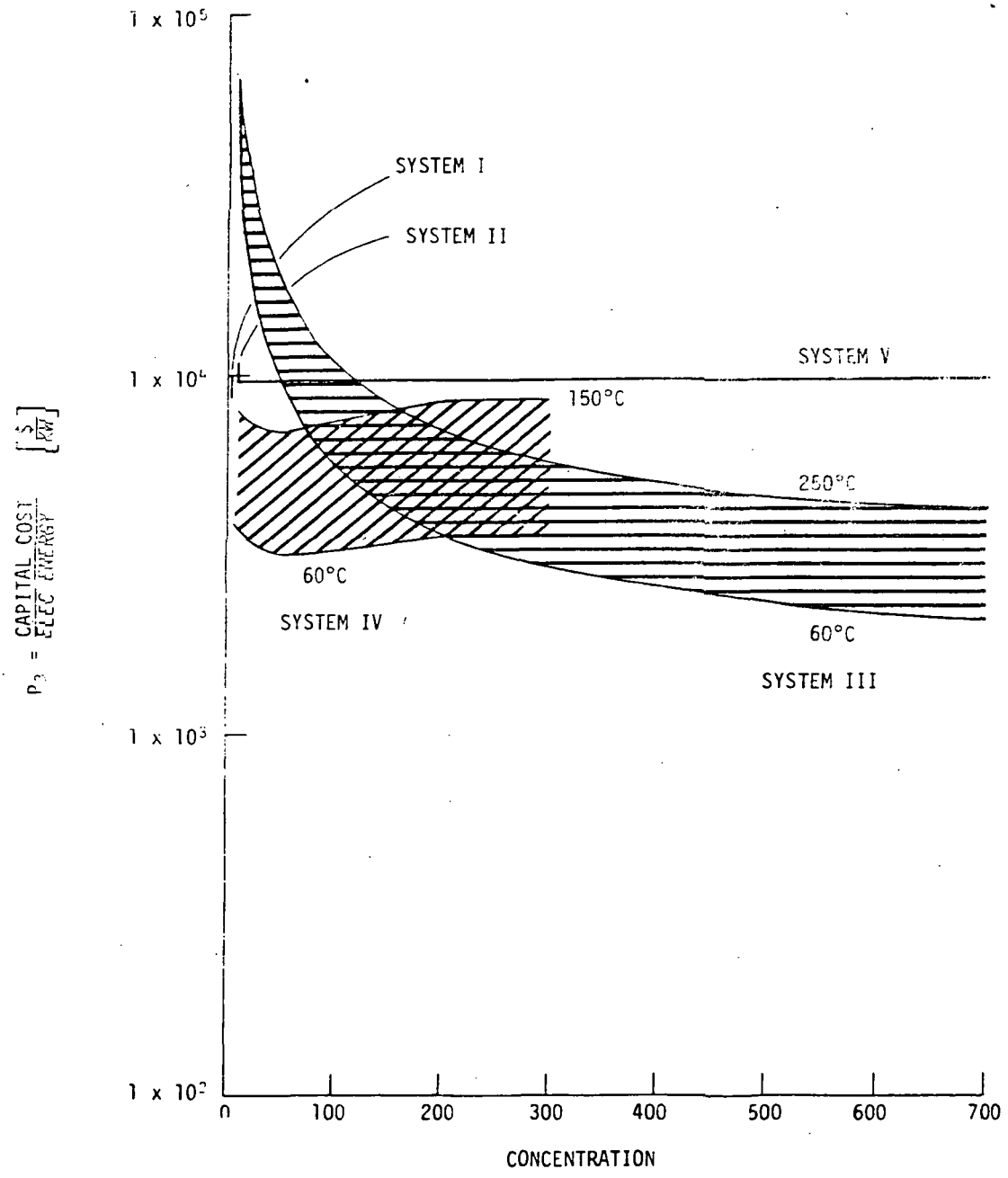
1 x 10⁵
1 x 10⁴
1 x 10³
1 x 10²
SYSTEM I
SYSTEM II
SYSTEM V
150°C
250°C
60°C
SYSTEM IV
60°C
SYSTEM III
0
100
200
300
400
500
600
700
CONCENTRATION
P₃ = CAPITAL COST / ELEC ENERGY [$/kW]

COMPARISON OF SYSTEMS III AND IV

ENERGY BALANCE

$$Q_{IN} = Q_{ELEC} + Q_{LOSS} + Q_{COOL}$$

$$\eta_1 I_N C_{TH} = \eta_1 I_N C_{TH} \eta_3 + 2h_1(T_C - T_{air}) + 2\epsilon\sigma(T_{CK}^4 - T_{airK}^4) + K(T_C - T_F)$$

FOR LINEAR MODEL

$$\eta_3 = \eta_r\left(1 - \beta(T_c - T_r)\right)$$

GaAs $\eta_r = .15$, $T_r = 25°C$, $\beta = .0024$

Si $\eta_r = .10$, $T_t = 25°C$, $\beta = .0047$

$$C_{TH} = \frac{Q_{LOSS} + Q_{COOL}}{\eta_1 I_N(1 - \eta_3)}$$

FOR NON-LINEAR MODEL

$$\eta_3 = \frac{V_{OC}(E,T_c) \cdot I_{sc}(E,T) \cdot FF(E,T)10^4}{E}$$

GaAs

$$V_{OC}(E,T) = VOCO_G + 7.36110^{-3})E^{.357} - 2.45(10^{-3})T$$

$$I_{sc}(E,T) = (.148E^{.363} + .388)T$$

$$FF_G(E,T) = FIFO_G + 1.922E^{-.162} - 1.11(10^{-3})T$$

Si

$$V_{OC}(E,T) = VOCO_S + (2.9(10^{-3})E^{.172} - 2.23(10^{-3})T$$

$$I_{sc}(E,T) = ISCO_S(A_0 + A_1T + A_2T^2 + A_3T^3 + A_4T^4 + A_5T^5) * E/10.$$

$$FF_S(E,T) = FF_G(E,T)$$

For T_c fixed, $E = \eta_1 I_N C_{TH_{OLD}}$ calculate η_3

$$C_{TH_{NEW}} = \frac{Q_{LOSS} + Q_{COOL}}{\eta_1 I_N (1 - \eta_3)}$$

$$Q_{COOL} = K(T_C - T_F)$$

$$Q_{ELEC} = \eta_1 I_N C_{TH} \cdot \eta_3$$

$$Q_{LT} = Q_{COOL} - W_{OUT}$$

$$W_{OUT} = .5\left(1 - \frac{T_{FK}}{T_{CK}}\right) \cdot Q_{COOL}$$

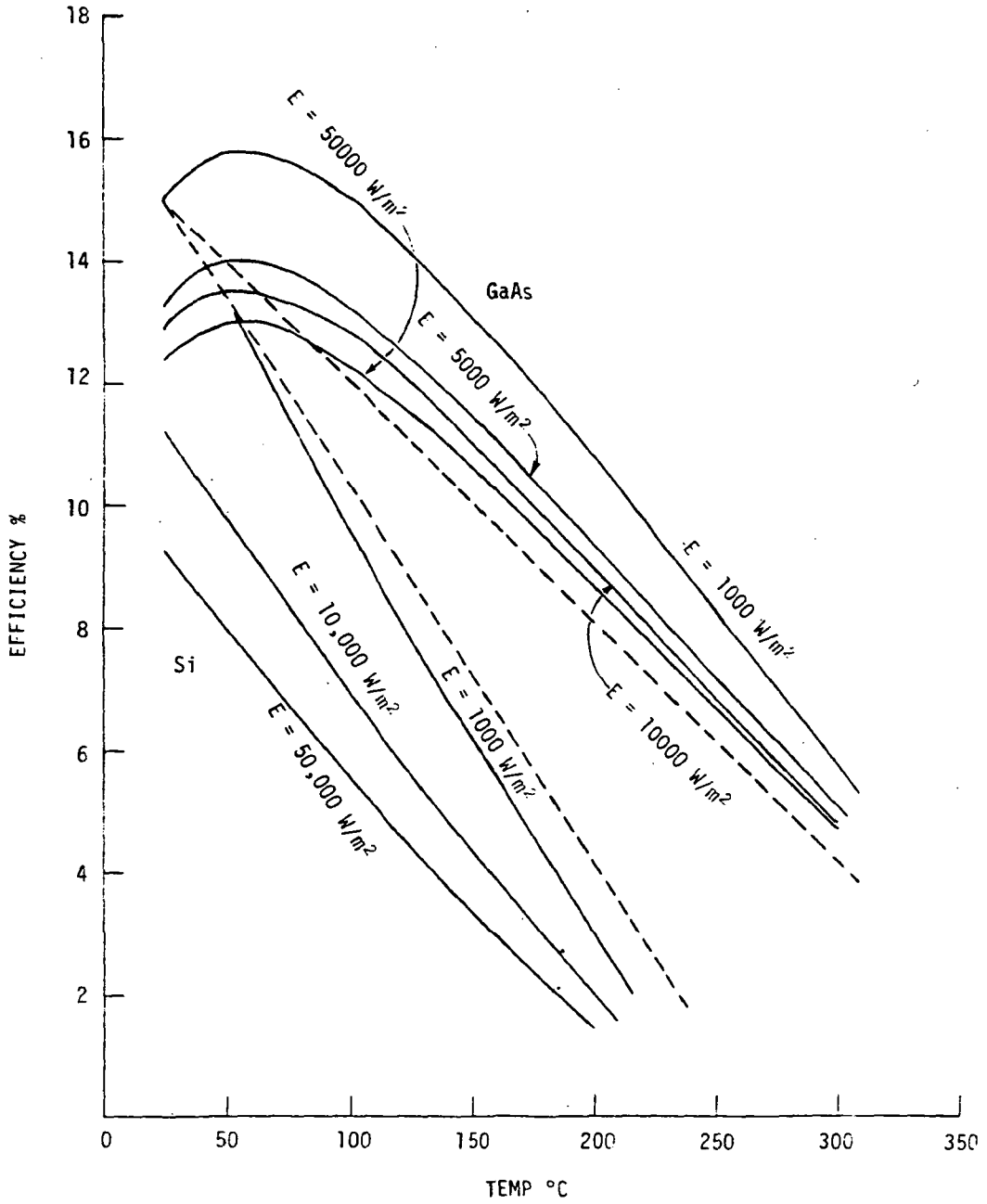
EFFICIENCY %
TEMP °C
GaAs
Si
E = 50000 W/m²
E = 5000 W/m²
E = 1000 W/m²
E = 10000 W/m²
E = 10,000 W/m²
E = 1000 W/m²
E = 50,000 W/m²
18
16
14
12
10
8
6
4
2
0
50
100
150
200
250
300
350

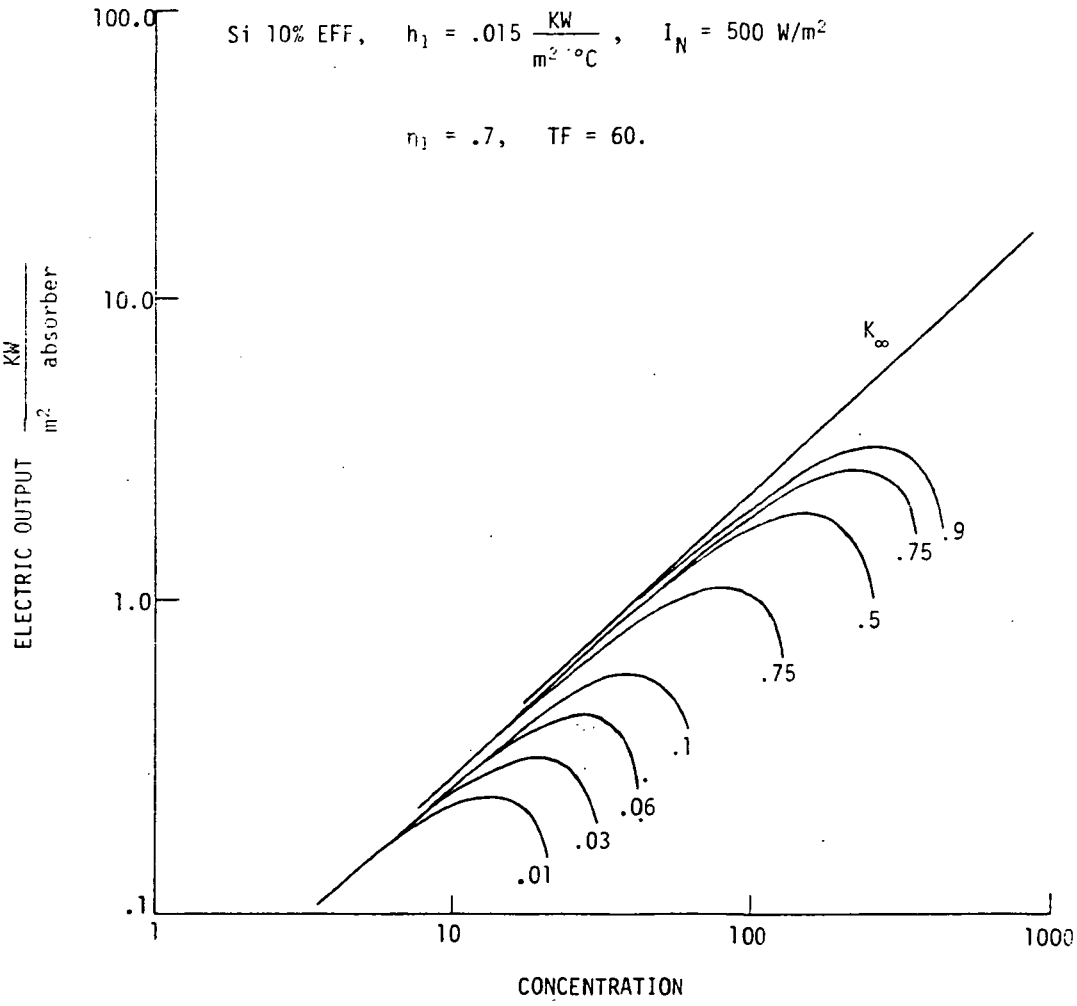

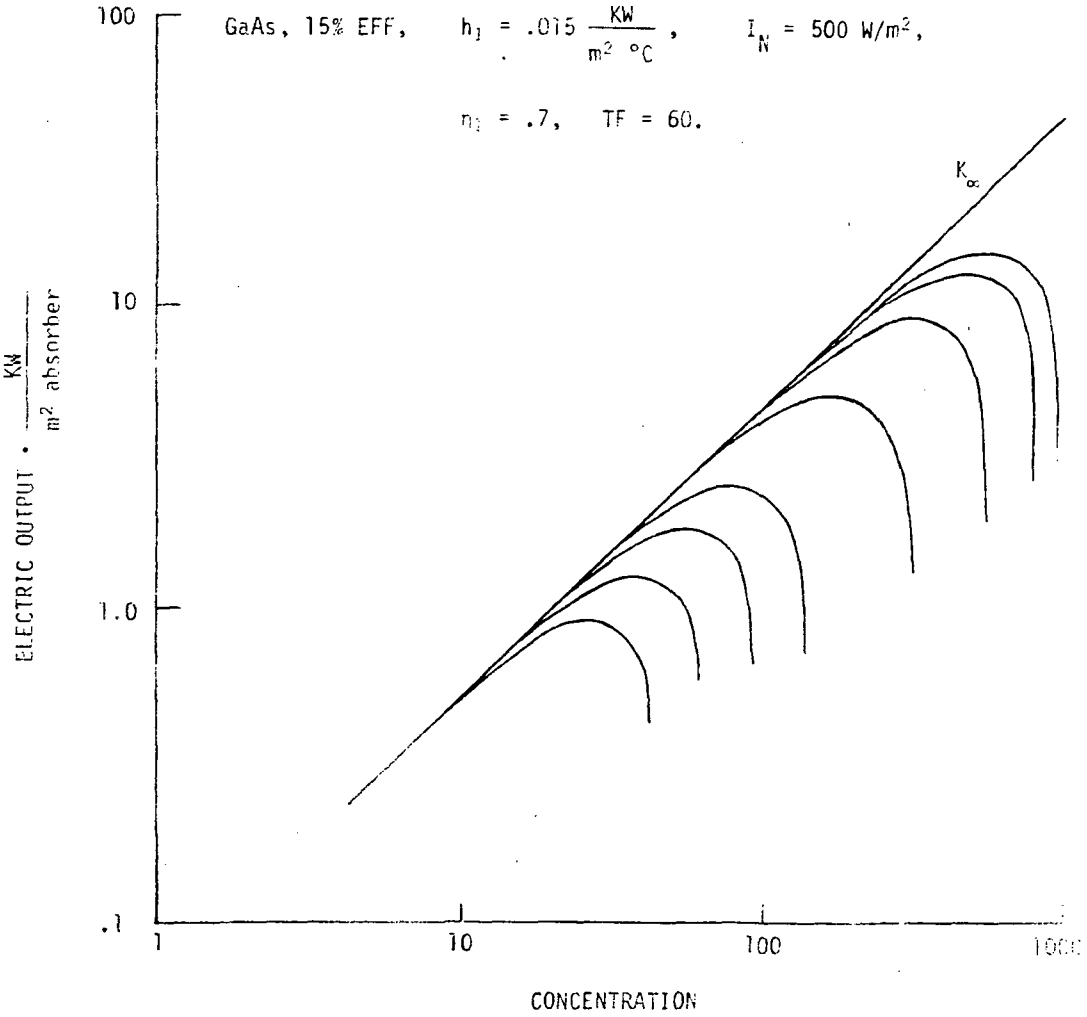
GaAs, 15% EFF, $h_j = .015 \frac{KW}{m^2\ °C}$, $I_N = 500\ W/m^2$,
$\eta_j = .7$, TF = 60.
K_∞
100
10
1.0
.1
1
10
100
ELECTRIC OUTPUT • $\frac{KW}{m^2\ absorber}$
CONCENTRATION

Rectangular Coordinate

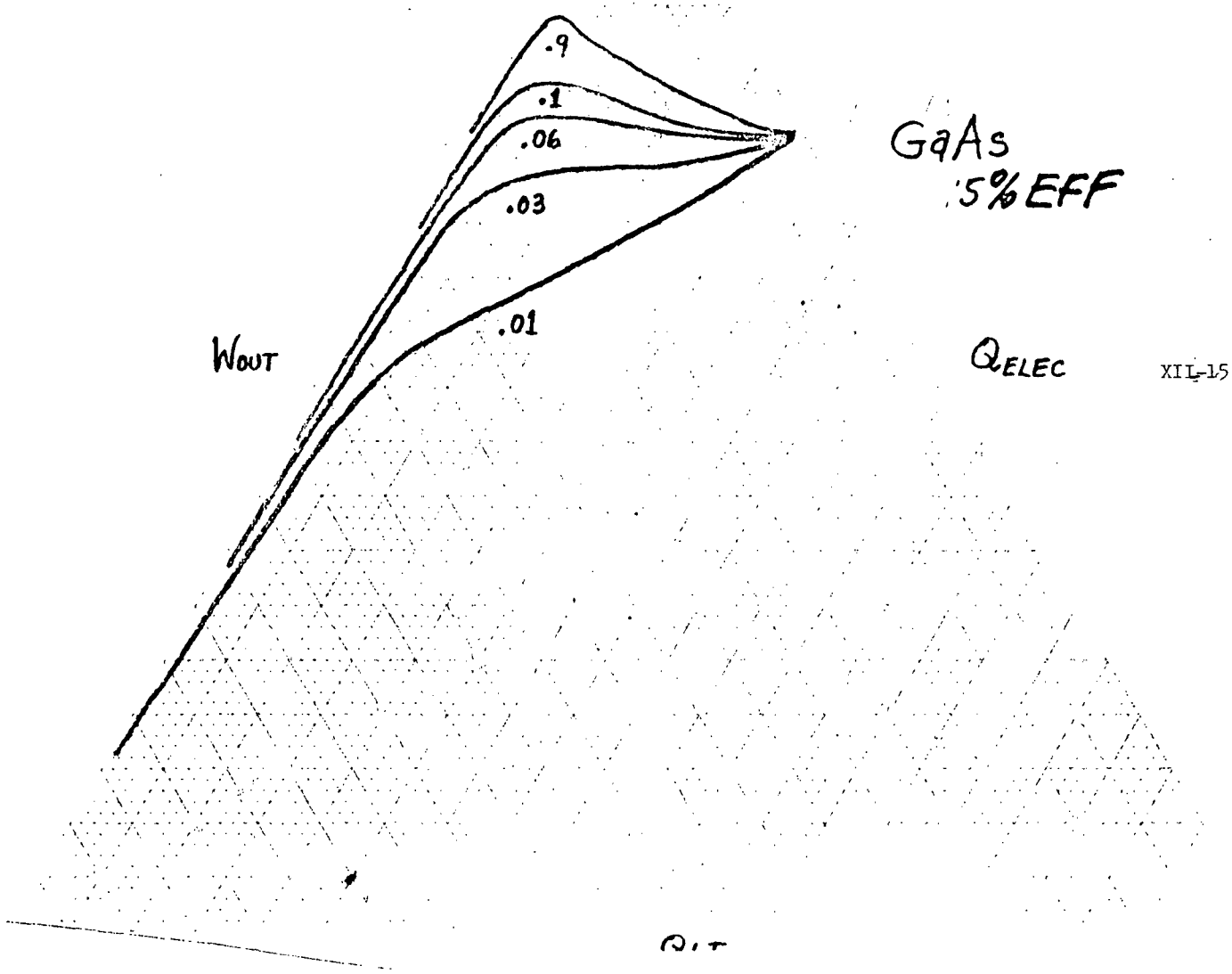
.9
.1
.06
.03
.01
GaAs
15% EFF
WOUT
QELEC
QIT

ANNUAL ENERGY PRODUCTION

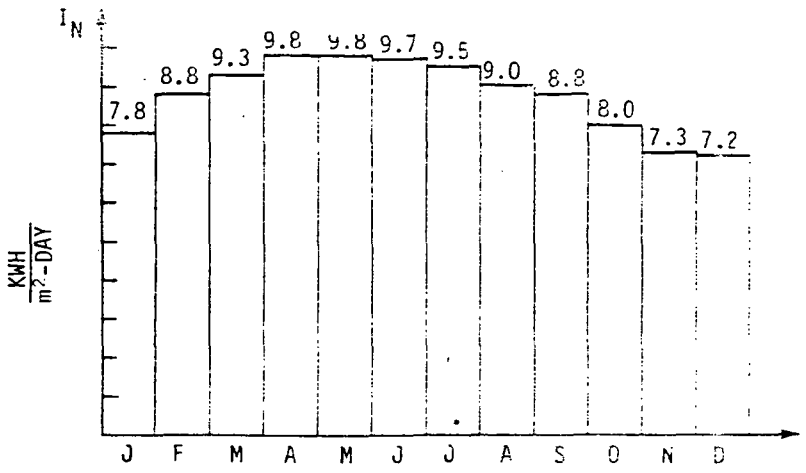

$I_N(n)$ = AVG. INTENSITY FOR nth MONTH

$$(1 - \eta_3)\eta_1 I_N(n) C_{TH} - 2h_1(T_{CK} - T_{airK}) - 2\varepsilon\sigma(T_{CK}^4 - T_{airK}^4) - K(T_{CK} - T_{FK}) = 0$$

Calculate

$$Q_{ELEC}(n) = \eta_1 I_N(n)\, C_{TH}\eta_3(24)DAYM(n)$$

$$Q_{COOL}(n) = K(T_{CK} - T_{FK})$$

$$Q_{WORK}(n) = \left[.5\left(1 - \frac{T_{FK}}{T_{CK}}\right) Q_{COOL}(n) + Q_{ELEC}(n)\right](24)\ DAYM(n)$$

$$\text{ANNUAL ELEC} = \left(\sum_{n=1}^{12} Q_{ELEC}(n)\right)\ Aabs$$

$$\text{ANNUAL WORK} = \left(\sum_{n=1}^{12} Q_{WORK}(n)\right)\ Aabs$$

$$\text{ANNUAL COST} = \left[\frac{(1+i)^n \cdot i}{(1+i)^n - 1} + m\right]\left(\begin{matrix}\text{CAPITAL}\\ \text{COST}\end{matrix}\right)$$

$$\left(\begin{matrix}\text{CAPITAL}\\ \text{COST}\end{matrix}\right) = \left(\begin{matrix}\text{COST}\\ \text{CON}\end{matrix}\right)(Aap) + \left(\begin{matrix}\text{COST}\\ \text{CELL}\end{matrix}\right)(Aabs)$$

$$\text{Performance Index 4} = P_4 = \frac{\text{annual cost}}{\text{annual elec}}$$

$$\text{Performance Index 5} = P_5 = \frac{\text{annual cost}}{\text{annual work}}$$

i = .08

n = 20 years

m = maintenance cost = .02

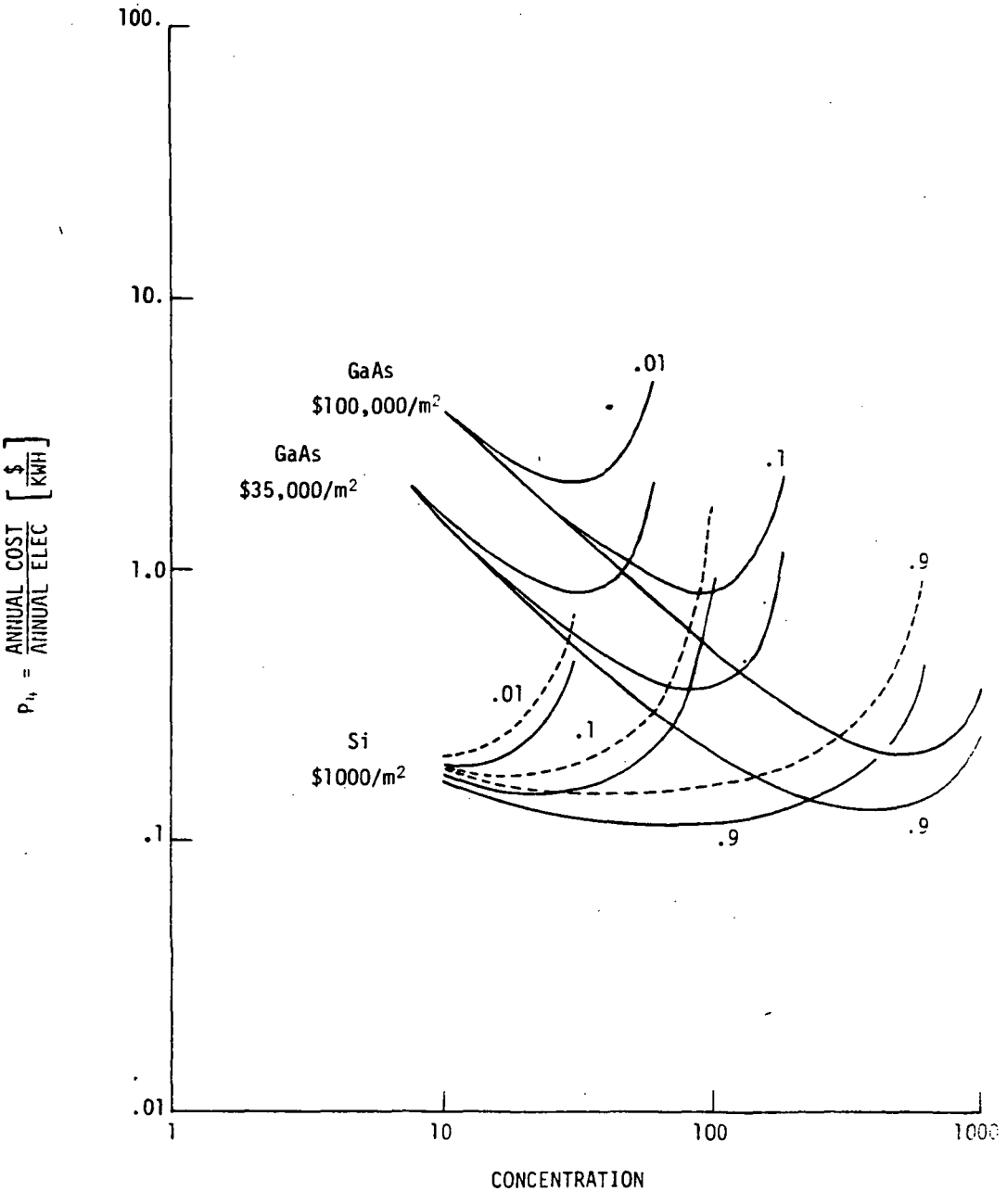
100.
10.
1.0
.1
.01
1
10
100
1000
CONCENTRATION
$P_{ij} = \frac{\text{ANNUAL COST}}{\text{ANNUAL ELEC}} \left[\frac{\$}{\text{KWH}}\right]$
GaAs
$100,000/m²
GaAs
$35,000/m²
Si
$1000/m²
.01
.1
.9

XII-17

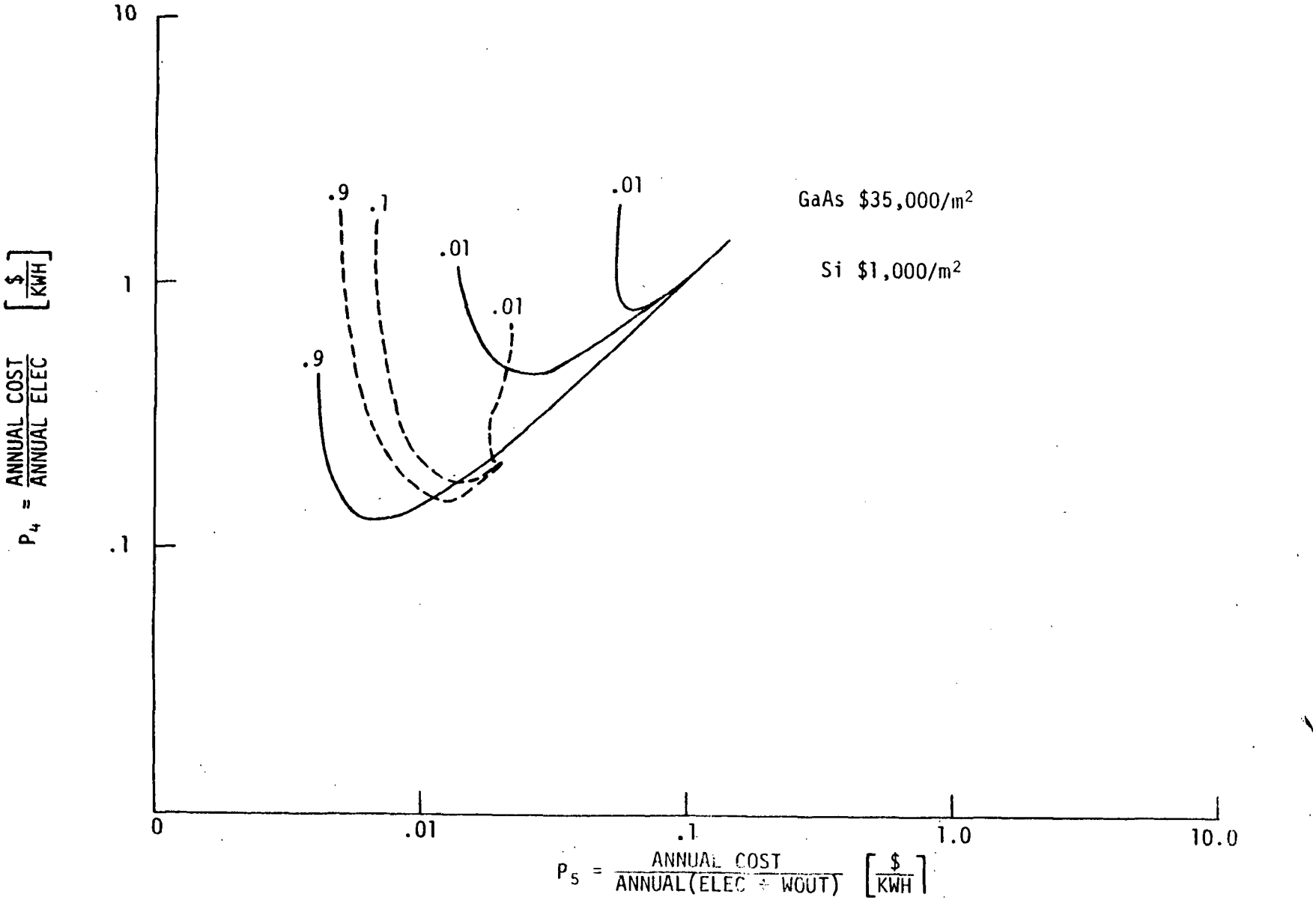
10
1
.1
0
.01
.1
1.0
10.0
.9
.1
.01
.01
.01
.9
GaAs $35,000/m²
Si $1,000/m²
$P_4 = \frac{\text{ANNUAL COST}}{\text{ANNUAL ELEC}}$ $\left[\frac{\$}{\text{KWH}}\right]$
$P_5 = \frac{\text{ANNUAL COST}}{\text{ANNUAL(ELEC + WOUT)}}$ $\left[\frac{\$}{\text{KWH}}\right]$

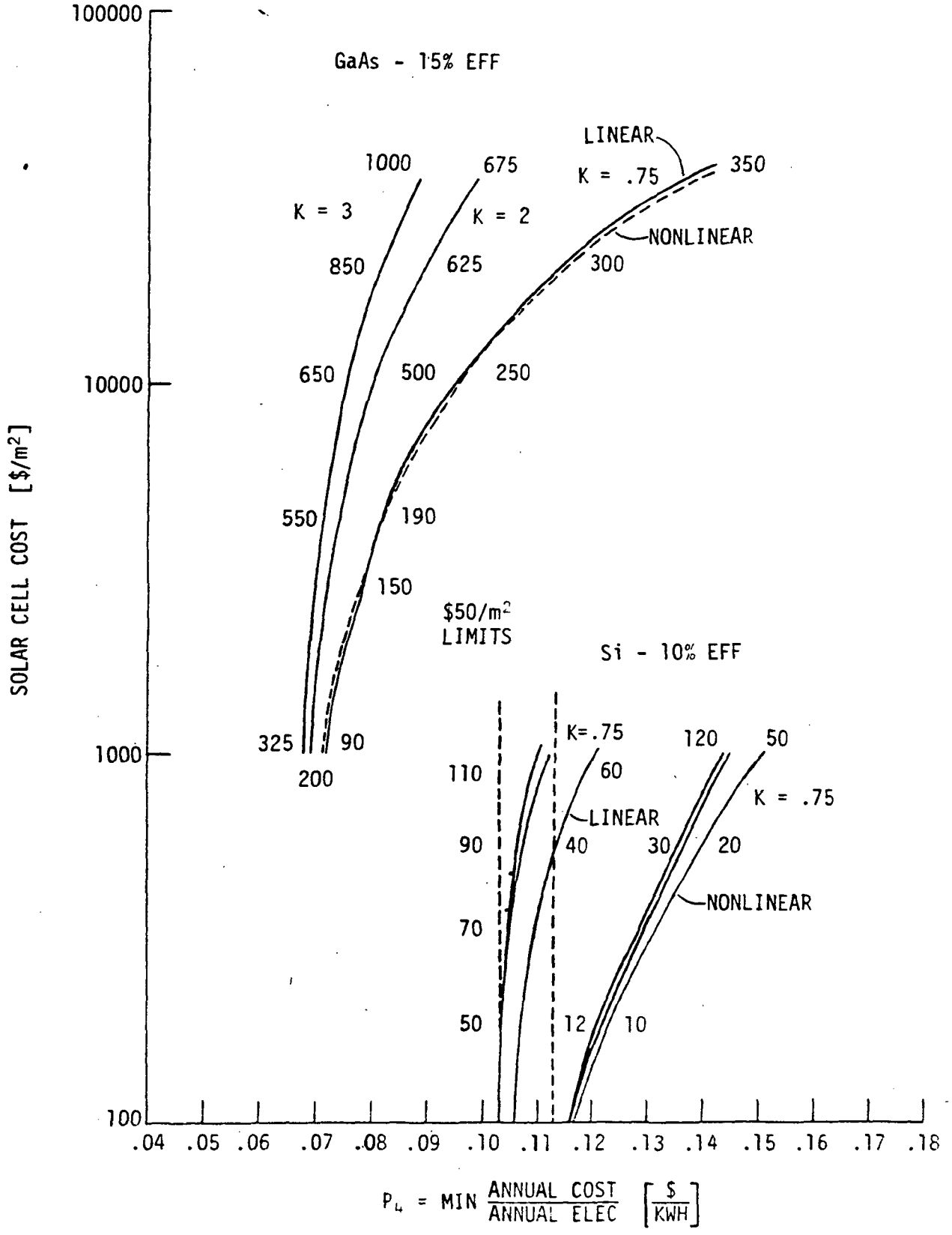
GaAs - 15% EFF
LINEAR
K = .75
350
1000
675
K = 3
K = 2
NONLINEAR
850
625
300
650
500
250
550
190
150
$50/m^2$
LIMITS
Si - 10% EFF
325
90
200
K=.75
120
50
110
60
LINEAR
K = .75
90
40
30
20
NONLINEAR
70
50
12
10
100000
10000
1000
100
SOLAR CELL COST [$/m^2]
.04 .05 .06 .07 .08 .09 .10 .11 .12 .13 .14 .15 .16 .17 .18
P_4 = MIN ANNUAL COST / ANNUAL ELEC [$/KWH]

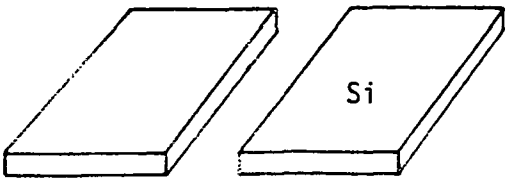

SYSTEM I

FLAT PLATE COLLECTOR (THERMAL POWER) SEPARATE FLAT PLATE COLLECTOR (Si) (ELECTRIC POWER)

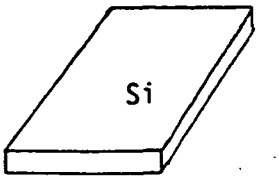

SYSTEM II

FLAT PLATE COLLECTOR WITH SILICON

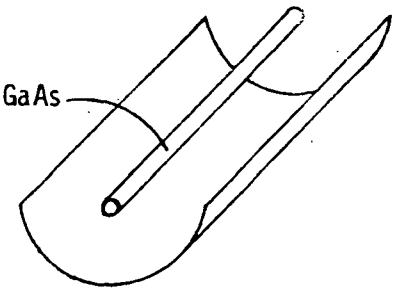

SYSTEM III

CONCENTRATOR WITH GaAs

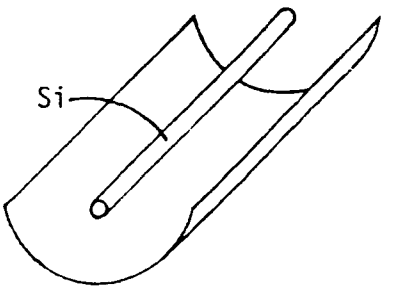

SYSTEM IV

CONCENTRATOR WITH Si

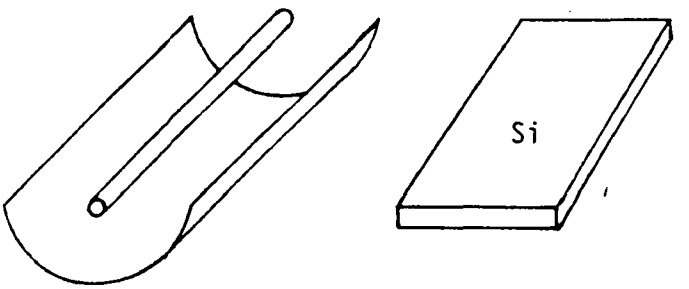

SYSTEM V

CONCENTRATOR FOR THERMAL POWER FLAT PLATE COLLECTOR WITH Si FOR ELECTRIC POWER

CONCLUSIONS

1. REALISTIC COSTS AND EFFICIENCES OF GaAs AND Si ARE:

   Si : $1000/m^2 - 10% eff. cells -AM1
   GaAs: $35000/m^2 - 15% eff. cells -AM1

2. LIMITING VALUES FOR ANNUAL COSTS ARE

	Si	GaAs
MINIMUM ($\frac{\text{ANNUAL COST}}{\text{KWH ELECTRIC}}$)	$\frac{10.5¢}{KWH}$	$\frac{6.8¢}{KWH}$

3. FOR A GIVEN FLOW RATE , THERE IS AN OPTIMAL OPERATING CONDITION FOR MAXIMUM PHOTOVOLTAIC OUTPUT FOR BOTH GaAs AND Si HYBRID SYSTEMS.

4. HIGH CONCENTRATION HYBRID SYSTEMS OFFER A DISTINCT COST ADVANTAGE OVER FLAT PLATE HYBRID SYSTEMS (CONCENTRATION REDUCES CELL AREA

5. THE THERMAL ENERGY ACHIEVABLE FROM HYBRID SYSTEMS OPERATING AT MAXIMUM ELECTRIC POWER IS MAINLY FOR HEATING AND AIR CONDITIONING PURPOSES.

   THE ENERGY IS DIVIDED APPROXIMATELY AS FOLLOWS:

Si	: 9% ELECTRIC	; 90% useable heat	:	1% MECH. WORK
GaAs	: 12% ELECTRIC	; 85% useable heat	:	3% MECH. WORK

6. FOR Si CELL COSTS OF $50/m^2 (NSF GOAL) AND GaAs A FACTOR OF 2 MORE EXPENSIVE, OPTIMAL Si OR GaAs HYBRID SYSTEM PERFORMANCE CAN BE ACHIEVED AT LOWER CONCENTRATIONS.

Summary of Discussion - E. J. Conway

Dr. Charles Byvik of Langley initiated the discussion by reviewing some high points of the meeting. His impression of the program was given in analogy. The program was like a diamond. The narrow top point was the number of important applications which needed GaAs solar cells. The wide central region was the broad range of device concepts and research currently underway in the program. The narrow point which supports the diamond was seen as the materials research base within the program. Dr. Byvik felt that our materials research was too limited for a stable program.

Discussion of applications centered around three areas: the Satellite Solar Power Station (a 15 GWe space satellite beaming power to earth for a lifetime of twenty years), near sun missions (such as a Mercury or solar orbiter), and terrestrial photovoltaic power. Applications oriented people asked questions to which there were no satisfactory answers, yet.

a. What will the AM-0 efficiency be for GaAs solar cells in the 1980's?

b. What will the temperature coefficient be for developed cells?

c. What will be the temperature stability to cyclic variations?

d. What will be the radiation damage efficiency-decrement at end of life?

e. Who will manufacture GaAs solar cells?

f. How much will cells cost?

The chief questions asked of GaAs solar cell users were, how many square meters of these cells will be needed, and when.

Device research discussion emphasized both problems and potential. The chief problem was the low short circuit current, due to nonuniformity of the liquid phase epitaxial (LPE) layer or of the substrate material. Other important problems mentioned were the labor intensiveness of LPE cells and low resistance ohmic front contacts to p-GaAlAs. On the positive side, vapor phase epitaxy (VPE) may supplant LPE for further cell development due to flexibility and scaling advantages. Also, device specialists felt that the best small GaAs cells would be more than 14-15% efficient in space. However, a final structure, best suited to development, has not yet been identified.

On the subject of materials, all participants were in general agreement. GaAs is being produced for LED applications and does not meet high quality standards. (For example, the reproducibility and yield of manufactured microwave devices are strongly dependent on substrate quality.) Although double epi-techniques can provide the required long diffusion length, substrate uniformity appears to limit the high efficiency area of the cell. Since VPE techniques provide no clean-up, VPE cells should require purer substrates than presently being used.

The areas needing further emphasis within the program are

1. Bulk GaAs for uniform large area cells and for VPE cells
2. Contact metallurgy for low resistance ohmic contacts with good adherence
3. New cell structures including one with indium oxide front contact and a GaAs film cell
4. Environmental testing such as radiation damage and end of life characteristics.

U. S. Government Printing Office : 1978---[illegible]-761/69 Region 3-11